Application of Molecularly Imprinted Polymer for Drug Delivery and Membrane Separation of Chiral Drugs

Chutima Jantarat

A Thesis Submitted in Fulfillment of the Requirements for the Degree of Doctor of Philosophy in Pharmaceutical Sciences

Prince of Songkla University

2009

Thesis Title	Application of Molecularly Imprinted Polymer for Drug Delivery and Membrane Separation of Chiral Drugs
Author	Miss Chutima Jantarat
Major Program	Pharmaceutical Sciences

Major advisor

……..

(Assoc. Prof. Dr. Roongnapa Srichana)

Co-advisor

……..

(Dr. Sarunyoo Songkro)

……..

(Prof. Dr. Wolfgang Lindner)

Examining Committee

…….Chairperson

(Assoc. Prof. Dr. Ruedeekorn Wiwattanapatapee)

……

(Assoc. Prof. Dr. Roongnapa Srichana)

……

(Assoc. Prof. Dr. Pornsak Sriamornsak)

……

(Assist. Prof. Dr. Chitchamai Ovatlarnporn)

……

(Dr. Sarunyoo Songkro)

The Graduate School, Prince of Songkla University, has approved this thesis as fulfillment of the requirements for the Doctor of Philosophy Degree in Pharmaceutical Sciences

...……

(Assoc. Prof. Dr. Krerkchai Thongnoo)

Dean of Graduate School

ชื่อวิทยานิพนธ์ การประยุกต์ใช้พอลิเมอร์ที่มีรอยพิมพ์ประทับโมเลกุลสำหรับการนำส่งยาและการแยกด้วยเยื่อแผ่นของยาไครัล
ผู้เขียน นางสาวชุติมา จันทรัตน์
สาขาวิชา เภสัชศาสตร์
ปีการศึกษา 2551

บทคัดย่อ

วัตถุประสงค์ของวิทยานิพนธ์นี้เพื่อพัฒนาวิธีการในการเตรียมเยื่อแผ่นและระบบนำส่งยาให้มีความสามารถสูงในการปลดปล่อยที่เลือกเฉพาะอิแนนทิโอเมอร์สำหรับยาไครัลโดยการประยุกต์ใช้พอลิเมอร์ที่มีรอยพิมพ์ประทับโมเลกุล (Molecularly imprinted polymer; MIP) เป็นตัวจดจำที่เลือกเฉพาะอิแนนทิโอเมอร์ โดยเซลลูโลสที่ผลิตจากเชื้อแบคทีเรียซึ่งเป็นวัสดุที่ผลิตได้ง่ายและมีราคาถูกในประเทศไทยถูกนำมาใช้เป็นเยื่อแผ่นพยุงและเป็นส่วนประกอบของระบบนำส่งยา เยื่อแผ่นประกอบที่ประกอบด้วย MIP และเซลลูโลส (MIP composite membrane) ถูกเตรียมขึ้นโดยการกราฟต์ชั้นบางของ MIP (MIP layer) บนแผ่นเซลลูโลสและการบรรจุอนุภาคของ MIP ลงในแผ่นเซลลูโลส จากการศึกษาพบว่าการปลดปล่อยที่เลือกเฉพาะอิแนนทิโอเมอร์ของเยื่อแผ่นประกอบที่ประกอบด้วย MIP layer ขึ้นอยู่กับชนิดของมอนอเมอร์ที่ใช้ในการสังเคราะห์ MIP โดยเยื่อแผ่นประกอบที่ประกอบด้วย MIP layer ที่เตรียมจากโคพอลิเมอร์ของ อะคริลามายด์-เอ็นเอ็น-เมทิลีน บิสอะคริลามายด์ ซึ่งถูกพิมพ์ประทับด้วยเอส-อิแนนทิโอเมอร์ของยาไอบูโปรเฟนหรือยานาโปรเซนให้ผลการปลดปล่อยที่เลือกเฉพาะอิแนนทิโอเมอร์ของเอส-อิแนนทิโอเมอร์ของยาได้ดีกว่าเยื่อแผ่นประกอบที่ประกอบด้วย MIP layer ที่เตรียมจากโคพอลิเมอร์ของ 4-ไวนิล-ไพรีดีน-เอทิลีน ไกลคอล ไดเมทาครีเลท อย่างไรก็ตามเยื่อแผ่นประกอบที่เตรียมจากการกราฟต์ MIP layer บนแผ่นเซลลูโลสให้ผลการเลือกเฉพาะอิแนนทิโอเมอร์ต่ำ เนื่องจาก MIP ส่วนใหญ่เกาะติดอยู่บนผิวของเซลลูโลสมากกว่าที่จะกระจายตัวอยู่ภายในเยื่อแผ่น ทำให้ความจำเพาะของเยื่อแผ่นประกอบในการจับกับโมเลกุลตัวพิมพ์มีประสิทธิภาพต่ำ

การเตรียมเยื่อแผ่นประกอบโดยการบรรจุอนุภาคของ MIP ลงในแผ่นเซลลูโลสทำให้รอยจดจำถูกกระจายตัวอยู่ภายในเนื้อของเยื่อแผ่น และเป็นการเพิ่มความจำเพาะของโมเลกุลตัวพิมพ์ในการจับกับรอยพิมพ์ประทับ อนุภาคของ MIP แบบ nanoparticle-on-microsphere (NOM) ถูกพัฒนาขึ้นมาใช้ในการศึกษานี้ อนุภาคนาโนซึ่งเกาะติดอยู่บนอนุภาคไมโครสเฟียร์ทำให้เพิ่มพื้นที่ผิวในการสัมผัส จึงทำให้โมเลกุลตัวพิมพ์เข้าจับที่รอยพิมพ์ประทับได้ง่าย เยื่อแผ่น

ประกอบที่ประกอบด้วย MIP-NOM จึงให้ผลการเลือกเฉพาะอิแนนทิโอเมอร์ดีกว่าเยื่อแผ่นประกอบที่ประกอบด้วยอนุภาคของ MIP แบบแกรนูลซึ่งสังเคราะห์มาจากส่วนประกอบที่เหมือนกัน เยื่อแผ่นประกอบที่ประกอบด้วย MIP-NOM ที่พิมพ์ประทับด้วยเอส-โพรพราโนลอล ซึ่งสังเคราะห์โดยใช้ เมทาครีลิก เอซิด เป็นมอนอเมอร์ฟังก์ชัน และ เอทิลีน ไกลคอล ไดเมทาครีเลท เป็นมอนอเมอร์เชื่อมโยง มีประสิทธิภาพสูงในการปลดปล่อยเอส-โพรพราโนลอล นอกจากนี้เยื่อแผ่นประกอบดังกล่าวยังให้ผลการปลดปล่อยที่เลือกเฉพาะอิแนนทิโอเมอร์สำหรับยาโพรพราโนลอล โปรดรักของยาโพรพราโนลอล (ไซโครโพรพาโนอิล-โพรพราโนลอล และ วาเลอริล-โพรพราโนลอล) และยาเบต้า-บล็อกเกอร์ตัวอื่นๆ (พินโดลอลและออกพรีโนลอล) ในการศึกษาแบบนอกกาย (*in vitro*) ผ่านหนังหนู (rat skin) เยื่อแผ่นประกอบที่ประกอบด้วย MIP-NOM อาจจะสามารถนำไปประยุกต์ใช้เพื่อควบคุมการปลดปล่อยโมเลกุลเป้าหมายได้

นอกจากนี้ยังได้ทำการศึกษาการประยุกต์ใช้ MIP-NOM ที่สังเคราะห์โดยใช้มอนอเมอร์ฟังก์ชันที่เป็นไครัล MIP-NOM ที่มีรอยจดจำที่เป็นไครัลอาจทำให้เพิ่มความจำเพาะในการจับกับอิแนนทิโอเมอร์ได้ อนุพันธ์ของควินิน (Methacryloylate quinine; MQN) และอนุพันธ์ของควินิดีน (Methacryloylate quinidine; MQD) ถูกสังเคราะห์ขึ้นเพื่อใช้เป็นมอนอเมอร์ฟังก์ชันในการสังเคราะห์ MIP-NOM ซึ่งพิมพ์ประทับด้วยเอส-โอเมพราโซล และ MIP-NOM ที่ประกอบด้วย 4-ไวนิลไพรีดีน (4-VPD) ซึ่งเป็นมอนอเมอร์ฟังก์ชันที่ไม่เป็นไครัลถูกสังเคราะห์ขึ้นมาเพื่อใช้ในการเปรียบเทียบ จากผลการศึกษาด้วย Fourier transform infrared spectroscopy (FT-IR) และ Confocal laser scanning microscopy (CLSM) แสดงให้เห็นว่า MQN-MIP-NOM น่าจะเกิดสารประกอบกับโมเลกุลตัวพิมพ์เอส-โอเมพราโซลได้ดีกว่า MQD-MIP-NOM การเลือกเฉพาะอิแนนทิโอเมอร์สำหรับยาโอเมพราโซลของ MQN-MIP-NOM มีประสิทธิภาพสูงกว่าของ MQD-MIP-NOM ในขณะที่ MQD-MIP-NOM ให้ผลการเลือกเฉพาะอิแนนทิโอเมอร์ที่ใกล้เคียงกับ 4-VPD-MIP-NOM ระบบนำส่งยาที่ประกอบด้วย MQN-MIP-NOM สามารถปลดปล่อยเอส-โอเมพราโซลออกมาได้ในปริมาณที่มากกว่าอาร์-โอเมพราโซล ซึ่งระบบนำส่งยาดังกล่าวมีประสิทธิภาพในการเลือกเฉพาะอิแนนทิโอเมอร์ดีกว่าระบบนำส่งยาที่ประกอบด้วย MQD-MIP-NOM ดังนั้น MQN-MIP-NOM อาจจะมีศักยภาพสูงสำหรับการประยุกต์ใช้ในการนำส่งยาที่เลือกเฉพาะอิแนนทิโอเมอร์ของยาโอเมพราโซลได้

Thesis Title	Application of Molecularly Imprinted Polymer for Drug Delivery and Membrane Separation of Chiral Drugs
Author	Miss Chutima Jantarat
Major Program	Pharmaceutical Sciences
Academic Year	2008

ABSTRACT

The purpose of this thesis is to develop a method for preparation of membrane and drug delivery system to have highly enantioselective release ability for chiral drugs by applying molecularly imprinted polymer (MIP) as enantioselective recognition phase. The bacterial cellulose, which is easily produced in a vast amount with low unit cost in Thailand, was used as membrane support and component in drug delivery system. The MIP composite membranes were prepared by grafting MIP layer on cellulose membrane and by integrating MIP particles into cellulose membrane. The enantioselective release of MIP layer composite membrane was dependent on type of monomer used in MIP synthesis. The MIP layer comprising of poly(acrylamide-*co*-*N,N'*-methylene bisacrylamide), which was imprinted with *S*-enantiomer of ibuprofen or naproxen, composite membrane demonstrated enantioselective release of *S*-enantiomer of the drugs greater than MIP layer comprising of poly(4-vinylpyridine-*co*-ethylene glycol dimethacrylate) composite membrane. However, the MIP composite membrane derived by grafting MIP layer on cellulose membrane gave the modest enantioselectivity due to more deposition of MIP onto the surface of cellulose than at deeper layer, thus the reduction in affinity of composite membrane to the template.

The preparation of MIP composite membrane by integration of MIP particles into cellulose membrane allowed an availability of the molecule recognition sites within a membrane matrix, and this improved the affinity of template and its binding sites. The MIP nanoparticle-on-microsphere (MIP-NOM) was successfully developed to use in this study. The adherent nanoparticles on microspheres provided an increased surface area enabling the composite membrane to be employed efficiently for the trans-membrane transport of the imprinted molecule. The MIP-NOM within the membrane were easily accessible for binding of

the imprinted molecule and appeared to maintain high selectivity compared to the MIP granules which were synthesized using the same composition. The high potential in the release of *S*-propranolol enantiomer from *S*-propranolol-MIP-NOM, synthesized by using methacrylic acid as functional monomer and ethylene glycol dimethacrylate as cross-linking monomer, composite membrane was achieved. The enantioselective release was also achieved *in vitro* skin permeation using rat skin for racemic propranolol, in addition its prodrug analogs (cyclopropanoyl- and valeryl-propranolol) and other β-blockers (pindolol and oxprenolol). The proposed MIP-NOM composite membrane controlled release system may be applicable for fabrication of novel membranes with self-controllable permeability responding to the presence of target solutes.

In addition, the application of MIP-NOM synthesized by using chiral functional monomers was studied. The chiral binding sites generated on MIP-NOM would provide an increased affinity for binding of enantiomer. The methacryloylate quinine (MQN) and methacryloylate quinidine (MQD) were synthesized to use as chiral functional monomers for MIP-NOM synthesis, which was imprinted with *S*-omeprazole, and the MIP-NOM composing 4-vinylpyridine (4-VPD), which is achiral functional monomer, was synthesized for comparison. The studies by Fourier transform infrared spectroscopy (FT-IR) and Confocal laser scanning microscopy (CLSM) revealed stronger complexation of MQN-MIP-NOM and *S*-omeprazole template than that of MQD-MIP-NOM. The enantioselectivity for omeprazole of MQN-MIP-NOM was achieved in superior than that of MQD-MIP-NOM, whereas MQD-MIP-NOM displayed comparative enantioselectivity to 4-VPD-MIP-NOM. The release of *S*-omeprazole in higher proportion than *R*-omeprazole was achieved from drug delivery system containing MQN-MIP-NOM, which demonstrated greater enantioselectivity than drug delivery system containing MQD-MIP-NOM. Therefore, the MQN-MIP-NOM may be potential for application in drug delivery selective to the enantiomer of omeprazole.

CONTENTS

CONTENTS (CONTINUED)

CONTENTS (CONTINUED)

CONTENTS (CONTINUED)

CONTENTS (CONTINUED)

CONTENTS (CONTINUED)

CONTENTS (CONTINUED)

CONTENTS (CONTINUED)

LIST OF TABLES

LIST OF TABLES (CONTINUED)

LIST OF TABLES (CONTINUED)

LIST OF FIGURES

LIST OF FIGURES (CONTINUED)

LIST OF FIGURES (CONTINUED)

LIST OF FIGURES (CONTINUED)

LIST OF FIGURES (CONTINUED)

LIST OF FIGURES (CONTINUED)

LIST OF FIGURES (CONTINUED)

CHAPTER 1

INTRODUCTION

1.1. General introduction

Approximately half of the drugs currently in use are chiral compounds and most of them (near 90%) are still marketed as racemates consisting of an equimolar mixture of two enantiomers (Nguyen et al., 2006). Although they have the same chemical structure, most isomers of chiral drugs exhibit marked differences in biological activities such as pharmacology, pharmacokinetics, toxicity etc. Therefore, the use of pure active enantiomer drugs is an important consideration in order to ensure the desired activity in the administration of drugs. There are many racemic compounds which are easily synthesized and which can be simply resolved into their respective enantiomers. However, the resultant optically pure enantiomer is not always stable and racemization, which will become a mixture of equal amounts of each isomer during pharmaceutical processing and storage.

A molecularly imprinted polymer (MIP) is a synthetic polymer possessing selective molecular recognition properties because of recognition sites within the polymer matrix that are complementary to the analyte molecule in the size, shape and positioning of functional groups (Komiyama et al., 2003). The selective recognition property in addition to the robustness and ease of preparation of MIPs have made them attractive for widely applications not only in analytical chemistry but also in drug delivery and have been extended to the enantioselective-controlled delivery of chiral drugs such as β-blockers and non-steroidal anti-inflammatory drugs (NSAIDs) *via* both the oral and transdermal routes (Suedee et al., 2002a, 2002b; Bodhibukkana et al., 2006). The discovery of novel phenomena and processes into the nano-scale has created great excitement in biomedical research and technologies that can provide numerous novel biomaterials such as nanoparticles, liposomes and micelles with appropriate dimension utilized potentially as drug-carriers for drug delivery technologies. In addition, nanotechnology can be employed to

produce MIPs which may be used as important recognition materials in the construction of biosensors, drug delivery technology or the development of novel separation phases. The improvement of MIP synthesis to obtain MIP micro-/nanoparticles could provide more potential use in areas such as assay technology and separation science because the binding sites should be at or near the surface, giving good accessibility and binding kinetics.

The use of molecular imprinting approach to develop new affinity membrane for sensor and separation technology is becoming more widespread, due to the potential high selective membranes can be achieved. MIP membranes were first easily prepared *via in situ* polymerization (Kobayashi et al., 1998). However, only moderate success was achieved since comparatively high selectivities for the template molecules were shaded by ineffective performance, especially due to small fluxes (Mathew-Krotz et al., 1996; Piletsky et al., 1998; Piletsky et al., 1999). Moreover, it is difficult to prepare thin and stable membranes with reproducible properties from highly cross-linked polymers. Several approaches for combining imprinting and membrane technologies have been proposed to develop stable permselective or affinity membranes for the separation of special target molecules from a mixture of structurally similar compounds (Yoshikawa et al., 1995; Mathew-Krotz and Shea, 1996; Piletsky et al., 1999). A number of composite membranes derived from MIPs could be synthesized to attain high separation specificity membranes (Ulbricht et al., 2002). Depending on pore size, the resulting membranes may be novel affinity membranes, but potentially pore-filling composite membranes with entirely novel separation properties could be achieved as well (Piletsky et al., 1999). Cellulose acetate (Ramamoorthy and Ulbricht, 2003), polysulfone (Yoshikawa et al., 2006), polyamide (Lehmann et al., 2002), polyvinylidene fluoride (Kochkodan et al., 2002; Hilal and Kochkodan, 2003; Hilal et al., 2003), and polypropylene (Piletsky et al., 2000) are commonly used as a membrane base for the production of MIP membranes. However, such synthetic membranes are not always suitable for use *in vivo* as a consequence of biocompatibility issues or unsuitable physical properties. In contrast, bacterial cellulose, a natural polysaccharide, has been identified as a promising material for use in medical care since it can be produced with high purity, high-water binding capacity, high-mechanical strength, and biodegradable (Klemm et al., 2001). Bacterial cellulose can be easily produced by the incubation of *Acetobacter sp*. such as *Acetobacter xylinum* in coconut juice or in any other fruit juices. Such bacterial cellulose is

therefore produced in vast amount at a low unit cost from readily available renewable resources found in Southeast Asian countries such as the Philippines, Indonesia, Thailand and Malaysia. These advantages render bacterial cellulose suitable as a possible membrane base for preparing MIP composite membrane for medical application.

The preparation and evaluation of enantioselective-controlled delivery systems for chiral drugs by the use of MIP as the enantioselective recognition phase composed with bacterial cellulose were concerned to the research in this thesis. The MIP and bacterial cellulose were composed as either MIP layer or MIP particle composite membranes to produce the enantioselective membranes. Moreover, MIP particles and cellulose were fabricated into other polymer support to produce the enantioselective drug delivery system. The MIP micro-/nanoparticles have been developed to use. This might be able to improve the enantioselective property of drug delivery system due to high accessibility of MIP particles. The drug permeability might be also improved because of the efficient packing of micro-/nanoparticles.

1.2. Stereochemistry

The study of the spatial arrangement of atoms and molecules is known as *stereochemistry*. One aspect of stereochemistry is *stereoisomerism*; isomers that have the same constitution but differ from each other only in the way that the atoms are oriented in three dimensional space are called stereoisomers (Atkins and Carey, 2002). The field of stereochemistry has been developing since the early 1800s when Jean-Baptists Biot, a French physicist, discovered the phenomenon of optical activity (the ability of a substance to rotate the plane of polarization of light). By the middle of the 18th century, Louis Pasteur first demonstrated the stereoisomeric forms of tartaric acid. Pasteur made the remarkable proposal that optical activity was caused by molecular asymmetry and that nonsuperimposable mirror-image structures resulted from that molecular asymmetry (Hyneck et al., 1990). By the end of the 18th century, Van't Hoff of Holland and Le Bel of France strengthened Pasteur's proposal by hypothesizing that the chiral nature of compounds was due to the fact that carbon constituents could have a non-

planar spatial arrangement giving rise to nonsuperimpossable mirror images (Drayer, 1988) as realized in Figure 1.1.

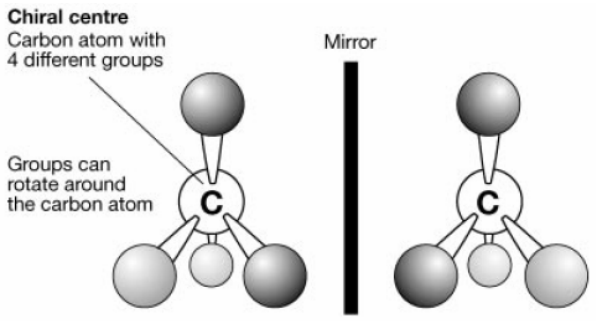

Figure 1.1. General depiction of a molecule with a chiral center and its enantiomers (Burke and Henderson, 2002).

Optical isomerism enables the existence of two nonsuperimposable mirror images or *enantiomers* (Greek *enantios*=opposite, *meros*=part) that share identical physicochemical properties but differ in their rotation of plane-polarized light. The two enantiomers can be identified according to the rotation direction of polarization of light. The symbols (+) or (*d*) are used to denote dextrorotatory (clockwise) and (-) or (*l*) to denote levorotatory (counterclockwise). The R/S system according to The Cahn-Ingold-Prelog (CIP) convention (Cahn et al., 1966) is currently recommended for specifying the two enantiomers based on attaching an order of priority to substituent ligands attached to the central chiral atom. A mixture of two enantiomers is called a *racemate* and has no optical activity. Optical isomers that are not enantiomers are called *diastereoisomers* or *diastereomers*. Unlike enantiomers, the physical and chemical properties of diastereomers can differ and consequently, their chemical characterization is easy and their biological activities are often different. This is the basis for derivatization of enantiomers to form diastereomers in chiral separation and also for the explanation of enantiomer activities with their chiral receptors in the body.

1.3. Importance of chirality in drug action

The body with its numerous homochiral compounds being amazingly chiral selector will interact with each enantiomer of racemic drug differently and metabolize each enantiomer by a separate pathway to generate different pharmacological activity. Thus one enantiomer may produce the desired therapeutic activities, while the other may be inactive or, in the worst cases, produce undesired or toxic effects (Nguyen et al., 2006). The reason for chiral recognition by drug receptors is a three-point interaction of the drug with the receptor site proposed by Easson and Stedman in 1933 (Easson and Stedman, 1933). The difference between two enantiomers of a drug with its receptor is illustrated in Figure 1.2 using a hypothetical interaction between a chiral drug and its chiral binding site. In this case, the active enantiomer has a three-dimensional structure that allows drug domain A to interact with binding site domain a, B to interact with b, and C to interact with c. In contrast, the inactive enantiomer cannot be aligned to bind the same three sites simultaneously. The difference in three-dimensional structure allows the active enantiomer to bind and have a biological effect, whereas the inactive enantiomer cannot.

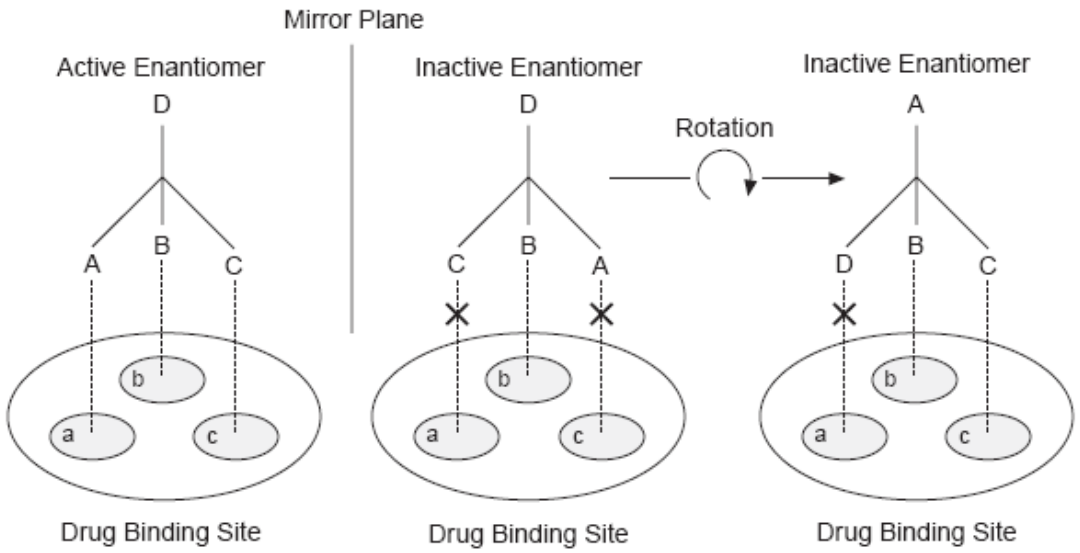

Figure 1.2. Easson-Stedman hypothetical interaction between the two enantiomers of a racemic drug with a receptor at the drug binding sites (McConalthy and Owens, 2003).

The tragic case of using chiral drugs as racemates occurred in the 1960's with sedative thalidomide. Its therapeutic activity resided exclusively in the *R*-enantiomer. It was discovered only after several hundred births of malformed infants that the *S*-enantiomer was teratogenic (Crossley, 1995). This had led to a greater awareness of the pitfalls inherent in the development of racemates. In May 1992, the US Food and Drug Administration (FDA) issued a policy statement for the development of new stereoisomeric drugs (this statement is available at the FDA web site at http://www.fda.gov/cder/guidance/stereo.htm), which served as an incentive to the current move to single enantiomer drugs.

1.4. Chiral separation

In recent years, there has been considerable interest in the biological activity of the enantiomers of chiral drugs. The potential benefits of using single enantiomer drugs could be (1) reduction of the total administered dose, (2) enhanced therapeutic window, (3) reduction of inter-subject variability, and (4) more precise estimation of dose-response relationships (Caner et al., 2004). Hence the achievement and identification of single enantiomer drugs has become one of the most important requirements in pharmaceutical, in order to ensure the desired activity in the administration of drugs.

There are two basic approaches to obtain the pure active enantiomers: asymmetric synthesis and separation. If the asymmetric synthesis approach is used, most or all of the inactive enantiomer would be converted into the desired enantiomers, thereby the yield of desired isomer would be maximized. However, this approach may require auxiliary chiral synthesis or asymmetric catalysis, and resolution involves separation methods or enantioselective catalysis, which may be direct or subtractive (Eikeren, 1997). At the early stages of development of new drugs, time constraints to have some amounts of pure enantiomers for the first pharmacological tests are usually crucial before a manufacture route (protocol) has to be selected. At these early stages, the development of an asymmetric synthesis would be both expensive and time consuming. Thus, the application of enantioseparation technique has become effective way and increasingly relevant on a preparative scale. The main groups of techniques for the separation

of enantiomers are schematized in Figure 1.3, considering their use at analytical or preparative scale. Chromatography methods such as capillary electrophoresis (CE), thin-layer chromatography (TLC) and particularly high-performance liquid chromatography (HPLC) have long been the methods of choice in enantioseparation and suited for enantioseparation analysis (Maier et al., 2001). HPLC can be used either indirectly with chiral derivatization reagents or directly with chiral stationary phase (CSP) or chiral mobile phase additives. Recently, CSPs produced from MIPs have been interested and extensively researching. The use of membrane technology for chiral separation has also been investigated and become one of interesting ways besides chromatography methods.

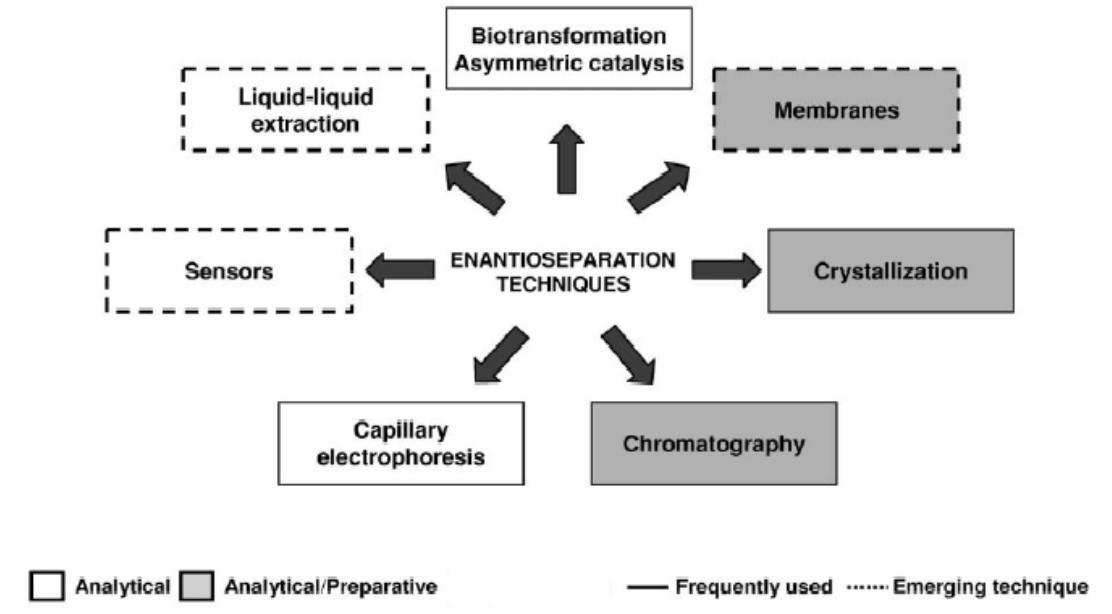

Figure 1.3. Techniques used for the separation of enantiomers (Maier et al., 2001).

Chiral separation with membranes is a promising way to obtain an enantiomerically pure molecule economically and continuously among several methods for optical resolution, such as diastereomer crystallization, chemically kinetic resolution, enzymatic kinetic resolution, and chromatography. Separation with membranes of racemic mixtures reported so far can be divided into two types of membrane systems: liquid membrane (Shinbo et al., 1993; Pickering and Chaudhuri, 1997; Maximini et al., 2006) and solid membrane (Maruyama et al., 1990; Higuchi et al., 2002; Kim et al., 2003). However, the development of liquid membrane may

be more limited, concerning the very poor stability due to the washing of membrane liquid or carrier (Newcomb et al., 1974; Bryjak et al., 1993; Keurentjes et al., 1996). Therefore, the solid membrane may be more applicable and can be prepared by several approaches such as chiral polymer (Thoelen et al., 2001; Kim et al., 2003), membrane immobilized chiral selector (Higuchi et al., 2002; Hadik et al., 2005) and molecularly imprinted technology (Yoshikawa et al., 1995; Ramamoorthy and Ulbricht, 2003).

1.5. Chiral stability

One major problem arising from the presence of elements of chirality is their possible lack of configurationally stability (Danel et al., 2006). As is well known, the optical activity of an optically active material changes with time (Cattani and Bassalo§, 1997). The sample, containing predominantly one stereoisomer, will become a mixture of equal amounts of each isomer. This relaxation process (racemization) is due to the interaction of the active molecule with the environment. The rate of racemization can vary with solvents (Yang and Lu, 1992) or conditions (Testa et al., 1993). Once obtaining the single enantiomer, the stability of such enantiomer to racemization process needs special attention to be understood properly and to determine whether this is going to occur during formulation or storage. Hence the well-controlled delivery system, which controls the release of an active enantiomer (eutomer) and retains the less active (or inactive) enantiomer (distomer) from the stable formulation of racemate drug, would be much more favorable.

1.6. Drug delivery systems

Delivery of a pharmaceutical agent to the systemic circulation, and consequently to the site of action to produce a desired pharmacological effect, is the ultimate goal of drug delivery (Han and Wang, 2005). The oral drug delivery is typically considered the preferred and most patient-convenient means of drug administration and prior selected for the research in drug

delivery. Transdermal drug delivery is also an important means for the research in drug delivery recently; it represents an attractive alternative to oral drug delivery. An understanding in drug delivery process may be useful for the design of drug delivery system. The drug delivery systems produced in this thesis may be able to further develop and use *via* conventional oral and transdermal routes.

1.6.1. Oral drug delivery

Oral administration of therapeutic agents represents by far the easiest and most convenient route of drug delivery, especially in the case of chronic therapies (Lavelle et al., 1995). While convenient from the patient's perspective, oral drug formulation presents a challenge to the chemist, who has to design delivery systems optimizing drug stability in the gastrointestinal (GI) tract, such that a desirable pharmacokinetic profile may be attained for a given drug (Daugherty and Mrsny, 1999).

Physicochemical characteristics of oral delivery

The human GI tract is a complex time-, position-, and patient-dependent absorptive, metabolizing, and excretive organ. Key physiological factors that control the absorption of drugs from the GI tract include gastric and intestinal transit profiles, fluid and food intake, build fluid and luminal pH, gastric and intestinal secretions, absorptive mechanisms, and enterocyte-based metabolism and secretion (efflux). Coupled with these physiological factors, the physicochemical properties of a drug, such as its solubility, ionization, stability, and lipophilicity, strongly influence the rate and extent of drug absorption from the GI lumen (Charman and Charman, 2003). Approximate fluid flux, pH, and residence times within the gastrointestinal tract are shown in Table 1.1. The interplay between GI physiology and drug delivery design (e.g., type of system, mechanism of release) is always a key determinant of the likely success of drug delivery system.

Table 1.1. Approximate fluid flux, pH, and residence times within the gastrointestinal tract (Charman and Charman, 2003).

Section	Fluid	Input/day (ml)	Output/day (ml)	pH[a]	Residence time (h)
Mouth	Water + saliva	1200 + 1500		1-3.5	0.5-12[a,b]
Stomach	Gastric fluid	2000[a]			
Duodenum	Pancreatic juice	1500		4-6.5	
Jejunum	Bile	500		5-7	3-4[c]
Ileum	Intestinal secretions	1500	⟶ 8500	6-8	
Colon	Fluid transfer	500	⟶ 350	6-8	~10[d]

[a] Varies depending on the postprandial state.

[b] Highly dependent on dosage form size.

[c] Relatively independent of dosage form size and postprandial state.

[d] not well defined.

***In vitro* evaluation of oral delivery system**

The majority of oral controlled release systems rely on dissolution, diffusion, or a combination of both mechanisms, to generate release of drug to the GI tract. Some consideration of the *in vitro* systems that can be used to assess drug release kinetics is necessary. Dissolution is now accepted as an *in vitro* standard for drug release from conventional dosage forms. The USP dissolution apparatus 1 (basket) and apparatus 2 (paddle) would be equally useful in this regard.

1.6.2. Transdermal drug delivery

Transdermal delivery is the term used to describe the application of a drug to the skin to treat systemic disease and is aimed to achieve systemically active levels of the drug (Flynn and Weiner, 1993). Transdermal drug delivery has many advantages that can overcome the deficiency of oral administration as follows: (1) avoidance of the first-pass elimination, (2) no

effects of complicated factors such as foods, digestive juices, gastrointestinal transit, and pH changes, (3) long-term and rate controlled administration using some devices, (4) arbitrary drug input and its interruption, and (5) increases in patient compliance (Ranade, 1991). An understanding of the nature, properties and functions of human skin is an essential preliminary to a design of drug delivery system and a study of the routes and mechanisms by which medicaments penetrate the skin barrier.

Skin structure and routes of drug penetration

Skin is one of the largest organs of the body, 15,000-20,000 cm^2 in area in most adults, varying in thickness from approximately 1.5 to 4 mm, and weighing approximately 2 kg. It consists of two parts: the cellular outermost layer, the epidermis, and the inner, relatively a cellular, connective tissue layer, the dermis (Figure 1.4). Lying between these two layers is a submicroscopic structure, the basal lamina or basement membrane zone, which serves as the anchoring structure by which the epidermis and dermis are held together. The blood supply to the skin resides exclusively in the dermis, and the nutritional needs of the epidermis are met entirely by diffusion. The epidermis is about 110 micrometers in thickness and is pierced by hair follicles and sebaceous glands; it is non-vascular. The outermost layer of the epidermis is called the *stratum corneum* or horny layer. It is composed of dense overlapping laminates of dead cells, each packed with keratin filaments in an amorphous matrix of proteins with lipids and water-soluble substances. The cells are polygonal when viewed perpendicularly and are arranged in layers about 15 cells deep. Lipid materials are mainly found in the intercellular region. Resistance to the diffusion of chemicals is greater in the stratum corneum than in the underlying living skin tissues. The stratum corneum is therefore recognized as the rate-limiting barrier to the ingress of materials and is the tissue predominantly responsible for the remarkable impenetrability of the skin. However, the layer is not an absolute barrier and trace amounts of penetrants can be detected. Other parts of skin that are important in transdermal drug delivery are the skin appendages, such as hair follicles, sebaceous glands, and eccrine sweat glands. These skin appendages are often considered as shunts through the stratum couneum that can facilitate the transdermal absorption of drugs. (Swarbrick and boylan, 1995).

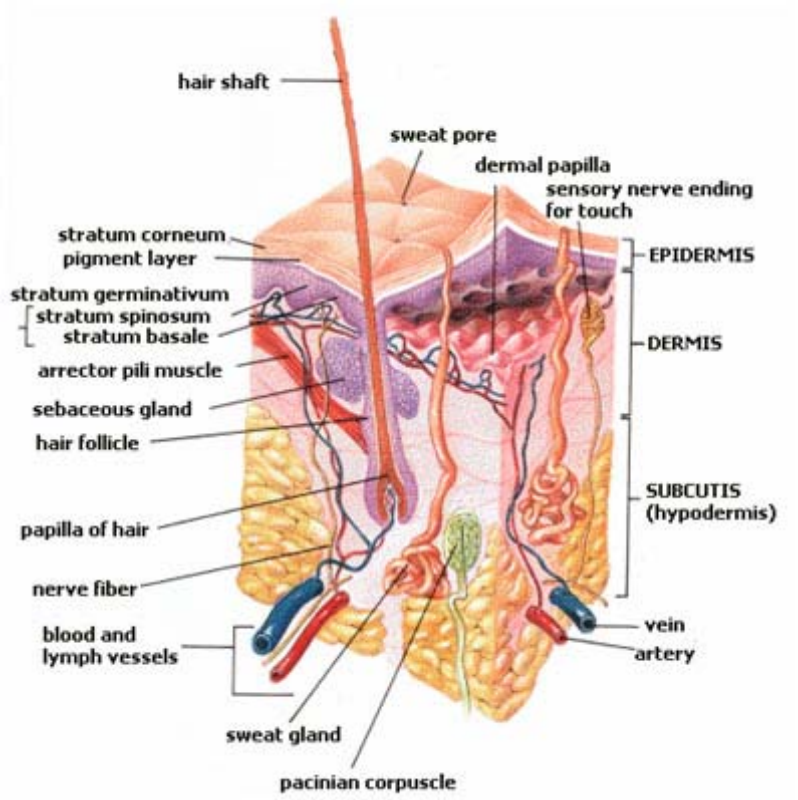

Figure 1.4. Cross-section of all skin (http://en.wikipedia.org/wiki/Epidermis_(skin).

A molecule may use two diffusional routes to penetrate normal intact skin: the skin appendages (sweat glands and hair follicles) or called *transappendageal*, or the intact epidermis or called *transepidermal*, as illustrated in Figure 1.5. There are two possible routes for the transepidermal absorption of drugs: between the cells of the stratum corneum and direct diffusion of the drug through the cells (Figure 1.5b). These two pathways are called the *intercellular* and *intracellular* routes. Hydrophilic drugs should partition preferentially into the intracellular domains, whereas lipophilic penetrants (log *P* octanol-water typically > 2) traverse the stratum corneum mainly *via* the intercellular route (Swarbrick and boylan, 1995).

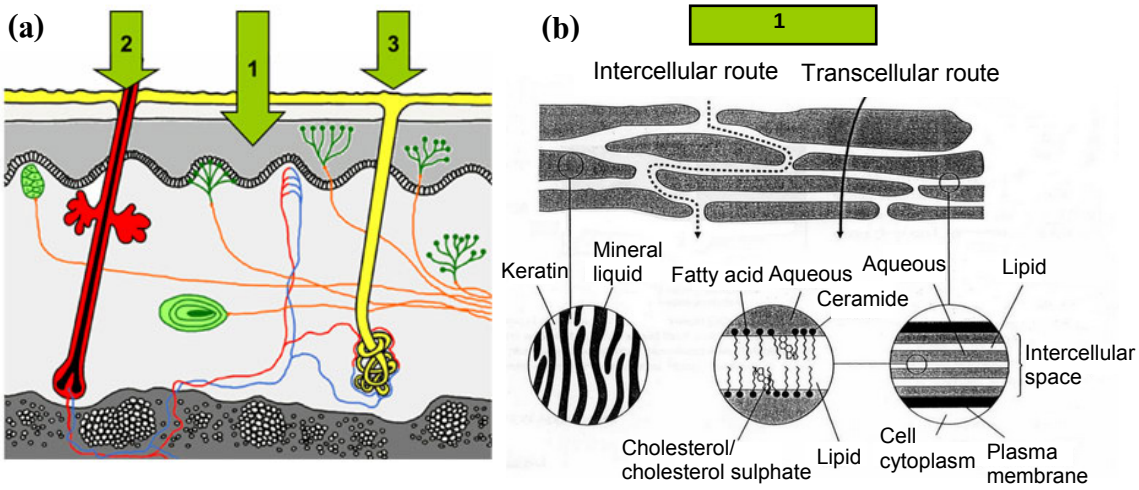

Figure 1.5. (a) Simplified structure of human skin, with potential routes for drug permeation indicated: (1) across the continuous skin, and *via* (2) the hair follicles, and (3) the sweat ducts; and (b) Schematic illustration of the stratum corneum and major transport routes of drugs across the stratum corneum (http://www.scf-online.com/german/43_d/absorption43_d.htm; Higaki et al., 2003).

Parameters important in transdermal delivery

The most basic diffusion equation is Fick's first law which describes steady state flux per unit area (J) in terms of the partition of the permeant between the skin and the applied formulation (K), its diffusion coefficient (D) in the intercellular channels of diffusional pathlength (h), the applied concentration of the permeant in the vehicle (c_{app}) and the concentration of the permeant in the receptor phase (c_{rec}):

$$J = KD\,(c_{app} - c_{rec})/h \qquad (1.1)$$

In most circumstances $c_{rec} << c_{app}$ and equation 1.1 is often simplified to

$$J = k_p c_{app} \qquad (1.2)$$

Where; k_p ($= KD/h$) is the permeability coefficient (Hadgraft, 2004).

In vitro evaluation of transdermal delivery system

The aim of *in vitro* experimentation in transdermal delivery is to understand and/or predict the delivery and penetration of molecule from the skin surface into the body *via* the skin of a living animal (Gummer, 1989). There is a wide variety of diffusion cells designed for *in vitro* measurement of skin permeation. These cells have generally been designed in one of two ways: side-by-side (bi-chambers) and vertical *in vivo* mimic diffusion cells. A primary goal of *in vitro* permeation studies is the prediction of skin permeation *in vivo*. In this regard, side-by-side diffusion cells are useful in delineating mechanisms of permeation under controlled conditions, but are of more limited usefulness in predicting skin permeation *in vivo*. Vertical cells are more versatile because a wide variety of experimental conditions can be used to gain information useful in the evaluation of formulations ultimately destined for clinical use (Friend, 1992). Normally, the *in vitro* evaluation is performed by using animal skin models. A practical reason for the use of animal skin models is the availability of animals or isolated animal skin (compared to the availability of isolated human skin). Many animal skin models have been described in the literatures and it is suggested that the barrier properties of pig skin most closely resemble those of human skin (Haigh and Smith, 1994; Schmook et al., 2001). However, it is evident from the reported literature that no single animal or synthetic model can mimic percutaneous absorption in man for the diverse range of chemicals which are investigated for clinical and toxicological effects. Researchers have for many years used skin excised from rodents. Laboratory rodents are a convenient source of animal skin for research purposes because theses animals are fairly easily handled and are relatively inexpensive when compared with larger species. The rat has been used extensively in the study of transdermal drug absorption. Excised rat skin has generally been considered more permeable than human or pig skin, however, in the diffusion of certain compounds rat skin appears to be as good as pig skin in modeling absorption through human tissue (Haigh and Smith, 1994).

1.7. Stereoselective-controlled drug delivery system

For controlled drug delivery, it denotes to system which can provide some control, whether this be of a temporal or spatial nature, or both, of drug release in the body. The design of formulation may offer an advantage in the therapeutic situation especially for chiral drug. Avgerinos et al. (1991) have investigated the enantiomeric composition of ibuprofen in plasma following the oral administration of the racemic drug in a novel controlled release formulation compared to conventional tablet formulation. The results were suggested that drug release from the controlled release preparation was suitably modified and the fluctuation between the peaks and troughs of *S/R* ratio was lower than in conventional tablet formulation.

The addition of excipients can play an important role in the characteristics of the finished product. For example, material can be added to promote stability or solubility of the drug and subsequently enhance release from the matrix. Some materials can be used to develop enantioselective-controlled release system. Several studies have proved that there exists the possibility of chiral discrimination in the release of chiral drugs from systems providing a chiral environment especially containing cellulose derivatives and cyclodextrin. Solinís et al. (2002) studied the release of salbutamol and ketoprofen enantiomers from hydroxypropylmethylcellulose (HPMC) K100M matrices. The authors concluded that stereoselectivity was dependent on the amount of chiral excipient in the formulation. Other dosage forms, such as propranolol in HPMC matrices (Duddu et al., 1993), ketoprofen or ricobendazole in matrix tablets with HPMC (Alvarez et al., 1999), and verapamil in matrix tablets containing pectin, galactomannan, or scleroglucan (Maggi et al., 1996) also showed stereoselective release of the enantiomers. Srichana and Suedee (2001) examined the *in vitro* dissolution of salbutamol from matrix tablets containing various chiral excipients such as γ-cyclodextrin, heptakis (2, 6-di-O-methyl)-β-cyclodextrin, sulfobutyl-β-cyclodextrin, HPMC and egg albumin. The formulation containing γ-cyclodextrin provided significant stereoselectivity throughout the dissolution profile, which the release of eutomer *R*-salbutamol was higher than that of the distomer *S*-salbutamol from the γ-cyclodextrin tablets. Moreover, MIPs could be considered to use as chiral excipient potential in enantioselective-controlled delivery of chiral drugs (see Section 1.8.5).

1.8. Molecular imprinting

The molecular imprinting method is quite simple and easy to perform in a tailor-made fashion. It allows the creation of artificial recognition sites in synthetic polymers (Wulff, 1993). The history of molecular imprinting is usually traced back to the experiments of Dickey in the 1940s and 1950s who was inspired to create affinity for dye molecules in silica gel (Mayes and Whitchombe, 2005). Dickey's silicas can be considered to be the first imprinted materials. Molecular imprinting in synthetic polymers was reported for the first time in 1972 by Wulff and Sahan (Wulff and Sahan, 1972). They used what is now termed a covalent approach to prepare an organic molecularly imprinted polymer capable of discriminating between the enantiomers of glyceric acid. The second major break through in organic polymer imprinting occurred in 1981 when Mosbach and Arshady reported that they had prepared an organic MIP using non-covalent interactions only (Arshady and Mosbach, 1981). So, it can be said that the initial idea was to obtain in the polymer highly specific binding clefts with a predetermined size, shape and three-dimensional arrangement of functional groups. Later, further experiments demonstrated that such functionalized cavities could be tailored to mimic the active sites of enzymes (enzyme analogue built polymer).

In common principle, the molecular imprinting procedure is generally based on the linkage of suitable monomers containing functional groups (binding site monomers) to template molecules by covalent (later also non-covalent) interactions. Subsequent copolymerization of the resulting template monomer assembly with an excess of a cross-linking agent in the presence of a porogen produces rigid macroporous polymers. Removal of the template molecules (see Figure 1.6) leaves behind cavities in the polymer whose size, shape and three-dimensional arrangement of binding sites are determined by the structure of the template molecules. If one of the enantiomers of a racemic compound is used as the template, the resulting polymer might be able to discriminate between the two enantiomers.

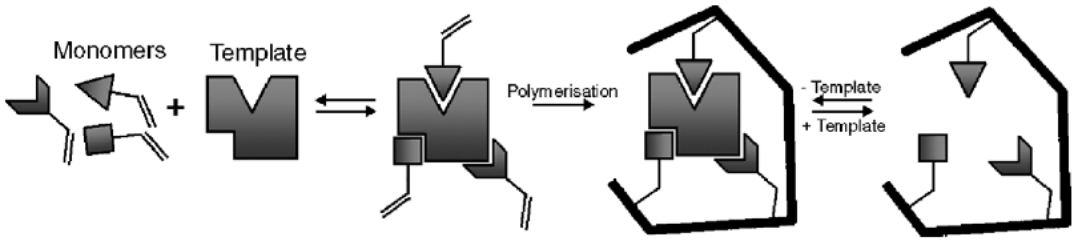

Figure 1.6. Schematic generalization of the molecular imprinting process (Sellergren and Allender, 2005).

1.8.1. MIP syntheses

In molecular imprinting processes, several components are involved, e.g., template, functional monomer, cross-linker, solvent and initiator. Their nature and properties can affect the obtained MIP behavior. The *template* (the blueprint on which a receptor is based) is of central importance in that it directs the organization of the functional groups pendent to the functional monomers. It should ideally be chemically inert under the polymerization conditions. The *functional monomer* is the building block responsible for the introduction of functionality into the polymer matrix, complementary to the functionality present in the template molecule. It is clearly very important to match the functionality of the template with the functionality of the functional monomer in a complementary fashion (e.g., hydrogen-bond donor with hydrogen-bond acceptor) in order to maximize complex formation and thus the imprinting effect. The *cross-linker* is the component in excess in most polymerization protocols. In an imprinted polymer the cross-linker fulfils three major functions: (1) the cross-linker is important in controlling the morphology of the polymer matrix, (2) it serves to stabilize the imprinted binding site, and (3) it imparts mechanical stability to the polymer matrix. High cross-link ratios are generally preferred in order to access permanently porous materials and in order to be able to generate materials with adequate mechanical stability. Polymers with cross-link ratios in excess of 80% are often the use. The presence of *solvent (porogen)* in traditional imprinting protocol is necessary, not only to dissolve the agents for polymerization, but also to provide porous structures to imprinted polymers, accessible for both the removal of the template as well as the rebinding of the analytes of interest. Choice of solvents is dependent on the kind of imprinting. In covalent imprinting,

many kinds of solvents are employable as long as they satisfactorily dissolve all the components. In non-covalent imprinting, the choice of solvent is more critical to the promotion of the formation of non-covalent adducts between the functional monomer and the template and thus to enhancement of the imprinting efficiency. Chloroform is one of the most widely used solvents, since it satisfactorily dissolves many monomers and templates and hardly suppresses hydrogen bonding. Finally, since most molecular imprinting protocols are based on free-radical polymerizations, a free-radical *initiator* is added, selected based upon the choice of thermal or photochemical polymerization. The azo-initiator azobis-(isobutyronitrile) (AIBN) is typically used. It can be conveniently decomposed by thermal or photolysis (Komiyama et al., 2003; Cormack and Elorza, 2004).

1.8.2. Approaches to molecular imprinting

MIPs have been prepared mainly by two approaches: covalent binding of the template to the functional monomer(s) and non-covalent binding (self-assembly) of the template and the functional monomer(s). Both have advantages and disadvantages, and thus the choice of the best method strongly depends on various factors. The covalent approach was developed by Wulff and Sahan (1972). Prior to polymerization, functional monomer and template are bound to each other by covalent linkage. Then, this covalent conjugate is polymerized under the conditions where the covalent linkage is intact. After the polymerization, the covalent linkage is cleaved and the template is removed from the polymer. Upon the guest binding by the imprinted polymers, the same covalent linkage is formed. The non-covalent approach, the more popular of the two due to its simplicity and multitude of combinations, was developed by Arshady and Mosbach (1981). In order to connect a functional monomer with a template, non-covalent interactions (e.g., hydrogen bonding, electrostatic interaction, and coordination-bond formation) are used. Thus, the adducts can be obtained *in situ* simply by adding the components to reaction mixtures. After the polymerization, the template is removed by extracting the polymer with appropriate solvents. The guest binding by the polymer occurs through the corresponding non-covalent interactions. It is generally accepted that there are pros and cons to both approaches. Some advantages and disadvantages of covalent and non-covalent imprinting are described in Table 1.2. In 1995,

Whitcombe et al. reported an intermediate approach that appeared to combine the advantages of both approaches (Whitcombe et al., 1995). This approach relies on covalent interaction during the polymerization stage but non-covalent interactions during rebinding. Importantly, in order to improve subsequent non-covalent binding geometry, Whitcombe's approach incorporated a sacrificial spacer group that was designed to be lost during template removal.

Table 1.2. Advantages and disadvantages of covalent and non-covalent imprinting (Komiyama et al., 2003).

	Covalent	Non-covalent
Synthesis of monomer-template conjugate	necessary	unnecessary
Polymerization conditions	rather free	restricted
Removal of template after polymerization	difficult	easy
Guest-binding and guest-release	slow	fast
Structure of guest-binding site	clearer	less clear

Covalent imprinting

Advantages:

1. Monomer-template conjugates are stable and stoichiometric, and thus the molecular imprinting processes (as well as the structure of guest-binding sites in the polymer) are relatively clear.
2. A wide variety of polymerization conditions (e.g., high temperature, high or low pH, and highly polar solvent) can be employed, since the conjugates are formed by covalent linkages and are sufficiently stable.

Disadvantages:

1. Synthesis of the monomer-template conjugate is often troublesome and less economical.
2. The number of reversible covalent linkages available is limited.
3. The imprinting effect is in some case diminished in the step of cleavage of covalent linkages, which requires rather severe conditions.
4. Guest binding and guest release are slow, since they involve the formation and breakdown of a covalent linkage.

Non-covalent imprinting

Advantages:

1. Synthesis of covalent monomer-template conjugates is unnecessary.

2. Template is easily removed from the polymer under very mild conditions, since it is only weakly bound by non-covalent interactions.

3. Guest binding and guest release, which take advantage of non-covalent interactions, are fast.

Disadvantages:

1. The imprinting process is less clear (monomer-template adduct is labile and not strictly stoichiometric).
2. The polymerization conditions must be carefully chosen to maximize the formation of non-covalent adduct in the mixtures.
3. The functional monomers existing in large excess (in order to displace the equilibrium for adduct-formation) often provide nonspecific binding sites, diminishing the binding selectivity.

1.8.3. MIP formats

The format in which the polymer is obtained is very important and will determine to a great extent the application for which the MIP will be suitable. Some applications require specific morphologies and properties, such as micron size beads for efficient packing into chromatographic columns or solid phase extraction (SPE) cartridges. Here, different procedures for producing MIPs in defined formats are described.

Bulk polymerization

The first polymerization method employed to synthesize MIP was based on bulk polymerization (Wulff, 1995; Mosbach and Ramson, 1996). This method is by far the most widely used by groups working on imprinting because of its simplicity and universality. After polymerization, it results in a brittle monolithic polymer network. The monolith is subsequently ground in order to expose a larger surface area which is molecularly imprinted. However, the ground particles tend to have extremely broad size and shape distributions. Sieving of the

particles typically yields approximately 20% of the original bulk polymer in particles of useful size (Brueggemann et al., 2000). The shape of individual particles however remains intrinsically irregular. This method is not only inefficient but often is difficult to control, which have restricted their functionality in certain applications.

Surface imprinting

The development of bead polymerization techniques serves a twofold objective. First it addresses the technical issues related to the conventional monolith procedure to produce MIPs, e.g., low yields of useful particles, irregular particle sizes, time-consuming crushing-sieving techniques. Secondly, packed beds of monodisperse spherical particles will exhibit less band broadening effects (in chromatography) than corresponding beds of irregular particles. If the particles are sufficiently small, the binding kinetics can also be expected to strongly improve since the binding sites are promoted on highly surface area of MIP particles. Recently, suspension polymerization, precipitation polymerization, two-step polymerization and core-shell particles appear very promising in this regard. *Suspension polymerization* in fluorocarbon solvent was first described by Mayes and Mosbach (1996). It is a fast and reliable methodology that synthesizes particles by UV irradiation in less than 2 h (or as little as 10-15 min for easily-polymerizing monomers). Perfluorocarbon solvent (perfluoro(methylcyclohexane); PMC) was employed as the continuous phase, and this allows the establishment of the same interactions that occur in bulk polymers (each particle acts like a mini-bulk reactor). The beads obtained have a diameter that can vary between 5 and 50 μm depending on the stirring speed and the amount of surfactant. The fluorocarbon suspending medium can be easily recycled by distillation. *Precipitation polymerization* is another method that can provide particles in the submicron scale (0.3-10 μm). It is based on the precipitation of the polymeric chains out of the solvent in the form of particles as they grow more and more insoluble in an organic continuous medium. In this case, particles are prevented from coalescence by the rigidity obtained from the cross-linking of the polymer, so there is no need of any extra stabilizer (Wang et al., 2003). *Two-step polymerization* was developed with MIP by Hosaya and co-workers in 1994 (Hosoya et al., 1994). It requires several swelling steps on the initial proceeds. In this case, the continuous phase of the polymerization

medium is water. This method produces monodisperse particles in the micron size range (2-50 μm) with good control of the final size and number of the particles. *Core-shell particles* are obtained by emulsion polymerization (Pérez et al., 2001). They have a structured morphology that allows the incorporation of any added property into the core of the particle without interfering with the imprinted shell. The continuous medium during polymerization is water. Particles obtained by this method are monodisperse and can be produced in a colloidal size range of 0.05-2 μm.

1.8.4. Molecularly imprinted membrane (MIM)

The main advantages of membrane technology are related to the unique separation principle, i.e., the transport selectivity of the membrane. The separations with membranes do not require additives, and they can be performed isothermally and at very competitive energy consumption. Both up-scaling and downscaling of membrane processes is easy. A high membrane performance depends on well-defined membrane morphology with respect to pore structure and layer topology (Ulbricht, 2004). MIP technology can compose with membrane technology to improve membrane selectivity and mostly used for separation or sensor applications. MIM can be prepared by either simultaneous formation of MIP structure and membrane morphology (self-supported MIM) or composing of MIP with support membrane (MIP composite membrane). *Self-supported flat-sheet membranes* could be synthesized by using two main routes: the traditional *in situ* crosslinking polymerization and the polymer solution phase inversion, both in the presence of templates. Piletsky et al. (1990) could prepare MIM by *in situ* crosslinking polymerization of acrylate monomer forming a film in the presence of adenosine monophosphate (AMP), in diffusion experiments possess selective permeability for this nucleotide. However, MIM obtained by this method normally have a poor mechanical stability. Phase inversion (PI), the main approach towards technical polymeric membranes, can be applied for molecular imprinting, i.e., the solidification of a polymer is used instead of an *in situ* polymerization. Yoshikawa et al. (1995) have used polystyrene resins with peptide recognition groups, in a blend with a matrix polymer, for MIM formation *via* a casting/solvent evaporation process (dry PI process). The permeability was much higher for the MIM as compared with the

blank membranes. Kobayashi et al. (1998) reported the preparation of selective membranes by using functional acrylate copolymers, prepared by a casting/immersion precipitation phase inversion method (wet PI process). This yielded asymmetric porous MIM. Recently, the polymer selection for wet PI imprinting has been extended to most of the commonly used membrane materials, e.g., cellulose acetate (Yoshikawa et al., 1999), polyamide (Reddy et al., 1999), polyacrylonitrile and polysulfone (Reddy et al., 2002). For *MIP composite membrane*, it may be prepared in the form of pore filling MIP, thin layer MIP or MIP particles composing membrane. In pore filling MIP composite membranes, MIP synthesis mixtures, e.g., methacrylic acid (MAA)/ethylene glycol dimethacrylate (EDMA), have been polymerized in mm-thick glass filters to fill their pores (Piletsky et al., 1998). Also, reaction mixtures have been cast into the pores of a symmetric microfiltration membrane and a cross-linking copolymerization of a functional polyacrylate has been performed (Dzgoev and Haupt, 1999). For thin layer MIP composite membrane, it could be obtained by grafting MIP layer on the surface of the already flux optimized microfiltration membranes, had been shown to be a feasible novel approach. The obtained membrane showed highly sorption capability (Sergeyeva et al., 2001). The highly affinity thin layer composite membrane could be also prepared by deposition/coating MIP layers on support membrane *via* photoinitiated copolymerization (Kochkodan et al., 2002). However, using grafting method would be more beneficial because it contributes to the stability between MIP layer and support membrane which chemical interaction involved. The selective MIP membranes prepared by grafting MIP layer onto supporting membranes have been extensively studied by Yoshimi et al. (2001). They prepared thin nanometer-ordered layer of theophylline-imprinted copolymer of EDMA and MAA grafted onto indium-tin oxide (ITO) electrode or cellulosic dialysis membrane (Hottori et al., 2004) to obtained high selective permeability membranes. For MIP particles composite membrane, several attempts have been reported yet and these include: coating MIP particles onto the surface of membrane disc (Ciardelli et al., 2006), encapsulation of MIP nanoparticles between two membrane layers (Lehmann et al., 2002) and encapsulation of MIP nanoparticles into a composite nanofiber membrane by electrospinning (Chronakis et al., 2006). MIP particles could be integrated with polymers to form composite membranes but commonly permeability and binding site accessibility can be low due to the close packing of the particles. In addition MIP particles with a very large size are not suitable for obtaining a rapid separation of

the imprinted substance from related compounds as such particles allow only low mass transfer. In contrasts, the generation and use of a monodisperse MIP in a composite membrane provides a promising approach for obtaining a reproducible flow distribution through the matrix (Ulbricht, 2004). The adoption of micro-/nanoparticles for molecular imprinting gives rise to a high statistical probability of easily accessible binding sites on the outer shell of the particle. Due to their high surface to volume ratio, they are good building blocks to obtain imprinted materials. Despite the synthetic methods for MIP micro-/nanoparticles being straightforward in principal, the final particle size of the generated specific MIPs has often proved difficult to control. Hence the production of the MIP particles and their integration or association with membranes to form a membrane or composite membrane such that the final membrane has a high selectivity (due to the availability of a large number of recognition sites) but with good permeability often proves challenging.

As a consequence of the binding selectivity of the template *versus* other species, two main categories of MIM function with respect to membrane transport selectivity can be distinguished: retardation or facilitation for the selected species (see Figure 1.7). As consequence of a binding selectivity obtained by imprinting for a substance A: (a) transport of A is facilitated *via* binding/desorption to MIP sites, while the nonspecific transport of another substance B by diffusion is hindered by the micropore structure of the membrane ("fixed carrier" membrane); (b) transport of A is retarded either by binding or binding/desorption to MIP sites on the surface of trans-membrane pores, while another substance B which has no specific interactions with the membrane surface will be transported by diffusion or convection (membrane adsorber).

Figure 1.7. Separation mechanisms for MIM as consequence of a binding selectivity obtained by imprinting for a substance A: (a) facilitated transport and (b) retarded transport (Ulbricht, 2006).

For MIM function, it is critically important to control both MIP specificity and membrane pore structure. With exclusively microporous MIM, template binding to imprinted sites can either change the pore network thus altering membrane permeability in general (gate effect) or the permeation rate is controlled by the interaction with the micropore walls. In MIM with larger trans-membrane pores, nonselective transport by diffusion or convection can only be compensated by binding to accessible imprinted sites, causing a retardation which can be used in membrane adsorbers (Ulbricht, 2006).

1.8.5. Application of MIPs in drug delivery

MIPs can be programmed to recognize a large variety of target structures with antibody-like affinities and selectivities. These properties, in addition to the robustness and ease of preparation of these artificial receptors, have made them extremely attractive for problem solving in the areas of preparative chemical separation, solid phase extraction, catalysis and sensing (Figure 1.8). In addition, MIPs are now receiving considerable attention for drug delivery applications. In this subject the application of MIPs in drug delivery and controlled release systems will be highlighted.

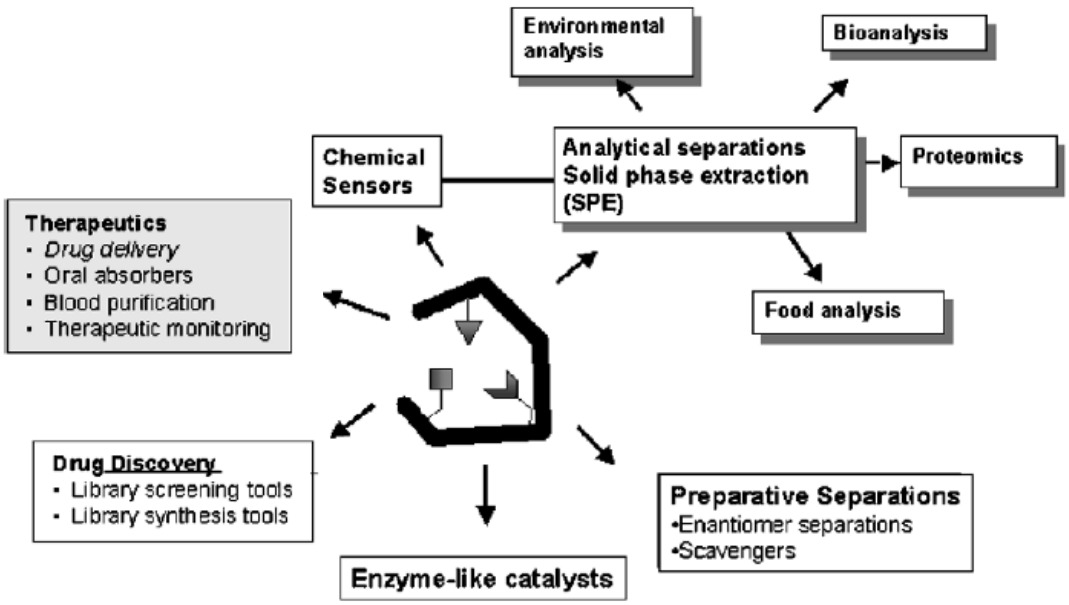

Figure 1.8. The main application envisaged for MIPs (Sellergren and Allender, 2005).

Drug delivery systems are required whenever an administered therapeutic agent needs to be protected against metabolic attack, or when there are absorption barriers or dosage limitations. The ideal delivery vehicle will ensure that the drug is released at the right site, in the right dose and for the required time (Cunliffe et al., 2005). MIPs have been proposed as base excipients for controlled release devices of drug. The first reports of imprinted polymer that afforded a sustained release mechanism were by Norell et al. (1998). Polymers imprinted with theophylline (drug with a narrow therapeutic index) used in the treatment of asthma, were evaluated for controlled release in an aqueous buffer. The release kinetics of theophylline in phosphate buffer pH 7 from polymers loaded with theophylline found that at the lowest theophylline loading displayed the slowest release characteristics and the release of drug from reference (non-imprinted) systems showed slightly faster. Later, Allender et al. (2000) has used MIPs as sustaining release excipients of transdermal drug delivery system for a β-blocker, propranolol. They embedded polymer imprinted with propranolol in a hydrophobic skin adhesive that was permeable to propranolol but did not allow water to permeate into the drug delivery device. As with the propranolol imprinted polymers, the device with the lowest loading of propranolol displayed the slower release profile again illustrating the heterogeneity of binding sites that can be obtained in non-covalent imprinted polymers. One promising example of using MIP to control the release of drug from the system as a response to a change in the conditions of the environment is the development of soft contact lens, which could be used directly as a drug delivery device on the surface of the eye (Hiratani and Alvarez-Lorenzo, 2002). Hiratani and Alvarez-Lorenzo synthesized the MIPs as hydrogels based on the use of hydrophilic monomer 2-hydroxyethyl methacrylate (HEMA) copolymerized with MAA, methyl methacrylate (MMA), *N,N*-dimethylacrylamide (DMAA), *N,N*-diethylacrylamide (DEAA), 1-(tristrimethylsiloxysilylpropyl) methacrylate (SiMA), and cross-linking with EDMA, imprinted with the β-blocker *S*-timolol, which can be used for the treatment of glaucoma. The uptake of timolol by imprinted and non-imprinted polymer at different pHs (1.5-10) was investigated and shown that timolol uptake was different in different pHs that relate to the swelling of device and the deprotonation of timolol. The imprinted soft contact lenses are an illustration of the potential utility of imprinted hydrogels as drug delivery devices.

MIPs are also promising to be capable of differentiating between the enantiomers of a racemic mixture. The goal of enantioselective-controlled delivery system is to administer a racemic drug and then the desired enantiomer is allowed to release from the system. Suedee et al. (2000; 2002a) studied enantioselective controlled release of propranolol by using MIP as chiral excipient in the system. The influence of the method of polymer synthesis, drug to polymer ratio, pH, and temperature on the release of two enantiomers was determined. The study revealed that release of eutomer can be controlled *via* means of formulation and the distomer was retained in the dosage form. Furthermore, the enantioselective controlled release by incorporating MIPs in the drug delivery system of NSAIDs was examined (Suedee et al., 2002b). Recently, Bodhibukkana et al. (2006) have prepared the enantioselective-controlled delivery system of propranolol as selective membrane intended to use in transdermal application. The system prepared by the *S*-propranolol imprinted polymer (MAA/EDMA) was grafted with bacterially-derived cellulose membrane showed very promising of the release of template *S*-propranolol higher than non-template *R*-propranolol. This selective membrane was further studied *in vivo* in rat and showed the efficient enantioselective release of eutomer *S*-propranolol than the respective enantiomer (Suedee et al., 2008).

1.9. Bacterial cellulose membrane

Cellulose is a polysaccharide made of many β-glucose monomers that is primarily used in nature for supplying structure to cells. Cellulose is the main component in cell walls of plants, algae, and fungi, making it the most abundant source of terrestrial biomass in the world today. There are four different pathways to form the biopolymer cellulose: (1) industrial isolation of cellulose from plants, (2) biosynthesis of cellulose by different types of microorganisms, (3) enzymatic synthesis, and (4) chemosynthesis (Klemm et al., 2001). The bacteria most known for their cellulose producing abilities are found in the genus *Acetobacter*, and of these is *Acetobacter xylinum*, a gram negative aerobic bacterium. Microorganisms of the genus *Acetobacter* usually found on fruits, vegetables, in vinegar, fruit juices, and alcoholic beverages. The production of cellulose by this microorganism was first reported by Brown in

1886 (Brown, 1886). The cellulose synthesized by *A. xylinum* is identical to that made by plants in respect to molecular structure, a linear β-1,4-linked glucose polymer (see structure in Figure 1.9), but the degree of polymerization differs from about 13000 to 14000 for plant and 2000-6000 for bacterial cellulose (Jonas and Farah, 1998). Figure 1.10 shows morphology of cellulose obtained from plant compared to from bacteria. Bacterial cellulose was found to be superior on many accounts as compared to the plant one. It is free of lignin, pectin, and hemicellulose as well as other biogenic product, which are associated with plant cellulose. Additionally, bacterial cellulose differs from plant cellulose with respect to its high crystallinity, high water absorption capacity, and mechanical strength in the wet state, ultra-fine network structure, mouldability *in situ*, and availability in an initial wet state (Ross et al., 1991; Jonas and Farah, 1998).

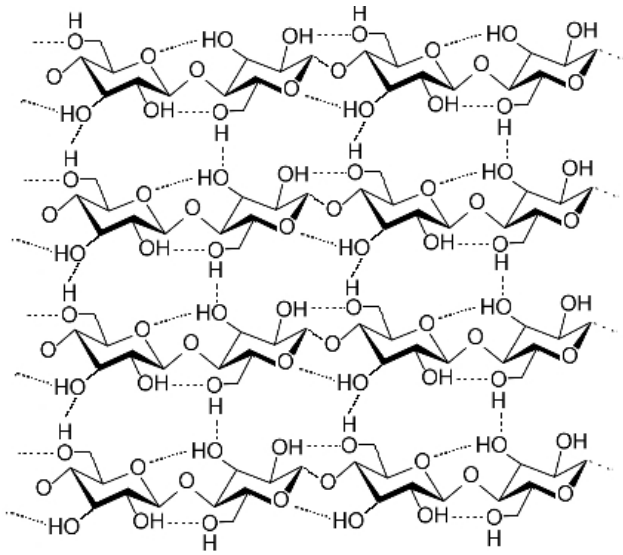

Figure 1.9. A strand of cellulose showing the hydrogen bonds (dashed) within and between cellulose molecules (http://en.wikipedia.org/wiki/cellulose).

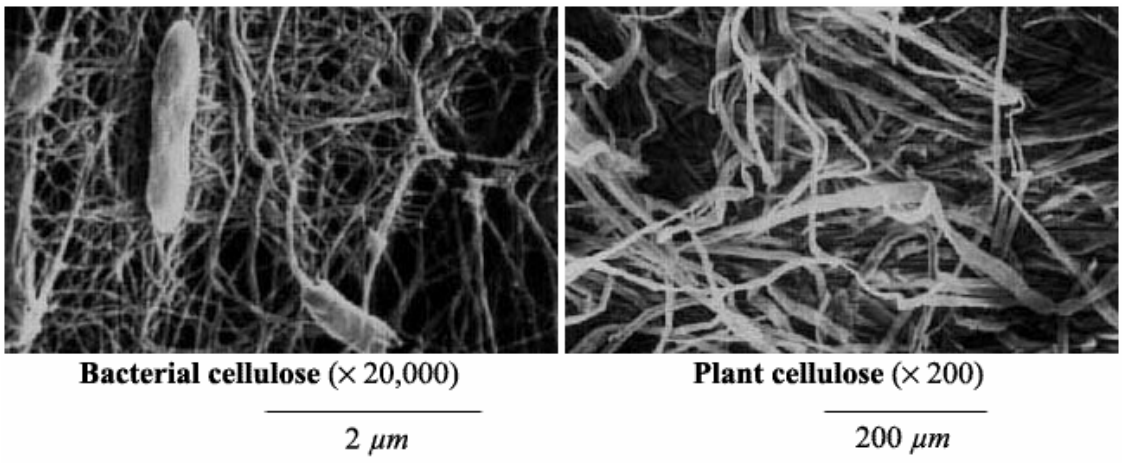

Figure 1.10. Cellulose morphology from bacteria (left) and plant (right) (http://www.res.titech.ac.jp/~junkan/english/cellulose).

Due to its high purity and unusual physicochemical properties bacterial cellulose offers a wide range of special applications e.g., as a food matrix (nata de coco), as dietary fiber, as acoustic or filter membrane, as ultra-strength paper and as a reticulated fine fiber network with coating, binding, thickening and suspending characteristics (Jonas and Farah, 1998; Klemm et al., 2001). Up to now several applications of bacterial cellulose in human and veterinary medicine are known. The high mechanical strength in the wet state, substantial permeability for liquids and gases, and low irritation of skin indicated that the gelatinous membrane of bacterial cellulose was usable as an artificial skin for temporary covering of wounds. Biofill® and Gengiflex® are products of bacterial cellulose with wide applications in surgery and dental implants and realities in the human health-care sector (Jonas and Farah, 1998). The unique properties of the bacterial cellulose have inspired to use it in this thesis as the supporting material in enantioseparation and drug delivery systems for chiral drugs.

1.10. Drugs of interest in this thesis

1.10.1. Non-steroidal anti-inflammatory drugs (NSAIDs)

The non-steroidal anti-inflammatory agents (NSAIDs) mainly affect the enzyme cyclooxygenase (COX) by inhibition of the transformation of the naturally occurring fatty acid arachidonic acid into prostaglandins and leukotrienes and other eicosanoids used for the treatment of inflammation, rheumatoid arthritis, headache and minor pain. The largest group of NSAIDs is the α-arylpropionic acids (profens) such as ibuprofen ($C_{13}H_{18}O_2$, MW 206.28), ketoprofen ($C_{16}H_{14}O_3$, MW 254.29) and naproxen ($C_{14}H_{14}O_3$, MW 230.26) (structures are shown in Figure 1.11). These drugs are all chiral molecules and *S*-enantiomer is responsible for the desired therapeutic effect. The *S*-enantiomer of ibuprofen and naproxen is more active than *R*-enantiomer about 165 and 30 times, respectively (Adams, 1976). Moreover, the inactive *R*-enantiomer undergoes a unidirectional metabolic inversion of configuration to afford the active *S*-enantiomer (Sheldon, 1993). The mechanism of metabolic inversion of ibuprofen and related profen drugs is established in Figure 1.12. The enantiospecificity of the inversion is controlled by the enzyme, acylcoenzyme-A synthetase, that converts *R*-ibuprofen to the corresponding coenzyme-A thioester. Racemization of the latter and subsequent hydrolysis yields *S*-ibuprofen. In competition with the hydrolysis, the thioester intermediate can also undergo acyl exchange with the endogenous triacylglycerols. This results in accumulation of ibuprofen residues in fatty tissue. Since the *S*-enantiomer does not form the coenzyme-A thioester, it cannot be incorporated into fatty tissue (Sheldon, 1993). *R*-ibuprofen is inverted to *S*-ibuprofen *in vivo* to extent of 57-69% (Lee et al., 1985; Cheng et al., 1994). The long term effects of accumulation of ibuprofen residues in fatty tissue are unknown but toxic side-effects cannot be completely ruled out. The risk of side-effects can, in any case, be avoided by administering the pure *S*-enantiomer (Sheldon, 1993).

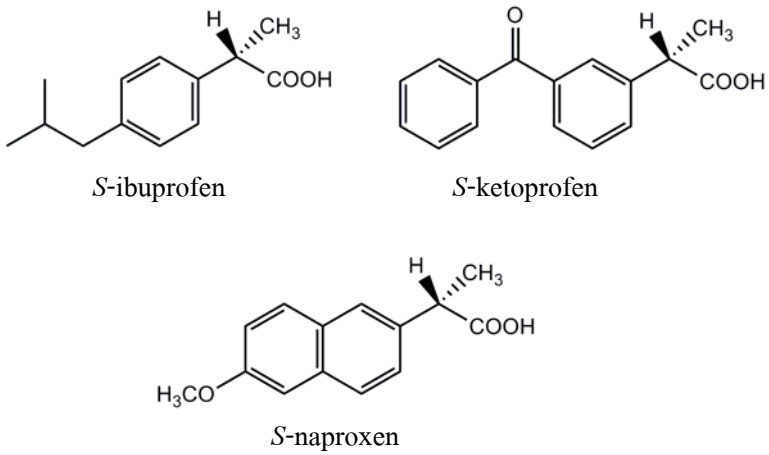

Figure 1.11. Structure of *S*-enantiomer of α-arylpropionic acid non-steroidal anti-inflammatory drugs.

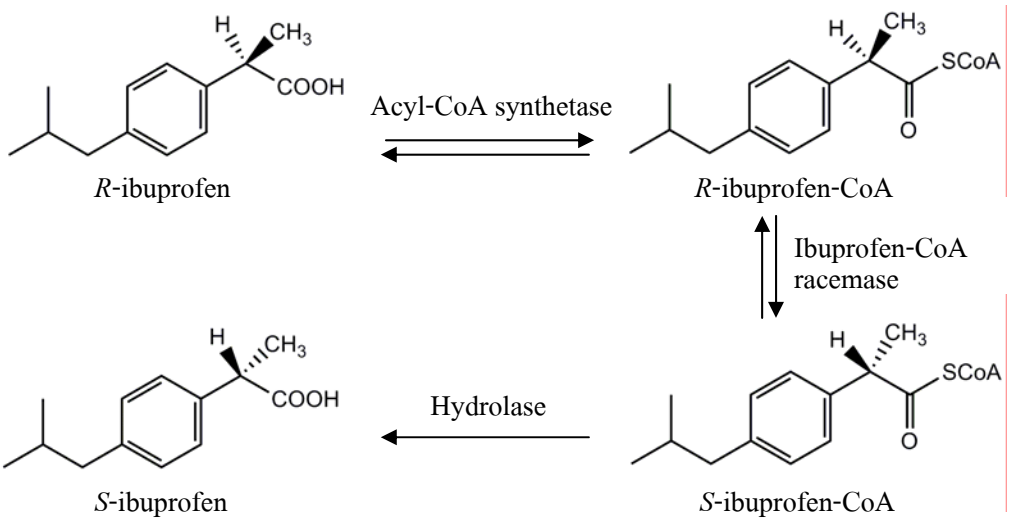

Figure 1.12. Mechanism of metabolic inversion of ibuprofen and related anti-inflammatory drugs (Sheldon, 1993).

It is commonly considered that molecule containing carboxylic acid, NSAIDs have a short biological half-life necessitating the frequent administration of conventional dosage forms to maintain therapeutic effectiveness. An additional problem associated with NSAIDs of short biological half-life is that they do not protect patients against morning joint stiffness which is common in rheumatoid disease states. Although the systemic treatment of such disease with NSAIDs has proven to be efficient, dose-dependent side effects, especially gastrointestinal

irritation, bleeding, ulceration or perforation after oral administration, are commonly seen. Considering the fact that NSAIDs are often used for a long-term period, transdermal delivery might be more appropriate to reduce the side effects while maintaining its therapeutic blood concentration (Park, 2000).

1.10.2. Propranolol

Propranolol ($C_{16}H_{21}NO_2$, MW 259.34), one of the most widely prescribed β-blockers in the long-term treatment of hypertension and cardiovascular diseases, is usually taken orally although an intravenous form is available for acute administration. Propranolol (Figure 1.13) possesses one chiral center and the *S*-isomer is 100-130 times as active as its *R*-isomer (Howe and Shanks, 1966; Barrett and Cullum, 1968). In pharmacokinetic, after oral administration, propranolol is almost completely and rapidly absorbed from the gastrointestinal tract. However, because of the high first-pass metabolism and hepatic tissue binding, the absolute bioavailability is only about 30% and varies greatly between individuals. About 90 to 95% of the drug is stereoselectively bound to plasma proteins (*R*-propranolol is bound higher than *S*-propranolol). Propranolol is extensively metabolized by the liver and is stereoselectively metabolized at different clearance rates (*R*-propranolol is metabolized higher than *S*-propranolol) (Pham-Huy et al., 1995). Therefore, the pharmacodynamic outcome can vary between patients (who may have different cytochrome P450 (CYP) compositions) and with the route of administration (Tucker and Lennard, 1990).

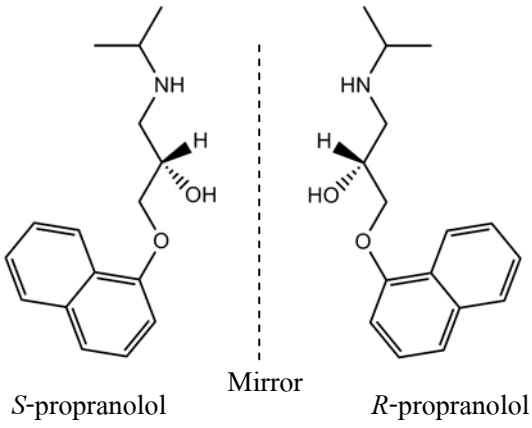

Figure 1.13. Structure and configuration of the *S*- and *R*-enantiomers of propranolol.

Transdermal controlled drug delivery provides a possible route for propranolol administration, but transdermal absorption of propranolol is poor, although a number of different approaches have been investigated with a view to improve permeation (Stott et al., 2001; Namdeo and Jain, 2002; Amnuaikit et al., 2005). Thus, if the *S*-enantiomer of propranolol were to be selectively transported across the skin, a better therapeutic response might be expected relative to that obtained using a racemic mixture of the drug.

1.10.3. Omeprazole

The racemic omeprazole ($C_{17}H_{19}N_3O_3S$, MW 345.42) is the first and the leading gastric proton-pump inhibitor used clinically as an anti-ulcer agent (Brunton, 1990), becoming the world's highest selling drug in 1997 ($5 billion) (Stinson, 1998). Omeprazole has a stereogenic center at the sulfur atom in sulfoxide group, and exists as two enantiomers, *S*-enantiomer and *R*-enantiomer (Figure 1.14). Omeprazole is a selective inhibitor of gastric acid secretion by interacting with H^+/K^+-ATPase in gastric parietal cells (Fellenius et al., 1981). It is effective in the treatment of gastro-esophageal reflux disease, gastric ulcer, or together with antibiotic therapy, in the eradication of *Helicobacter pylori* infections (Gomollon and Calvet, 2005). It is demonstrated that both enantiomers have the same *in vitro* capacity to decrease gastric acid formation (Erlandsson et al., 1990), but stereoselective metabolism is different. Omeprazole is extensively metabolized in the liver by the CYP450 enzyme family, particularly by the enzymes CYP2C19 and CYP3A4 (Figure 1.15). The metabolic pathway is enantioselective in such a way that CYP3A4 acts mainly on *S*-omeprazole to produce achiral omeprazole sulfone, whereas CYP2C19 acts mainly on *R*-omeprazole to produce *R*-5-hydroxyomeprazole, together with minor amounts of *S*-5-hydroxyomeprazole (Abelo et al., 2000). The clinical efficacy of omeprazole depends in part on the CYP2C19 phenotype of the patient. CYP2C19 fast metabolizers show relatively lower serum values of omeprazole and have lower success rates in the treatment of various disorders than CYP2C19 poor metabolizers (Klotz, 2006). The frequency of poor metabolizer is approximately 2-6% of Caucasians, whereas the frequency of poor metabolizer in Asians (19-23%) is much higher (Kanazawa et al., 2003). Recently, this chiral drug has been marketed as the pure *S*-enantiomer (esomeprazole) under the commercial name of Nexium®. This

single isomer is subjected to less first pass metabolism by CYP2C19 and lower plasma clearance than racemic omeprazole, resulting in an AUC almost two times greater than omeprazole, when equivalent doses are administered (Olbe et al., 2003).

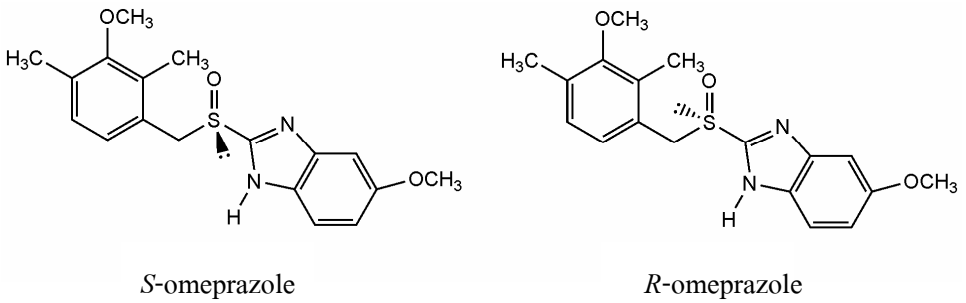

S-omeprazole *R*-omeprazole

Figure 1.14. Structure of two enantiomers of omeprazole.

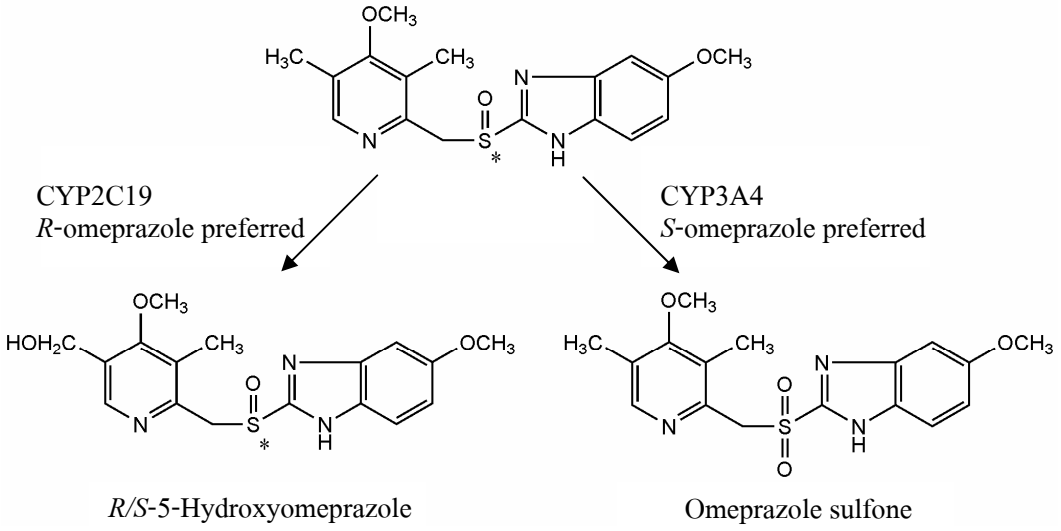

R/S-5-Hydroxyomeprazole Omeprazole sulfone

Figure 1.15. Molecular structure of omeprazole and its two main metabolites. CYP2C19 acts principally on the *R*-enantiomer of omeprazole, whereas *S*-omeprazole is the main target of CYP3A4 (Martens-Lobenhoffer et al., 2007).

1.11. Aims of the thesis

If highly enantioselective release was achieved, the prepared delivery systems may possibly be developed to use for chiral drugs administration which would be able to improve the efficiency of chiral drugs use. The objectives of this study were to characterize and evaluate the enantiomeric separation of a separation membrane and applicability of molecularly imprinted polymer (MIP) in drug delivery technologies of chiral drugs. More specifically, the aims of this thesis were:

1. The MIP composite cellulose membranes selective to *S*-enantiomer of ibuprofen, ketoprofen and naproxen were synthesized and their enantioselective release properties were evaluated. The composite membranes composed of MIP and bacterially-derived cellulose were prepared by using *S*-enantiomer of NSAIDs as template molecule.

2. The MIP composite membranes composed of the MIP particles and cellulose were prepared and examined for enantioselective-controlled release of racemic propranolol. The pre-made MIP granules and MIP-nanoparticle-on-microsphere (NOM) were prepared with the use of either *R*- or *S*-propranolol as imprint molecule by the use of methacrylic acid (MAA) as functional monomer and ethylene glycol dimethacrylate (EDMA) as cross-linker. Granules and beads were also prepared from corresponding non-imprinted polymers to act as control.

3. The drug delivery systems containing MIP-NOM were prepared and examined for enantioselective-controlled release of racemice omeprazole. The MIP-NOM selective to *S*-omeprazole was prepared regarding to the use of chiral functional monomers: quinine and quinidine derivatives, which the MIP-NOM synthesized by the use of non-chiral (achiral) functional monomer: 4-vinylpyridine (4-VPD) was prepared for comparison.

CHAPTER 2

THE MIP COMPOSITE MEMBRANE DERIVED FROM MOLECULARLY IMPRINTED POLYMER AND CELLULOSE

2.1. Introduction and objectives

This chapter was involved the study of MIP composite membranes based on the grafting of MIP layer onto bacterial cellulose membrane. The *S*-form of ibuprofen, ketoprofen and naproxen were used as template molecules for the preparation of MIPs. 4-Vinylpyridine (4-VPD) and acrylamide (ACM) (see structure in Figure 2.1) were selected to use as functional monomers since the amine group of 4-VPD and the amide group of ACM could interact with the carboxyl group of the templates *via* hydrogen bonding interaction. Ethylene glycol dimethacrylate (EDMA) and *N,N*'-methylene bisacrylamide (MBA) (see structure in Figure 2.1) were used as cross-linkers copolymerized with 4-VPD and ACM, respectively. The MIP comprising of poly(4-VPD-*co*-EDMA) was a rigid structural polymer, whereas the MIP comprising of poly(ACM-*co*-MBA) was a more flexible structural network. The ability in enantioselective release of these two types of MIP layer composite membranes were studied in comparison. 4-VPD, EDMA, ACM and MBA are found to have biocompatibility and normally used in biomedical researches. From literatures, copolymer of alkylated 4-VPD did not show hemolysis of human red blood cells (Allison et al., 2007); poly(*N*-vinylpyrrolidinone) crosslinked with EDMA showed biocompatibility and could stimulate fibroblast viability of skin cell (Smith et al., 2006); acrylamide-based hydrogel was shown to have biocompatible studied with human sera (Karadag et al., 1996); and the adhesive containing MBA-siloxane system demonstrated to show less cytotoxic (< 2% cell death) in WST-1 assay (Wilson et al., 2005). These kinds of monomers were considered to be suitable for using as materials in drug delivery system.

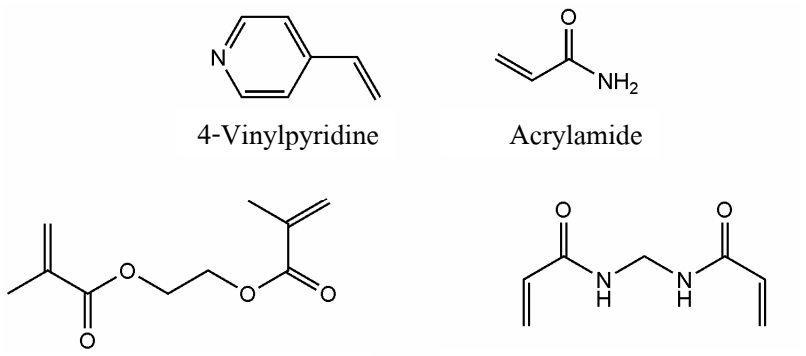

Figure 2.1. Structure of functional monomers (4-VPD and ACM) and cross-linkers (EDMA and MBA) used in this study.

The objectives of this study were to prepare the MIP composite membranes by grafting MIP layer selective to *S*-enantiomer of the NSAIDs (ibuprofen, ketoprofen and naproxen) onto bacterial cellulose membrane and their enantioselective release properties were examined. The composite membrane composed of MIP and cellulose was produced by derivatizing the cellulose membrane to obtain anchor isopropenylates which subsequently grafted with MIP layer. The MIP comprising of poly(4-VPD-*co*-EDMA) and poly(ACM-*co*-MBA) were prepared by using thermal polymerization. The non-imprinted polymer (NIP) composite cellulose membranes were also prepared as the control. The composite membranes were characterized in terms of morphology, mechanical strength and electrical resistance. The enantioselective release of MIP composite membranes and NIP composite membranes for NSAIDs was examined using Franz-type diffusion cell. The effects of amount of monomer in MIP synthesis and electrolyte (NaCl) were investigated in term of enantioselective release of the composite membranes. Furthermore, the composite membrane that gave the highest enantioselective release for the NSAIDs was evaluated the ability in enantioselective release *in vitro*.

2.2. Experimental

2.2.1. Materials

4-Vinylpyridine (4-VPD), acrylamide (ACM), ethylene glycol dimethacrylate (EDMA), *N,N'*-methylene bisacrylamide (MBA) and 3-methacryloxypropyltrimethoxysilane (3-MPS) were purchased from Aldrich Chemical Company (Milwaukee, WI, USA). *RS*-ibuprofen, *RS*-ketoprofen, *S*-ibuprofen, *S*-ketoprofen and *S*-naproxen sodium were obtained from Aldrich Chemical Company (Milwaukee, WI, USA). 2,2'-Azobis-(isobutyronitrile) (AIBN) was obtained from Janssen Chimica (Geel, Belgium). All solvents used were of analytical grade and were dried with molecular sieves before use. EDMA was purified by extraction with 1 M aqueous sodium hydroxide, washing with water, drying over anhydrous sodium sulfate and subsequent distillation under reduced pressure. 4-VPD was distilled under reduce pressure before use. Since only the *S*-form of naproxen is commercially available, *RS*-naproxen was obtained from racemization according to the method described by Gyo Lee et al. (2001). Briefly, *S*-naproxen sodium (30 g) was dissolved in ethylene glycol (120 ml). The solution was refluxed for 2 h at 150^{o}C. The reaction mixture was cooled to room temperature, and 1N HCl (120 ml) was added. *RS*-naproxen precipitated as a white powder and was washed with distilled water. The precipitate was overdried and the racemization was verified by stereospecific HPLC analysis. Bacterial cellulose membrane was a gift from Assist. Prof. Dr. Sanae Kaewnopparat, Department of Pharmaceutical Technology, Faculty of Pharmaceutical Sciences, Prince of Songkla University. The buffer solutions with different pH values were prepared as follows:

pH 5.5 buffer (0.16 M, μ=0.37): add 118 mmol of Na_2HPO_4 and 42 mmol of citric acid in 1 L volume distilled water.

pH 7.4 buffer (0.22 M, μ=0.57): add 180 mmol of Na_2HPO_4, 9 mmol of citric acid and 30 mmol of NaCl in 1 L volume distilled water.

2.2.2. Stereospecific HPLC analysis and method validation for ibuprofen, ketoprofen and naproxen enantiomers

2.2.2.1. Stereospecific HPLC analysis

The amounts of ibuprofen, ketoprofen and naproxen enantiomers were analyzed by stereospecific HPLC method using chiral column. The HPLC system consisted of a Water 600 HPLC system (Bedford, USA) with a Water 717 plus autosampler equipped with a 486 variable wavelength UV detector connected to Water 746 integrator. The chiral column used was Chiral-AGP column (150 mm × 4 mm, 5 μm) (Chiral-AGP^{TM}, ChromTech Ltd., UK). The mobile phase compositions for analysis of ibuprofen, ketoprofen and naproxen enantiomers are shown in Table 2.1. A flow rate of 1.0 ml.min^{-1} was used throughout with the injection volume of 20 μl. The UV detector was set at 273, 260 and 225 nm for ibuprofen, ketoprofen and naproxen enantiomers determination, respectively and the temperature ambient (25±1^{o}C). The retention times of *R*- and *S*-enantiomers of all the drugs studied are shown in Table 2.1.

Table 2.1. Mobile phase compositions and retention times of ibuprofen, ketoprofen and naproxen enantiomers for/from stereospecific HPLC assay.

Drug	**Mobile phase**	**Retention time (min)**	
		***R*-isomer**	***S*-isomer**
Ibuprofen	1 mM dimethyloctylamine in 100 mM sodium phosphate buffer pH 7.4	4.0	6.0
Ketoprofen	1 mM dimethyloctylamine in 10 mM sodium phosphate buffer pH 7	4.5	7.0
Naproxen	25 mM sodium phosphate buffer pH 7	3.9	10.7

2.2.2.2. Validation

To demonstrate whether the stereopecific HPLC method was suitable for determination of ibuprofen, ketoprofen and naproxen enantiomers in experiments as well as *in*

vitro skin permeation study, it was validated through the analysis of linearity, precision, accuracy, limit of detection and limit of quantification.

Linearity

The standard calibration curves were constructed separately for the *R*- and *S*-enantiomers, using racemic drugs. The stock solution of each drug (ibuprofen, ketoprofen or naproxen) was prepared by dissolving the drug in pH 7.4 buffer to make the concentration of 100 $\mu g.ml^{-1}$. The solutions at concentrations range of 2-25, 1-25 and 0.5-10 $\mu g.ml^{-1}$ of ibuprofen, ketoprofen and naproxen, respectively were obtained by appropriate dilutions with pH 7.4 buffer. Each concentration was prepared in sets of three and each one was analyzed by stereospecific HPLC method in triplicate. Linearity was evaluated from standard curves constructed by plotting concentration ($\mu g.ml^{-1}$) of drug as function of peak area on HPLC chromatogram.

Precision

The precision was evaluated through repeatability and expressed by relative standard deviation (RSD). Three different concentrations (2, 5 and 10 $\mu g.ml^{-1}$) of each drug were prepared in pH 7.4 buffer. Each concentration was prepared in sets of three and each one was injected to stereospecific HPLC method in triplicate. For precision evaluation *in vitro* skin permeation study (only ibuprofen was studied in this experiment), ibuprofen solutions (2, 5 and 10 $\mu g.ml^{-1}$) were prepared by spiked mouse skin solution about 50% v/v. The mouse skin solution was obtained from pH 7.4 phosphate buffer saline (PBS) (2.5 ml) incubated with mouse skin (1 cm^2) at $37\pm1^{o}C$ for 24 h. Each concentration was prepared in sets of three and each one was analyzed by stereospecific HPLC method in triplicate.

Accuracy

The accuracy was evaluated by comparing the measured concentration with the actual concentration and expressed by %recovery which used the data obtained in precision study.

The limit of detection (LOD) and the limit of quantification (LOQ)

Calibration curves were constructed according to linearity study. The limit of detection (LOD) and the limit of quantification (LOQ) were calculated as:

$$LOD = \frac{3\sigma}{S} \quad (2.1)$$

$$LOQ = \frac{10\sigma}{S} \quad (2.2)$$

Where; σ is the standard deviation of the response.

S is the slope of the calibration curve.

2.2.3. Stability aspects of the drugs used in this study

The stability of *S*-enantiomer of NSAIDs (ibuprofen, ketoprofen and naproxen) was studied in various conditions related with experiments. The study was carried out in the conditions of polymerization, drug release and *in vitro* skin permeation. Each of *S*-ibuprofen, *S*-ketoprofen and *S*-naproxen solution was prepared in dimethylformamide (DMF) and made the final concentration to 10 $\mu g.ml^{-1}$. Each drug solution was incubated at 60°C for 24 h. *S*-ibuprofen, *S*-ketoprofen and *S*-naproxen solutions were prepared in pH 5.5 and pH 7.4 buffers and made the final concentrations to 10 $\mu g.ml^{-1}$. Each drug in each buffer was incubated at room temperature (30±1°C) and 37±1°C for 7 days. In addition, *S*-ibuprofen solution (10 $\mu g.ml^{-1}$) in pH 7.4 buffer which spiked with mouse skin solution (50% v/v) was prepared. The solution was incubated at 37±1°C for 3 days. The amounts of drugs before and after incubation in various conditions were analyzed by stereospecific HPLC method. Each experiment was carried out in triplicate.

2.2.4. Solubility study of racemic drugs used in this study

The solubility of racemic drugs (ibuprofen, ketoprofen and naproxen) in pH 7.4 buffer was determined at room temperature (30±1°C). An excess amount of each racemic drug

was added into 5-ml vials containing 2 ml of pH 7.4 buffer to ensure saturation and the solutions were constantly agitated under 250 rpm speed for 24 h using magnetic bar and a magnetic stirrer. The saturated solutions were filtered through a 0.2 μm filter and the amounts of racemic drugs were measured by using stereospecific HPLC method after suitable dilutions. The standard curves of ibuprofen, ketoprofen and naproxen were established in pH 7.4 buffer and from the slope of the standard curves the solubility of each drug was calculate. The studies were repeated in triplicate for each drug.

2.2.5. Preparation of MIP composite cellulose membranes

The grafting of MIP layer onto the surface of a bacterial cellulose membrane is shown in Figure 2.2. Bacterial cellulose membrane was derivatized to modify the OH group of cellulose membrane to obtain the anchor C=C group by reacted with 3-MPS (10% w/w in toluene) at 80^{o}C for 4 h. The resulting membrane was then thoroughly washed in methanol and dried. The derivatized cellulose membrane was then placed in a Petri-dish (10 cm in diameter). The imprinting solution containing 0.4 mmol of the template (*S*-ibuprofen, *S*-ketoprofen or *S*-naproxen), 1.6 mmol of the functional monomer (4-VPD or ACM), 8 mmol of the cross-linker (EDMA or MBA) and 0.35 mmol of AIBN in DMF (1 ml) was poured onto the membrane surface. The dish was then purged with nitrogen gas for 5 min to remove oxygen (which acts as a radical scavenger) before closure and polymerized in the oven at 60^{o}C for 24 h. After polymerization, membrane was transferred to a Soxhlet extractor and extracted with tetrahydrofuran (THF) for 72 h before further extraction with methanol for 72 h to remove any non-grafted polymer, residual substances and template molecule. The resulting membranes were dried in vacuum overnight. The complete removal of the template molecule from the grafted membranes was confirmed by its absence from the final rinse of grafted membrane, as verified by stereospecific HPLC method. In this study, two different types of MIP layers were prepared for each drug studied; when 4-VPD was used as a functional monomer, EDMA was used as a cross-linker (poly(4-VPD-*co*-EDMA)); and when ACM was used as a functional monomer, MBA was used as a cross-linker (poly(ACM-*co*-MBA)). The control, non-imprinted polymer (NIP)

membranes were prepared in parallel with MIP membranes in the same procedure as MIP membranes but in the absence of template molecule in the monomer mixture.

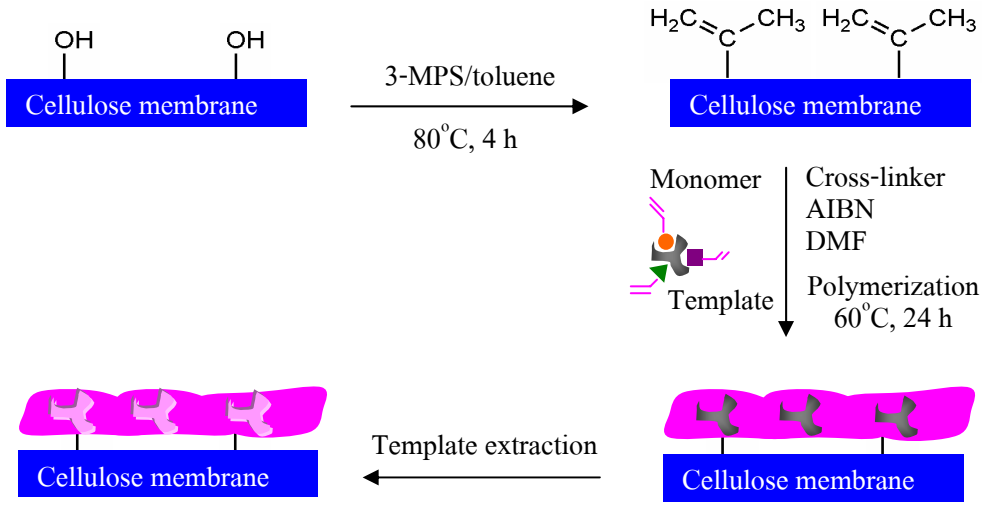

Figure 2.2. Schematic representation of MIP grafted onto a cellulose membrane.

2.2.6. Characterization of MIP composite cellulose membranes

2.2.6.1. Scanning electron microscope (SEM) analysis

The morphology of membranes (grafted and ungrafted) in both surface and cross-section was observed by scanning electron microscopy (SEM). The membrane samples were sputter-coated with gold before imaging by SEM (Jeol serie JSM 5800LV, CA, USA) at an accelerating voltage of 10 kV. The pore size of membranes was estimated from surface images of the membranes observed by SEM (n=10).

2.2.6.2. Atomic force microscope (AFM) analysis

The morphology of grafted and ungrafted membranes was also examined with an atomic force microscope (AFM) using a Digital Instruments NanoScope IIIa scanning probe microscope (Veeco Instruments GmbH, Germany). AFM observations were carried out at room

temperature without any previous treatment, using rectangular silicon nitride cantilevers with pyramidal tips.

2.2.6.3. Degree of modification (DM) measurement

The degree of modification (DM) of composite membranes was calculated from the difference in weight between the grafted membrane and the ungrafted membrane.

2.2.6.4. Fourier transform infrared spectroscopy (FT-IR) study of the attachment of polymer with cellulose membrane

Using Attenuated total reflectance (ATR) technique in the IR spectroscopy, it is possible to determine the chemical composition of a surface of the thin films/plates or multilayered sample up to the sampling depth of ~5 μm. The attachment of grafted polymer with cellulose membrane was investigated by using FT-IR spectrometer (Perkin-Elmer series 2000, Perkin-Elmer, Beaconsfield, UK) in an Attenuated total reflectance (ATR). The membrane (1cm×1cm) was placed on the crystal (ZnSe) of the ATR module and the spectra were recorded (100 scans).

2.2.6.5. Electrical resistance measurement

The degree of membrane fibrillation was assessed from the value obtained for the electrical resistance of membrane. Electrical resistance value of the membrane was also used to investigate the deposition of MIP on the surface of cellulose membrane. The electrical resistance measurement of the membranes was carried out by short-circuits current technique using a Revision G Voltage-Current Clamp, Model VCC 600 (Harvard Apparatus, CA, USA). The chamber used has effective area of 1 cm^2. The four electrodes potentiostat assured a passage of current between the two calomel electrodes in such a manner as to hold constant amplitude of voltage between the two identical reversible silver-silver chloride electrodes and the intensity and phase of current in the circuit. A 180 μA current was applied and the membrane potential

difference, PD (mV) and the short circuit current, I_{sc} (μA) were recorded simultaneously. The membrane resistance, R_m ($\Omega.cm^2$) was calculated based on the Ohm's law as:

$$R_m = \frac{PD}{I_{sc}} \tag{2.3}$$

These were corrected by eliminating the offset voltage between the electrodes and solution resistance, which was determined prior to each experiment using identical bathing solutions. All experiments were carried out at 25±1°C. At least three replicates were carried out for each membrane.

2.2.6.6. Mechanical property measurement

The mechanical strength of the membranes was measured using a Universal testing machine (Lloyd LRX, Fareham, UK) with an operating head load of 100 N. The membrane was placed between the grips of testing machine. The grip length was 2.5 cm and the speed of testing was set at the rate of 30 $mm.min^{-1}$. Each membrane was tested in triplicate. Tensile strength was calculated according to the equation:

$$\text{Tensile strength } (kN.m^{-2}) = \frac{\text{Max load (kN)}}{\text{Cross section area } (m^2)} \tag{2.4}$$

2.2.6.7. Thermogravimetric analysis

Thermogravimetric analysis (TGA) of membranes was carried out using a Perkin-Elmer DTA7 analyzer (Perkin Elmer, CT, USA). A portion of membrane (0.5 mg) was heated from 50 to 800°C at $10^{o}C.min^{-1}$ in nitrogen gas.

2.2.6.8. Water absorption measurement

The water absorption of unmodified and modified cellulose membranes was evaluated in pH 5.5 and pH 7.4 buffers. The membranes were vacuum-dried at room temperature for at least 3 days before testing. The membrane samples were weighted and then soaked in individual tubes containing pH 7.4 or pH 5.5 buffers at room temperature (30±1^{o}C). The membranes were incubated in the medium until the weight of wet membranes remained stable, which usually occurred after approximately 7 h of incubation. Before measuring the weight of the wet membrane, surface water was gently removed with a tissue. Each membrane was tested in triplicate. The water absorption (%) was calculated from the equation:

$$\text{Water absorption (\%)} = \frac{W_{wet} - W_{dry}}{W_{dry}} \times 100 \qquad (2.5)$$

Where; W_{dry} and W_{wet} are the weights of dried and wet samples, respectively.

2.2.7. Measurement of partition coefficient

The membrane partition coefficients at pH 5.5 and pH 7.4 were evaluated by equilibrating of the drug solution with a membrane. In a typical binding assay, the membrane (1cm×1cm) was added to 5 ml of an aqueous solution containing 10 μg.ml^{-1} of racemic ibuprofen (or naproxen), and stirred (250 rpm) overnight at room temperature (30±1^{o}C) for equilibrium to be established. The difference between the initial and equilibrium concentrations of each enantiomer in the aqueous phase was determined by stereospecific HPLC method and hence the amounts of enantiomers of drugs adsorbed to the membranes were calculated. Each experiment was carried out in sets of three. The partition coefficient (K) was calculated from the equation:

$$K = \frac{C_p}{C_s} \qquad (2.6)$$

Where; C_p is the concentration of the analyte associated with the membrane.

C_s is the concentration of the analyte in the solution.

The enantioselectivity factor representing the effect of the imprinting process was the ratio of *K* of the *S*-isomer to *K* of the *R*-isomer.

2.2.8. Enantioselective transport determination

The enantioselective transport of racemic drugs across unmodified and modified cellulose membranes was evaluated by dialysis method using vertical Franz-type diffusion cell (Figure 2.3) with a normal receptor volume of 2.5 ml and diffusional area of 0.8 cm^2. The cell flanges were greased with high performance vacuum grease and the membrane was mounted between the receptor and donor compartments. Clamps were used to hold the membrane into position before the receptor compartment was filled with pH 7.4 buffer. Micromagnetic stirrer bar was added to the receptor compartment and set to stir at 250 rpm during experiment. The required amount of racemic drug was dissolved in either pH 5.5 or pH 7.4 buffer solutions to obtain the donor solution (1 ml was applied in donor compartment). The test was performed at room temperature (30±1^{o}C). Drug transport was measured by the removal of samples (200 µl) from the receptor phase at appropriate time intervals over 6 h. The volume of the sample withdrawn was replaced by the same volume of the fresh medium. The diffusion of each enantiomer of drugs was determined using the stereospecific HPLC method. Each test was carried out in sets of six. The cumulatively permeated amounts per unit area (µg.cm^{-2}) were calculated and plotted against time (min). The flux (*J*, µg.cm^{-2}.min^{-1}) of each enantiomer was measured from the best fit linear slope of the graph. The steady-state portion of the line was extrapolated to the time axis and the point of intersection was recorded as the lag time. The diffusion coefficient (*D*, µm^2.min^{-1}) was obtained from the equation:

$$D = \frac{h^2}{6T_L} \tag{2.7}$$

Where; h is the membrane thickness (µm).

T_L is the lag time (min).

The enantioselectivity factor was expressed as the ratio of *D* of the *S*-isomer to *D* of the *R*-isomer.

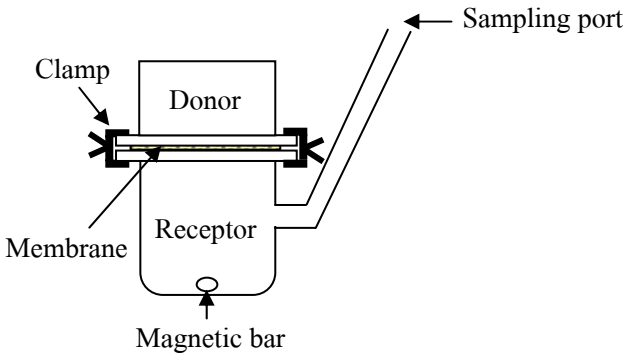

Figure 2.3. Vertical Franz-type diffusion cell used in this study.

2.2.9. *In vitro* skin permeation study

The *in vitro* skin permeation study of the modified membranes was performed with a vertical Franz-type diffusion cell similar to that of enantioselective transport determination. Male mice (8-9 weeks), weighing 28-32 g were sacrificed by snapping the spinal cord at the neck. Rectangular section of dorsal skin were shaved and excised from the animal using surgical scissors. Adhering fat and other visceral dermis were removed from the undersurface with tweezers. The excised skin was immediately mounted between the half-cells, with and without a coupled test membrane, such that the dermal surface was in contact with the receptor fluid and the epidermal side in contact with the test membrane (if present). Racemic ibuprofen was dissolved in pH 5.5 buffer to produce drug concentration of 240 $\mu g.ml^{-1}$, and 1 ml of the drug solution was applied in the donor compartment to expose with membrane surface. The receptor compartment containing 2.5 ml PBS was placed on magnetic stirring plate (Variomag, FL, USA) submersed in a water bath maintained the temperature at $37\pm1^{o}C$ to allow the receptor compartment to expose with water in water bath. The solution in receptor compartment was stirred with a magnetic bar constantly at 250 rpm. An aliquot (200 µl) of receptor fluid was collected at the set time intervals over 3 days and replaced with the same volume of fresh PBS. The concentrations of ibuprofen enantiomers in the collected samples were determined by stereospecific HPLC method. The

experiment was carried out in sets of six. Cumulative amounts of ibuprofen enantiomers permeated per unit area (μg.cm^{-2}) were plotted against time (h) over the 60 h experimental period.

2.2.10. Statistical analysis

The statistical significance of the observed difference of *R*- and *S*-enantiomers of each drug in every experimental test was examined by paired *t*-test using SPSS version 13.0 (SPSS, Cary, NC, USA). A *p*-value of <0.05 was considered significant.

2.3. Results and discussion

2.3.1. Method validation

The linearity, precision, accuracy, limit of detection (LOD) and limit of quantification (LOQ) of ibuprofen, ketoprofen and naproxen enantiomers from stereospecific HPLC assay were summarized in Table 2.2. The linearity was obtained with correlation coefficients (R^2) of higher 0.999 for the concentrations range of 2-25, 1-25 and 0.5-10 μg.ml^{-1} of ibuprofen, ketoprofen and naproxen enantiomers, respectively. The stereospecific HPLC assay method was accurate and precise with a relative percent standard deviation (%RSD) of lower 2% and %recovery was in the range of 99.10-100.76% for both *R*- and *S*-enantiomers of every drug in pH 7.4 buffer and in pH 7.4 buffer spiked mouse skin solution.

Table 2.2. Linearity, precision, accuracy, limit of detection (LOD) and limit of quantification (LOQ) of ibuprofen, ketoprofen and naproxen enantiomers from stereospecific HPLC assay.

Drug	Isomer	Linearity (R^2)	Precision (%RSD)	Accuracy (%recovery)	LOD ($\mu g.ml^{-1}$)	LOQ ($\mu g.ml^{-1}$)
Ibuprofen	*R*	0.9998	0.92 [a], 0.98 [b]	99.32 [a], 100.24 [b]	0.19	0.63
	S	0.9997	1.01 [a], 1.12 [b]	99.10 [a], 100.76 [b]	0.26	0.86
Ketoprofen	*R*	0.9999	0.89	100.12	0.12	0.40
	S	0.9999	1.02	100.26	0.15	0.50
Naproxen	*R*	0.9999	0.88	99.68	0.05	0.17
	S	0.9998	0.97	100.36	0.06	0.21

[a] refer to %RSD or %recovery of ibuprofen enantiomers in pH 7.4 buffer.

[b] refer to %RSD or %recovery of ibuprofen enantiomers in pH 7.4 buffer spiked mouse skin solution.

2.3.2. Stability of the drugs used in this study

The *S*-enantiomer of NSAIDs used in this study (i.e., ibuprofen, ketoprofen and naproxen) were evaluated the stability in various conditions to verify whether the drugs had good stability throughout experiments. It was found that the stability of *S*-enantiomer for all drugs in DMF incubated at 60^{o}C for 24 h and in pH 5.5 and pH 7.4 buffers incubated at room temperature (30±1^{o}C) and 37±1^{o}C for 7 days was shown higher than 99% content of drugs remained after incubation times (Table 2.3), indicating good stability of the enantiomers under polymerization condition and drug release study. The stability of *S*-ibuprofen enantiomer in pH 7.4 buffer incubated with mouse skin solution showed that more than 98% content of enantiomer was found after 3 days incubation and no chiral inversion was observed. This indicated that *S*-ibuprofen enantiomer was stable under *in vitro* skin permeation study.

2.3.3. Solubility of the drugs used in this study

The solubility of drug in release study solvent would provide information of sink condition. The solubility of ibuprofen, ketoprofen and naproxen in pH 7.4 buffer at 30±1^{o}C was 7.42±0.68, 6.11±1.21 and 10.32 μg.ml^{-1}, respectively.

2.3.4. Membranes characterization

2.3.4.1. Morphologic analysis

SEM and AFM were used to visualize the surface of bacterial cellulose membranes before and after modified with MIP. The cross-section of each membrane was also observed by SEM. The SEM images (Figure 2.4) showed that the modified cellulose membranes had additives incorporated onto the fiber surface, while the cellulose membrane (reference) did not. Cellulose membranes with imprinted layer leaded to increase the surface roughness. AFM image of reference membrane (Figure 2.6) showed distinct area of pores (dark color), indicating a porous nature of bacterial cellulose membrane, while cellulose membrane modified with MIP exhibited a rough surface and the pores were smaller than reference membrane. The pore size of the modified membranes observed from SEM surface images was smaller than that of reference membrane and some pores were covered with the polymer matrix. The poly(ACM-*co*-MBA) could cover the outer surface of the cellulose membrane more efficiently than poly(4-VPD-*co*-EDMA). From SEM cross-section images (Figure 2.5), the modified membranes showed slightly more solidity of cellulose sheets than reference membrane. This may be due to some of imprinting mixture applied on membrane surface was penetrated into the membrane and subsequently polymerized to form polymer attached with the fibril inside membrane. However, the imprinting mixture should not penetrate as effectively into the tight meshed polymer chains, causing accumulating and form polymer matrix at the initial surface of membrane. The SEM images indicated the increase of membrane base thickness (10-14 μm) about 2-3 μm after grafting with a MIP. The modified membranes have an average degree of modification (DM) of 1 mg.cm^{-2}.

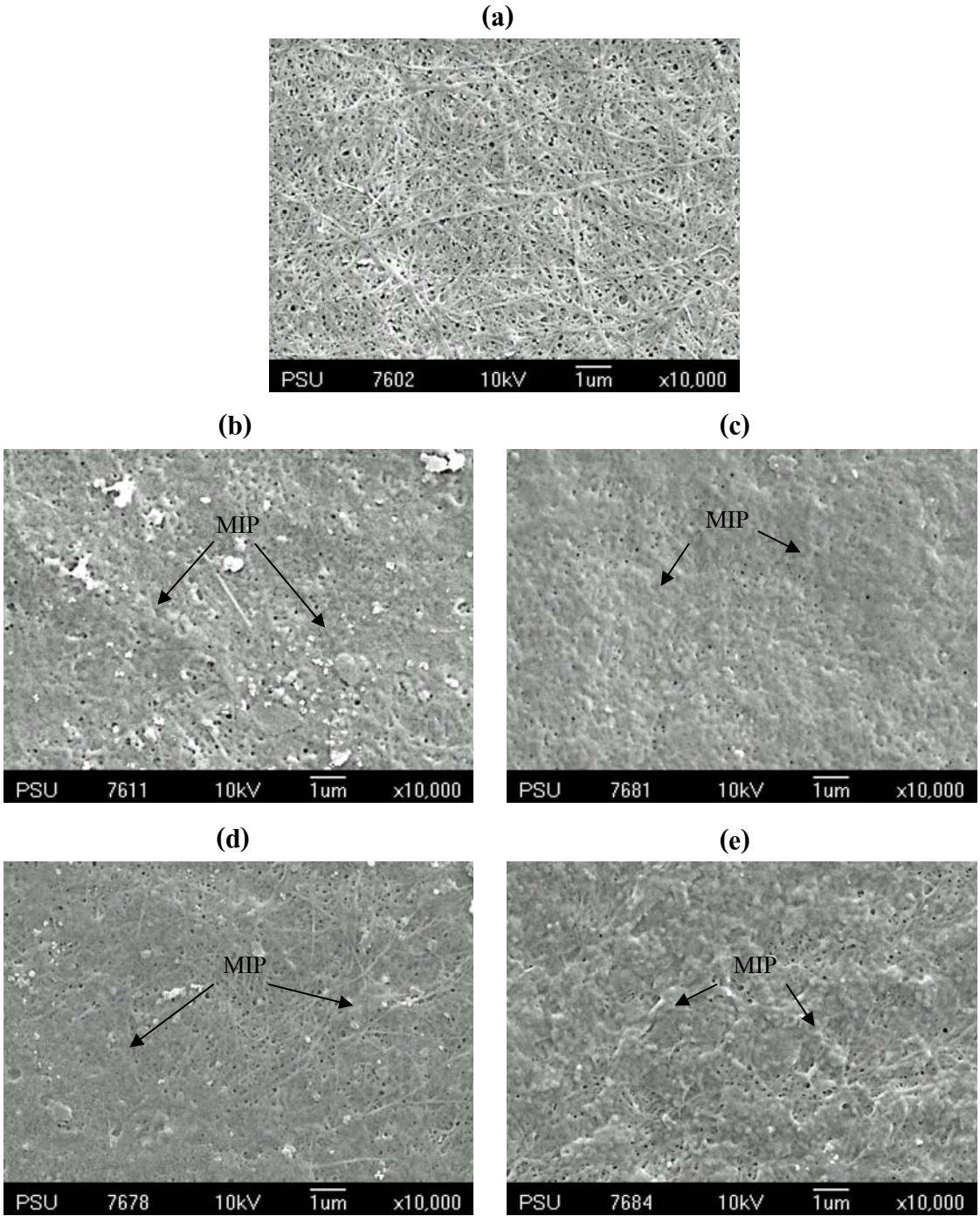

Figure 2.4. SEM images showing surface morphology of (a) the initial cellulose membrane, the *S*-ibuprofen-MIP modified membranes using (b) poly(4-VPD-*co*-EDMA) and (c) poly(ACM-*co*-MBA), and the *S*-naproxen-MIP modified membranes using (d) poly(4-VPD-*co*-EDMA) and (e) poly(ACM-*co*-MBA).

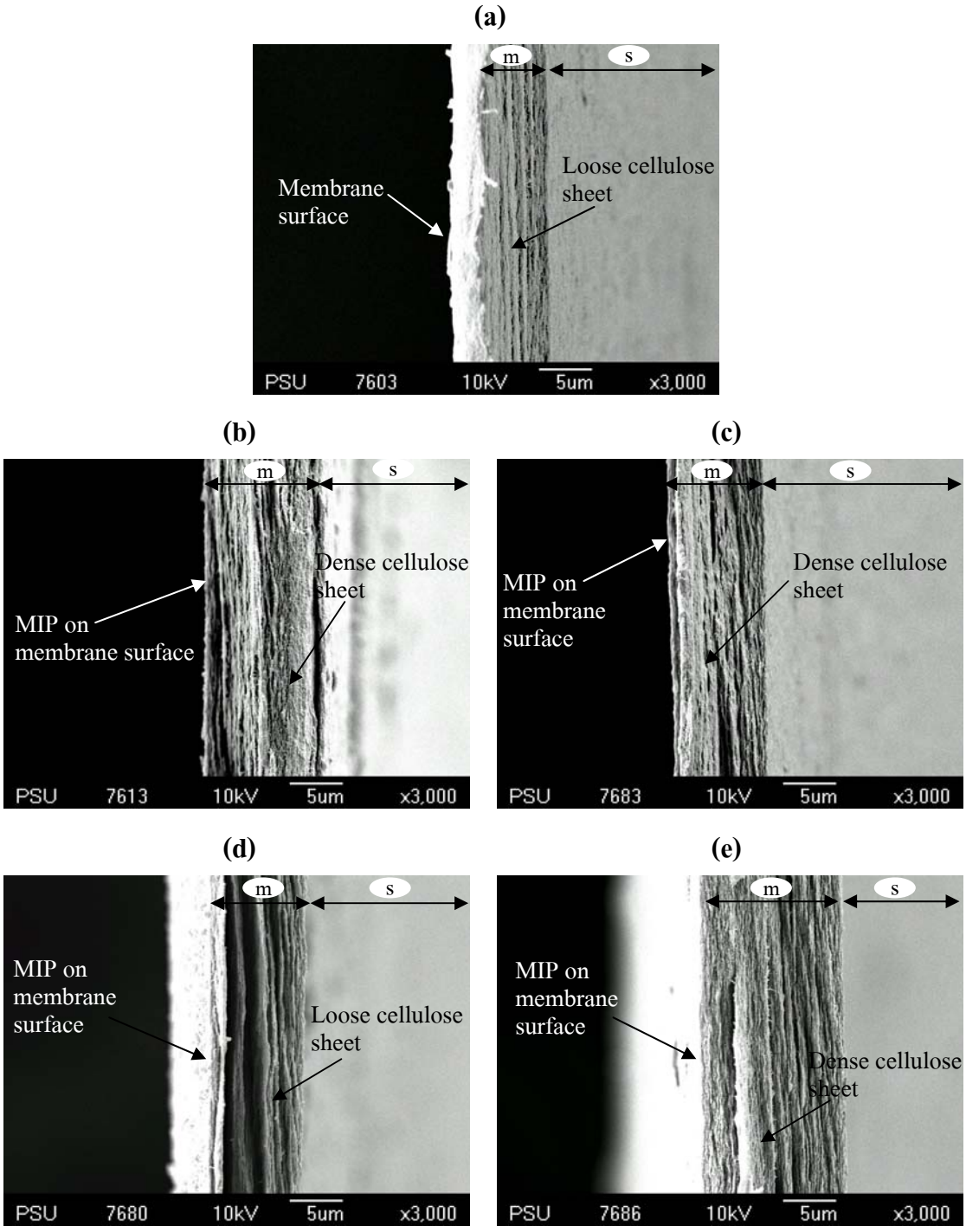

Figure 2.5. SEM cross-section images of (a) the initial cellulose membrane, the *S*-ibuprofen-MIP modified membranes using (b) poly(4-VPD-*co*-EDMA) and (c) poly(ACM-*co*-MBA), and the *S*-naproxen-MIP modified membranes using (d) poly(4-VPD-*co*-EDMA) and (e) poly(ACM-*co*-MBA) (s=stub, m=membrane).

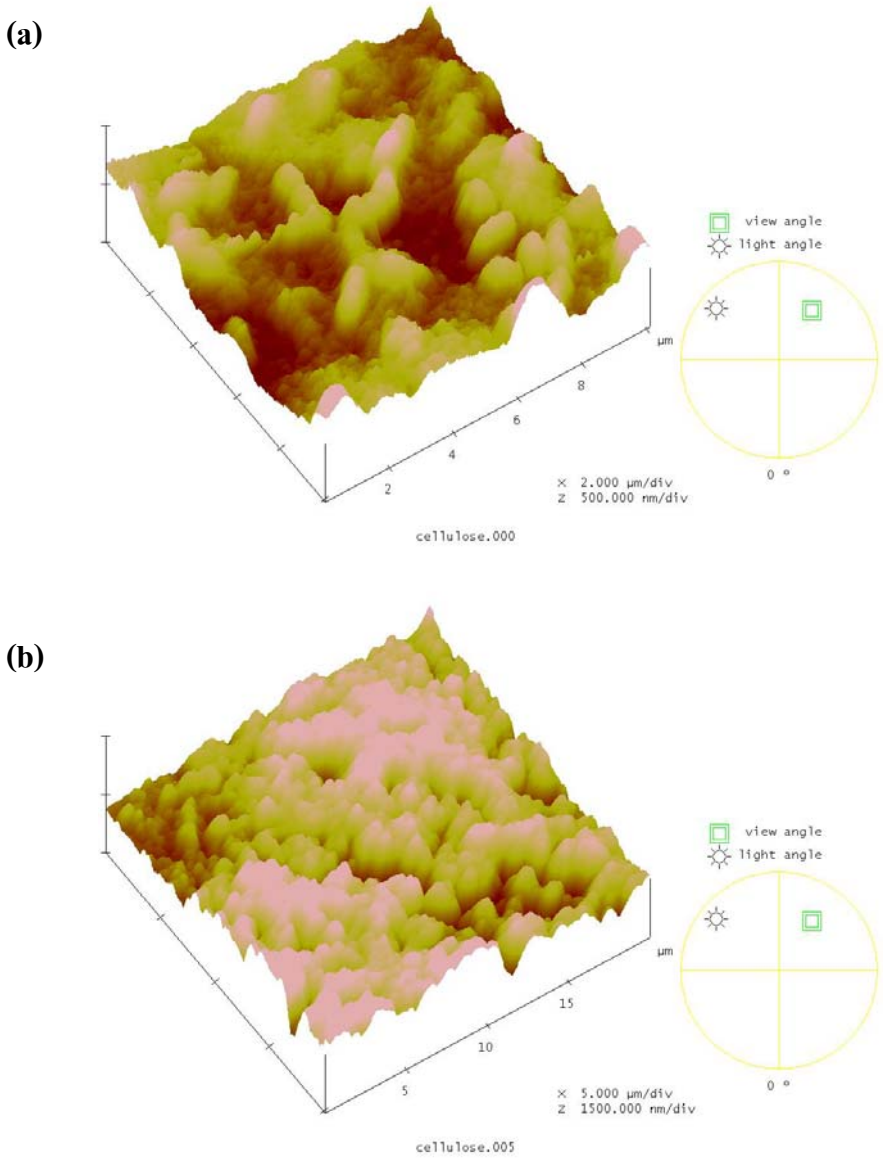

Figure 2.6. AFM images showing (a) initial cellulose membrane and (b) *S*-ibuprofen-MIP composite cellulose membrane comprising of poly(4-VPD-*co*-EDMA).

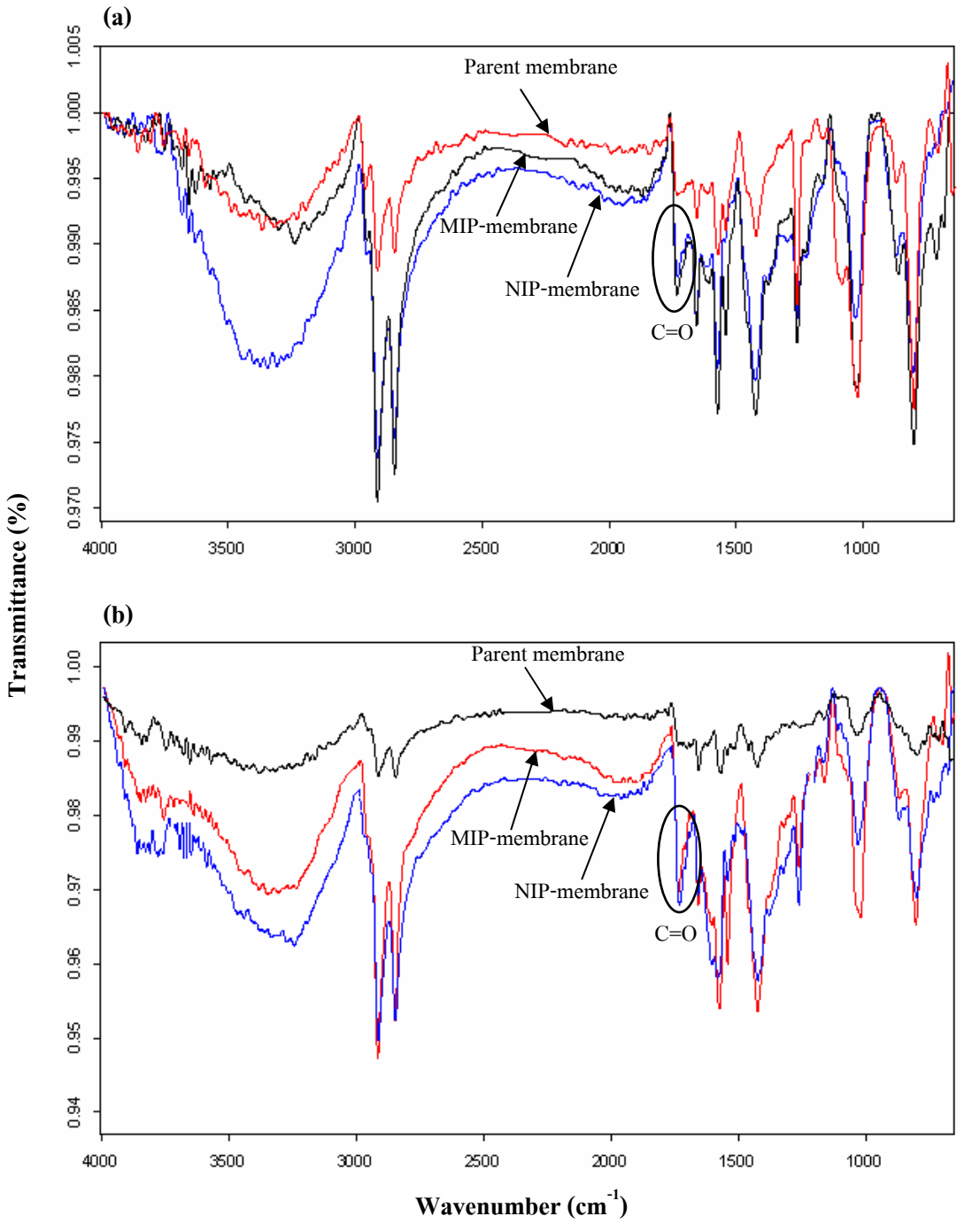

Figure 2.7. ATR-FTIR spectra of parent cellulose membrane, *S*-ibuprofen-MIP and NIP membranes comprising of (a) poly(4-VPD-*co*-EDMA), and (b) poly(ACM-*co*-MBA).

2.3.4.2. ATR-FTIR characterization

The presence of grafted polymer onto cellulose membrane was further supported from ATR-FTIR investigations. The IR spectra of the parent cellulose membrane, *S*-ibuprofen-MIP and NIP grafted cellulose membranes comprising of poly(4-VPD-*co*-EDMA) and poly(ACM-*co*-MBA) are shown in Figure 2.7. An absorption peak at 1720 cm^{-1} was apparent in the MIP and NIP grafted membranes in both types of copolymers which assigned to the stretching of the introduced C=O from the copolymer, suggesting the successful polymerization on the cellulose.

2.3.4.3. General properties of MIP composite cellulose membranes

The general properties (i.e., membrane resistance, tensile strength, water content, pore size and water absorption) of *S*-ibuprofen- and *S*-naproxen-MIP composite cellulose membranes comprising of poly(4-VPD-*co*-EDMA) and poly(ACM-*co*-MBA) were compared with those of corresponding NIP membranes which were all produced from the same basic cellulose membrane and reference cellulose membrane (Table 2.3-2.6).

Table 2.3. Characteristics of cellulose membrane, *S*-ibuprofen-MIP composite membrane comprising of poly(4-VPD-*co*-EDMA) and NIP membrane (mean±S.D., n=3).

Membrane	**Membrane resistance ($\Omega.cm^2$)**	**Tensile strength ($kN.m^{-2}$)**	**Water content (%)**	**Pore size* (nm)**	**Water absorption (%)**	
					pH 5.5	**pH 7.4**
Cellulose	1.88±0.43	10.73±4.13	3.10	142.7±14.6	91.66±7.21	70.83±7.21
MIP	3.76±0.26	15.05±7.74	2.07	62.8±17.3	78.76±5.24	51.51±13.88
NIP	3.76±0.26	12.70±2.04	4.02	56.3±13.8	60.60±18.92	48.48±10.49

* n=10

Table 2.4. Characteristics of cellulose membrane, *S*-ibuprofen-MIP composite membrane comprising of poly(ACM-*co*-MBA) and NIP membrane (mean±S.D., n=3).

Membrane	Membrane resistance ($\Omega.cm^2$)	Tensile strength ($kN.m^{-2}$)	Water content (%)	Pore size* (nm)	Water absorption (%)	
					pH 5.5	pH 7.4
Cellulose	1.88±0.43	10.73±4.13	3.10	142.7±14.6	91.66±7.21	70.83±7.21
MIP	3.13±0.73	6.06±2.53	3.33	47.3±15.5	88.88±11.11	59.21±6.41
NIP	3.13±0.73	5.81±2.71	4.88	42.7±17.6	85.18±6.41	51.85±6.52

* n=10

Table 2.5. Characteristics of cellulose membrane, *S*-naproxen-MIP composite membrane comprising of poly(4-VPD-*co*-EDMA) and NIP membrane (mean±S.D., n=3).

Membrane	Membrane resistance ($\Omega.cm^2$)	Tensile strength ($kN.m^{-2}$)	Water content (%)	Pore size* (nm)	Water absorption (%)	
					pH 5.5	pH 7.4
Cellulose	1.88±0.43	10.73±4.13	3.10	142.7±14.6	91.66±7.21	70.83±7.21
MIP	3.13±0.73	4.52±2.70	2.77	62.4±15.8	85.18±12.83	66.66±11.11
NIP	3.13±0.73	8.21±2.08	3.52	56.6±18.5	97.40±12.83	59.25±23.12

* n=10

Table 2.6. Characteristics of cellulose membrane, *S*-naproxen-MIP composite membrane comprising of poly(ACM-*co*-MBA) and NIP membrane (mean±S.D., n=3).

Membrane	Membrane resistance ($\Omega.cm^2$)	Tensile strength ($kN.m^{-2}$)	Water content (%)	Pore size* (nm)	Water absorption (%)	
					pH 5.5	pH 7.4
Cellulose	5.02±0.21	8.20±2.88	3.02	142.7±18.2	73.80±4.12	64.28±7.14
MIP	6.27±0.25	4.75±2.85	3.83	42.0±4.16.0	92.85±7.14	78.57±7.14
NIP	6.27±0.25	9.08±2.79	3.44	59.9±16.7	92.85±0.10	80.95±4.12

* n=10

The characteristics of membranes, i.e., membrane resistance, tensile strength, water content, pore size and water absorption were changed after modification but these characteristics were not different between MIP and NIP composite cellulose membranes. The values obtained for the electrical resistance of membranes provided an indication of the leakage of membrane and it was found that the electrical resistance of the cellulose membrane increased upon modification. This was presumably a consequence of the occlusion of the pores by copolymer or the pores at membrane surface were covered by polymer layer. An increase in the tensile strength of the membranes after modification was found, possibly as a consequence of the introduction of a rigid poly(4-VPD-*co*-EDMA) within the pores of cellulose membrane, leading to a decrease in chain movement. A reduction in the tensile strength of cellulose membranes was also observed, suggesting that poly(4-VPD-*co*-EDMA) or poly(ACM-*co*-MBA) covered onto the surface of cellulose membrane rather than fill into the pore of cellulose membrane. Thermogravimetric analysis indicated that the parent cellulose was a thermostable polymer, with 80% of the weight loss occurring at temperature of 460^{o}C. This was the only sharp weight loss that occurred and it was ascribed to the decomposition of polymer main chain. When the MIP and NIP membranes were analyzed by TGA, two sharp transition of loss in weight (occurred in two separate temperature ranges). The first, at around 100^{o}C was attributed to desorption of water from the membrane, and this allowed the water content of the membranes to be determined and this was found to be about 2-4%. The second large weight loss occurred at approximately 460^{o}C, corresponding to the composition of the cellulose membrane. The pore size of membranes was decreased about two times after modification. This was the consequence that MIP layer covered onto membrane surface as observed from SEM and AFM images. Cellulose membranes swelled greatly in aqueous solvents confirming the hydrophilic and highly porous nature, which promotes water absorption capacity. Swelling of parent cellulose membrane in pH 5.5 buffer was slightly greater than in pH 7.4 buffer. When poly(4-VPD-*co*-EDMA) and poly(ACM-*co*-MBA) were modified with cellulose membranes, these tended a decrease in the water absorption. The swelling of membranes modified with poly(ACM-*co*-MBA) was slightly higher than that of the membranes modified with poly(4-VPD-*co*-EDMA). This was presumably a consequence that poly(4-VPD-*co*-EDMA) is a rigid polymer, while poly(ACM-*co*-MBA) is more flexible polymer. However, both types of modified cellulose membranes still showed a great degree of swelling.

This suggested that the swelling of the modified membranes were governed predominantly by the cellulose membrane.

2.3.5. Enantiomer uptake and imprinting effect

2.3.5.1. Effect of type of monomer on imprinting effect of membranes

The effect of type of functional monomer and cross-linker used for MIP composite membranes preparation was evaluated from partition coefficient (*K*) and diffusion coefficient (*D*) of membranes (Table 2.7 and 2.8). For *K* measurement, the drug concentration of incubating solution of either ibuprofen or naproxen was 10 $\mu g.ml^{-1}$ (pH 5.5). For *D* measurement, the drug concentration in donor phase was 120 $\mu g.ml^{-1}$ (pH 5.5) for ibuprofen and 16 $\mu g.ml^{-1}$ (pH 5.5) for naproxen since these concentrations gave optimal flux and sufficient amount of the drugs diffused across membranes to enable sufficient assay sensitivity. The enantioselectivity of the membranes was expressed as the ratio of *K* of the *S*-isomer to *K* of the *R*-isomer and as the ratio of *D* of the *S*-isomer to *D* of the *R*-isomer. In preliminary study, bacterial cellulose membrane grafted with *S*-ketoprofen-(4-VPD-*co*-EDMA)-MIP was prepared and tested for enantioselective transport of ketoprofen enantiomers. It was found that no enantioselectivity was observed. This finding is similar to the previous work (Ansell, 2005) showing that MIP gave the lowest capability in enantioseparation for ketoprofen compared to ibuprofen and naproxen studied in the same type of MIP (poly(4-VPD-*co*-EDMA)).

Table 2.7. Partition coefficient (*K*) and diffusion coefficient (*D*) of bacterial cellulose membrane and *S*-ibuprofen-MIP composite cellulose membranes comprising of poly(4-VPD-*co*-EDMA) and poly(ACM-*co*-MBA) in pH 5.5 buffer (mean±S.D., n=3).

Solute	Bacterial cellulose membrane		4-VPD-*co*-EDMA MIP membrane		ACM-*co*-MBA MIP membrane	
	K	***D*** **(μm^2.min^{-1})**	***K***	***D*** **(μm^2.min^{-1})**	***K***	***D*** **(μm^2.min^{-1})**
R-ibuprofen	263.79±12.90	6.43±0.25	110.02±17.69	6.21±0.34	68.91±9.14	1.58±0.25
S-ibuprofen	282.28±15.58	6.82±0.38	353.22±14.76	8.21±0.69	332.95±15.67	3.13±0.45
S/R ratio	1.11±0.04	1.06±0.02	3.21±0.73	1.32±0.05	4.83±0.34	1.98±0.04

Table 2.8. Partition coefficient (*K*) and diffusion coefficient (*D*) of bacterial cellulose membrane and *S*-naproxen-MIP composite cellulose membranes comprising of poly(4-VPD-*co*-EDMA) and poly(ACM-*co*-MBA) in pH 5.5 buffer (mean±S.D., n=3).

Solute	Bacterial cellulose membrane		4-VPD-*co*-EDMA MIP membrane		ACM-*co*-MBA MIP membrane	
	K	***D*** **(μm^2.min^{-1})**	***K***	***D*** **(μm^2.min^{-1})**	***K***	***D*** **(μm^2.min^{-1})**
R-naproxen	94.73±8.52	7.78±0.85	35.63±7.97	2.97±0.29	56.02±9.33	3.92±0.10
S-naproxen	24.41±6.75	6.80±0.44	9.70±1.44	3.66±0.13	9.21±4.36	5.31±1.01
S/R ratio	0.24±0.03	0.87±0.04	0.28±0.05	1.23±0.06	0.17±0.08	1.34±0.08

The binding results showed that the parent cellulose membrane adsorbed *R*-naproxen greater than *S*-naproxen (Table 2.8). In contrast, cellulose membrane similarly adsorbed *R*- and *S*-enantiomers of ibuprofen (Table 2.7). The *S*-ibuprofen template was bound to *S*-ibuprofen-MIP composite membranes higher than *R*-ibuprofen in both types of MIPs. This result indicated that the imprinting cavities occurred in the MIP layer. However, in the case of naproxen, the non-template isomer was bound to the *S*-naproxen-MIP composite membranes higher than the template isomer, indicating that the enantioselective sorption was still predominant from the effect of parent cellulose membrane. The enantioselective sorption for ibuprofen of the MIP composite cellulose membrane prepared with poly(ACM-*co*-MBA) was greater than that prepared with poly(4-VPD-*co*-EDMA).

Diffusion measurement of ibuprofen and naproxen enantiomers indicated an overall slightly faster transport of the template *S*-enantiomer for MIP composite cellulose membranes. Ratio of effective diffusion coefficients for MIP composite cellulose membranes indicated a slightly facilitated transport of the template enantiomers determined by imprinting. The enantioselective diffusion of the MIP composite cellulose membrane prepared with poly(ACM-*co*-MBA) was greater than that prepared with poly(4-VPD-*co*-EDMA). This may be suggested from more effective of poly(ACM-*co*-MBA) to graft with cellulose membrane than poly(4-VPD-*co*-EDMA), which can be seen from SEM images (Figure 2.4).

2.3.5.2. Effect of amount of monomer on imprinting effect of membranes

The effect of amount of monomer on the enantioselective recognition ability of membrane was investigated for cellulose membrane grafted with MIP comprising of ACM as the functional monomer and MBA as the cross-linking monomer. Four different concentrations of ACM: 0.8, 1.6, 3.2 and 6.4 M in the polymerizing mixture were studied. It was found that increasing of the ACM contents in polymer layer resulted in a decrease of partition coefficient (*K*) of both enantiomers (Table 2.9) as this was due to an increase in the thickness of barrier, hence the decreased binding of ibuprofen enantiomers on cellulose membrane. The enantioselectivity of the membranes expressed as the ratio of *K* of the *S*-ibuprofen to *K* of the *R*-ibuprofen increased at various amounts of the monomer increased, but when the contents of ACM were higher than

3.2 M, the enantioselectivity of membranes was decreased in both pH 5.5 and pH 7.4 buffers. This may be due to the excess of ACM monomer caused a higher non-specific binding on the resulting MIPs, thus the decrease in enantioselectivity. The optimal content of the ACM monomer used in synthesizing of MIP was found at 1.6 M.

Table 2.9. Partition coefficient (*K*) of *S*-ibuprofen-(ACM-*co*-MBA)-MIP composite cellulose membranes prepared by using different amounts of ACM (mean±S.D., n=3).

Amount of ACM (M)	**Solute***	***K***	
		pH 5.5	**pH 7.4**
0.8	*R*	303.70±16.29	179.50±11.67
	S	335.59±15.28	235.49±19.35
	S/R ratio	1.10±0.02	1.31±0.02
1.6	*R*	68.91±9.14	127.22±3.12
	S	332.95±15.67	297.38±13.18
	S/R ratio	4.83±0.34	2.33±0.11
3.2	*R*	53.72±18.66	107.36±14.81
	S	240.89±8.14	267.31±16.24
	S/R ratio	4.48±0.30	2.48±0.16
6.4	*R*	57.02±6.69	96.23±13.95
	S	219.59±12.12	200.36±14.81
	S/R ratio	3.85±0.05	2.08±0.07

* refer to *R*- or *S*-isomer of ibuprofen.

2.3.6. The evaluation in enantioelective release of the MIP composite cellulose membranes

The release study of bacterial cellulose membrane (membrane base) revealed that there was no differential release of ibuprofen enantiomers in all the cases of concentrations studied (Figure 2.8). Bacterial cellulose membrane tended to release *S*-ibuprofen greater than *R*-ibuprofen. However, bacterial cellulose membrane retarded the release of *S*-naproxen at low

concentration (Figure 2.9), whereas there was no enantioselectivity of release for naproxen at the higher concentration.

Cellulose membrane modified with *S*-ibuprofen-(4-VPD-*co*-EDMA)-MIP showed the release of *S*-ibuprofen enantiomer higher than *R*-ibuprofen enantiomer (Figure 2.10) compared to the corresponding NIP membrane. However, the enantioselective release obtained was not significantly different ($p>0.05$). The enantioselective release for ibuprofen was obtained from cellulose membrane modified with *S*-ibuprofen-(ACM-*co*-MBA)-MIP (Figure 2.11) which the template *S*-ibuprofen enantiomer was released faster than *R*-ibuprofen enantiomer at every time point ($p<0.05$) compared to the control NIP membrane. The enantioselective release for ibuprofen enantiomers obtained from the ACM-*co*-MBA-MIP composite membrane was higher than that from the 4-VPD-*co*-EDMA-MIP composite membrane. This may be due to the higher poly(ACM-*co*-MBA) content grafted onto the cellulose membrane, as shown in SEM image (Figure 2.4). There was no enantioselectivity of release for ibuprofen from the control NIP membranes comprising of both copolymers studied. Since cellulose membrane did not show enantioselective release for ibuprofen enantiomers, the enantioselective release obtained from the MIP modified cellulose membrane was due to the imprint polymer itself. It appeared that the template enantiomer of ibuprofen was released greater than the other enantiomer for *S*-ibuprofen-(ACM-*co*-MBA)-MIP membrane. Although the enantioselectivity obtained from *S*-ibuprofen-(ACM-*co*-MBA)-MIP membrane in aqueous solvent was modest, it is statistically significant ($p<0.05$). The facilitated transport of the template isomer for *S*-ibuprofen-MIP was not yet known, however the preferable adsorption together with mobility of the template molecule has been considered. The selectivity of *S*-ibuprofen enantiomer to the *S*-ibuprofen-(ACM-*co*-MBA)-MIP membrane occurred due to the hydrogen bonding interaction of carboxyl of *S*-ibuprofen and amide of ACM, or electrostatic interaction. In addition, the non-enantioselectivity for release of naproxen enantiomers was observed in either 4-VPD-*co*-EDMA- or ACM-*co*-MBA-MIP membranes.

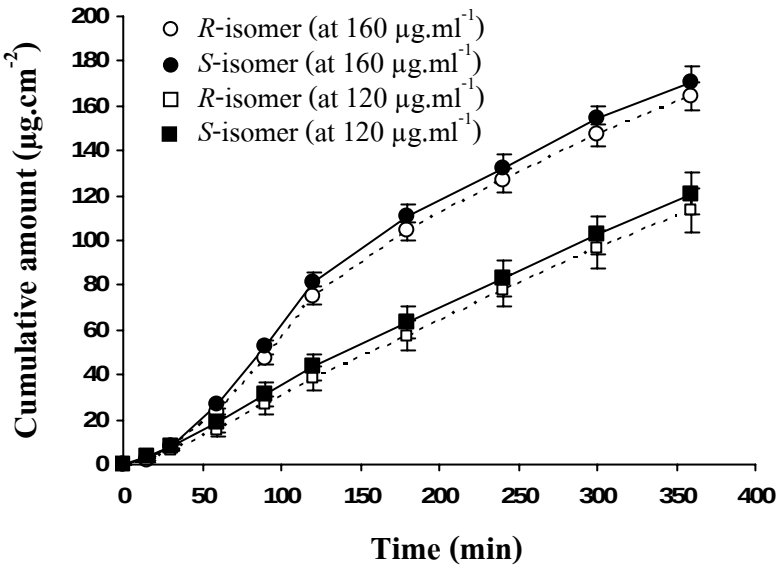

Figure 2.8. Cumulative amount (µg.cm^{-2}) of ibuprofen enantiomers release through parent bacterial cellulose membrane in various drug concentrations in donor phase (mean±S.D., n=3).

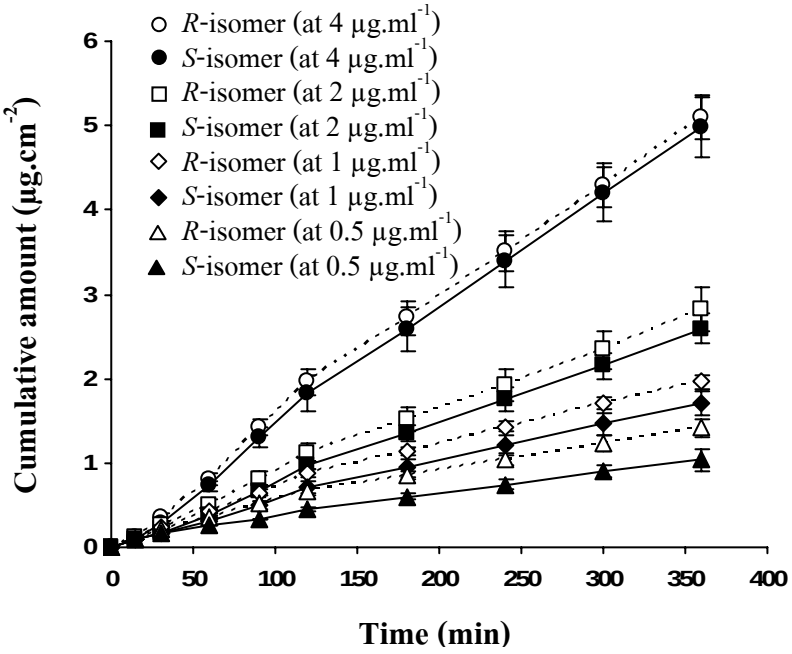

Figure 2.9. Cumulative amount (µg.cm^{-2}) of naproxen enantiomers release through parent bacterial cellulose membrane in various drug concentrations in donor phase (mean±S.D., n=3).

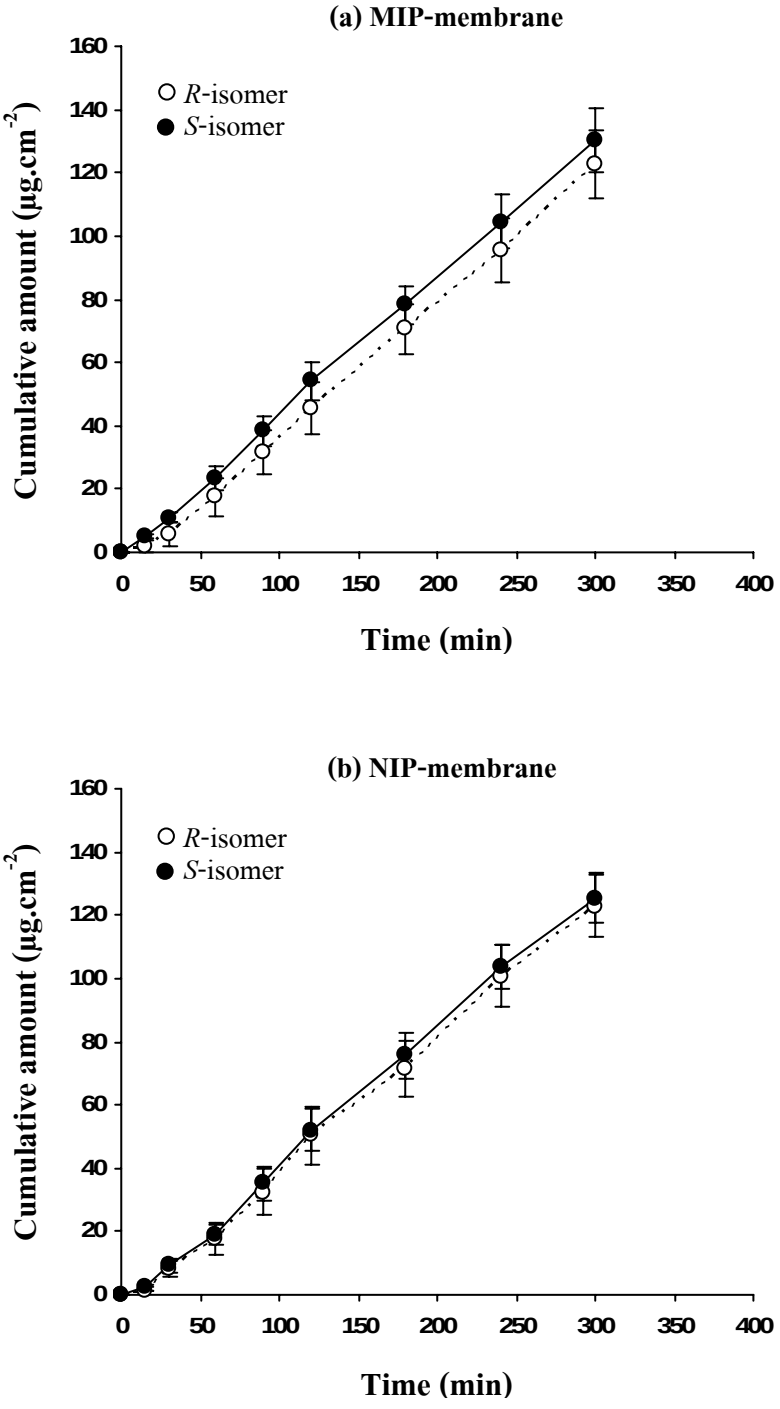

Figure 2.10. Cumulative amount (µg.cm^{-2}) of ibuprofen enantiomers release through (a) *S*-ibuprofen-(4-VPD-*co*-EDMA)-MIP and (b) NIP composite cellulose membranes (mean±S.D., n=6).

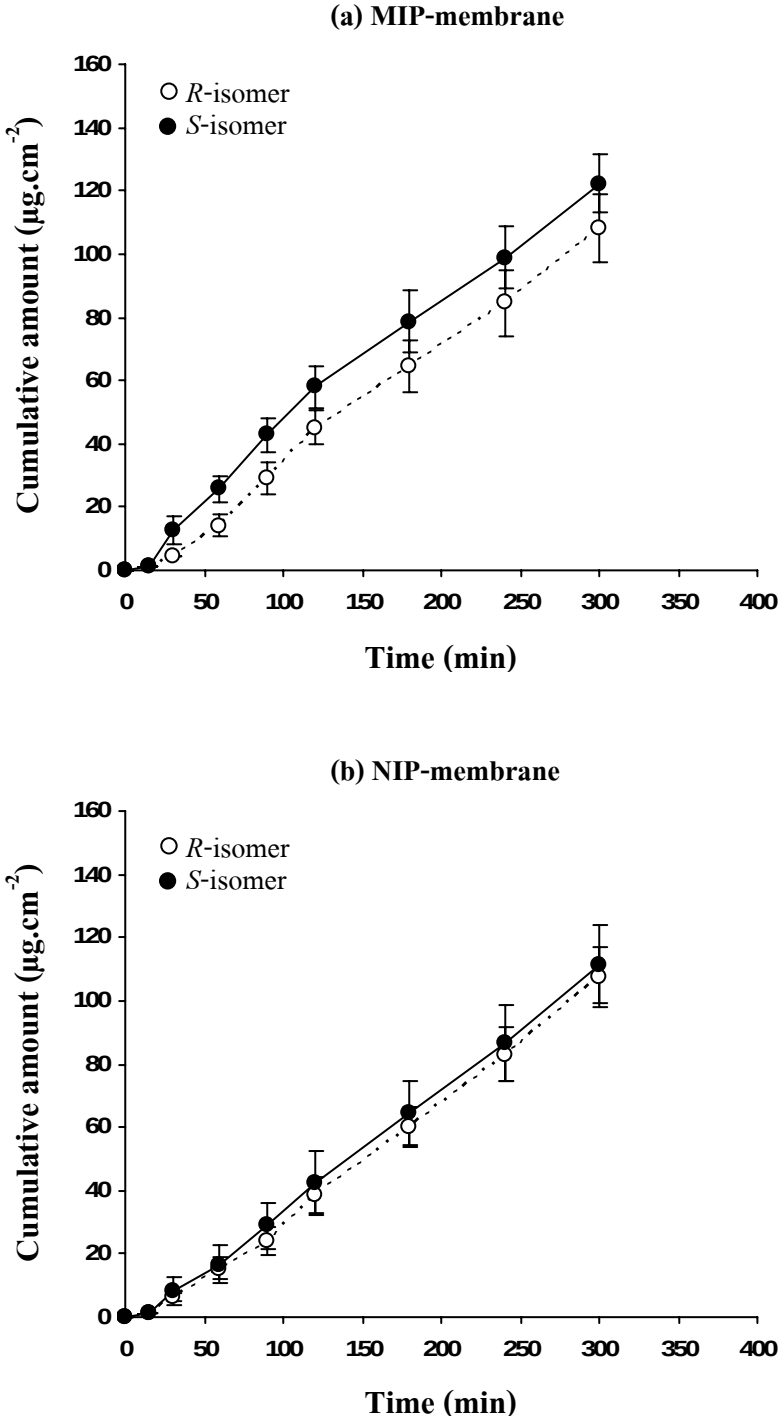

Figure 2.11. Cumulative amount (µg.cm^{-2}) of ibuprofen enantiomers release through (a) *S*-ibuprofen-(ACM-*co*-MBA)-MIP and (b) NIP composite cellulose membranes (mean±S.D., n=6).

2.3.7. Effect of electrolyte on the enantioselective release of MIP composite cellulose membrane

The effect of electrolyte on the enantioselective release of MIP composite membrane was studied to evaluate the electrostatic interaction of MIP and drug molecule. NaCl in various contents (0, 0.1, 0.3 M) was added in ibuprofen solution (pH 5.5) in donor phase of Franz-type diffusion cell for enantioselective release evaluation of *S*-ibuprofen-(ACM-*co*-MBA)-MIP composite membrane. It was found that increasing NaCl concentration decreased the flux of both *R*- and *S*-ibuprofen enantiomers (Figure 2.12). NaCl added to donor phase is a source of co-ion. This co-ion (Na^+/Cl^-) is generally more mobile and smaller in size than the drug molecule and can compete to transport across membrane thereby causing a decrease in flux of the drug (Dixit et al., 2007). In pH 5.5 buffer, ibuprofen (pKa=4.4) and ACM (pKa=7.9) would be in ionized form, allowing ibuprofen and ACM can form electrostatic *via* polar non-ion interaction. The addition of electrolyte decreased the enantioselectivity of MIP membrane by reducing the electrostatic interaction between MIP and *S*-ibuprofen template. With the increase of salt concentration, the electrostatic interaction would be more interfered by Na^+/Cl^- counter ions which this is due to the binding of sodium ions into the carboxyl groups of ibuprofen. The enantioselectivity was not observed in the present of NaCl at high concentration (0.3 M). This result suggested that the ionic interaction would be the main interaction involving the enantioselectivity of *S*-ibuprofen-(ACM-*co*-MBA)-MIP composite membrane.

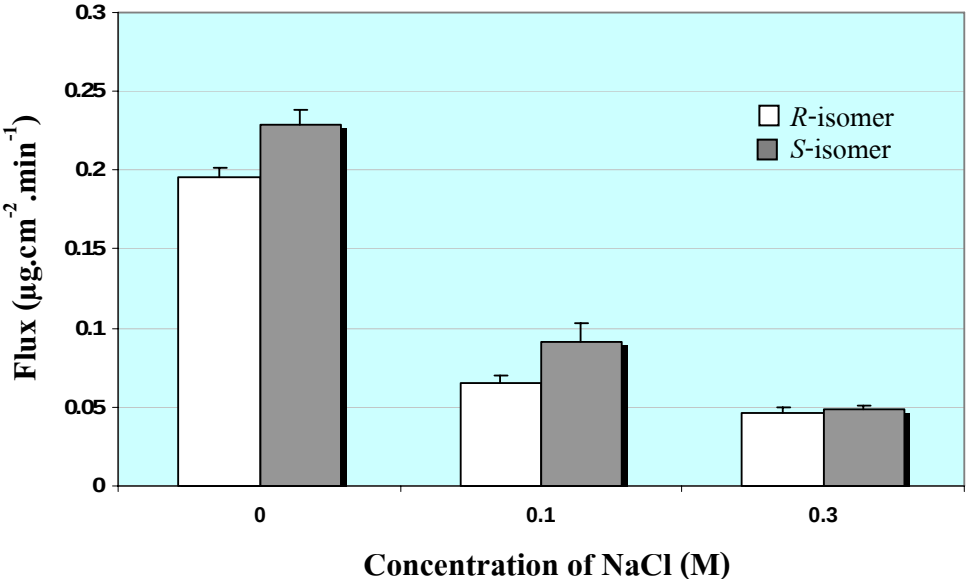

Figure 2.12. Effect of sodium chloride on flux of ibuprofen enantiomers release through *S*-ibuprofen-(ACM-*co*-MBA)-MIP composite cellulose membrane (mean±S.D., n=3).

2.3.8. Transdermal enantioselective-controlled release of *S*-ibuprofen-(ACM-*co*-MBA)-MIP composite cellulose membrane

The *in vitro* skin permeation of *S*-ibuprofen-(ACM-*co*-MBA)-MIP composite membrane that showed the greatest enantioselectivity for release of ibuprofen enantiomers was examined with pH in donor phase was 5.5 in order to simulate the pH of skin. Racemic ibuprofen in donor phase was 240 µg.ml^{-1} to ensure that sufficient amount of the drug permeated into the skin to enable sufficient assay sensitivity. A control experiment was carried out with NIP membrane. Figure 2.14 shows the cumulative amounts of ibuprofen enantiomers across mouse skin as function of time, when the MIP and NIP composite membranes were placed onto the surface of mouse skin. The differential transport of ibuprofen enantiomers across skin alone showed not to be significant (Figure 2.13). The transport of ibuprofen enantiomers through the control NIP membrane was not significantly difference (Figure 2.14b). For the MIP composite membrane, Figure 2.14a, the diffusion of *R*-ibuprofen enantiomer through MIP membrane and

skin slightly delayed compared to that of *S*-ibuprofen enantiomer. The observed differential release of ibuprofen enantiomers was however not to be statistically significant (p>0.05). The decrease in the enantioselectivity of MIP composite membrane *in situ* mouse skin than that of MIP composite membrane alone can be attributed to the effect of skin barrier.

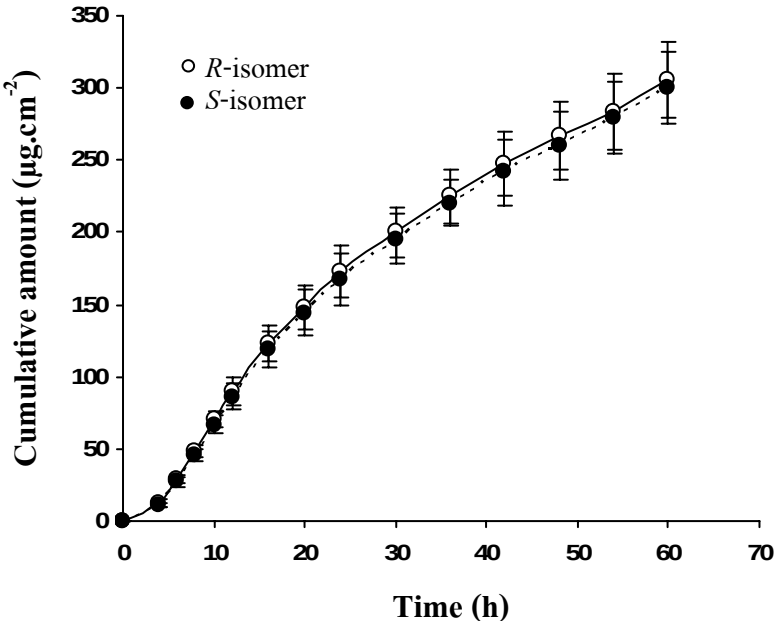

Figure 2.13. Permeation of ibuprofen enantiomers from pH 5.5 buffer solution across full-thickness mouse skin at 37±1°C (mean±SD, n=6).

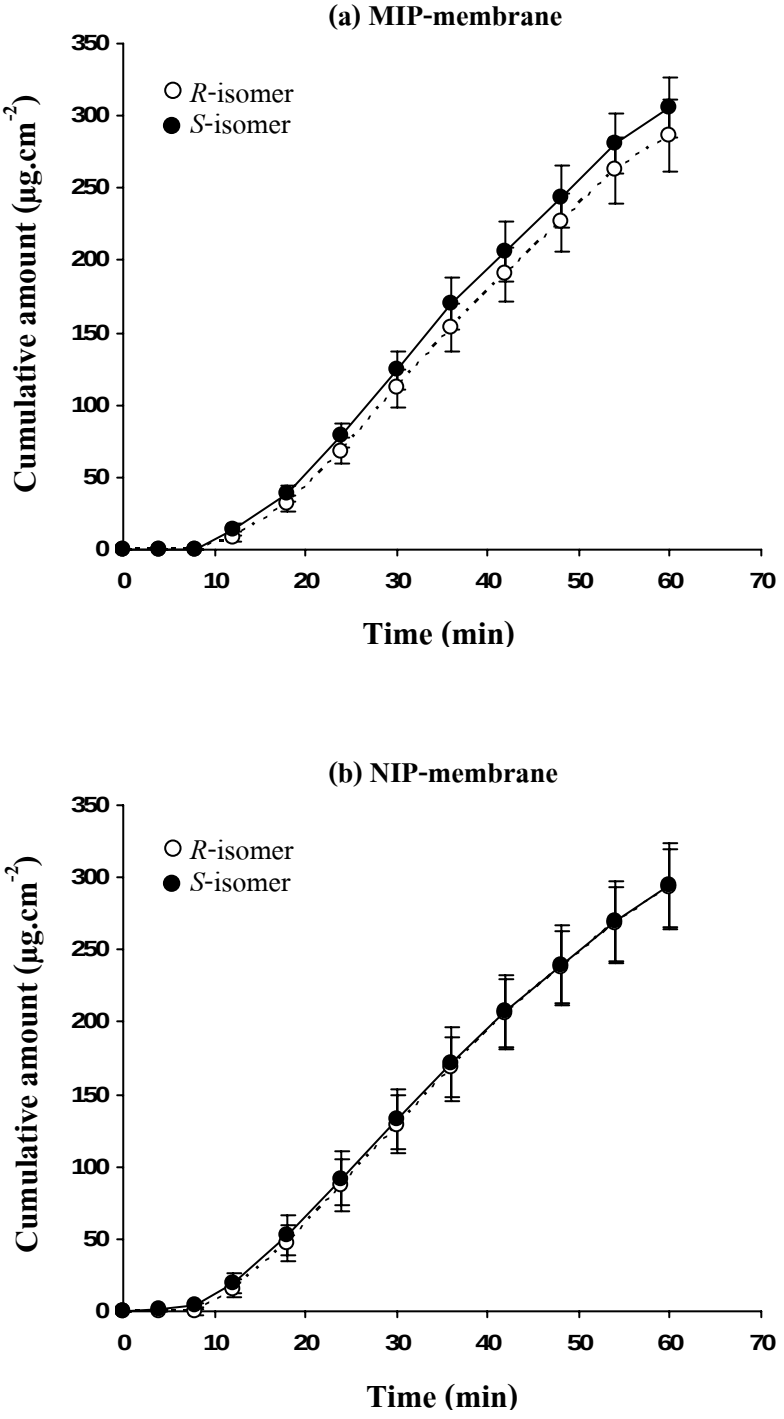

Figure 2.14. Permeation of ibuprofen enantiomers from pH 5.5 buffer solution across full-thickness mouse skin at 37±1°C in the presence of (a) *S*-ibuprofen-(ACM-*co*-MBA)-MIP composite cellulose membrane or (b) NIP composite cellulose membrane placed on the surface of mouse skin (mean±S.D., n=6).

In summary, the composite membrane composed of MIP layer that functionalized onto the cellulose membrane surface showed the modest enantioselectivity of the release of ibuprofen enantiomers. This low enantioselective release of *S*-ibuprofen enantiomer by the *S*-ibuprofen-MIP composite membrane can be attributed to the more deposition of MIP onto the surface of cellulose than at deeper layer membrane.

CHAPTER 3

THE MIP GRANULE COMPOSITE CELLULOSE MEMBRANE

3.1. Introduction and objectives

In this chapter, the MIP granule composite cellulose membranes had been prepared and their enantioselective release properties were examined. The selectivity of the pre-made MIP particles within the cellulose membrane can be examined as well as good dispersity of MIP into membrane might be obtained. Propranolol was the chiral drug of interest for this study. Methacrylic acid (MAA) (see structure in Figure 3.1) was used as the functional monomer. Ethylene glycol dimethacrylate (EDMA) which is a common cross-linker was chosen as the cross-linking agent due to its giving rigidity for the polymer. Propranolol (see structure in Figure 1.12) contains the amino and hydroxyl groups enable to the hydrogen bond formation with the carboxyl group of MAA functional monomer. MAA was found to have biocompatibility and non-toxicity. Since poly(methacrylic acid) are also used for producing pharmaceutical products such as pharmaceutical tablets, capsules, confectionary or food with water-based ingestible. Methacrylic acid-methacrylic acid ester copolymer with the trademark "Eudragit" is widely used as enteric polymer in controlled drug delivery (Devine et al., 2006; Smith et al., 2006). The methacrylic acid-based polymer exhibited no cytotoxic effects on the caco-2 cell cultures (Torres-Lugo et al., 2002; Foss and Peppas, 2004).

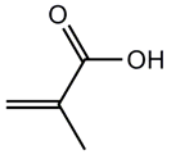

Methacrylic acid

Figure 3.1. Structure of functional monomer (MAA) used in this study.

In this study, the MIP granules selective to propranolol enantiomer were synthesized by bulk polymerization using MAA as functional monomer and EDMA as cross-linker. The selectivity of synthesized MIP granules was evaluated in term of selective rebinding of propranolol enantiomers. Further, the MIP granule composite cellulose membranes were prepared by a phase inversion using *N*-methylmorpholine-*N*-oxide (NMMO) as casting solvent. The ability in enantioselective rebinding of MIP granules and the ability in enantioselective release of MIP granule composite membranes were evaluated regarding to the content of drug (racemic propranolol): polymer granules ratio.

3.2. Experimental

3.2.1. Materials

Methacrylic acid (MAA), poly(caprolactone triol) (PCL-T), *RS*-propranolol HCl, *R*-propranolol HCl and *S*-propranolol HCl were purchased from Aldrich Chemical Company (Milwaukee, WI, USA). *N*-methylmorpholine-*N*-oxide (NMMO) was obtained from Fluka Chemie (Buchs, Switzerland). All solvents used were of analytical grade and were dried with molecular sieves before use. MAA was purified by distillation under reduced pressure. *R*- and *S*-propranolol used in this study were as free base. Five hundred mg *R*- or *S*-propranolol HCl was dissolved in 25 ml of distilled water to which an excess of a 0.5 M aqueous solution of sodium hydroxide (purity 99.99%, Aldrich) was added to precipitate the base. The precipitate was filtered off and dissolved in chloroform. The chloroform solution was then washed three times with distilled water and the organic layer was collected. The chloroform was removed under vacuum to yield propranolol base. Racemic propranolol was used as hydrochloride salt. Bacterial cellulose sheet was purchased locally in Songkhla, Thailand, under the Thai government's project "One Tombon, One Product" program (a government sponsored economic development program). The weight of the bacterial cellulose sheet was 273.33±32.14 $\mu g.cm^{-2}$ (n=3) and the thickness was 20-30 μm (as measured by SEM).

3.2.2. Stereospecific HPLC analysis and method validation for propranolol enantiomers

3.2.2.1. Stereospecific HPLC analysis

The amounts of enantiomers of propranolol and propranolol prodrugs were determined using the stereospecific HPLC method. The mobile phase for determination of propranolol and propranolol prodrugs enantiomers was prepared by comprising of 0.5% 2-propanol in 20 mM ammonium acetate buffer pH 4.1. The wavelength of the assay was set at 290 nm. The flow rate was set at 1 $ml.min^{-1}$ throughout and the temperature ambient ($25\pm1^{o}C$). The volume of injection was 20 µl. The retention times of *R*- and *S*-enantiomers of propranolol were 4.2 and 8.5 min, respectively.

3.2.2.2. Validation

In order to demonstrate whether the stereospecific HPLC method was suitable for determination of propranolol enantiomers in experiments, it was validated through the analysis of linearity, precision, accuracy, limit of detection and limit of quantification.

Linearity

The standard calibration curves were constructed separately for the *R*- and *S*-propranolol enantiomers, using racemic propranolol. The stock solution of *RS*-propranolol HCl was prepared at the concentration of 100 $\mu g.ml^{-1}$ by dissolving the *RS*-propranolol HCl in pH 7.4 buffer. The stock solution was diluted with pH 7.4 buffer to obtain the standard solutions of propranolol HCl at the concentrations of 1-20 $\mu g.ml^{-1}$. Each concentration was prepared in sets of three and each one was analyzed by stereospecific HPLC method in triplicate. To assess the linearity, the standard curves for propranolol enantiomers were constructed by plotting the concentrations ($\mu g.ml^{-1}$) of drug as function of peak area on HPLC chromatogram.

Precision

The precision was evaluated through repeatability and evaluated through relative standard deviation (RSD) at two different days. Three different concentrations (2, 5 and 10 $\mu g.ml^{-1}$) of racemic propranolol HCl were prepared in pH 7.4 buffer. Each concentration was prepared in sets of three and analyzed in triplicate.

Accuracy

The accuracy was evaluated by comparing the measured concentration with the actual concentration and expressed by %recovery which used the data obtained in precision study.

The limit of detection (LOD) and the limit of quantification (LOQ)

Calibration curves were constructed according to linearity study. The limit of detection (LOD) and the limit of quantification (LOQ) were calculated by equation 2.1 and 2.2.

3.2.3. Stability aspects of *R*- and *S*-propranolol

The stability of *R*- and *S*-propranolol was studied under the polymerization condition for MIP preparation and the release condition. *R*- and *S*-propranolol solutions were prepared in chloroform separately and made the final concentration to 10 $\mu g.ml^{-1}$. The solutions were incubated at $60^{o}C$ for 24 h. After incubation time, chloroform was evaporated and the samples were reconstituted with mobile phase before analyzed by stereospecific HPLC method. For the study drug stability in drug release condition, *R*- and *S*-propranolol HCl solutions were prepared in pH 7.4 buffer separately and made the final concentration to 10 $\mu g.ml^{-1}$. The solutions were incubated at room temperature ($30\pm1^{o}C$) and $37\pm1^{o}C$ for 7 days. The drug remained in the solutions was analyzed by stereospecific HPLC method. The stability was determined by comparing the amount of drug before and after incubation. Each experiment was carried out in triplicate.

3.2.4. Solubility study of racemic propranolol

The solubility of racemic propranolol HCl in pH 7.4 buffer was determined at room temperature (30±1^{o}C). An excess amount of racemic propranolol HCl was added into 5-ml vials containing 2 ml of pH 7.4 buffer. Vials were constantly agitated under 250 rpm for 24 h using magnetic bar and a magnetic stirrer. After 24 h, the solution was passed through a 0.2 µm filter, diluted with mobile phase and the amount of propranolol HCl solubilized was then measuring by using stereospecific HPLC method. The standard curve for racemic propranolol HCl was established in pH 7.4 buffer and from the slope of the standard curve the solubility of racemic propranolol HCl was calculated. The study was repeated in triplicate.

3.2.5. Synthesis of MIP granules

The MIP granules selective to either *R*- or *S*-propranolol enantiomers were prepared by using thermal polymerization using MAA as a functional monomer, EDMA as a cross-linker, AIBN as a radical initiator and chloroform as a porogen. Figure 3.2 shows the procedure for synthesis of MIP granules. The print molecule (*S*- or *R*-propranolol as free base) (2 mmol) was first dissolved in chloroform (15 ml) before addition of MAA (8 mmol), EDMA (0.05 mol) and AIBN (0.7 mmol). The imprinting mixture (in a 120-ml vial, 5 cm in diameter) was then degassed under vacuum for 5 min and purged with nitrogen gas for 5 min to remove oxygen (which acts as a radical scavenger) before closure the vial. The polymerization was performed by oven-heating the mixture at 60^{o}C for 24 h. The polymer matrix obtained was crushed with a mortar and pestle and sieved through a 100 mesh-sieve (that has sieve opening of 150 µm). The print molecule was extracted from the polymer particulates by sequential washing with 1:9 (v/v) acetic acid and methanol mixture (500 ml, three times) followed by washing with methanol several portions (500 ml, ~three times) until no residue of print molecule was found in the rinses, as verified by stereospecific HPLC analysis method. The resultant polymer was dried under vacuum for 24 h and stored at ambient temperature. Non-imprinted polymer (NIP), which was used as a control polymer to determine selectivity of the MIPs, was prepared in the same

procedure as the MIPs but no template molecule was included in the reaction mixture. The MIP and corresponding NIP granules synthesized in this study are summarized in Table 3.1.

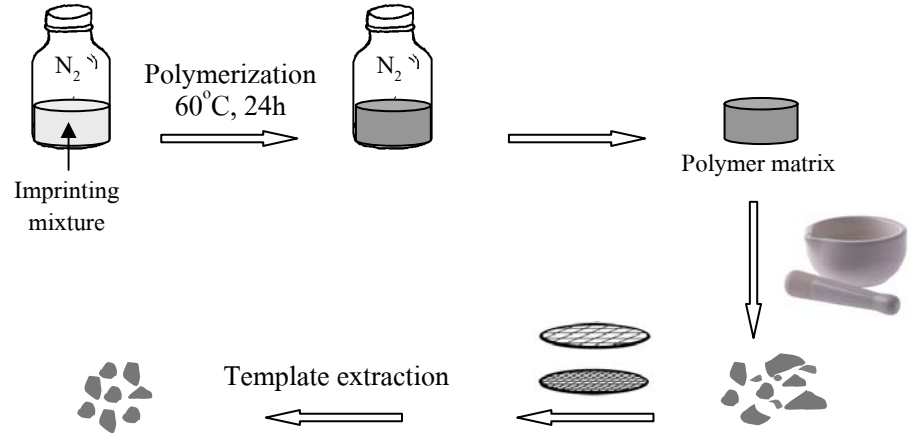

Figure 3.2. Schematic representation of the synthetic procedure of MIP granules.

Table 3.1. Types and compositions of MIP and corresponding NIP granules synthesized in this study.

Polymer	**Composition**		
	Template	**Functional monomer**	**Cross-linker**
R-MIP granule	*R*-propranolol	MAA	EDMA
S-MIP granule	*S*-propranolol	MAA	EDMA
NIP granule	-	MAA	EDMA

3.2.6. Evaluation of enantioselective binding of MIP granules

The ability of the MIP granules to selective rebind propranolol enantiomers from aqueous solution was investigated in a batch binding experiment. The study was investigated in pH 7.4 buffer which this pH value represents the physiological pH. Four different weights of MIP (2, 5, 10 and 15 mg) and separately, the corresponding NIP granules were incubated in 3 ml of pH 7.4 buffer containing 60 $\mu g.ml^{-1}$ racemic propranolol HCl at room temperature ($30\pm1^{o}C$) for 12 h to reach equilibrium. The incubated dispersions were centrifuged at 3000 G using a HERMLE rotor Z323K model (Wehingen, Germany) for 5 min. The concentrations of propranolol

enantiomers in the supernatant were determined using the stereospecific HPLC method. The amount of each enantiomer bound was calculated from the difference in concentrations before and after incubation. All experiments were run in triplicate.

3.2.7. Preparation of MIP granule composite cellulose membranes

In this experiment, the optimal ratio of cellulose and polymer particles was verified in terms of capability and performance of membrane. For this purpose, R-MIP, S-MIP or NIP granules were loaded in phase inversion cellulose membrane at three different concentrations, i.e., 18, 23 and 35% w/w of cellulose. In preliminary study, the ratio between cellulose and NMMO was varied until obtained the suitable membrane. The preparation of the composite cellulose membranes was described as following (see Figure 3.3): cellulose sheet (96 mg) was dispersed in an aqueous solution of NMMO (50% w/w) (5 ml). The suspension was then heated at 60-80^{o}C until cellulose mass dissolved and a clear, brown, viscous solution was appeared. Then PCL-T (0.3 ml) and appropriate amount of MIP granules were added. The polymer mixture was cast on a Petri-dish (10 cm in diameter). After 5 min, the generated membrane was transferred into a beaker containing 500 ml distilled water for 12 h. The resulting membranes with a surface area of 28 cm^2 were dried in air overnight and kept in a dessiccator for further use. The thickness of the prepared membranes varied between 50-70 μm as measured by a SEM (JEOL series JSM 5800LV, CA, USA). The control composite membranes were prepared as the MIP granule composite membranes but used NIP granules instead of MIP granules. The blank cast cellulose membrane was prepared using the procedure described above but in the absence of polymer particles.

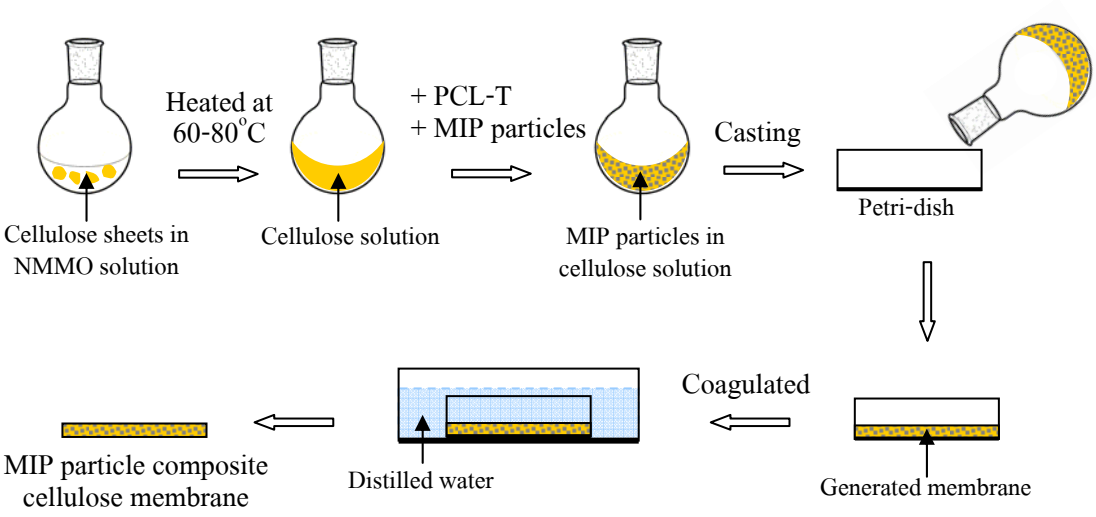

Figure 3.3. Schematic representation of the preparation of MIP particle composite cellulose membrane.

In addition, the MIP granule composite membranes containing racemic propranolol HCl were prepared for using in the study of enantioselective release of propranolol enantiomers from the MIP granule composite membranes (Section 3.2.10). In this case, the racemic propranolol HCl and MIP granules mixture was prepared before loading into cellulose solution. The mixture of 100 mg of MIP granules containing 10 mg of racemic propranolol HCl was first prepared for sample dilution. Thirty five milligram of granules was then titrated with aliquots of the drug by physical mixing. The corresponding drug-polymer mixture (containing 35 mg of MIP granules) was added into the cellulose solution. Drug: polymer weight ratios of 1:5, 1:20, 1:35, 1:70 and 1:170 were employed. The entrapment of racemic propranolol HCl in each of the composite membranes was examined by measuring the drug content in the washing solution derived from the cast membranes (n=3) using the stereospecific HPLC analysis method and the amount of drug entrapped was obtained by subtracting the amount of drug in the rinse solution from the amount of formulation. The control composite cellulose membranes containing NIP granules were prepared using the same methodology as the equivalent MIP granule composite cellulose membranes, with drug being included in the reaction mixture in the same ratios.

3.2.8. Characterization of MIP granules and MIP granule composite membranes

3.2.8.1. Morphology of polymer particles and composite membranes

The morphology of polymer particles and membranes (original cellulose membrane, blank cast cellulose membrane (without polymer particles loading), and MIP granule composite membrane) were examined by SEM (JEOL series JSM 5800LV, CA, USA). The samples were sputter-coated with gold before imaging, using an accelerating voltage of 20 kV. The particle size of polymer particles and pore size of membranes were estimated from the pictures obtained by SEM (n=10).

3.2.8.2. Porosity of polymer particles

The porosity of polymer particles was determined by nitrogen adsorption/desorption analysis using a nitrogen surface area analyzer (SA3100, Beckman Coulter, Hialeah, FL, USA). Prior to measurement, 200 mg of the polymer particles were heated at 80^{o}C for 5 h in vacuum. The specific surface areas were calculated using the BET method, and the specific pore volumes and average pore diameters were calculated according to the BJH method.

3.2.8.3. Degree of swelling of polymer particles

The degree of swelling of polymer particles was evaluated in chloroform, methanol, pH 5.5 and pH 7.4 buffers, since these mediums were related to the preparation and the application of MIP particles. Chloroform is solvent used in MIP synthesis, methanol is the template extracting solvent, and pH 5.5 and pH 7.4 buffers were related to the enantioselective release study. The polymer particles were vacuum-dried at room temperature (30±1^{o}C) for at least 3 days before testing. The polymer particles were then placed in a syringe (2.0 ml in capacity) to obtain the volume of 500 µl then 1.5 ml individual solvents were placed to incubate the polymer particles at room temperature (30±1^{o}C) for 12 h (the volume of wet particles reached stable).

Each experiment was run in sets of three. The degree of swelling of the polymer particles (%) was calculated from the equation:

$$\text{Degree of swelling (\%)} = \frac{V_2 - V_1}{V_1} \times 100 \quad (3.1)$$

Where; V_1 and V_2 are the volumes of dried and wet samples, respectively.

3.2.8.4. Mechanical property of composite membranes

The mechanical strength of blank cast membrane and composite membranes with different contents of MIP granules loading was measured. Each membrane was tested in triplicate. The method used for measurement was as described in Section 2.2.6.6.

3.2.8.5. Friability of composite membranes

The loss of polymer particles from the composite membranes was examined using friability apparatus (Eraweka Abrasion Tester) operated at a constant speed of 25±1 rpm. Samples from MIP granule and corresponding NIP granule composite membranes were rotated in apparatus until the weight of membranes remained constant (about 30 min). Each experiment was run in sets of three. The percentage of particles loss from the membrane was calculated according to the following equation:

$$\%\text{friability} = \frac{W_1 - W_2}{W_1} \times 100 \quad (3.2)$$

Where; W_1 and W_2 is the initial and final weight of membrane, respectively.

In addition, the change in membrane resistance of the composite membranes after each friability test was determined using the method described in Section 2.2.6.5.

3.2.9. Determination in enantioselective transport of MIP granule composite membranes

The ability of MIP granule composite membranes in enantioselective transport of propranolol enantiomers was determined using vertical Franz-type diffusion cell with a normal receptor volume of 2.5 ml and diffusional area of 0.8 cm^2. The cell flanges were greased with high performance vacuum grease and the cellulose membrane composing MIP granules was placed between the receptor and donor compartments of a vertical Franz-type diffusion cell. Clamps were used to hold the membrane into position. The donor phase was contained 1 ml of 40 $\mu g.ml^{-1}$ racemic mixtures of propranolol HCl in pH 7.4 buffer and the receptor phase was contained 2.5 ml of pH 7.4 buffer. The receptor phase was stirred with a magnetic bar constantly at 250 rpm. 200 µl samples were taken at appropriate time points between 0-6 h and were replaced by the same volume of fresh buffer. Each test was carried out in sets of three. The diffusion of each propranolol enantiomer was determined using the stereospecific HPLC method. The cumulative amount ($\mu g.cm^{-2}$) of each enantiomer permeated was calculated and plotted as a function of time (min). The diffusion coefficient (D, $\mu m^2.min^{-1}$) was calculated as the equation 2.7 and the enantioselectivity was defined as the ratio of D of the *S*-isomer to that of the *R*-isomer (or *R*-isomer to that of the *S*-isomer). Control experiments were carried out with cellulose membrane containing NIP particles.

3.2.10. Determination in enantioselective release of MIP granule composite membranes

In this study, the ability of MIP granule composite membranes in enantioselective-controlled release of propranolol enantiomers was evaluated by dissolution testing method. The composite membranes were prepared as that the MIP granules were loaded together with the racemic propranolol HCl in the cellulose membrane. The test membrane (1.5cm×1.5cm) was placed in 3 ml of pH 7.4 buffer which was stirred at a rate of 250 rpm using a magnetic bar. Samples (200 µl) were withdrawn at appropriate time points between 0-6 h and these were replaced by the same volume of fresh buffer. Each test was carried out in triplicate at

room temperature (30±1^{o}C) and the release of each propranolol enantiomer was determined using the stereospecific HPLC method. The flux (J, μg.cm^{-2}.h^{-1}) of each propranolol enantiomer from the membrane loaded with different ratios of drug: polymer was measured from the best fit linear slope of graph (over 60-180 min) plotted between the cumulative amount of drug release per unit area (μg.cm^{-2}) as function of time (h). The diffusion coefficient (D, cm^{2}.h^{-1}) was obtained from the equation:

$$D = \frac{Jx}{C} \tag{3.3}$$

Where; C (μg.cm^{-3}) is the concentration of propranolol enantiomer inside the membrane.

x (cm) is the membrane thickness as measured by SEM.

Control experiments were carried out using the composite cellulose membranes containing NIP granules, in order to examine selectivity of the MIP granule composite membranes.

3.2.11. Statistic analysis

Statistical analyses were carried out using SPSS version 13.0 (SPSS, Cary, NC, USA). Paired *t*-tests were used to investigate differences of *R*- and *S*-propranolol enantiomers in every experimental test. A *p*-value of <0.05 was considered significant.

3.3. Results and discussion

3.3.1. Method validation

The linearity, precision, accuracy, limit of detection (LOD) and limit of quantification (LOQ) of propranolol enantiomers from stereospecific HPLC assay were summarized in Table 3.2. The standard curves for propranolol enantiomers showed good linearity

in the range of 1-20 μg.ml^{-1}, with correlation coefficients (R^2) of higher 0.999 of both *R*- and *S*-propranolol enantiomers. The repeatability demonstrated small RSD for each day analyzed (lower 0.92% in the first day and lower 1.56% in the second day for both *R*- and *S*-enantiomers). The accuracy was found in the range of 99.32-100.53% for both *R*- and *S*-propranolol enantiomers. These results suggested that the method was accurate and precise for analysis of propranolol enantiomers in the concentration range of validation (1-20 μg.ml^{-1}).

Table 3.2. Linearity, precision, accuracy, limit of detection (LOD) and limit of quantification (LOQ) of propranolol enantiomers from stereospecific HPLC assay.

Isomer	**Linearity (R^2)**	**Precision (%RSD)**	**Accuracy (%recovery)**	**LOD (μg.ml^{-1})**	**LOQ (μg.ml^{-1})**
R-propranolol	0.9997	0.84[a], 1.20[b]	99.93[a], 100.53[b]	0.06	0.18
S-propranolol	0.9998	0.91[a], 1.55[b]	99.32[a], 100.16[b]	0.08	0.26

[a] refer to %RSD or %recovery of propranolol enantiomers in the first day.

[b] refer to %RSD or %recovery of propranolol enantiomers in the second day.

3.3.2. Stability of *R*- and *S*-propranolol

To ensure that propranolol enantiomers were stable in the conditions of experiments, the stability of *R*- and *S*-propranolol enantiomers was investigated in the polymerization condition and in the drug release condition. The results of stability study showed that more than 99% content of both *R*- and *S*-propranolol enantiomers was found after 7 days incubation in pH 7.4 buffer at room temperature (30±1^{o}C) and 37±1^{o}C and after 24 h incubation in chloroform at 60^{o}C. These results indicated that propranolol enantiomers had good stability under the conditions studied.

3.3.3. Solubility of racemic propranolol

The solubility of racemic propranolol HCl in pH 7.4 buffer at 30±1^{o}C was 73.4±3.2 mg.ml^{-1}.

3.3.4. MIP granules synthesis and characterization

The MIP granules were synthesized by radical polymerization using MAA as functional monomer, EDMA as cross-linker, *R*- or *S*-propranolol as template and chloroform as porogen. The bulk polymerization was accomplished by AIBN that generated free radical at 60^{o}C. After polymerization step, the polymer particles were sequentially washed with 1:9 (v/v) acetic acid and methanol mixture and methanol in order to remove the unreacted monomers and template molecules. Figure 3.4 shows scanning electron micrographs of MIP granules. The monolithic particles obtained after bulk polymerization, followed by grinding and sieving have an irregular, rough morphology with diameters ranging of 15-35 μm. Table 3.2 shows physical properties (i.e., particle size, porosity and degree of swelling) of MIP and NIP granules. The pore structure (total pore volume and average pore diameter) of the R-MIP and S-MIP granules was found to be similar and was slightly higher than NIP particles. The surface area of MIP particles was slightly larger than NIP particles. Large surface area was convenient for the analytes to diffuse and be adsorbed (Qin et al., 2008). The polymer particles composing of poly(MAA-*co*-EDMA) can swell in polar solvents (methanol and aqueous media) better than in non-polar solvent (chloroform). The rather high swelling of MIP granules in methanol would favor in template extraction.

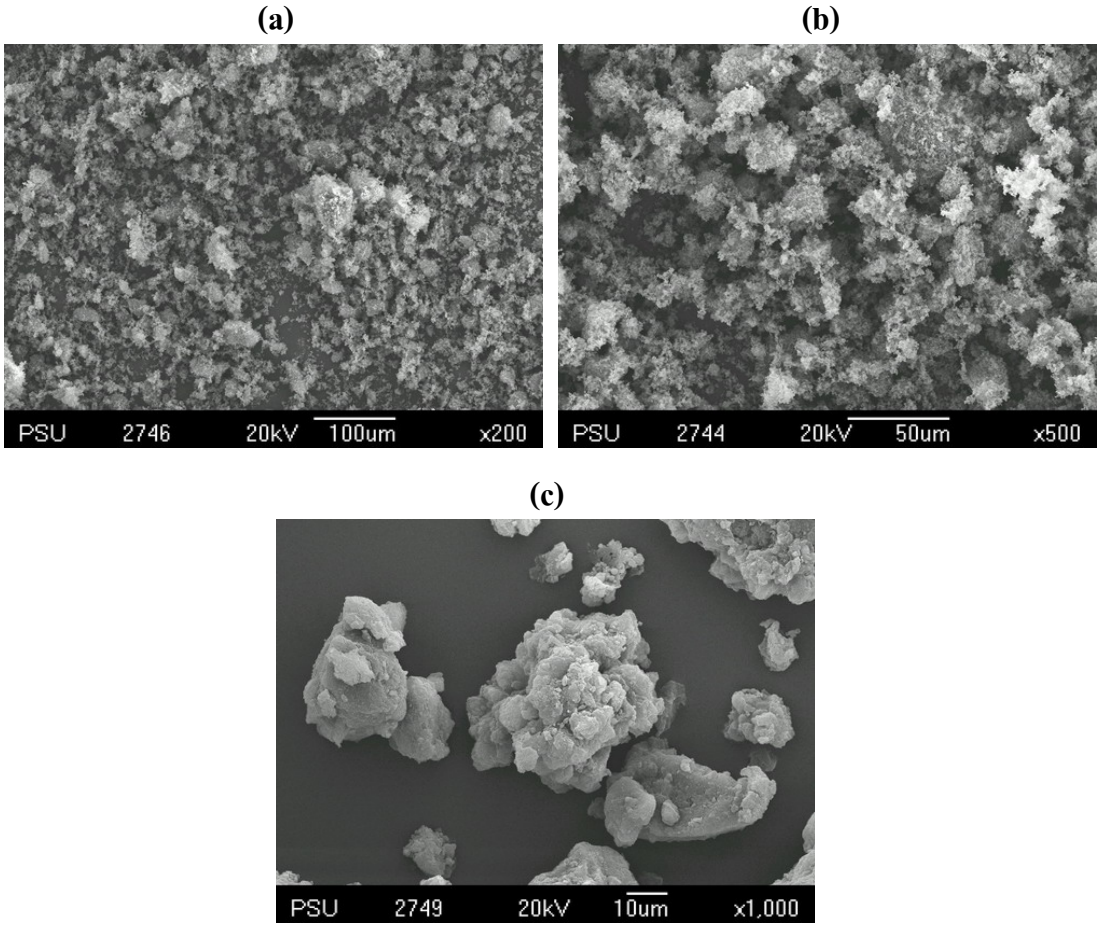

Figure 3.4. SEM images of MIP granules at (a) ×200, (b) ×500, and (c) ×1,000 magnifications.

Table 3.3. Physical properties of MIP and corresponding NIP granules (mean±S.D., n=3).

Polymer	Particle size*	Porosity			Degree of swelling (%)			
	(µm)	Surface area ($m^2.g^{-1}$)	Total pore volume ($ml.g^{-1}$)	Average pore diameter (nm)	methanol	chloroform	pH 5.5	pH 7.4
R-MIP granule	23.81±14.33	62.53	0.243	39.18	96.3±2.7	24.6±2.3	100.6±7.0	84.8±8.9
S-MIP granule	24.25±10.40	64.30	0.244	39.36	98.0±5.4	25.5±1.3	120.4±6.0	76.4±6.1
NIP granule	24.89±10.16	54.92	0.130	38.0	78.0±5.6	20.0±1.9	80.5±6.4	70.2±3.3

*n=10

3.3.5. Enantioselective binding of MIP granules

The enantioselective binding ability of individual polymer particles (R-MIP granule, S-MIP granule and NIP granule) in pH 7.4 buffer at the polymer particle content of 10 mg and the incubation drug concentration of 60 μg.ml^{-1} is shown in Figure 3.5. The MIP granules bound the template enantiomer higher than non-template enantiomer, i.e., R-MIP granule bound *R*-propranolol enantiomer higher than *S*-propranolol enantiomer, while S-MIP granule bound *S*-propranolol enantiomer higher than *R*-propranolol enantiomer. However, the enantioselectivity obtained from R-MIP granule and S-MIP granule was very low (*R/S* or *S/R* ratios <1.1). The control NIP granule bound propranolol enantiomers slightly lower than MIP granules with no enantioselectivity (*R/S* or *S/R* ratios ≈1.0). Since the NIP did not have any specific cavities, the binding amount obtained in NIP granule would be from non-specific binding.

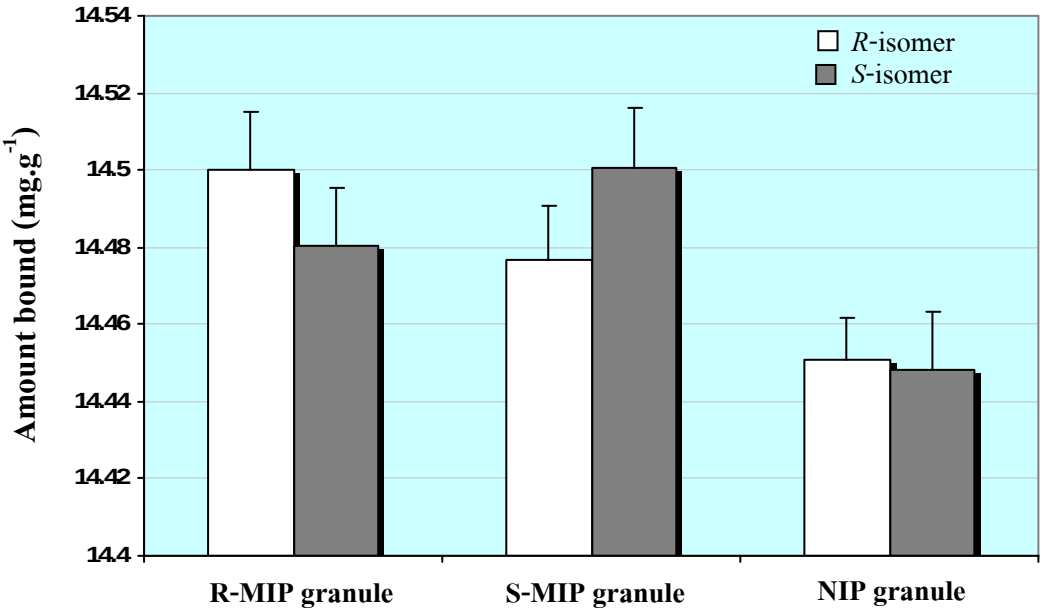

Figure 3.5. Amount bound (mg.g^{-1}) of propranolol enantiomers for R-MIP, S-MIP and NIP granules after incubation with racemic propranolol HCl in pH 7.4 buffer at room temperature (30±1^{o}C) (mean±S.D., n=3).

Figure 3.6 shows the enantioselective binding ability of the S-MIP granule and corresponding NIP granule when different amounts of granules were incubated with a fixed concentration of racemic propranolol HCl (60 μg.ml^{-1}) in pH 7.4 buffer solution at room temperature (30±1^{o}C). The MIP granule showed %bound slightly higher than NIP granule in every polymer content. This may be due to the higher porosity of MIP granule compared to NIP granule. The %bound was slightly increased with the increase of polymer contents which can be observed in both MIP and NIP granules. The S-MIP granule bound the template *S*-propranolol enantiomer higher than *R*-propranolol enantiomer, however the differences were statistically insignificant (p>0.05) over the entire range of polymer content. It would indicate that the production of granules led to the generation of a material that displayed high non-specific binding sites.

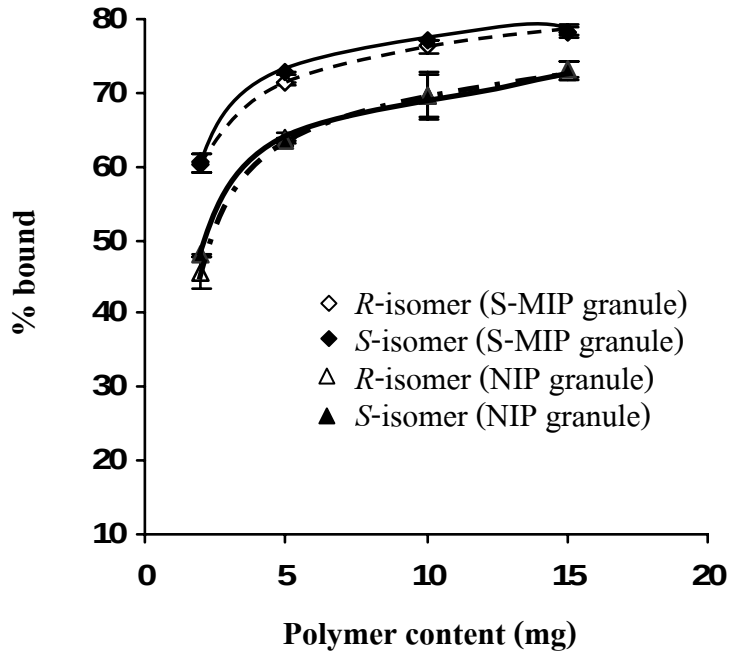

Figure 3.6. The percentage of bound propranolol enantiomers after incubation of different weights of S-MIP and NIP granules with 60 μg.ml^{-1} racemic propranolol HCl in pH 7.4 buffer solution at room temperature (30±1^{o}C) (mean±S.D., n=3).

3.3.6. MIP granule composite membranes preparation and characterization

Cellulose does not dissolve in most conventional solvents due to the strong hydrogen bonds that exist between cellulose chains (see Figure 1.9). There are variety solvents exploited for dissolving cellulose but most of them are complex solvent systems and environmentally hazardous problems. *N*-methylmorpholine-*N*-oxide (NMMO) was discovered and become the most powerful solvent, which can be used as single component solvent. NMMO is normally used for manufacture of textile cellulose fibers and filaments with environmentally friendly (Fink et al., 2001; Heinze and Koschella, 2005). The morphology of membrane is considered to strongly influence the transport properties. Dense membranes are generally less permeable but provide more stringent selectivity of small compound, compared with more porous counterparts. The presence of plasticizer in membrane preparation can affect the permeation of drug through a membrane because the plasticizer agent can reduce the intermolecular forces between the polymer chains, increasing the free volume. The amounts of cellulose, NMMO, poly(caprolactone triol) (PCL-T) and MIP particles were optimized to obtain good performance composite membrane.

Figure 3.7 shows SEM images of (a) the original cellulose membrane and (b) a cellulose membrane with no added components after casting. The bacterial cellulose membrane comprised a porous pellicle with good mechanical strength. After casting, the bacterial cellulose is converted to non-porous membrane with a smooth surface. The mechanical strength of the cast bacterial cellulose membrane (tensile strength = 1.53 $kN.cm^{-2}$) was markedly lower than that of the original (tensile strength = 10.16 $kN.cm^{-2}$). However, the swelling properties in water of the cast bacterial cellulose membrane (147.50±24.74%) were not significantly different to the original membrane (122.72±16.42%).

When PCL-T was added to the bacterial cellulose membrane during phase inversion, then numerous pores were introduced into the matrix (Figure 3.7c). The introduction of PCL-T has been reported previously to promote pore formation within polymer membranes (Meier et al., 2004). In this study the bacterial cellulose membrane cast in the presence of PCL-T was more flexible and the tensile strength was lower (1.35±0.13 $kN.cm^{-2}$) than the bacterial cellulose membrane prepared in the absence of the added component.

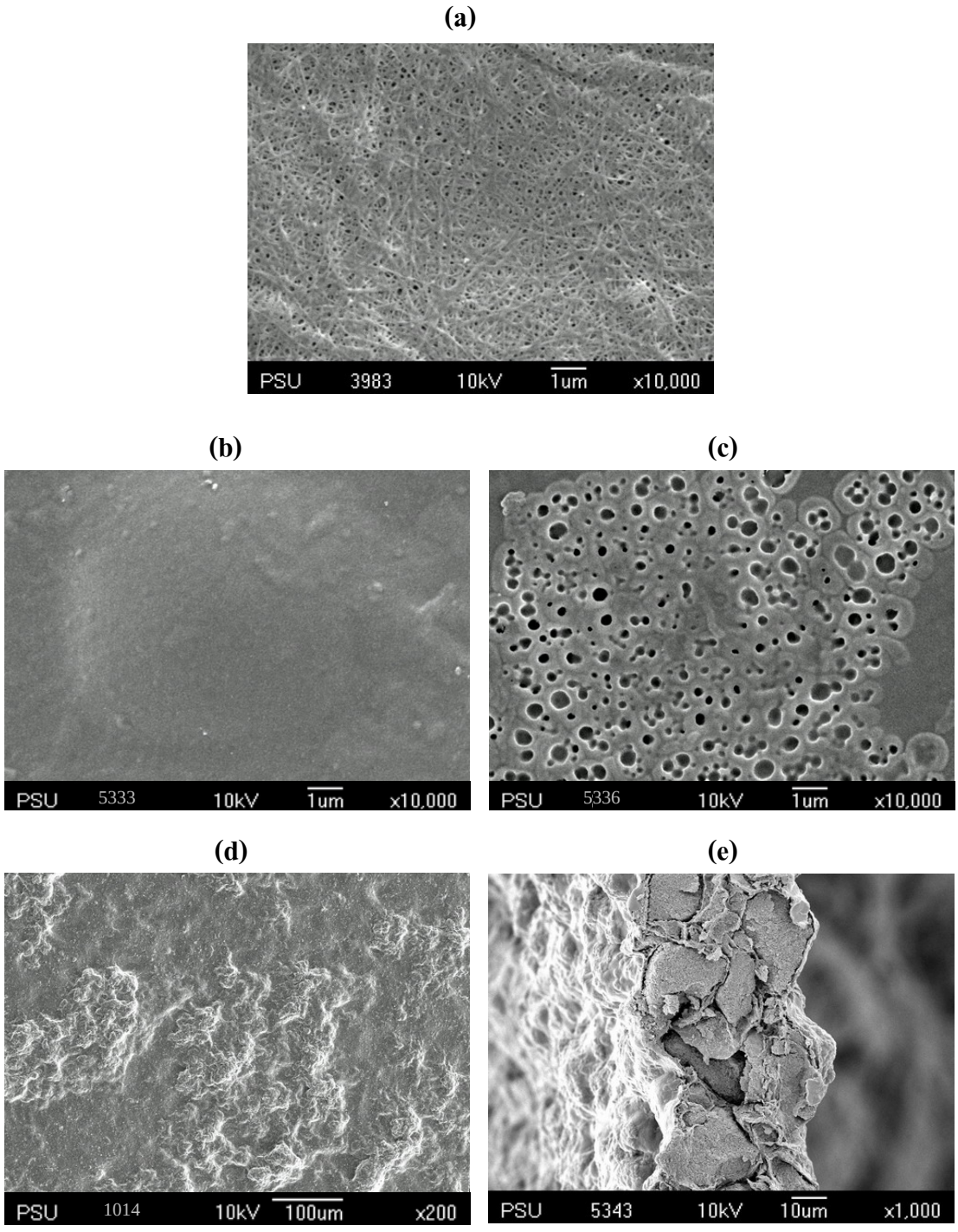

Figure 3.7. SEM images of (a) original bacterial cellulose, (b) cast cellulose without PCL-T, (c) cast cellulose with PCL-T, (d) surface and (e) cross-section of MIP granule (35% w/w) composite membrane.

The surface morphology and cross-sectional architecture of bacterial cellulose membrane loaded with MIP granules (35% w/w) are also shown in Figure 3.5d and e. The SEM images showed that the surface of the membrane that contained particles exhibited a rough appearance with quite low porosity. This may have been due to the bulkiness of the polymer granules coupled with their tendency to form aggregates, which packed in a layer at the bottom of the composite membrane.

The physical properties (i.e., pore size, membrane resistance, tensile strength and friability) of the bacterial cellulose composite membrane containing 35% w/w granules are shown in Table 3.3. The physical properties studied showed no difference between MIP and corresponding NIP granule composite membranes. The pore size of granule-containing composite membranes, which exhibited quite low porosity as revealed in Figure 3.5d, was in the range of 0.3-0.4 μm. The friability of membranes was reduced about 2-3% after the test. The electrical resistance of the membranes was redetermined, after the friability test had been carried out but this was found to change less than 2.5%. The composite membranes retained a good appearance after testing.

Table 3.4. Characteristics of MIP and NIP granule composite membranes (mean±S.D., n=3).

Membrane	**Polymer loaded (%)**	**Pore size* (μm)**	**Membrane resistance ($\Omega.cm^2$)**	**Tensile strength ($kN.cm^{-2}$)**	**Friability (%)**
MIP granule	35	0.3 ± 0.05	1.26 ± 0.42	0.25 ± 0.20	2.60 ± 0.19
NIP granule	35	0.4 ± 0.10	1.26 ± 0.42	0.50 ± 0.33	3.11 ± 0.31

* n=10

3.3.7. Mechanical property of MIP granule composite cellulose membranes

In this section, the optimal content of MIP granules loaded into cellulose membrane was evaluated. MIP granules were loaded in self-assembly porous cellulose membrane at three different contents: 18, 23 and 35% w/w of cellulose. Figure 3.8 shows the tensile strength of composite membranes which loaded with those three different contents of MIP granules compared to the cast membrane with no polymer particles loading. It was found that polymer particles loaded into cellulose membrane caused a decrease in the strength of the membrane. The cellulose membrane loaded with polymer particles at 18% w/w showed about 4-fold lower tensile strength than the cast cellulose membrane without polymer particles. In addition, there was no difference in tensile strength of cellulose membranes loaded with polymer particles in the range of 18-35% w/w. However, when MIP granules were loaded in higher content (> 35% w/w), the membrane became unstable.

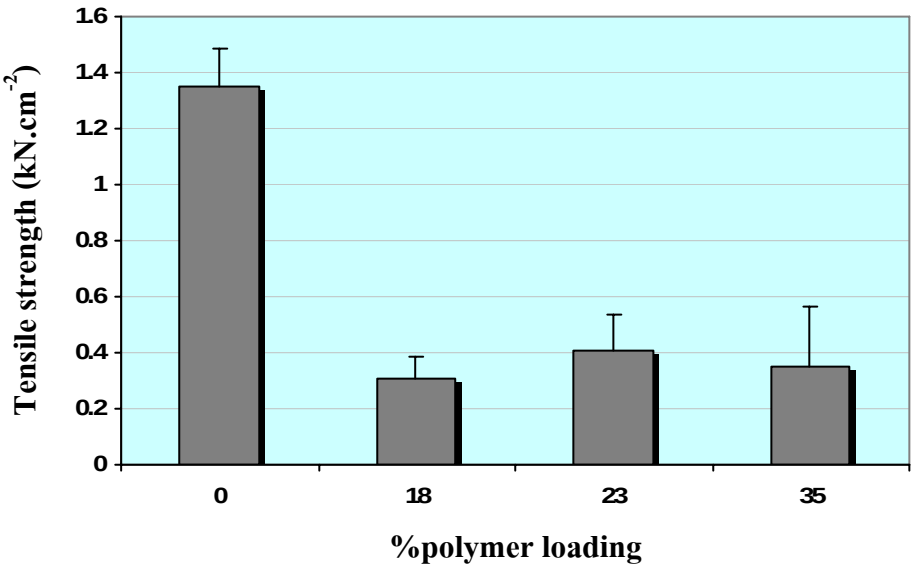

Figure 3.8. Tensile strength of MIP granule composite membranes in different contents of MIP granules (18, 23 and 35% w/w) compared to the cast cellulose membrane without polymer particles loading (mean±S.D., n=3).

3.3.8. Enantioselective transport of propranolol enantiomers across MIP granule composite membranes

To determine the enantioselective transport of composite membranes, permeation experiment of racemic propranolol HCl in pH 7.4 buffer solution was carried out, using a vertical Franz-type diffusion cell. The cast cellulose membrane without polymer particles, cellulose membrane loaded with R-MIP granules, cellulose membrane loaded with S-MIP granules and control membrane (cellulose membrane loaded with NIP granules) were tested. Figure 3.9 shows the time course of *R*- and *S*-enantiomers of propranolol HCl permeated across composite cellulose membranes loaded with R-MIP and S-MIP granules (35% w/w) when 40 $\mu g.ml^{-1}$ of racemic propranolol HCl in pH 7.4 buffer was loaded into donor phase. The selective transport of the enantiomers was achieved by means of enantiospecific interactions between the active imprinted polymer particles and the propranolol HCl. It was evidenced that MIP in the membrane retarded the transport of template isomer. *S*-propranolol enantiomer was diffused through R-MIP granule composite membrane faster than *R*-propranolol enantiomer, while *R*-propranolol enantiomer was diffused through S-MIP granule composite membrane faster than *S*-propranolol enantiomer. This implied that the template isomer was preferentially adsorbed on MIP granules. The permeability of MIP granule composite membranes was quite low which propranolol enantiomers were permeated in lower amount than 20% in 3 h due to quite compact texture with low porosity of MIP granule composite membranes.

The transport measurements with racemic propranolol HCl indicated an initial delay for diffusion (higher sorption) and an overall faster transport of the opposite imprinted enantiomer (Table 3.5). Further increase in polymer loading resulted in a decrease in the diffusion of propranolol enantiomers, but the enantioselectivity increased from 1.07 to 1.42 for cellulose membrane loaded with R-MIP granules and from 1.07 to 1.31 for cellulose membrane loaded with S-MIP granules. Cellulose membrane loaded with NIP granules did not show any enantioselectivity under identical conditions. The *S/R* selectivity as high as 1.4 was achieved with the R-MIP granule composite cellulose membrane, while the *S*/*R* ratio of diffusion for the control membranes were approximately 1.0 for any loading contents. The enantioselectivity of both S-MIP granule and R-MIP granule composite membranes at the %polymer loading of 23 and 35

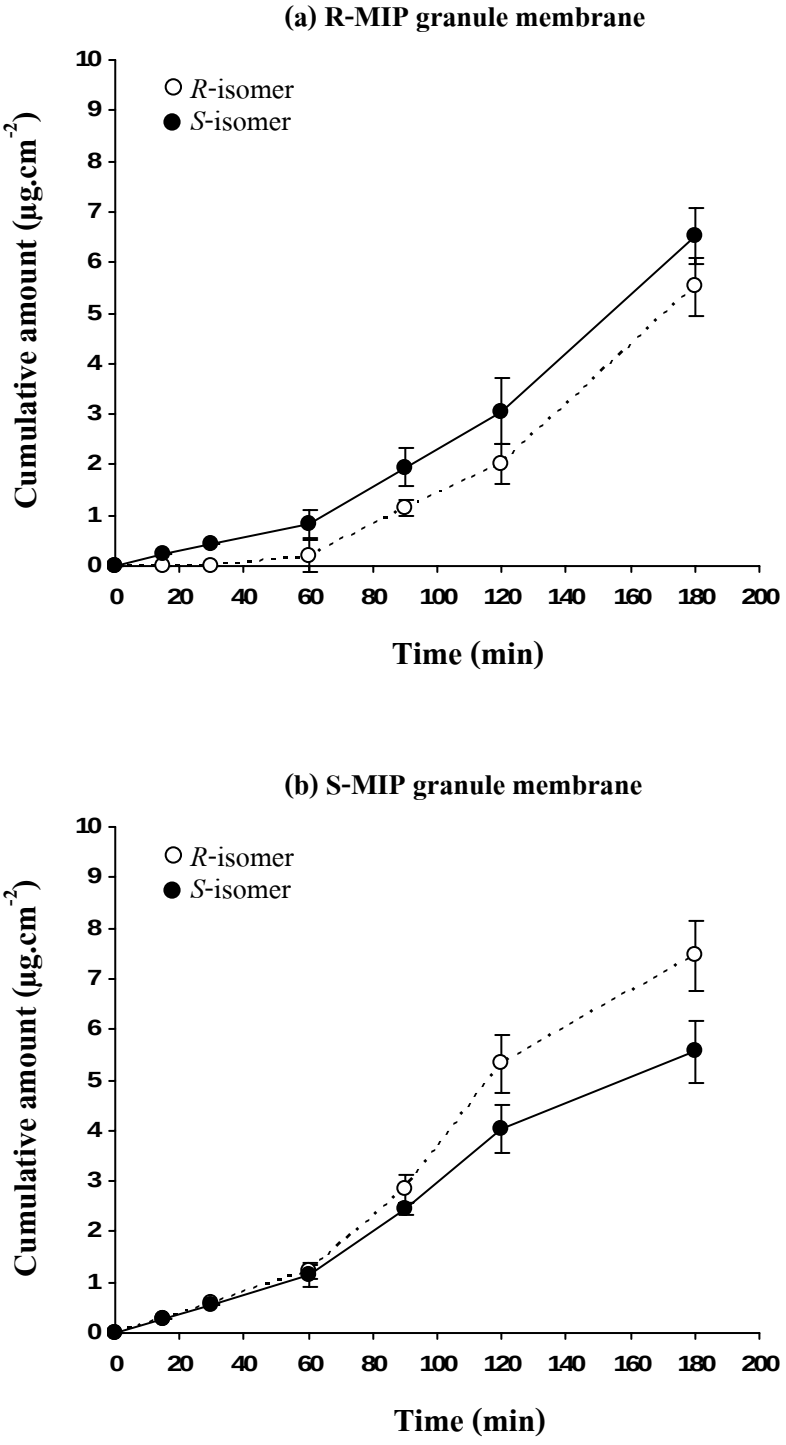

Figure 3.9. Cumulative amount (µg.cm^{-2}) of propranolol enantiomers transport across cellulose membranes loaded with (a) R-MIP granules and (b) S-MIP granules at 35% w/w (mean±S.D., n=3).

were found to be statistically significant (p<0.05) compared with each NIP granule composite membrane. But the differences in enantioselectivity between MIP and NIP granule composite membranes at the %polymer loading of 18 were statistically insignificant (p>0.05). The permeation result of blank cast cellulose membrane (without polymer particles loading) revealed that cellulose membrane was not able to produce enantioselective transport of propranolol enantiomers. However, the previous work showed that the parent cellulose membrane gave a high enantioselective release for propranolol enantiomers which *S*-propranolol enantiomer was released higher than *R*-propranolol enantiomer (Bodhibukkana et al., 2006). The decrease in enantioselectivity of the cast cellulose membrane may be due to the reduction in crystallinity of bacterial cellulose membrane (see Figure 5.10).

Table 3.5. Diffusion coefficient (D) of cast cellulose membrane without polymer particles loading, and cellulose membranes loaded with NIP, R-MIP and S-MIP granules in different contents (18, 23 and 35% w/w) (mean±S.D., n=3).

Membrane	**% polymer loaded**	***D*** **(μm^2.min^{-1})**		
		***R*-isomer**	***S*-isomer**	**Enantioselectivity***
Cast cellulose	-	24.19 ± 1.73	24.72 ± 1.06	1.02 ± 0.01
R-MIP$_1$ granule	18	21.14 ± 1.32	22.57 ± 1.50	1.07 ± 0.01
S-MIP$_1$ granule	18	25.34 ± 1.06	23.57 ± 0.92	1.07 ± 0.01
NIP$_1$ granule	18	19.48 ± 0.63	18.86 ± 1.71	1.03 ± 0.01
R-MIP$_2$ granule	23	15.67 ± 2.77	18.24 ± 2.76	1.16 ± 0.05
S-MIP$_2$ granule	23	20.45 ± 1.43	17.84 ± 2.20	1.15 ± 0.02
NIP$_2$ granule	23	18.34 ± 1.60	18.63 ± 1.51	1.01 ± 0.01
R-MIP$_3$ granule	35	13.71 ± 0.86	19.53 ± 1.35	1.42 ± 0.03
S-MIP$_3$ granule	35	20.31 ± 1.35	16.65 ± 1.22	1.31 ± 0.08
NIP$_3$ granule	35	15.83 ± 0.42	16.36 ± 0.88	1.03 ± 0.02

* refer to *S*/*R* ratio for R-MIP granule composite membrane and *R*/*S* ratio for S-MIP granule composite membrane.

3.3.9. Enantioselective release of propranolol enantiomers from MIP granule composite membranes

The purpose of this section was to determine the ability of S-MIP granule composite membrane for control the release of propranolol enantiomers which loaded together with S-MIP granules in the composite membrane. The total amount of drug incorporated in S-MIP granule and corresponding NIP granule composite membranes at various drug: polymer ratios is displayed in Table 3.6. The amounts of *R*- and *S*-propranolol enantiomers incorporated in the S-MIP granule and corresponding NIP granule composite membranes were not significantly different for the equivalent drug: polymer ratios. Also, there were no stereoselective differences in the amounts of propranolol enantiomers entrapped in the S-MIP granule or NIP granule composite membranes. Sequential release study, the diffusion coefficient of *S*-propranolol enantiomer and the enantioselectivity of S-MIP granule composite cellulose membranes at different drug: polymer ratios are shown in Figure 3.10. The cumulative amounts of the individual propranolol enantiomers released from the S-MIP granule composite membrane at the drug: polymer ratio of 1:35 were plotted as a function of time and those are shown in Figure 3.11. The cumulative release from the corresponding NIP membrane was also determined for comparison purposes. As shown in Figure 3.11, both *R*- and *S*-propranolol enantiomers were released faster through the NIP granule composite membrane than through the S-MIP granule composite membrane. The resulting curves indicated that the template *S*-propranolol enantiomer was slightly facilitated to release across S-MIP granule composite membrane compared to the *R*-propranolol enantiomer. As the polymer loading increased the diffusivity of propranolol enantiomers was slightly decreased (Figure 3.10). As a consequence of the nature of granules, which have a high volume/weight ratio, the MIP granules could not be loaded into the membrane at higher content than 35% w/w. The maximum loading of granular MIP was 1:170, drug: polymer weight ratio. The *S/R* selectivity obtained from S-MIP granules-loading membrane did not change with increased polymer loading and a low *S*/*R* selectivity (~1.1) was obtained for all drug: polymer ratios employed.

Table 3.6. The entrapment of propranolol enantiomers in the membranes loaded with different drug: polymer granules ratios (mean±S.D., n=3).

Drug: polymer ratio	Entrapment (μg.cm^{-2})			
	MIP granule membrane		NIP granule membrane	
	***R*-isomer**	***S*-isomer**	***R*-isomer**	***S*-isomer**
1:5	104.6 ± 9.0	106.0 ± 10.2	104.2 ± 10.2	106.0 ± 9.0
1:20	19.9 ± 1.8	21.2 ± 2.8	20.8 ± 2.0	21.2 ± 1.8
1:35	10.4 ± 1.0	10.6 ± 0.9	9.9 ± 1.4	9.9 ± 0.9
1:70	4.9 ± 0.4	5.0 ± 0.4	5.0 ± 0.3	5.2 ± 0.5
1:170	2.6 ± 0.3	2.6 ± 0.2	2.4 ± 0.2	2.6 ± 0.3

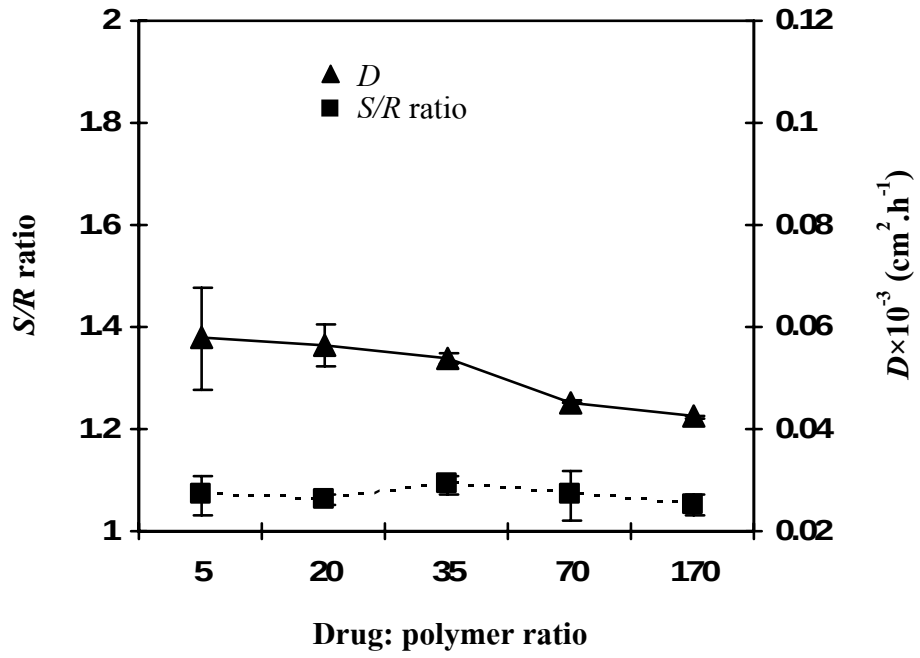

Figure 3.10. The diffusion coefficient (*D*) of *S*-propranolol enantiomer and the *S/R* ratio obtained from release study of S-MIP granule composite cellulose membranes at various polymer loadings after incubation in pH 7.4 buffer at room temperature (30±1°C) (mean±S.D., n=3).

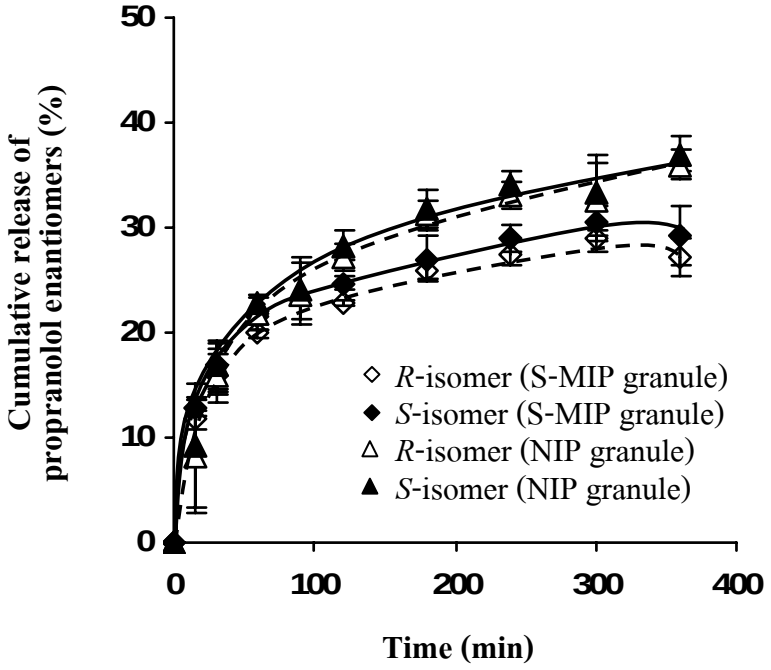

Figure 3.11. The release profiles of propranolol enantiomers from release study of S-MIP granule and corresponding NIP granule composite cellulose membranes at the drug: polymer loading ratio of 1:35. The experiment was performed by applying pH 7.4 buffer as medium to the membranes at room temperature (30±1^{o}C) (mean±S.D., n=3).

The composite membrane composed of MIP granules and cellulose displayed quite low enantioselective release for propranolol enantiomers. The heterogeneous morphology and broad population of binding site of MIP granules may restrict their functionality in certain application. The improvement in the morphology of MIP particles to obtain micro- or nano-spheres with regular size and shape may enhance the rebinding efficiency to the template molecule due to the high surface/volume ratio (Ye and Mosbach, 2001).

CHAPTER 4

THE MIP NANOPARTICLE-ON-MICROSPHERE COMPOSITE CELLULOSE MEMBRANE

4.1. Introduction and objectives

The aim of this chapter was to produce MIP particles having high enantioselectivity to compose with cellulose membrane in order to improve the enantioselective efficiency of composite membrane. In general, materials in form of micro-/nanospheres are particularly suitable for the selective binding properties required to imprinted polymer, providing an easy access of template molecule. The previous study reported that the MIP microspheres gave recognition to the template by far better than MIP granules when prepared with same functional monomer and cross-linker as in case of this study (Pérez-Moral and Mayes, 2004). A number of different strategies have been proposed to produce MIP-based membranes and a number of the developed methods can involve both the simultaneous formation of MIP sites and the formation of a self-supported membrane with an appropriate morphology. Other technologies have also evolved to incorporated pre-formed MIP particles with or into membranes and these include: coating MIP particles onto the surface of membrane disc (Ciardelli et al., 2006), encapsulation of MIP nanoparticles between two membrane layers (Lehmann et al., 2002), pore-filling of thin track-etched membranes with MIP (Ulbricht et al., 2002), surface grafting of the MIP onto the membrane pores by photoinitiation polymerization (Hattori et al., 2004) and encapsulation of MIP nanoparticles into a composite nanofiber membrane by electrospinning (Chronakis et al., 2006). Clearly the method employed influences the degree of resultant membrane selectivity and influences also its resultant applicability.

Suspension polymerization in fluorocarbon is a fast and reliable methodology that synthesizes particles by UV irradiation (Mayes and Mosbach, 1996). The beads obtained have a diameter that can be vary depending on the stirring speed and the amount of surfactant. By

modifying suspension polymerization method described by Mayes and Mosbach with high speed agitation of polymerizing mixture, the MIP beads can be obtained as nanoparticles supported onto microspheres, so called nanoparticle-on-microsphere MIP or NOM-MIP, which were used in this study. Such MIP particles loaded cellulose membrane may enable efficiency enantioselective release with good permeability due to high surface area of MIP, which provides large number of recognition sites with good accessibility.

The objectives of this study were to produce self-assembled composite porous cellulose membranes containing MIP-NOM and to evaluate enantioselective release of the obtained membranes for propranolol enantiomers. The compositions of MIP-NOM used in the preparation process were same as that of MIP granules. MIP-NOM was synthesized by suspension polymerization using agitation the imprinting mixture at high speed. The selectivity of MIP-NOM was examined in term of ability in enantioselective rebinding for propranolol enantiomers by batch binding experiment before incorporated into cellulose membrane. The enantioselective release of MIP-NOM composite membrane for propranolol enantiomers was evaluated when drug: MIP particles were loaded in the composite membranes in different ratios. Moreover, it was investigated the enantioselective release of propranolol, propranolol prodrugs (cyclopropanoyl-propranolol and valeryl-propranolol, see structure in Figure 4.1) and other β-blockers (oxprenolol and pindolol, see structure in Figure 4.1) enantiomers across excised rat skin.

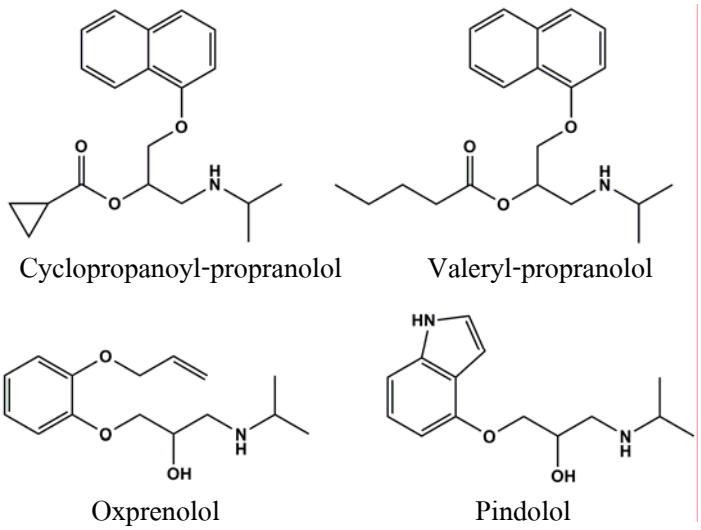

Figure 4.1. Structure of propranolol prodrugs (cyclopropanoyl- and valeryl-propranolol), oxprenolol and pindolol.

4.2. Experimental

4.2.1. Materials

Perfluoro(methylcyclohexane) (PMC), *RS*-oxprenolol and *RS*-pindolol were purchased from Sigma-Addrich (Milwaukee, WI, USA). The perfluoro polymeric surfactant (PFPS) comprising of 95% acryloyl-2-*N*-ethylperfluoroalkylsulfonamide (PFA) and 5% acryloyl PEG2000 monomethyl ether (PEG2000MME) was prepared, according to the method described by Mayes and Mosbach (1996). Cyclopropanoyl-propranolol and valeryl-propranolol were prepared by esterification of the racemic propranolol HCl with the acid chloride of the fatty acid, as described by Quigley et al. (1994). All solvents were analytical grade and dried with molecular sieves to eliminate trace of water before use.

4.2.2. Stereospecific HPLC analysis and method validation for the drugs used in this study

4.2.2.1. Stereospecific HPLC analysis for propranolol prodrugs, oxprenolol and pindolol enantiomers

The amounts of propranolol prodrugs, oxprenolol and pindolol enantiomers in the samples obtained in this study were determined using stereospecific HPLC method. For analysis of propranolol prodrugs enantiomers, the condition was used same as for determination of parent propranolol enantiomers. For analysis of oxprenolol enantiomers, the mobile phase comprising of 1% 2-propanol in 10 mM sodium acetate buffer pH 4.5 and an assay wavelength at 273 nm were used. For analysis of pindolol enantiomers, the mobile phase comprising of 10% acetonitrile in 10 mM sodium phosphate buffer pH 7.0 and an assay wavelength at 264 nm were used. The flow rate was set at 1 $ml.min^{-1}$ and the injection volume of 20 µl was used for both drugs analysis. The retention times of *R*- and *S*-enantiomers of propranolol prodrugs were 4.5 and 8.9 min, respectively. The typical retention times of oxprenolol enantiomers were 3.6 and 6.7 min, and that of pindolol enantiomers were 4.3 and 9.2 min.

4.2.2.2. Validation

In order to demonstrate whether the stereospecific HPLC method was suitable for determination of propranolol, cyclopropanoyl-propranolol, valeryl-propranolol, oxprenolol and pindolol enantiomers *in vitro* skin permeation study, it was validated through the linearity, precision, accuracy, limit of detection and limit of quantification.

Linearity

The standard calibration curves were constructed separately for the *R*- and *S*-enantiomers, using racemic drugs. The stock solution of each drug (cyclopropanoyl-propranolol, valeryl-propranolol, oxprenolol and pindolol) was prepared at the concentration of 100 $\mu g.ml^{-1}$ in pH 7.4 phosphate buffer saline (PBS). The stock solution of each drug was diluted with PBS to obtain the drug concentrations in the range of 1-20 $\mu g.ml^{-1}$. Each concentration was prepared in sets of three and each one was analyzed by stereospecific HPLC method in triplicate. Linearity was evaluated from standard curves constructed by plotting concentration ($\mu g.ml^{-1}$) of drug as function of peak area on HPLC chromatogram.

Precision

The precision was evaluated through repeatability and expressed through relative standard deviation (RSD). In each drug (propranolol HCl, cyclopropanoyl-propranolol, valeryl-propranolol, oxprenolol or pindolol), three different concentrations (2, 5 and 10 $\mu g.ml^{-1}$) were prepared by spiked rat skin solution about 50% v/v. The rat skin solution was obtained from PBS (2.5 ml) incubated with rat skin (1 cm^2) at 37±1^{o}C for 24 h. Each concentration was prepared in sets of three and each one was analyzed in triplicate.

Accuracy

The accuracy was evaluated by comparing the measured concentration with the actual concentration and expressed by %recovery by using the data obtained in precision study.

The limit of detection (LOD) and the limit of quantification (LOQ)

Calibration curves were constructed according to linearity study. The limit of detection (LOD) and the limit of quantification (LOQ) were calculated by equation 2.1 and 2.2.

4.2.3. Stability aspects of the drugs used in this study

Since the MIP-NOM was synthesized by using chloroform as solvent and polymerized under UV 365 nm for 4 h at room temperature (30±1^{o}C), the stability of the template *S*-propranolol was test under this condition. *S*-propranolol solution was prepared in chloroform and made the final concentration to 10 μg.ml^{-1}. The solution was then incubated under UV 365 nm for 4 h at room temperature (30±1^{o}C). After incubation time, chloroform was evaporated and the sample was reconstituted with mobile phase before analyzed by stereospecific HPLC method. For the study *in vitro* skin permeation condition, each drug (*RS*-propranolol HCl, *RS*-cyclopropanoyl-propranolol, *RS*-valeryl-propranolol, *RS*-oxprenolol or *RS*-pindolol) solution was prepared in PBS and made the final concentration to 10 μg.ml^{-1}. The solutions were spiked with rat skin solution (50% v/v) and incubated at 37±1^{o}C for 3 days. The samples were injected to analyze with stereospecific HPLC method. The stability was determined by comparing the amount of drug before and after incubation. Each experiment was carried out in triplicate.

4.2.4. Synthesis of MIP nanoparticle-on-microsphere

The MIP-NOM was prepared by a suspension polymerization method involving the use of the perfluoro polymeric surfactant (PFPS) as surfactant and the perfluoro (methylcyclohexane) (PMC) as dispersing phase (modified from the procedure used for

microspheres preparation described by Mayes and Mosbach (1996)). For MIP-NOM production in this study (see Figure 4.2), MAA (1.6 mmol), EDMA (9.2 mmol), *S*-propranolol as free base (0.4 mmol), AIBN (0.04 mmol), PFPS (25 mg) and PMC (20 ml) were added to chloroform (5 ml). The resultant microsuspension was placed in a 120-ml vial (5 cm in diameter) and purged with nitrogen gas stream for 5 min. The mixture was vigorously stirred using a 4cm×1cm magnetic bar and a magnetic stirrer set at 1000 rpm. Polymerization of the mixture was effected by irradiation for 4 h using UV light with a wavelength set at 365 nm at room temperature (30±1^{o}C). After obtaining polymer particles, the template molecule was removed by centrifuging the formed MIP-NOM with three portions of 1:9 (v/v) acetic acid and methanol mixture (50 ml) and then with a further three portions of methanol (50 ml) at 3000 G using a HERMLE rotor Z323K model (Wehingen, Germany) for 5 min after each wash. The polymer particles were then dried in a vacuum for 24 h and stored at ambient temperature. As control, corresponding NIP-NOM was produced using exactly the same synthetic route in MIP-NOM but omitting the template molecule from the preparation procedure.

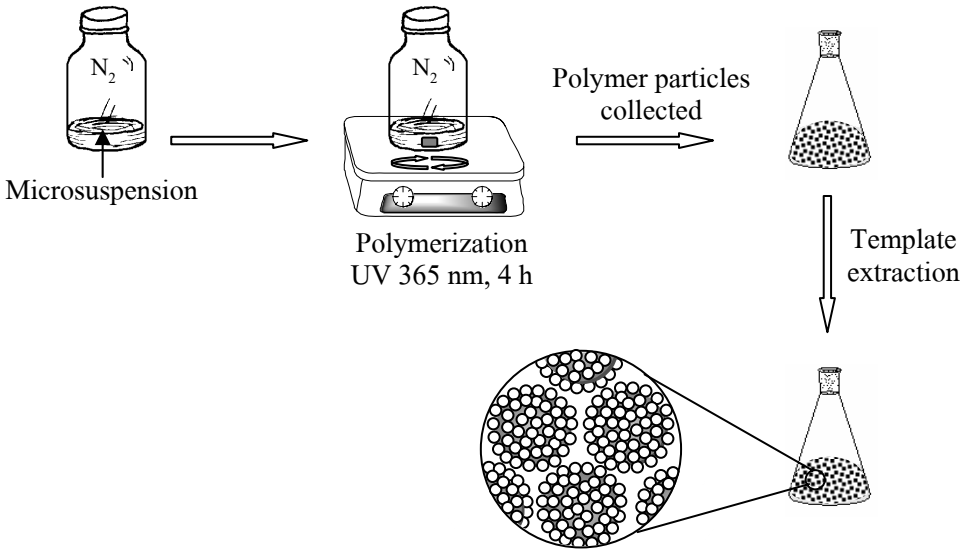

Figure 4.2. Schematic representation of the synthetic procedure of MIP-NOM.

4.2.5. Evaluation of recognition property of MIP-NOM

The ability of the MIP-NOM to selective rebind propranolol enantiomers was evaluated using a solid phase extraction procedure. In order to determine the recovery of bound drug enantiomers from aqueous solution, four different weights of MIP-NOM (2, 5, 10 and 15 mg) and separately, the corresponding NIP-NOM were incubated in 3 ml of pH 7.4 phosphate buffer saline (PBS) containing 60 $\mu g.ml^{-1}$ racemic propranolol HCl at room temperature ($30\pm1^{o}C$) for 12 h to reach equilibrium. The incubated dispersions were centrifuged at 3000 G for 5 min. The concentrations of propranolol enantiomers in the supernatant were determined using the stereospecific HPLC method. The amount of each enantiomer bound was calculated from the difference in concentrations before and after incubation. All experiments were run in triplicate.

4.2.6. Preparation of MIP-NOM-contained composite cellulose membranes

It was found that 3.7% w/w cellulose dissolved in 50% aqueous NMMO could incorporate up to 104% w/w MIP-NOM and still form intact composite membrane. For MIP-NOM composite membrane preparation, cellulose sheet (96 mg) was dispersed in an aqueous solution of NMMO (50% w/w) (5 ml) held initially at a temperature of $60^{o}C$. The suspension was then heated at $80^{o}C$ until the cellulose dissolved and a clear, brown, viscous solution was obtained. Subsequently, the mixture of 100 mg of MIP-NOM containing 10 mg of racemic propranolol HCl was prepared for sample dilution. One hundred mg of NOM particles was then titrated with aliquots of the drug by physical mixing. A mixture of 0.3 ml of PCL-T and the corresponding drug-polymer mixture (containing 100 mg of NOM particles) were added into the cellulose solution. Drug: polymer weight ratios of 1:10, 1:50, 1:100, 1:200 and 1:500 were used. The resulting suspension was cast into a membrane by pouring the melt into a Petri-dish (10 cm in diameter). After 5 min, generated membrane was transferred into a beaker containing 500 ml distilled water for 12 h. Finally, the membranes with a surface area of 28 cm^2 were recovered, dried in air overnight and stored in a dessiccator for until required. The entrapment of racemic propranolol HCl in each of the composite membranes was examined by measuring the drug content in the washing solution derived from the cast membranes (n=3) using an stereospecific

HPLC analysis method and the amount of drug entrapped was obtained by subtracting the amount of drug in the rinse solution from the amount of formulation. The thickness of the prepared membranes varied between 50-70 μm as measured by a SEM (JEOL series JSM 5800LV, CA, USA). The control composite cellulose membranes containing NIP-NOM were prepared using the same methodology as the equivalent MIP-NOM composite cellulose membranes, with drug being included in the reaction mixture in the same weight ratios.

4.2.7. Characterization of MIP-NOM and MIP-NOM composite membranes

The obtained MIP-NOM and MIP-NOM composite membranes were characterized in terms of morphology, porosity, degree of swelling, electrical resistance, mechanical strength and/or friability. The morphology of MIP-NOM and MIP-NOM composite membranes as well as the size of polymer particles and the pore size of composite membranes were examined by SEM. The porosity and degree of swelling of MIP-NOM were examined by nitrogen adsorption/desorption analysis and equilibrium incubation method, respectively. The electrical resistance, mechanical strength and friability of composite membranes were carried out.

4.2.8. Determination in enantioselective release of MIP-NOM composite membranes

The ability of MIP-NOM composite membranes for enantioselective-controlled release of propranolol enantiomers was evaluated regarding the difference in drug: polymer ratios, which was evaluated by dissolution testing method.

4.2.9. *In vitro* skin permeation study

Male Wistar rat dorsal skin was used in this study. Dorsal hair was removed by shaving, the skin gently excised using surgical scissors and the subcutaneous tissue and adipose tissue were carefully removed. The skin preparations were mounted in a vertical Franz-type diffusion cell and the composite membrane (0.8 cm^2) placed in turn on the surface of the stratum corneum in the donor compartment. PBS (2.5 ml) was filled the receptor compartment and 300 μl

of PBS was placed in contact with the membrane surface in the donor compartment. The receptor compartment was maintained at 37±1^{o}C by an external circulating water-bath. The receptor phase was placed on magnetic stirring plate (Variomag, FL, USA) submersed in a water bath to allow the receptor phase exposed to the water in water-bath. The receptor phase was stirred with a magnetic bar constantly at 250 rpm. Samples (200 μl) were collected from receptor fluid at set time intervals up to 48 h and immediately replaced with the same volume of fresh PBS of each time collecting. The amount of each propranolol enantiomer permeated at any time point was determined by stereospecific HPLC method. The steady-state portion of the line was extrapolated to the time axis and the point of intersection was recorded as the lag time.

In addition, the permeation rates of racemic mixtures of propranolol prodrugs (cyclopropanoyl-propranolol and valeryl-propranolol) and other β-blockers (oxprenolol and pindolol) were determined. To ensure that sufficient amount of the drugs permeated into the skin to enable sufficient assay sensitivity, 100 mg of each drug with 100 mg of NOM particulates were incorporated in the production of composite membrane. Each permeation test was carried in sets of three. The entrapment of racemic propranolol HCl, cyclopropanoyl-propranolol, valeryl-propranolol, oxprenolol or pindolol in the obtained composite membranes was found to be about the same in each case (2.1 mg.cm^{-2}).

4.2.10. Statistic analysis

Statistical analyses were carried out using SPSS version 13.0 (SPSS, Cary, NC, USA). Paired *t*-tests were used to investigate differences of *R*- and *S*-enantiomers in every experimental test. A *p*-value of <0.05 was considered significant.

4.3. Results and discussion

4.3.1. Method validation

The linearity, precision and accuracy for *in vitro* skin permeation study, limit of detection (LOD) and limit of quantification (LOQ) of propranolol HCl, cyclopropanoyl-propranolol, valeryl-propranolol, oxprenolol and pindolol enantiomers are shown in Table 4.1. Correlation coefficients (R^2) for the calibration curves in the range of 1-20 μg.ml^{-1} for cyclopropanoyl-propranolol, valeryl-propranolol, oxprenolol and pindolol enantiomers were higher than 0.999. It was indicated that the method for determination of drug enantiomers for *in vitro* skin penetration study was precise and accurate with the %RSD of repeatability was lower than 5% and the accuracy was found in the range of 98.41-99.92% for every drug studied.

Table 4.1. Linearity, precision, accuracy, limit of detection (LOD) and limit of quantification (LOQ) of propranolol HCl, cyclopropanoyl-propranolol, valeryl-propranolol, oxprenolol and pindolol enantiomers from stereospecific HPLC assay.

Drug	**Isomer**	**Linearity (R^2)**	**Precision (%RSD)**	**Accuracy (%recovery)**	**LOD (μg.ml^{-1})**	**LOQ (μg.ml^{-1})**
Propranolol HCl	*R*	0.9997	2.13	99.60	0.06	0.18
	S	0.9998	1.38	99.70	0.08	0.26
Cyclopropanoyl-	*R*	0.9999	2.21	98.41	0.08	0.28
propranolol	*S*	0.9995	2.64	99.36	0.08	0.28
Valeryl-	*R*	0.9996	1.58	98.65	0.07	0.25
propranolol	*S*	0.9997	1.56	99.81	0.08	0.27
Oxprenolol	*R*	0.9994	2.04	99.31	0.14	0.44
	S	0.9996	1.15	99.68	0.12	0.46
Pindolol	*R*	0.9998	1.26	99.20	0.04	0.13
	S	0.9999	1.69	99.92	0.04	0.14

Note: the *R*- and *S*-enantiomers of oxprenolol and pindolol were pretended from the first and second peaks of HPLC chromatogram, respectively.

4.3.2. Stability of the drugs used in this study

The stability study of *S*-propranolol under polymerization condition was revealed that the amount remaining as intact *S*-propranolol was 97.59±3.90% (n=3) with racemization was not observed. The stability of the drugs incubated in PBS spiked with rat skin solution was also shown high stability with the value of %recovery of 98.50-100.86%. The obtained drug after incubation was as racemic mixtures of *R*- and *S*-enantiomers for every drug. These results indicated the good stability of drugs under the experiments.

4.3.3. MIP-NOM synthesis and characterization

Figure 4.3 shows scanning electron micrographs of MIP-NOM in three different magnifications. Nano-sized imprinted polymer would be expected to provide a large imprinted surface with a high-selective potential due to the small size of the nanoparticle. However, in preliminary studies it was found that polymer in nano-size particles were difficult to embed in a composite membrane *via* phase inversion and subsequent casting. In addition, such particles tended to form aggregate that would reduce the available surface area of particles. The advantages of MIP-NOM are that in addition to providing a high accessibility of imprint sites they resolved the handling problems associated with generating and incorporating nanoparticles. The MIP microspheres synthesized by suspension polymerization method, involving dispersion of the polymerizing mixture in a liquid perfluorocarbon, generated spherical uniformly sized particles with a size range of 50-65 μm, which could be suitable for use as a separation phase in chromatography and/or in solid-phase extraction techniques (Mayes and Mosbach, 1996). Such MIP beads, if packed into a column would be expected to confer a low back pressure and rapid diffusion of the analyte molecule. The method used for agitating the polymeric mixture during polymerization was found to affect the morphology of polymer particles. By using rotating blade (250 rpm), the particles obtained as microsphere with smooth surface, while using magnetic stirring bar at high speed (~1000 rpm) could generate polymer NOM particles. The technique of suspension polymerization, involved the monomer having only sparing solubility in the continuous phase, in this case PMC. When initiation occurred in this phase the polymer chain

radical generated in reaction medium grew to a certain critical chain length, where upon nucleation into primary particles occurred. However, in addition monomer would coalesce into droplets. The formation of NOM in this study may be explained by the core-shell theory, where the primary particles have a polymer-rich core with little monomer but with an outer surrounding shell layer comprising practically pure monomer (Hansen and Ugelstad, 1978; Bataille et al., 1982). The surfactant used in this procedure was a preformed-polymer obtained from the grafted copolymerization of PFA acrylate and PEG2000MME acrylate, and this stabilized and allowed the formed composed of poly(MAA-*co*-EDMA) to grow. The agitation of the polymerizing mixture with magnetic bar at very high speed (~1000 rpm) appeared to induce the formation of nanoparticulate monomer droplets as well as the primary microspheres. As the propagation continues, monomer molecules from the monomer droplets may diffuse toward the propagating chains within the polymer microspheres. The diffusion of monomer to the polymer nanoparticles also continued at a rapid rate. The polymer particles obtained were in form of uniform nanoparticles, in the size range of 100-300 nm, that were attached onto the surface of microspheres in the size range of 3-10 μm.

The typical characteristics (i.e., particle size, porosity and degree of swelling) of NOM are shown in Table 4.2. The porosity data (surface area, total pore volume and average pore diameter) of NOM-MIP showed slightly higher than the control polymer. However, the surface area, total pore volume and average pore diameter for MIP-NOM were lower than those of MIP granule. The difference in polymerization method allowed obtaining polymer in different morphology and this affected the porosity. The NOM-MIP showed little lower swelling in chloroform than in methanol and aqueous solvents. There was not different in swelling of NOM-MIP and -NIP in every solvents studied.

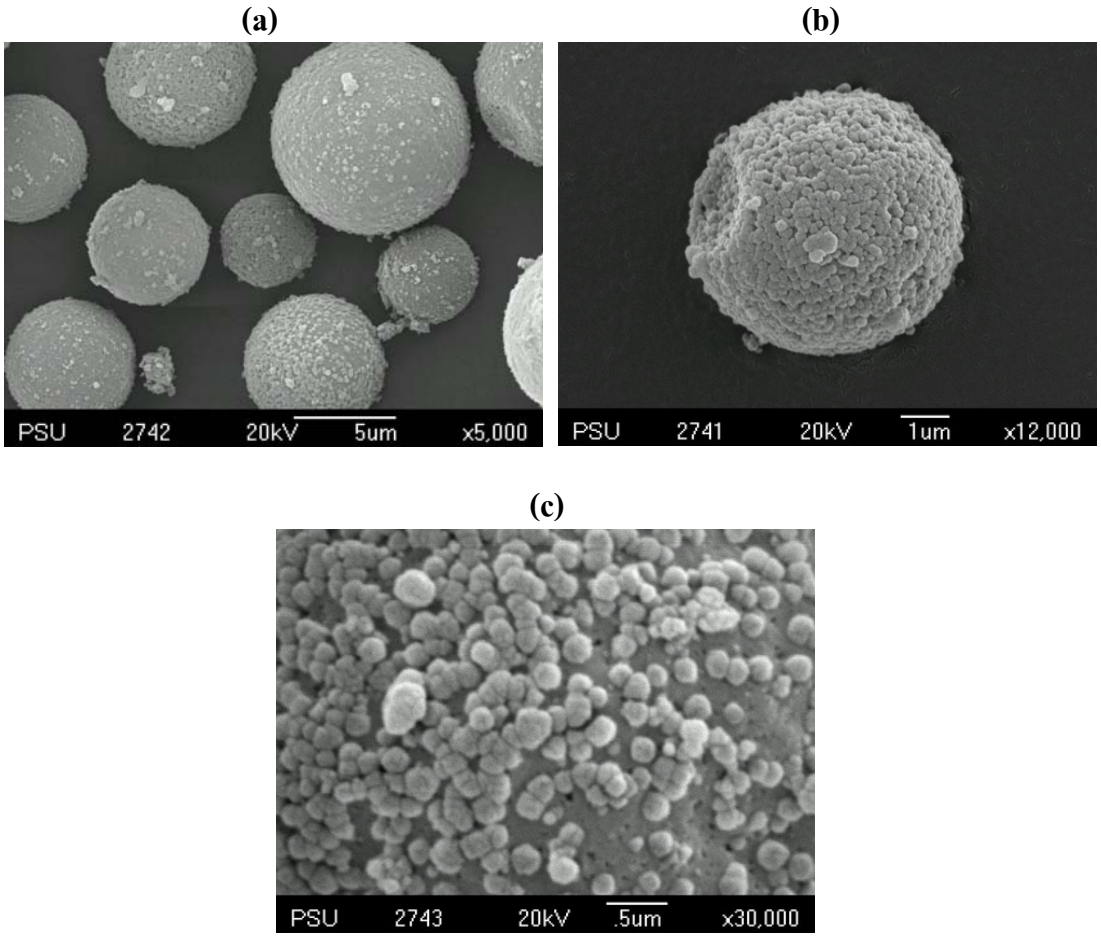

Figure 4.3. SEM images of MIP-NOM at (a) ×5,000, (b) ×12,000, and (c) ×30,000 magnifications.

Table 4.2. Physical properties of MIP-NOM and corresponding NIP-NOM (mean±S.D., n=3).

Polymer	Particle size*	Porosity			Degree of swelling (%)			
	(μm)	Surface area ($m^2.g^{-1}$)	Total pore volume ($ml.g^{-1}$)	Average pore diameter (nm)	methanol	chloroform	pH 5.5	pH 7.4
MIP-NOM	0.29±0.09[a]	21.03	0.053	10.87	60.2±6.5	30.0±7.3	50.5±6.2	50.3±5.7
NIP-NOM	0.27±0.05[a]	14.26	0.047	9.01	50.2±6.3	20.5±7.2	40.9±6.4	40.4±3.3

*n=10

[a] refer to the size of nanoparticles attached on microspheres (3-10 μm).

4.3.4. Selectivity of propranolol enantiomers binding to MIP-NOM

The selective extraction of enantiomer of a fixed concentration of racemic propranolol HCl in pH 7.4 buffer by increasing amounts of MIP particles were evaluated at room temperature (30±1°C). The enantioselectivity of the binding of propranolol HCl was measured as the amount of each enantiomer bound to the particles expressed as a percentage of the original concentration and this was plotted as a function of polymer content (Figure 4.4). The binding of both propranolol enantiomers to the MIP-NOM was markedly greater than to the corresponding NIP-NOM. MIP-NOM displayed marked enantioselectivity over the entire range of polymer content (2-15 mg) and the degree of enantioselectivity was similar at every level of polymer content. As the content of MIP particles was increased, then the percentage of each enantiomer bound increased significantly. This suggested that the binding sites may be more accessible in the particles produced by suspension polymerization and the increased surface area provided by the MIP-NOM provided an increased efficiency in the rebinding of the template molecule.

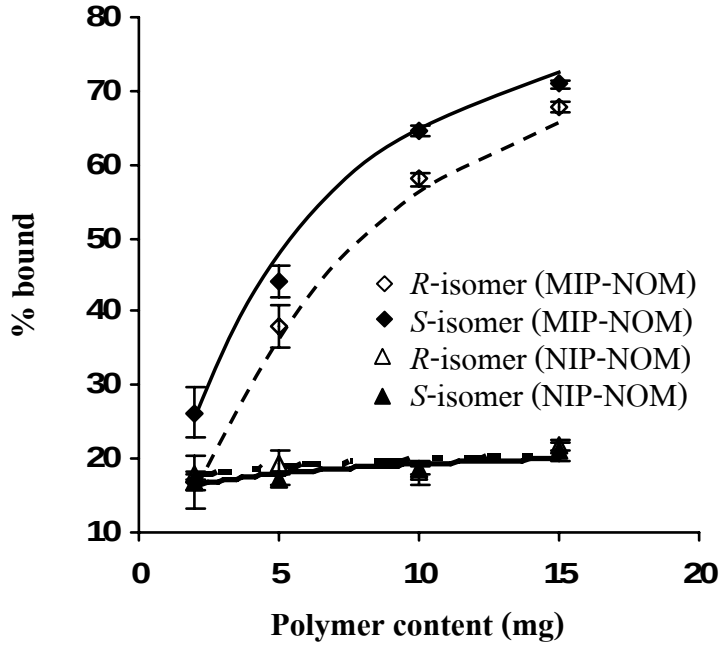

Figure 4.4. The percentage of bound propranolol enantiomers after incubation of different weights of imprinted and non-imprinted NOM polymer with 60 μg.ml^{-1} racemic propranolol HCl in pH 7.4 buffer solution at room temperature (30±1°C) (mean±S.D., n=3).

4.3.5. MIP-NOM composite membranes preparation and characterization

Figure 4.5 shows the surface morphology and cross-sectional architecture of cast bacterial cellulose membrane loaded with MIP-NOM. The surface image exhibited a rough appearance with a rather high porosity. The pore of composite membranes was induced by PCL-T during the phase inversion preparation procedure and the resultant pore size of the composite membranes was partly dependent on the size of the polymer beads size. From the enlargement image of MIP-NOM composite membrane, the nanoparticles were still visible as being attached on the surface of microsphere (Figure 4.4c). This indicated that the nanoparticles are adhered strongly to the microsphere.

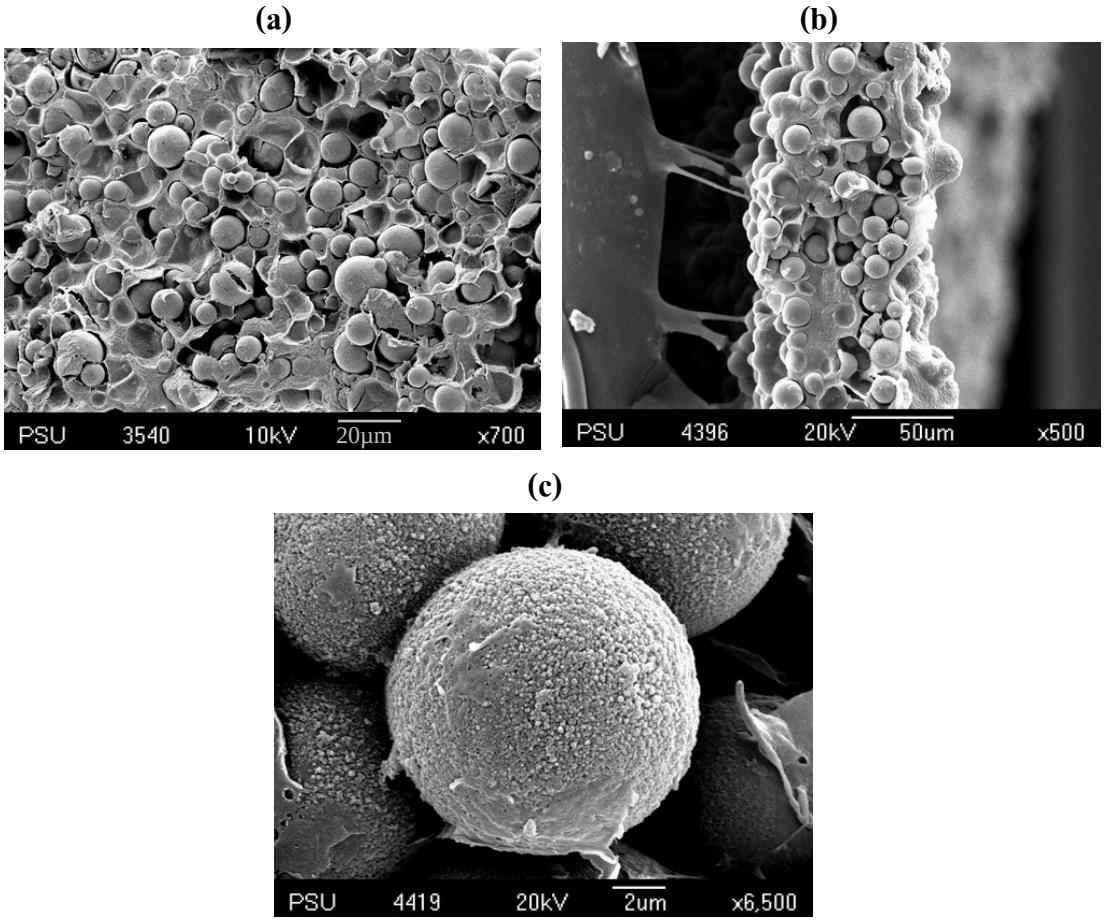

Figure 4.5. SEM images of (a) surface and (b) cross-section of MIP-NOM composite cellulose membrane and (c) the enlargement image of MIP-NOM composite membrane.

The physical properties (i.e., pore size, membrane resistance, tensile strength and friability) of the bacterial cellulose composite membranes containing 104% w/w NOM are shown in Table 4.3. The pore size of NOM contained composite membranes was approximately 6-10 μm, related with the size of NOM particles. This result confirmed the visual finding apparent from the SEM image (Figure 4.4). The mechanical strength of NOM composite cellulose membranes was in the range of 0.5-0.7 $kN.cm^{-2}$. The friability of NOM composite membranes was reduced about 2-3% after the test. The electrical resistance of the membranes was redetermined, after the friability test had been carried out but this was found to change less than 2.5%. The NOM composite membranes retained a good appearance after testing and it was concluded that the NOM composite membranes would have sufficient robustness for experimental application purposes.

Table 4.3. Characteristics of MIP-NOM and NIP-NOM composite cellulose membranes (mean±S.D., n=3).

Membrane	**Polymer loaded (%)**	**Pore size* (μm)**	**Membrane resistance ($\Omega.cm^2$)**	**Tensile strength ($kN.cm^{-2}$)**	**Friability (%)**
MIP-NOM	104	10.5 ± 2.0	2.22 ± 0.92	0.56 ± 0.38	2.70 ± 0.53
NIP-NOM	104	6.3 ± 2.1	2.95 ± 0.85	0.73 ± 0.14	2.54 ± 0.31

* n=10

4.3.6. Enantioselective release of propranolol enantiomers from MIP-NOM composite membranes

The diffusion coefficient (*D*) of both *R*- and *S*-propranolol enantiomers and the enantioselectivity (*S*/*R* ratio) of MIP-NOM composite cellulose membrane were dependent upon the drug: polymer ratio (Figure 4.6). The total amount of drug incorporated in each of the MIP-NOM and corresponding NIP-NOM composite cellulose membranes at various drug: polymer ratios is displayed in Table 4.4. The amount of *R*- and *S*-propranolol enantiomers incorporated in the MIP-NOM composite membranes and the NIP-NOM composite membranes was not

significantly different for the equivalent drug: polymer ratios. Also, there was no stereoselective difference in the amounts of propranolol enantiomers entrapped in the MIP-NOM or the NIP-NOM composite membranes. The cumulative amount of the individual propranolol enantiomers released was plotted as a function of time and the profiles obtained are shown in Figure 4.7. The cumulative release from the corresponding NIP-NOM composite membranes was also determined for comparison purposes. As shown in Figure 4.7, the MIP-NOM composite membrane showed the release of *S*-isomer similar to the NIP-NOM composite membrane. The resulting curves indicated that the diffusion of *R*-propranolol enantiomer across the MIP-NOM composite membrane was delayed, whereas a relatively facilitated transport of *S*-propranolol enantiomer across MIP-NOM membrane. The preferential sorption of *S*-propranolol enantiomer to MIP-NOM particles enhances the transport selectivity of the MIP-NOM composite membrane. Enantioselective release was obtained from MIP-NOM composite membrane, with the template *S*-propranolol enantiomer being released preferentially in comparison to the *R*-propranolol enantiomer. As the polymer loading increased the diffusivity of both propranolol enantiomers decreased (Figure 4.6), but the stereoselectivity increased. The great enantioselectivity of release from the membrane-containing MIP-NOM was probably as a consequence of the high surface area of the incorporated particles which allowed good accessibility of the template molecule to the MIP-NOM binding sites. The *S/R* selectivity of the MIP-NOM composite membranes was increased when the MIP-NOM loading was increased but above a drug: polymer ratio of 100 (*S/R* flux ratio = 1.7), there was no further increase. This result indicated that the selectivity was likely to be influenced by the capacity of the available MIP particles within the bacterial cellulose membrane to bind the template molecule.

Table 4.4. The entrapment of propranolol enantiomers in the membranes loaded with different drug: polymer-NOM ratios (mean±S.D., n=3).

Drug: polymer ratio	Entrapment (μg.cm^{-2})			
	MIP-NOM membrane		NIP-NOM membrane	
	***R*-isomer**	***S*-isomer**	***R*-isomer**	***S*-isomer**
1:10	106.2 ± 7.0	109.7 ± 5.2	108.6 ± 7.8	109.0 ± 11.0
1:50	20.8 ± 1.0	21.2 ± 1.5	19.9 ± 0.9	19.8 ± 0.8
1:100	11.0 ± 0.9	10.6 ± 0.5	9.3 ± 0.3	9.6 ± 0.4
1:200	5.3 ± 0.3	5.3 ± 0.2	5.3 ± 0.3	4.9 ± 0.3
1:500	2.4 ± 0.1	2.8 ± 0.1	2.7 ± 0.2	2.5 ± 0.1

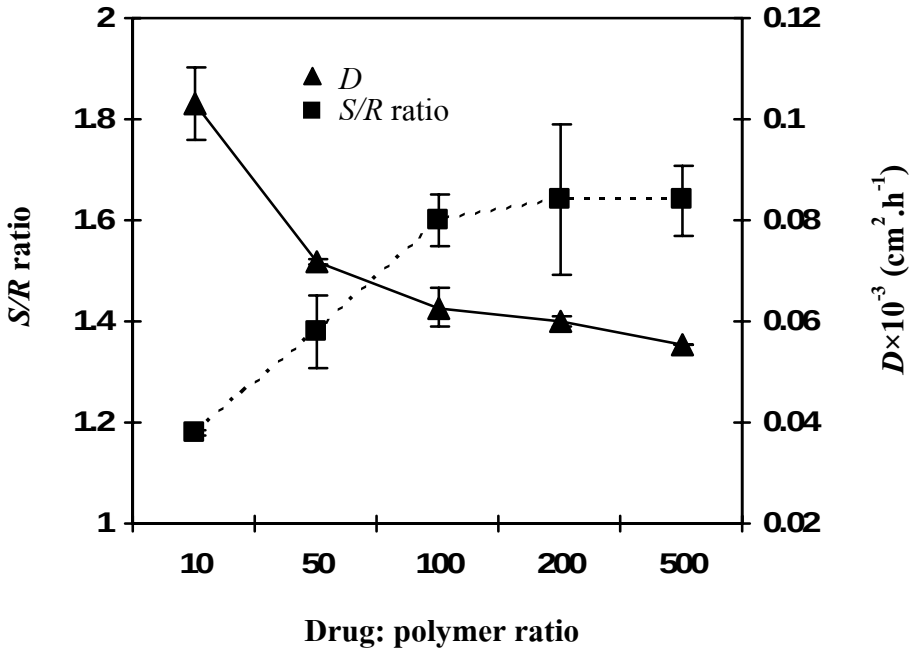

Figure 4.6. The diffusion coefficient (*D*) of *S*-propranolol enantiomer and the *S/R* ratio obtained from release study of MIP-NOM composite cellulose membranes at various polymer loadings after incubation in pH 7.4 buffer saline at room temperature (30±1°C) (mean±S.D., n=3).

The release profiles of *R*- and *S*-propranolol enantiomers from the composite membranes loaded with MIP-NOM and NIP-NOM at a fixed drug: polymer ratio of 1:100, when pH 7.4 buffer was employed as the diffusing dissolution medium, are shown in Figure 4.7. Initially, the drug release was rapid with low enantioselectivity, possibly as a consequence of the drug located at the membrane surface dissolving into the aqueous medium. After the burst release of propranolol, subsequent release of the enantiomers was slower but stereoselectivity was increased. Drug at this stage was presumably being release from the binding sites of MIP-NOM in the membrane. Release from the control membrane, containing equivalent NIP-NOM, showed the release rate of drug to decrease as a function of time in a similar manner to the membrane loaded with MIP-NOM. However, no enantioselectivity in the release of propranolol enantiomers was found for NIP-NOM composite membrane.

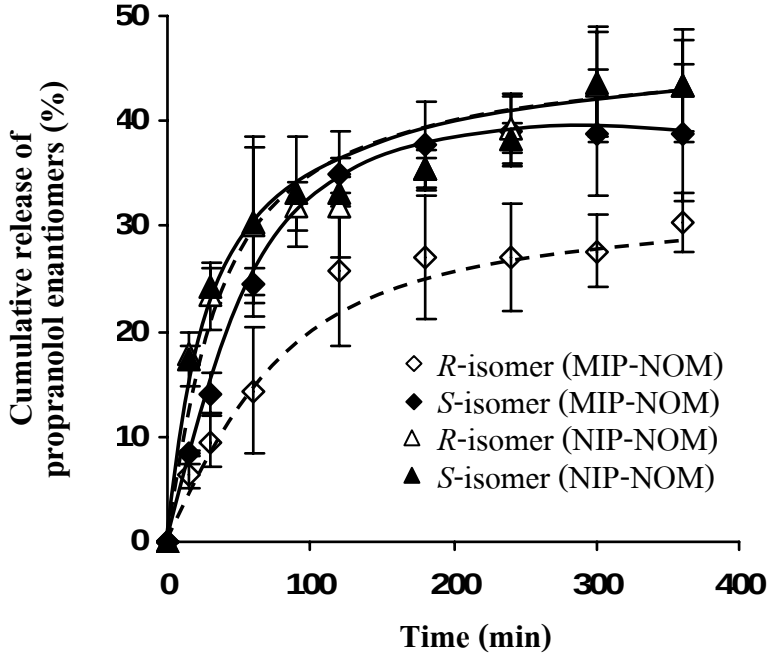

Figure 4.7. The release profiles of propranolol enantiomers from MIP-NOM and corresponding NIP-NOM loaded cellulose membranes at the drug: polymer loading ratio of 1:100. The experiment was performed by applying pH 7.4 buffer as medium to the membranes at room temperature (30±1^{o}C) (mean±S.D., n=3).

4.3.7. *In vitro* skin permeation study

The enantiomeric release and the subsequent transdermal transport of propranolol HCl and propranolol prodrugs (cyclopropanoyl-propranolol and valeryl-propranolol) as well as other β-blockers (oxprenolol and pindolol) from the MIP-NOM loaded bacterial cellulose membrane *in situ* with excised rat skin was determined. The results (Table 4.5) indicated that the transport of *S*-propranolol enantiomer across rat skin after release from MIP-NOM composite membrane was higher than the concomitant transport of *R*-propranolol enantiomer. Also, the transport of the more lipophilic propranolol prodrug enantiomers occurred at a higher rate than that of the parent enantiomers. The transport rates of the *R*- and *S*-enantiomers of the propranolol and its prodrugs were found to be different ($p<0.05$). The various esterases present in the skin would be expected to act upon the prodrug during its transport through the viable epidermis and dermis. The rate of hydrolysis of valeryl-propranolol and cyclopropanoyl-propranolol within the rat skin has been reported to be enantiomer dependent, with that *R*-isomer enantiomer prodrug being hydrolyzed faster than *S*-isomer prodrug (Ahmed et al., 1997). However, no overall difference was apparent in the extent of enantioselectivity of transport of either of the propranolol prodrugs, nor indeed when the degree of enantioselectivity of the prodrugs was compared to that obtained for propranolol itself. The MIP-NOM bacterial cellulose composite membrane also produced statistically significant differences in the fluxes of the oxprenolol and pindolol enantiomers ($p<0.05$). The results obtained indicate that there was a cross-reactivity between the *S*-propranolol imprinted MIP-NOM and compounds that are structurally related to the template. Nevertheless, no enantioselectivity was detected in the lag times determined for the diffusion through skin for any of the racemic compounds studied.

Table 4.5. *In vitro* rat skin permeation data of racemic propranolol HCl, prodrugs of propranolol and other β-blockers release from MIP-NOM and NIP-NOM loaded bacterial cellulose membranes after application of pH 7.4 phosphate buffer at 37±1°C (mean ± S.D., n = 3).

Drug	Membrane	J_{ss} (μg.cm^{-2}.h^{-1})[a]			τ (h)[b]		
		R-isomer	*S*-isomer	*S/R* ratio	*R*-isomer	*S*-isomer	*S/R* ratio
Propranolol HCl	MIP-NOM	0.43 ± 0.09	0.57 ± 0.08	1.33 ± 0.18	20.27 ± 6.74	18.13 ± 10.27	0.85 ± 0.19
	NIP-NOM	0.32 ± 0.06	0.31 ± 0.12	0.95 ± 0.18	28.53 ± 0.46	27.73 ± 0.92	0.97 ± 0.02
Cyclopropanoyl-	MIP-NOM	8.72 ± 0.07	11.79 ± 0.13	1.36 ± 0.03	20.23 ± 7.43	16.53 ± 6.22	0.81 ± 0.01
propranolol	NIP-NOM	2.17 ± 0.01	1.96 ± 0.03	0.91 ± 0.01	20.50 ± 2.26	20.23 ± 2.70	0.99 ± 0.02
Valeryl-	MIP-NOM	4.62 ± 0.11	5.87 ± 0.02	1.27 ± 0.02	15.33 ± 2.57	12.00 ± 2.80	0.88 ± 0.03
propranolol	NIP-NOM	4.86 ± 0.92	5.08 ± 0.33	1.05 ± 0.13	13.20 ± 2.11	12.93 ± 1.84	0.98 ± 0.03
Oxprenolol	MIP-NOM	16.77 ± 0.88	19.48 ± 0.69	1.16 ± 0.02	12.60 ± 3.34	11.06 ± 2.72	0.86 ± 0.02
	NIP-NOM	9.85 ± 3.63	10.44 ± 4.56	1.04 ± 0.14	12.46 ± 3.44	12.73 ± 3.90	1.01 ± 0.03
Pindolol	MIP-NOM	3.83 ± 0.32	4.48 ± 0.26	1.16 ± 0.03	13.46 ± 2.01	11.65 ± 1.60	0.86 ± 0.02
	NIP-NOM	5.04 ± 0.68	4.91 ± 0.74	0.97 ± 0.01	10.53 ± 0.92	10.46 ± 0.98	0.99 ± 0.01

[a] Steady state transdermal flux.

[b] Lag time.

CHAPTER 5

THE MIP NANOPARTICLE-ON-MICROSPHERE COMPOSITE CELLULOSE MEMBRANE: CHARACTERIZATION AND EVALUATION IN ENANTIOSELECTIVE RELEASE OF RACEMIC OMEPRAZOLE

5.1. Background and rationale

The biological receptors constructed by protein molecule, considered as chiral receptors and indeed, can recognize the two enantiomers as two different substances due to the different interactions explained by a three-point interaction of the drug with the receptor site proposed by Easson and Stedman (1933). The attachment of an enantiomer to the chiral receptor is similar to a hand fitting into a glove or to a key into a lock. A particular enantiomer can only fit (interact) into a receptor site and can produce an active biological effect, while the other enantiomer will not fit and consequently, there is no active response (Nguyen et al., 2006). The transmembrane receptors (proteins) can potentially control the transduction of signal in response to the activation of the binding molecule. The enantioselective recognition of biological receptors inspired to the preparation of MIP having recognition site like protein receptor for enantiomer selective purpose of a chiral drug. In order to obtain a MIP containing the enantioselective recognition site, chiral material was used in the polymerization process.

Cinchona alkaloids have been successfully used as chiral auxiliaries and selectors for enantioseparation of chiral compounds in HPLC (Pettersson, 1984; Pettersson and Schill, 1986) as well as in capillary electrophoresis (CE) (Piette et al., 2000; Piette et al., 2002). The most often used cinchona alkaloids are quinine, quinidine, cinchonine and cinchonidine, especially quinine (QN) and quinidine (QD), have received much attention as a cheap natural source for stereo-discriminating auxiliaries in HPLC. To use as chiral selectors for direct chromatographic enantioseparations, quinine and quinidine are either added to the mobile phase as counterions in chiral ion-pair chromatography (Pettersson, 1984; Pettersson and Schill, 1986)

or covalently immobilized onto silica thus obtaining chiral stationary phases (CSPs) (Mandl et al., 1999; Asnin et al., 2005). Structurally, QN and QD consist of a planar quinoline and a rigid quinuclidine ring, which are connected by a secondary methyl alcohol bridge (Figure 5.1). The arrangement of the five stereogenic centers within the rigid molecules QN and QD (at position 1, 3, 4, 8 and 9) may provide an excellent basis for effective chiral recognition. QN and QD are diastereomers which N1, C3 and C4 have identical (1S, 3R, 4S) and C8, C9 have opposite configurations. The high stereoselectivity potential obtained by QN or QD might be from simultaneously acting multiple interactions such as ionic interaction, hydrogen bonding, dipole-dipole, charge transfer (π-π), hydrophobic and steric interactions (Piette et al., 2000). QN and QD were selected to modify and used as functional monomers for MIP preparation in this study. The present of nitrogen atom especially in quinuclidine ring would be an important role in hydrogen bond formation, which is often a key step in molecular imprinting, with omeprazole free acid.

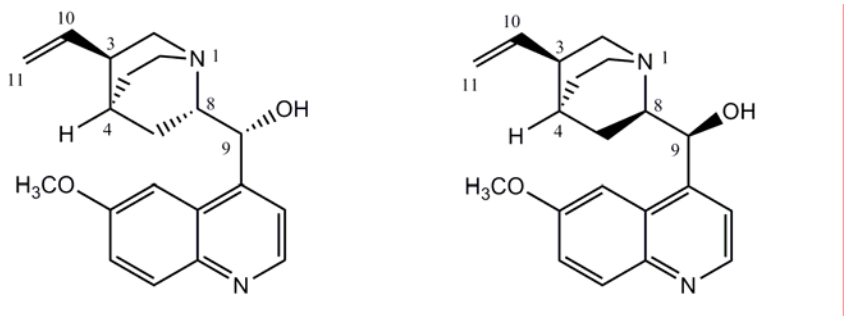

1S, 3R, 4S, 8S, 9R Quinine (QN) 1S, 3R, 4S, 8R, 9S Quinidine (QD)

Figure 5.1. Structure and stereochemistry of quinine (QN) and quinidine (QD).

The MIP-NOMs were prepared by using methacryloylate QN and methacryloylate QD, see structure in Figure 5.2, as functional monomers. Moreover, the MIP-NOM using 4-vinylpyridine (4-VPD), see structure in Figure 2.1, as functional monomer which is non-chiral (achiral) molecule was prepared for comparative purposes. A 4-VPD is the most widely basic functional monomer used in molecular imprinting and has been reported to successfully use in the imprinting of *S*-naproxen (Kempe and Mosbach, 1994; Donato et al., 2005) and amino acid derivatives (Kempe et al., 1993; Kempe and Mosbach 1995). The 4-VPD was selected to use regarding to the capability in interaction formation with omeprazole and the

stability of omeprazole in the polymerization process. The 4-VPD represents an amine group which can interact with the NH group on the benzimidazole ring of omeprazole through hydrogen bonding interaction.

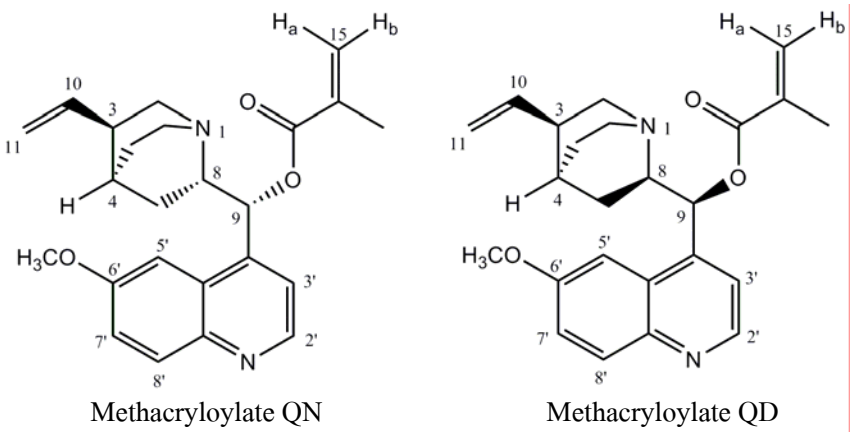

Figure 5.2. Structure of methacryloylate QN and methacryloylate QD.

The objective in this study was to determine the enantioselective recognition properties of NOM-MIPs prepared by using either chiral functional monomers: methacryloylate QN and methacryloylate QD or achiral functional monomer: 4-VPD. The methacryloylae QN and methacryloylate QD were obtained from esterification reaction of QN and QD with methacryloyl chloride. *S*-omeprazole and ethylene glycol dimethacrylate (EDMA) were used as template and cross-linker, respectively. EDMA was selected to use as the cross-linking monomer since it could produce the polymer with rigidity property. The ability in enantioselective rebinding of different types of MIP particles was evaluated by batch binding experiment in various solvents, i.e., chloroform, pH 6.8, pH 7.4 and pH 10 buffers. The ability of MIPs to form complexation with omeprazole enantiomers was investigated by using Attenuated total reflectance-Fourier transform infrared (ATR-FTIR) and X-ray diffraction (XRD) techniques. The enantioselective release and the enantioselective permeation abilities of MIP-NOM composite cellulose membranes for omeprazole enantiomers were evaluated. The effects of drug concentration and pH medium were investigated in enantioselective permeation of composite membranes when MIP particles were added in donor phase of diffusion cell. In addition, the permeation of omeprazole enantiomers into MIP-NOM composite cellulose membranes was studied by using Confocal laser scanning microscopy (CLSM).

5.2. Experimental

5.2.1. Materials and apparatus

Nexium® (esomeprazole sodium salt) i.v. 40 mg, AstraZeneca, quinine (QN) and quinidine (QD) were purchased from Kwizda (Vienna, Austria). *RS*-omeprazole was purchased from Sigma-Aldrich (Milwaukee, WI, USA). Methacryloyl chloride was supplied by Fluka (Buchs, Switzerland). *n*-butyllithium (1.6 M in hexane) was purchased from Sigma-Aldrich (Vienna, Austria). Tetrahydrofuran (THF) used for synthesis of methacryloylate QN and methacryloylate QD was purified by reflux with calcium hydride for 4 h and subsequently distilled before use. All solvents used were of either analytical grade or HPLC grade. The *S*-omeprazole used as template in MIP preparation was extracted from Nexium® i.v. 40 mg, AstraZeneca using the procedure as follows. Nexium® i.v. (53.20 mg, 0.14 mmol) was dissolved in distilled water (2 ml). 0.1 N HCl (1.44 ml, 1 equivalent) was added. The chloroform was added to extract the omeprazole free base (3 ml, three times), washed with brine (3 ml) and distilled water (3 ml) and then dried in magnesium sulfate. The chloroform was evaporated by rotary evaporator at ambient temperature (25±1^{o}C). The recovery of *S*-omeprazole was determined by stereospecific HPLC analysis method which was found to be 98.0±1.0% (using *RS*-omeprazole as standard assuming to contain 50% *S*-omeprazole) with high purity which given as 100% measured by elemental analysis (FLASH EA 1112 CHNS-O Analyzer, CE Instruments, UK). Buffers used in this study were prepared as follows:

pH 6.8 buffer (0.07 M, μ=0.07): add 50 mmol of KH_2PO_4 and 22 mol of NaOH in 1 L volume distilled water.

pH 7.4 buffer (0.1 M, μ=0.22): add 39 mmol of NaH_2PO_4 and 61 mmol of Na_2HPO_4 in 1 L volume distilled water.

pH 10 buffer (0.1 M, μ=0.16): add 68 mmol of $NaHCO_3$ and 32 mmol of Na_2CO_3 in 1 L volume distilled water.

Melting points of synthesized methacryloylate QN and methacryloylate QD were determined with a Kofler apparatus, equipped with a Leica microscope. Optical rotation

values were recorded on a Jasco P-1020 Polarimeter (Jasco, Tokyo, Japan). IR spectra were obtained by using FT-IR spectrometer (Perkin-Elmer system 2000, Perkin-Elmer, Beaconsfield, UK). ^{1}H NMR spectra were acquired on a Bruker DRX 200 MHz spectrometer.

5.2.2. Stereospecific HPLC analysis and method validation for omeprazole enantiomers

5.2.2.1. Stereospecific HPLC analysis

The stereospecific HPLC analysis for determination of omeprazole enantiomers in the samples was performed using a Dionex ICS-3000 system includes Dionex AS-Autosampler, ICS 3000 DC-Detector/Chromatography module, ICS 3000 SP-Single Pump equipped with PDA-100 Photodiode array detector. The column used was Chiral-AGP column (150 mm × 4 mm, 5 µm) (Chiral-AGP^{TM}, ChromTech Ltd., UK). The mobile phase contained 10% acetonitrile in 10 mM sodium phosphate buffer pH 6.5. Ten µl volume sample loop was used and the temperature of column was set at 25^{o}C. The wavelength was set at 302 nm and the flow rate of 1 ml.min^{-1} was used throughout. The retention times of *R*- and *S*-enantiomers of omeprazole were 4.5 and 8.8 min, respectively.

5.2.2.2. Validation

The stereospecific HPLC method was validated to ensure that it was suitable for determination of omeprazole enantiomers in the buffer solutions used in enantioselective release study.

Linearity

The standard calibration curves were constructed separately for the *R*- and *S*-omeprazole enantiomers, using racemic omeprazole. The stock solution of *RS*-omeprazole was prepared at the concentration of 100 µg.ml^{-1} by dissolving *RS*-omeprazole in pH 10 buffer. The

solution was further diluted with pH 10 buffer to obtain the concentrations of 1-50 μg.ml^{-1}. Each concentration was prepared in sets of three and each one was analyzed by stereospecific HPLC method in triplicate. To assess the linearity, the standard curves for omeprazole enantiomers were constructed by plotting concentration (μg.ml^{-1}) of drug as function of peak area on HPLC chromatogram.

Precision

The precision was evaluated through repeatability and evaluated through relative standard deviation (RSD). Three different concentrations (5, 10 and 20 μg.ml^{-1}) of racemic omeprazole were prepared in pH 10 buffer. Each concentration was prepared in sets of three and each one was injected to stereospecific HPLC methods in triplicate.

Accuracy

The accuracy was evaluated by comparing the measured concentration with the actual concentration and expressed by %recovery which used the data obtained in precision study.

The limit of detection (LOD) and the limit of quantification (LOQ)

Calibration curves were constructed according to linearity study. The limit of detection (LOD) and the limit of quantification (LOQ) were calculated by equation 2.1 and 2.2.

5.2.3. Stability aspects of *S*-omeprazole and racemic omeprazole

The stability of *S*-omeprazole was studied in polymerization condition to ensure that *S*-omeprazole was stable during MIP preparation. The *S*-omeprazole solution in chloroform (10 μg.ml^{-1}) was incubated under UV 365 nm for 4 h at room temperature (25±1^{o}C). After the incubation time, chloroform was evaporated and the residue was reconstituted with mobile phase and the amount of *S*-omeprazole was analyzed by stereospecific HPLC method.

A stock solution containing 1000 μg.ml^{-1} of racemic omeprazole in ethanol was prepared using a simple solution method. This stock solution was further diluted to a concentration of 10 μg.ml^{-1} using pH 6.8, pH 7.4 or pH 10 buffers. The freshly prepared solutions were injected to stereospecific HPLC for zero day (or min) record. The solutions were stored in vial and protected from light at room temperature (25±1^{o}C), 4 and/or 37±0.5^{o}C. The concentration of omeprazole enantiomers was measured again at the appropriate intervals. For the stability study of omeprazole in chloroform, racemic omeprazole solution was prepared in the same procedure as above but with chloroform as the solvent. After incubation time, chloroform was evaporated and the residue was reconstituted with the mobile phase before the determination of omeprazole enantiomers by stereospecific HPLC method.

In addition, the stability of racemic omeprazole was studied in the condition of drug delivery system preparation to ensure that racemic omeprazole was stable during the preparation of drug delivery system. The racemic omeprazole solution in ethanol (10 μg.ml^{-1}) was incubated under UV 365 nm for 30 min at room temperature (25±1^{o}C). After incubation time, ethanol was evaporated and the sample was reconstituted with the mobile phase and the amount of omeprazole enantiomers remained was analyzed by stereospecific HPLC method. Each experiment was carried out three times.

5.2.4. Solubility study of racemic omeprazole

The solubility of racemic omeprazole was determined in chloroform, pH 6.8, pH 7.4 and pH 10 buffers at room temperature (25±1^{o}C). An excess amount of racemic omeprazole was added into 10-ml vial containing 3 ml individual solvents. The mixtures were sonicated for 10 min and constantly stirred at 250 rpm for 6 h using magnetic bar and magnetic stirrer. After 6 h, the solutions were passed through a 0.2 μm filter, diluted with mobile phase and the amount of omeprazole solubilized was then estimated by stereospecific HPLC method. The standard curve for omeprazole was established in pH 10 buffer and from the slope of the standard curve the solubility of omeprazole was calculate. The studies were repeated in triplicate and mean was calculated.

5.2.5. Synthesis of methacryloylate quinine and methacryloylate quinidine

Quinine or quinidine (as free base) (2.5 g, 7.70 mmol) was dissolved in tetrahydrofuran (THF) (25 ml). The solution was cooled to -80^{o}C (ethanol-dry ice mixture). Then 1.6 M solution of *n*-butyllithium/hexane (5.30 ml, 8.47 mmol, 1.1 equivalents) was added dropwise *via* a syringe. The reaction mixture was allowed to warm up to ambient temperature and a solution of methacryloyl chloride (0.82 ml, 8.47 mmol, 1.1 equivalents) in THF (5 ml) was added *via* a dropping funnel. The reaction mixture was stirred for 30 min. After evaporation of the solvent, the residue was dissolved in ethyl acetate (50 ml). The solution was washed with 0.5 M aqueous sodium hydroxide (50 ml, two times) and brine (50 ml, two times). After drying in magnesium sulfate, the solvent was evaporated at ambient temperature and the residue was dried in high vacuum. The resultant was purified by column chromatography on silica with methanol-ethyl acetate 1:4 (v/v) as the eluent. Evaporation of solvent gave methacryloylate QN (white solid) and methacryloylate QD (yellowish oil). Yield: 2.0 g (5.10 mmol), 65% for the methacryloylate QN and 1.90 g (4.84 mmol), 62% for the methacryloylate QD.

Physical properties of methacryloylate QN: m.p. 124-126^{o}C; $[\alpha]_{589}^{25}$ = +19.02 (*c*=1.00, $CHCl_3$); IR (KBr): 1711 (C=O stretching of carbonyl ester), 1230 (C-O stretching) and 1156 (C-O-C stretching) cm^{-1}; ^{1}H NMR (200 MHz, $CDCl_3$): δ 8.7 (d, *J*=4.5 Hz, 1H, H-2'), 8.0 (d, *J*=9.1 Hz, 1H, H-8'), 7.4 (m, 3H, H-3',5',7'), 6.5 (d, *J*=6.8 Hz, 1H, H-9), 6.2 (s, 1H, H_a-15 or H_b-15), 5.8 (m, 1H, H-10), 5.6 (s, 1H, H_a-15 or H_b-15), 5.0 (m, 2H, CH_2, H-11), 3.9 (s, 3H, OCH_3), 3.4-2.3 (m, 6H, quinuclidineH), 2.0 (s, 3H, CH_3), 1.8-1.5 (m, 5H, quinuclidineH) ppm.

Physical properties of methacryloylate QD: m.p. -; $[\alpha]_{589}^{25}$ = +39.81 (*c*=1.00, $CHCl_3$); IR (NaCl window): 1715 (C=O stretching of carbonyl ester), 1230 (C-O stretching) and 1154 (C-O-C stretching) cm^{-1}; ^{1}H NMR (200 MHz, $CDCl_3$): δ 8.7 (d, *J*=4.4 Hz, 1H, H-2'), 8.0 (d, *J*=9.1 Hz, 1H, H-8'), 7.4 (m, 3H, H-3',5',7'), 6.6 (d, *J*=6.9 Hz, 1H, H-9), 6.2 (s, 1H, H_a-15 or H_b-15), 6.0 (m, 1H, H-10), 5.6 (s, 1H, H_a-15 or H_b-15), 5.1 (m, 2H, CH_2, H-11), 3.9 (s, 3H, OCH_3), 3.3-2.3 (m, 5H, quinuclidineH), 1.9 (s, 3H, CH_3), 1.8-1.3 (m, 6H, quinuclidineH) ppm.

5.2.6. Preparation of MIP-NOMs selective to *S*-omeprazole

The template (*S*-omeprazole, 0.4 mmol), functional monomer (4-VPD, methacryloylate QD or methacryloylate QN, 1.6 mmol), cross-linker (EDMA, 9.2 mmol), AIBN (0.04 mmol), PFPS (25 mg) and PMC (20 ml) were added in chloroform (5 ml). The resultant microsuspension was placed in a 120-ml vial (5 cm in diameter) and degassed by sonication for 5 min and purged with nitrogen stream for 5 min before polymerizing at 365 nm for 4 h at room temperature (25±1^{o}C). During polymerization, the imprinting mixture was stirred vigorously by magnetic stirrer and a magnetic bar (0.9 cm length, 0.4 cm in diameter) at 1000 rpm. The MIP particles were collected by filtration and dried in dessiccator under vacuum for 24 h. The template molecule was removed by washing in 1:9 (v/v) acetic acid and methanol mixture (50 ml, three times) and then in methanol several portions (50 ml, ~three times) until no trace of *S*-omeprazole was detected in the final rinsing analyzed by stereospecific HPLC method. In each wash, the MIP particles were centrifuged at 3000 G using a HERMLE rotor Z323K model (Wehingen, Germany) before changing the solvent. The resulting MIP particles were then dried in dessiccator under vacuum and kept in dessiccator at room temperature (25±1^{o}C) until use. The variety types of MIP-NOM and corresponding NIP-NOM synthesized in this study are summarized in Table 5.1.

Table 5.1. Types and compositions of MIP-NOM and NIP-NOM synthesized in this study.

Polymer	**Composition**		
	Template	**Functional monomer**	**Cross-linker**
4-VPD-MIP-NOM	*S*-omeprazole	4-VPD	EDMA
4-VPD-NIP-NOM	-	4-VPD	EDMA
MQD-MIP-NOM	*S*-omeprazole	Methacryloylate QD	EDMA
MQD-NIP-NOM	-	Methacryloylate QD	EDMA
MQN-MIP-NOM	*S*-omeprazole	Methacryloylate QN	EDMA
MQN-NIP-NOM	-	Methacryloylate QN	EDMA

5.2.7. Characterization of MIP-NOMs

The MIP particles were characterized in terms of morphology, porosity and degree of swelling. The morphology of 4-VPD-MIP-NOM, MQD-MIP-NOM and MQN-MIP-NOM was examined to confirm the success of NOM formation using SEM. The porosity was examined using nitrogen adsorption/desorption analysis. The degree of swelling was examined using equilibrium incubation method in chloroform and various pH buffers (pH 6.8, pH 7.4 and pH 10 buffers).

5.2.8. Enantioselective binding evaluation of MIP-NOMs

The enantioselective rebinding ability of various types of MIP-NOM (4-VPD-, MQD- and MQN-MIP-NOMs) for omeprazole enantiomers was determined by batch binding experiment in various solvents. 20 mg of imprinted and non-imprinted polymer particles was incubated separately in 10-ml vial containing 2 ml of 500 $\mu g.ml^{-1}$ racemic omeprazole in chloroform or pH 6.8, pH 7.4 or pH 10 buffers at room temperature ($25\pm1^{o}C$) for 6 h. The incubation mixtures were stirred at 250 rpm throughout the study. After the incubation time, the polymer particles were separated by centrifugation at 3000 G for 5 min. The amounts of omeprazole enantiomers were analyzed by stereospecific HPLC method. All experiments were run in triplicate. The amount of each enantiomer bound to the MIP particles was calculated by subtracting the free amount of drug remained in the solution from initial amount added. The enantioselectivity of binding of MIP-NOMs was presented as the ratio of amount bound *S*-omeprazole enantiomer to amount bound *R*-omeprazole enantiomer.

5.2.9. Preparation of MIP-NOM composite cellulose membranes

The MIP-NOM composite membranes were prepared by phase inversion technique. Various types of MIP-NOMs were loaded into cellulose membrane either with or without omeprazole enantiomers. For drug release study, MIP particles (100 mg) were loaded together with *RS*-omeprazole (10 mg). For FT-IR study, MIP particles (100 mg) was loaded

together with *S*-omeprazole (4 mg for 4-VPD-MIP-NOM and MQN-MIP-NOM membranes and 3 mg for MQD-MIP-NOM membrane) in order to obtain an equivalent mole ratio of the amount of binding sites of MIP and template *S*-omeprazole (The amount of binding sites of 4-VPD-MIP-NOM, MQD-MIP-NOM and MQN-MIP-NOM were 1.20×10^{-4}, 8.68×10^{-5} and 1.16×10^{-4} $mol.g^{-1}$, respectively, which were calculated from the amount bound *S*-omeprazole enantiomer to MIP particles according to the binding study). For XRD and Differential scanning calorimetry (DSC) study, MIP particles (100 mg) were loaded together with *S*-omeprazole (3 or 4 mg) same as those for FT-IR study. Moreover, the MIP-NOM composite membranes loaded with *RS*-omeprazole at low amount (8 mg for 4-VPD-MIP-NOM and MQN-MIP-NOM membranes and 6 mg for MQD-MIP-NOM membrane) and at high amount (80 mg for 4-VPD-MIP-NOM and MQN-MIP-NOM membranes and 60 mg for MQD-MIP-NOM membrane) were prepared. The MIP particles were incubated in chloroform (2 ml) containing omeprazole enantiomer(s) for 6 h and followed by evaporating chloroform by using nitrogen stream to obtain dry polymer-drug mixture, which sequentially loaded into cellulose membrane. The entrapment of drug into composite membranes was assumed to be a hundred percent due to no amount of drug was detected in precipitating medium measured by stereospecific HPLC analysis method. For drug permeation and CLSM study, the MIP-NOM composite membranes were prepared without drug loading; 100 mg of MIP particles was used per membrane. The composite membranes with a cross-sectional area of 28 cm^2 were recovered in both the cases of with and without drug loading. The control composite membranes were prepared as the MIP-NOM composite membranes but used NIP-NOMs instead of MIP-NOMs.

5.2.10. Enantioselective release study

The enantioselective release properties of MIP-NOM composite membranes were evaluated by dissolution testing method in chloroform and buffers. The test membrane (1.5cm×1.5cm) was placed in 10-ml vial containing different media (i.e., chloroform, pH 10, pH 7.4 and pH 6.8 buffers) (3 ml) and the vial was placed on the magnetic stirring plate (Variomag, FL, USA). The medium was gently stirred by magnetic bar at 250 rpm throughout the study time period at room temperature ($25\pm1^{o}C$). Two hundred µl of sample was taken from the vial at

different time points between 0-6 h with replacing medium of the same volume (200 µl) into the vial. The amounts of omeprazole enantiomers were determined by stereospecific HPLC method. All experiments were run in triplicate. According to the equation 3.3, the diffusion coefficient (D, $cm^2.h^{-1}$) of each enantiomer was obtained from the slope of graph plotted between the release fraction $\left(\frac{\text{cumulative amount } (\mu g.cm^{-2}) \times \text{membrane thickness (cm)}}{\text{drug concentration inside membrane } (\mu g.cm^{-3})} \right)$ and time (h).

The release mechanism was examined by fitting the first 60% data according to the well-known Korsmeyer-Peppas semi-empirical equation:

$$\frac{M_t}{M_\infty} = kt^n \tag{5.1}$$

Where; M_t/M_∞ is fractional release of the drug, t denotes the release time, k represents a constant, incorporating structural and geometrical characteristics of the system, and n is the release exponent and characterizes the type of release mechanism of drug from the composite membrane. For non-Fickian release, the value of n falls between 0.5 and 1.0; while in case of Fickian diffusion, n=0.5; for zero-order release (Case-II transport), n=1; and for Super Case-II transport, n>1 (Table 5.2) (Costa and Lobo, 2001). The values of n were estimated by linear regression of log (M_t/M_∞) versus log (t).

Table 5.2. Interpretation of diffusional release mechanisms from polymeric films (Costa and Lobo, 2001).

Release exponent (*n*)	**Drug transport mechanism**	**Rate as function of time**
0.5	Fickian diffusion	$t^{-0.5}$
$0.5 < n < 1.0$	Anomalous (non-Fickian) transport	t^{n-1}
1.0	Case-II transport	Zero order release
Higher than 1.0	Super Case-II transport	t^{n-1}

5.2.11. Fourier transform infrared spectroscopy (FT-IR) study

The complexation between MIP and template was investigated by Fourier transform infrared spectroscopy (FT-IR). FT-IR spectra of the complexes of MIP particles and *S*-omeprazole loaded into cellulose membranes were evaluated to compare with MIP particles without drug loading membrane by using FT-IR spectrometer (Perkin-Elmer series 2000, Perkin-Elmer, Beaconsfield, UK) in an Attenuated total reflectance (ATR). The test membrane (1cm×1cm) was placed on the crystal (ZnSe) of the ATR module and the spectra were recorded (16 scans).

5.2.12. X-ray diffraction (XRD) study

The MIP-NOM composite membranes as in the case of FT-IR experiment were further examined in X-ray spectra using PHILIPS X'Pert MPD X-ray diffractometer (Philips Analytical, Natick, MA, USA). Also, the complexation of MIP particles and *RS*-omeprazole loaded into cellulose membrane, which prepared by loading MIP particles together with *RS*-omeprazole in different contents were examined. The samples were scanned in 2θ range of 5-60^{o} with 5^{o}.min^{-1} scan speed.

5.2.13. Differential scanning calorimetry (DSC) study

The composite membranes which MIP-NOM loaded together with drug were also characterized by differential scanning calorimeter (DSC7, Perkin-Elmer, Beaconsfield, UK). The DSC measurement was performed at a heating rate of 10^{o}C.min^{-1} in the temperature range -50 to 250^{o}C under an ambient nitrogen atmosphere.

5.2.14. Enantioselective permeation study

In this study, the MIP-NOM composite cellulose membranes without drug loading were used. The permeation of omeprazole enantiomers across composite membranes

loaded with different types of MIP-NOM (4-VPD-, MQD- and MQN-MIP-NOMs) was performed using side-by-side diffusion cell (Figure 5.3) at room temperature (25±1^{o}C). The cell flanges were greased with high performance vacuum grease and the membrane was clamped between donor and receptor chambers of the diffusion cell, which each chamber had a capacity for 2.5 ml and the effective area for membrane was 0.8 cm^{2}. The receptor chamber was filled with fresh buffer solution (pH 7.4 or pH 10) and the donor chamber was filled with the same solution as in the receptor chamber containing racemic omeprazole in the different concentrations (in the range of 80-500 μg.ml^{-1}). Micromagnetic stirrer bars were added to both donor and receptor chambers and set to stir at 250 rpm throughout the experiment. Samples (200 μl) were collected from receptor chamber at a preset time (0-6 h), and the amount of each enantiomer of omeprazole permeated through the MIP-NOM composite membranes was determined by stereospecific HPLC method. The permeation medium was replaced into the diffusion cell. The experiments were performed in triplicate.

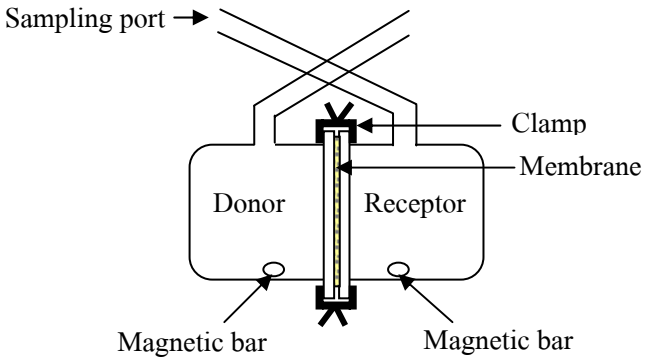

Figure 5.3. Side-by-side diffusion cell used in this study.

In addition, the effect when MIP particles were loaded in drug solution in donor chamber was studied. The racemic omeprazole solution in each concentration (2.5 ml/ pH 7.4) was incubated with MIP-NOM (5 mg) for 6 h before loading such drug solution containing MIP particles into donor chamber. The enantiomeric excess (%ee) which is the excess of predominant enantiomer in the diffusion medium in receptor phase expressed as percent was calculated, which for *R*>*S* was given by:

$$\%ee = \frac{(R-S)}{(R+S)} \times 100 \quad (5.2)$$

5.2.15. Confocal laser scanning microscopy (CLSM) study

Confocal laser scanning microscopy (CLSM) is now a routine instrument to obtain high resolution fluorescence images and sequentially reconstruct the three-dimensional (3D) structure of specimens. It can capture the fluorescence images sliced in the plane perpendicular to the optical axis and can scan the plane position along the optical axis.

CLSM images of the test membrane were collected under CLSM measurement: CLSM (Fluoview FV300, Olympus, Tokyo, Japan) equipped with an argon ion laser (488 nm, Melles Griot, Carlsad, CA, USA) and dry objective lens (UPLAPO 10×, Olympus, Tokyo, Japan). The fluorescence emission was detected at 560 nm. A confocal pinhole (60 μm) was used to reject the out-of-focus emission light and the signal through the pinhole was collected by a photomultiplier detector (FV5-TD, Olympus, Tokyo, Japan). Samples were observed through the *XYZT* scanning mode with the scanning rate of 1.08 sec/scan. The fluorescent intensity (*I*) of the obtained images was quantified by Fluoview FV300 software. The fluctuated fluorescence in each *Z*-stack (the distance in *Z* direction; depth) was calculated as the equation:

$$\text{Fluctuated fluorescence} = \Delta I_0 - \Delta I_t \quad (5.3)$$

Where; ΔI_0 is fluorescent intensity fluctuation of membrane before exposure to the test compound and ΔI_t is fluorescent intensity fluctuation of membrane after exposure to the test compound at time t. ΔI_0 was calculated from $I - I_{(20\ \mu m)}$ of membrane before exposure to the test compound and ΔI_t was calculated from $I - I_{(20\ \mu m)}$ of membrane after exposure to the test compound at time t. $I_{(20\ \mu m)}$ is the fluorescent intensity at the *Z*-stack of 20 μm of membrane. The subtraction of the viable fluorescent intensity and nonviable fluorescent intensity was plotted as a function of time at the *Z*-stack of 5, 20 and 50 μm.

The test membrane (MQN-MIP-NOM or MQD-MIP-NOM composite cellulose membranes without drug loading) (0.5cm×0.5cm) was placed on glass slide and fixed by two

coverslips on the left and right edge sides of membrane, allowing the middle sides (~0.3 cm in width) was available for dropping the test compounds. 10 µl of pH 7.4 buffer was gently dropped by micropipette onto membrane as being viewing solution. The test drugs solutions (pH 7.4) including: *S*-omeprazole (100 µg.ml^{-1}, 10 µl), *S*-omeprazole (100 µg.ml^{-1}, 10 µl) and *RS*-omeprazole (200 µg.ml^{-1}, 10 µl) were gently dropped sequentially onto membrane. The membrane in viewing solution was scanned by CLSM as blank and the same membrane was scanned after exposure with each test drug solution. Each experiment was repeated two times.

5.2.16. Statistic analysis

Statistical analyses were carried out using SPSS version 13.0 (SPSS, Cary, NC, USA). Paired *t*-tests were used to investigate differences of *R*- and *S*-enantiomers of omeprazole in every experimental test. A *p*-value of <0.05 was considered significant.

5.3. Results and discussion

5.3.1. Method validation

The linearity, precision, accuracy, limit of detection (LOD) and limit of quantification (LOQ) of omeprazole enantiomers from stereospecific HPLC assay are shown in Table 5.3. The stereospecific HPLC method used for determination of omeprazole enantiomers in buffers was found that calibration curves of omeprazole enantiomers were linear over the concentration range of 1-50 µg.ml^{-1} in all pH buffers (correlation coefficients were higher than 0.999 for both *R*- and *S*-omeprazole enantiomers). The %RSD of repeatability was found lower than 2% for both enantiomers and the recovery was found in the range of 99.85-100.34% for both enantiomers. The stereospecific HPLC method was considered to be precise and accurate for determination of omeprazole enantiomers in the enantioselective release study.

Table 5.3. Linearity, precision, accuracy, limit of detection (LOD) and limit of quantification (LOQ) of omeprazole enantiomers from stereospecific HPLC assay.

Isomer	Linearity (R^2)	Precision (%RSD)	Accuracy (%recovery)	LOD ($\mu g.ml^{-1}$)	LOQ ($\mu g.ml^{-1}$)
R-omeprazole	0.9998	0.62	99.85	0.42	1.40
S-omeprazole	0.9998	0.55	100.34	0.51	1.71

5.3.2. Stability of omeprazole enantiomers

Figure 5.4 shows stability results of omeprazole enantiomers in various conditions related to the experiments. Both *R*- and *S*-omeprazole enantiomers had similar characteristic of stability profile in every solvent studied. The stability of omeprazole enantiomers in pH 7.4 buffer at room temperature (25±1^{o}C) was gradually decreased within 7 days. The omeprazole enantiomers were remained about 90% after one day. At lower pH 7.8, the decomposition of omeprazole occurred about 6% in 24 h at 25^{o}C (Mathew et al., 1995). The storage of omeprazole solutions at 4^{o}C can delay the degradation of omeprazole enantiomers as revealed that omeprazole enantiomers were still remained above 80% after 5 days in pH 7.4 buffer. Omeprazole enantiomers had a good stability (>95%) in pH 10 buffer as well as in chloroform at least 7 days at room temperature (25±1^{o}C). The stability of omeprazole enantiomers was also evaluated in pH 6.8 and pH 7.4 buffers at 37±0.5^{o}C. It was found that omeprazole enantiomers were remained higher than 95% in both pH buffers after 6 h.

Furthermore, *S*-omeprazole in chloroform as well as *RS*-omeprazole in ethanol were found to be stable under the polymerization condition which the amount remaining *S*-omeprazole and *RS*-omeprazole was higher than 98% with no racemization was observed.

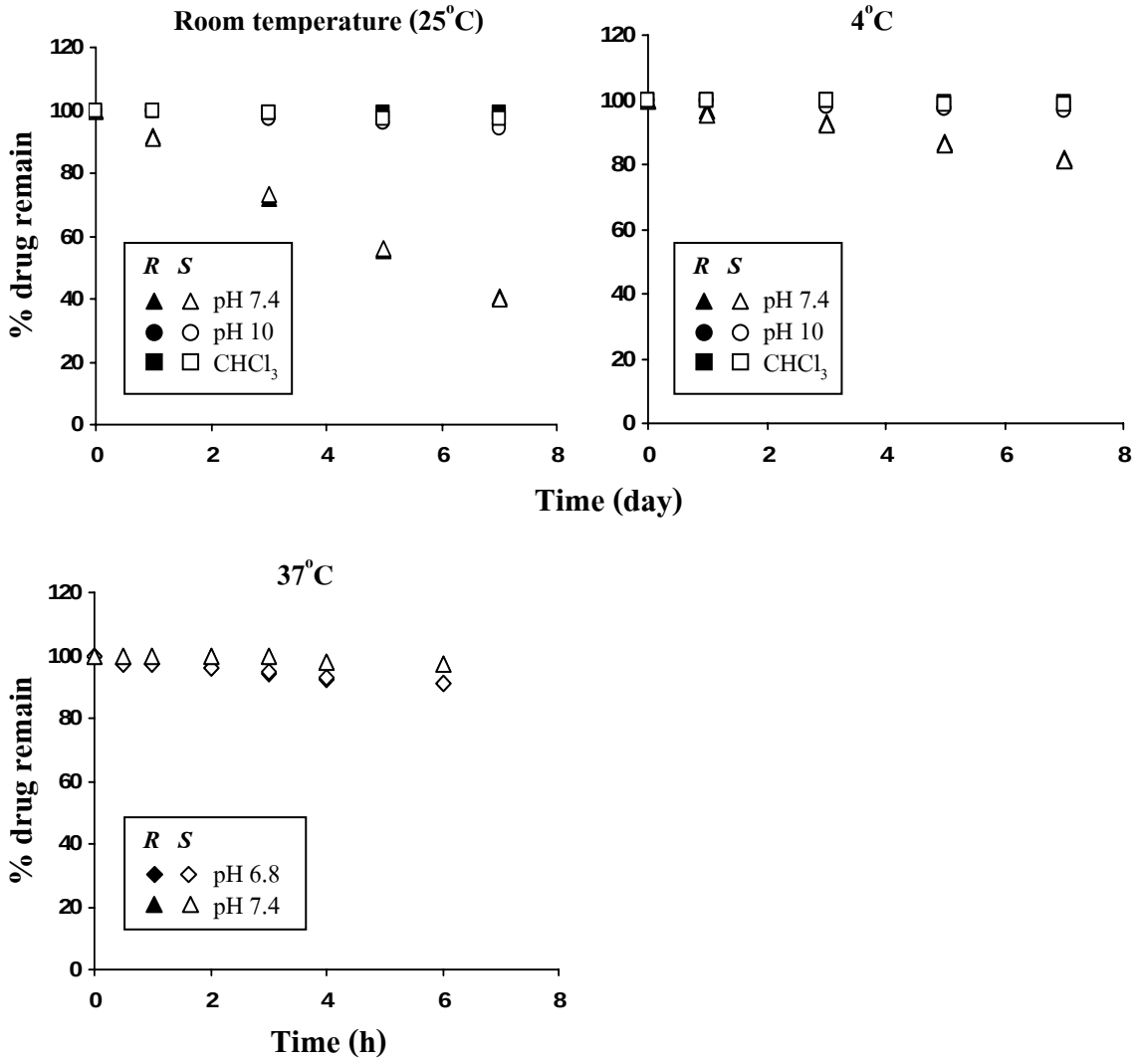

Figure 5.4. Stability of omeprazole enantiomers in different media at room temperature (25±1°C), 4 and/or 37±0.5°C.

5.3.3. Solubility of racemic omeprazole

The solubility of *RS*-omeprazole in chloroform and in various pH buffers (i.e., pH 6.8, pH 7.4 and pH 10) was examined. *RS*-omeprazole was freely soluble (> 100 $mg.ml^{-1}$) in chloroform. The solubility of *RS*-omeprazole in pH 6.8, pH 7.4 and pH 10 buffers were 1.5±0.3, 1.7±0.8, 6.0±1.2 $mg.ml^{-1}$, respectively.

5.3.4. MIP-NOMs preparation and characterization

Figure 5.5 shows morphology of 4-VPD-MIP-NOM, MQD-MIP-NOM and MQN-MIP-NOM obtained from SEM. The SEM images revealed that the resulting polymer particles in all three types were quite uniform spherical with approximately 5-10 μm in diameter for microspheres and approximately 100-300 nm in diameter for nanoparticles attached onto microspheres.

Table 5.4 shows physical characteristics (i.e., particle size, porosity and degree of swelling) of all three types of MIP-NOM and corresponding NIP-NOM. The surface area, total pore volume and average pore diameter of imprinted polymers was slightly higher than the non-imprinted polymers. The polymer particles swelled in chloroform greater than in buffers. The polymer particles containing 4-VPD showed little swelling property in buffers, while the polymer particles containing QD- and QN-derived did not swell in buffers in every pH. This may be due to the higher hydrophobic property of cinchona alkaloids: QN and QD (Log *P*=2.48) than of 4-VPD (Log *P*=1.33).

(a) 4-VPD-MIP-NOM

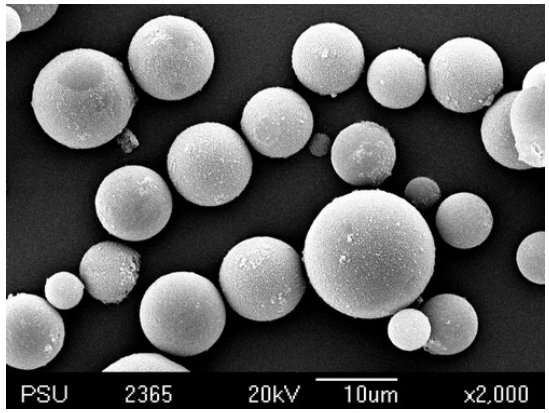

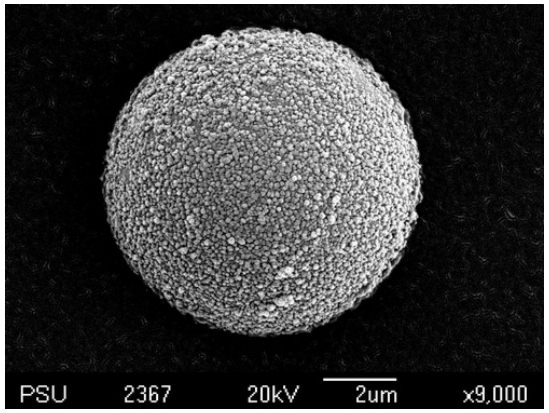

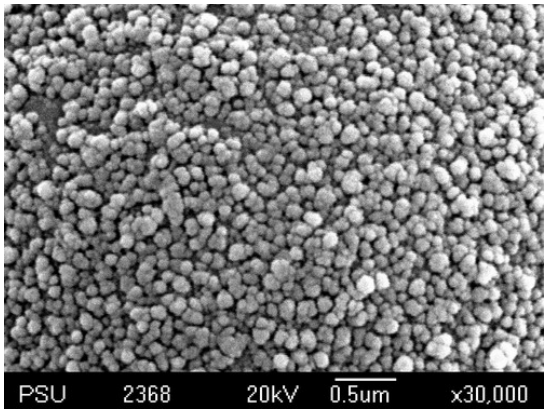

(b) MQD-MIP-NOM

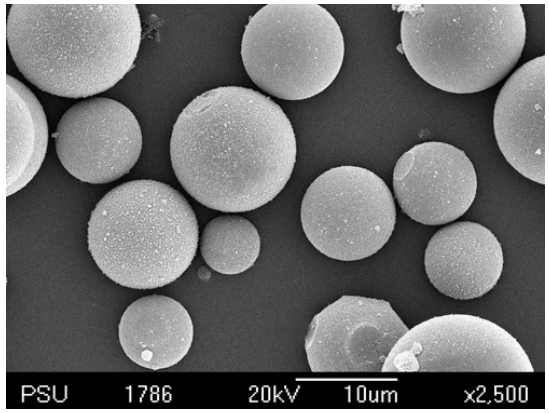

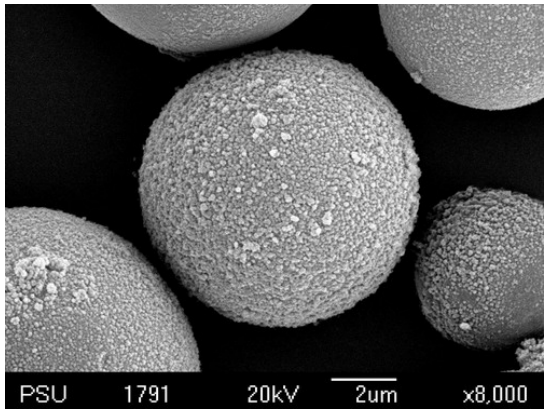

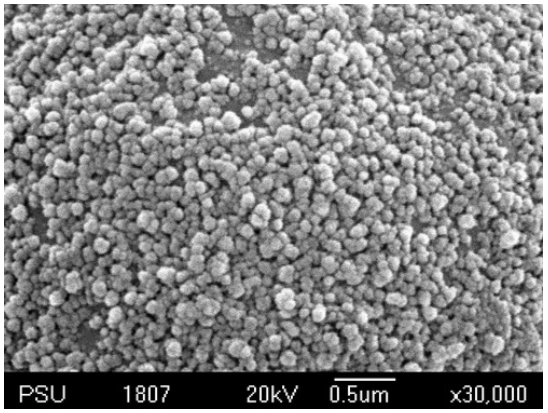

Figure 5.5. SEM images of (a) 4-VPD-MIP-NOM, (b) MQD-MIP-NOM, and (c) MQN-MIP-NOM.

(c) MQN-MIP-NOM

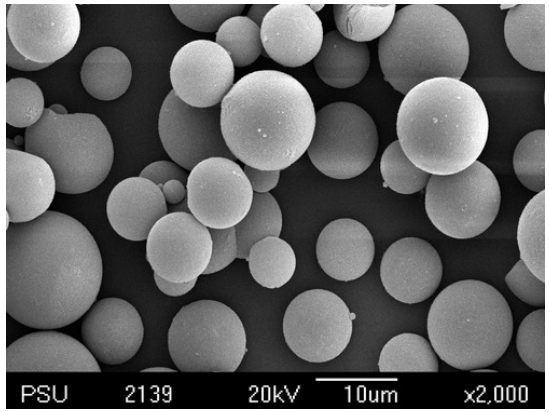

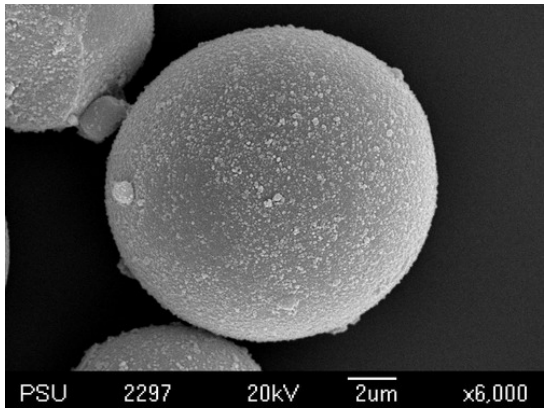

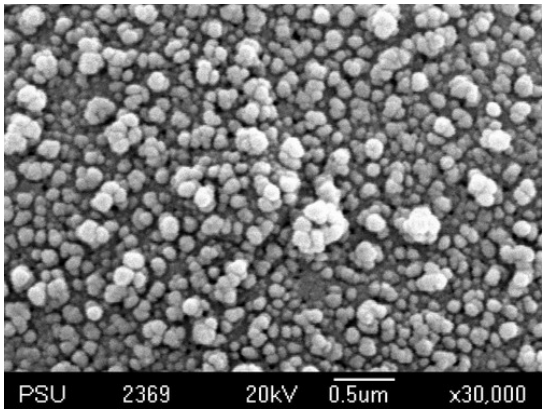

Figure 5.5. (continued)

Table 5.4. Physical properties of 4-VPD-MIP-NOM, MQD-MIP-NOM and MQN-MIP-NOM and corresponding NIP-NOMs (mean±S.D., n=3).

Polymer	Particle size*	Porosity			Degree of swelling (%)			
	(μm)	Surface area ($m^2.g^{-1}$)	Total pore volume ($ml.g^{-1}$)	Average pore diameter (nm)	chloroform	pH 6.8	pH 7.4	pH 10
4-VPD-MIP-NOM	0.13±0.02[a]	11.63	0.054	8.41	137.5±12.6	2.5±0.7	2.7±0.3	3.7±1.7
4-VPD-NIP-NOM	0.12±0.02[a]	9.43	0.039	7.81	135.2±16.3	2.5±0.7	2.7±0.3	3.7±1.7
MQD-MIP-NOM	0.13±0.02[a]	16.37	0.054	8.47	112.5±17.6	ND	ND	ND
MQD-NIP-NOM	0.13±0.02[a]	12.38	0.056	7.82	105.7±19.6	ND	ND	ND
MQN-MIP-NOM	0.13±0.04[a]	13.33	0.049	8.44	112.5±17.6	ND	ND	ND
MQN-NIP-NOM	0.12±0.03[a]	11.47	0.042	6.78	112.5±17.6	ND	ND	ND

*n=10

[a] refer to the size of nanoparticles attached onto microspheres (5-10 μm).

ND: not detectable.

5.3.5. Enantioselective binding of MIP-NOMs

The ability in enantioselective binding of MIP-NOMs was evaluated by using batch binding experiment in chloroform and in various pH buffers at room temperature (25±1°C). Figure 5.6 shows %bound *R*- and *S*-omeprazole enantiomers for 4-VPD-MIP-NOM, MQD-MIP-NOM and MQN-MIP-NOM and corresponding NIP-NOMs in chloroform, pH 10, pH 7.4 and pH 6.8 buffers. The enantioselectivity of binding was presented as *S/R* ratio of amount bound *S*- and *R*-omeprazole enantiomers, and the results are shown in Figure 5.7.

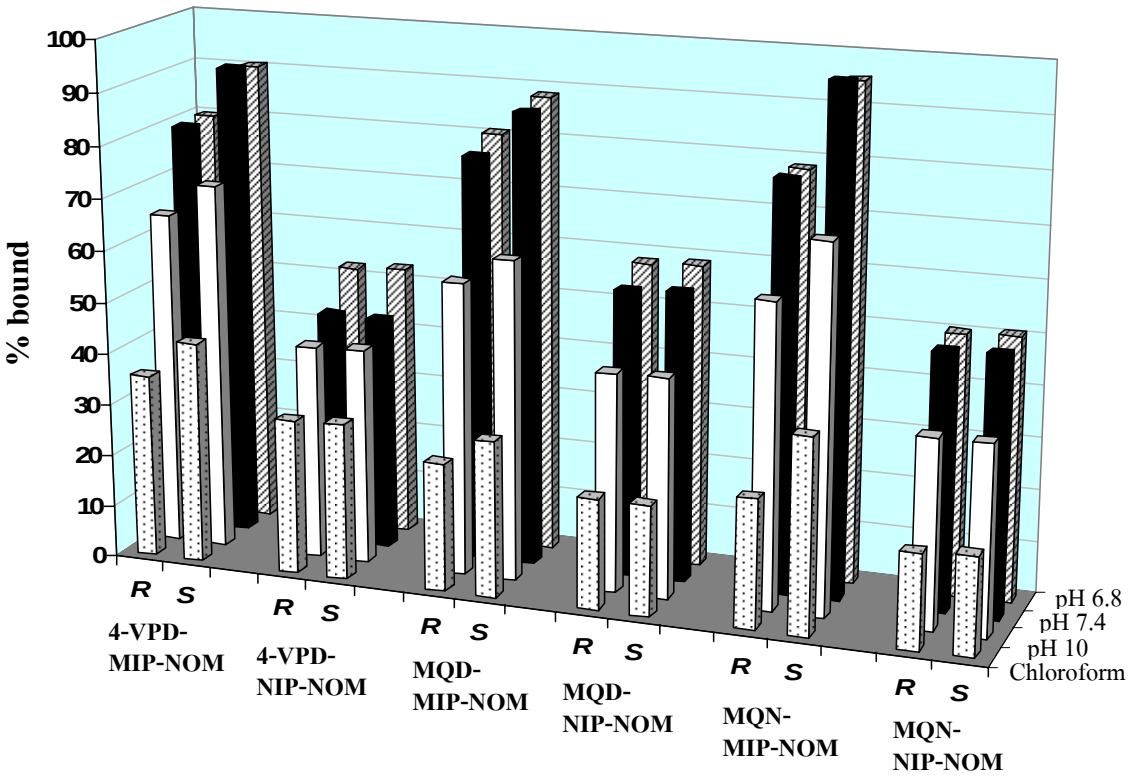

Figure 5.6. The percentage of bound *R*- and *S*-omeprazole enantiomers for 4-VPD-MIP-NOM, MQD-MIP-NOM and MQN-MIP-NOM and corresponding NIP-NOMs after incubation each type of polymers with racemic omeprazole in different media at room temperature (25±1°C).

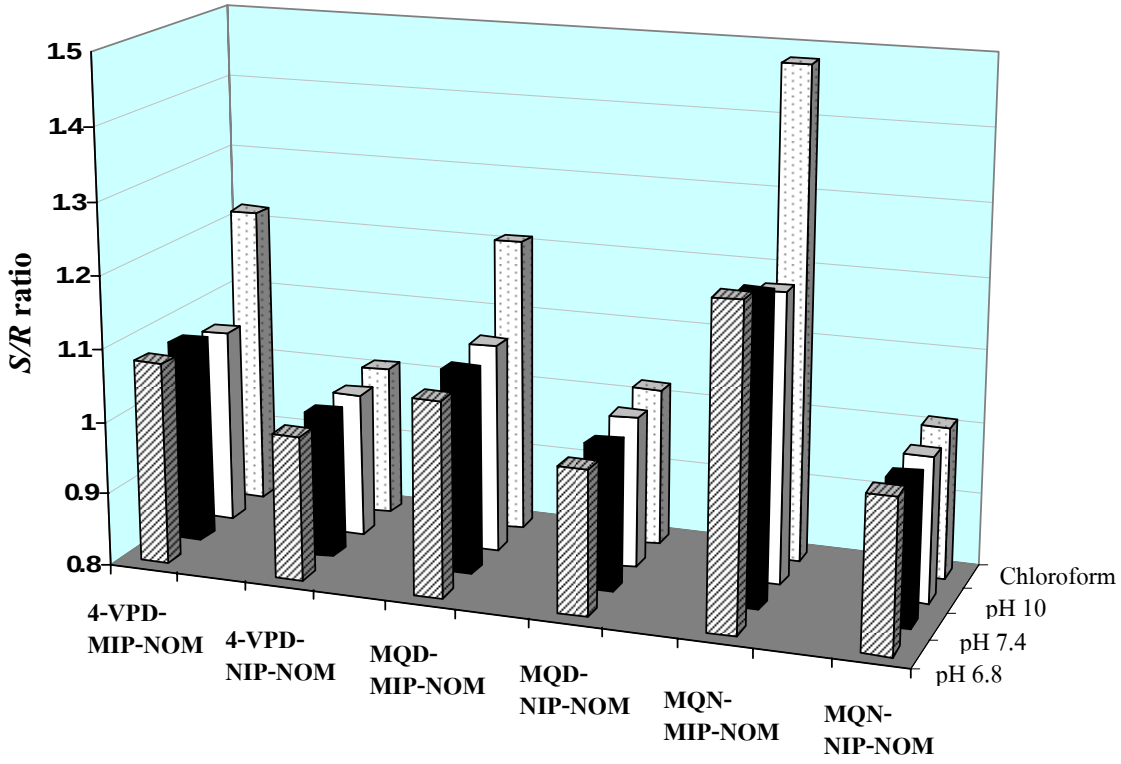

Figure 5.7. *S/R* ratio of bound omeprazole enantiomers for 4-VPD-MIP-NOM, MQD-MIP-NOM and MQN-MIP-NOM and corresponding NIP-NOMs after incubation each type of polymers with racemic omeprazole in different media at room temperature (25±1°C).

In comparison, the *S*-omeprazole imprinted NOMs bound both *R*- and *S*-omeprazole enantiomers higher than the control non-imprinted NOMs in all the solvents studied. The higher amount of omeprazole enantiomers bound on the MIP-NOMs can be explained by that the MIP-NOMs had a higher porosity, compared to NIP-NOMs, thus the drug molecules can easily diffuse and be adsorbed. The NIP was prepared by the same procedure of polymerization as MIP but in the absence of the template, so it possesses the same chemical properties as the MIP but without possessing any specific cavities. So, the high amount of omeprazole enantiomers bound to NIP-NOMs is due to the non-specific interaction. In addition, the binding amount of omeprazole enantiomers for the MIP-NOMs and NIP-NOMs in chloroform was rather low and this increased when studied in aqueous media. This is because that the lipophilic omeprazole molecule (Log *P*=2.17) causes higher non-specific binding in aqueous solvents. Under aqueous

condition, the binding amount of omeprazole enantiomers to MIP-NOMs and NIP-NOMs was increased dramatically in all types of polymers. This may be due to the hydrophobic interaction between omeprazole and polymeric matrix. The binding amount of omeprazole enantiomers for MIP-NOMs and NIP-NOMs in aqueous solvents depended on medium pH, which was slightly decreased with the increase of pH value. This can be explained as that the NH group on the benzimidazole ring of omeprazole molecule can deprotonate which this causes the reduction in binding of *S*-omeprazole template on MIP in pH 10 buffer.

For enantioselectivity evaluation, the MIP particles bound the template *S*-omeprazole enantiomer higher than *R*-omeprazole enantiomer (*S/R* ratio > 1), while the *R*- and *S*-omeprazole enantiomers were bound with NIP-NOMs in an equal (*S/R* ratio ≈ 1). The ability of MIPs to bind the template *S*-omeprazole enantiomer higher than *R*-omeprazole enantiomer indicated the imprinting effect. In all three types of MIP, the highest enantioselectivity was obtained when studied in chloroform. This implied that the molecular recognition of MIPs would be driven mainly by hydrogen bonding of template *S*-omeprazole enantiomer and functional monomers forming MIP binding sites. The enantioselective binding of MQN-MIP-NOM was the highest compared to the other MIP-NOMs. This suggested that the interaction of template *S*-omeprazole enantiomer and MQN-MIP-NOM may be stronger than that of *S*-omeprazole enantiomer and MQD-MIP-NOM. For this aspect, the further studies to evaluate the complexation formation of template *S*-omeprazole enantiomer and MIP-NOMs by using Fourier transform infrared spectroscopy (FT-IR) were performed.

5.3.6. The investigation of complexation between *S*-omeprazole and MIP-NOM by FT-IR

The complexation between *S*-omeprazole and MIP was characterized by ATR-FTIR. Figure 5.8 shows ATR-FTIR spectra of MIP-NOM composite membranes with and without *S*-omeprazole loading, in the frequency region of 1200-2600 cm^{-1}, which assigned to the group frequency region of MIPs. The absorption peak around 1730-1630 cm^{-1} was assigned to C=O stretching vibration of ester in EDMA. It appeared quite strong peak especially in the case of MQD- and MQN-MIP (Figure 5.8b and c) which contained carbonyl ester groups in cross-

linker EDMA and functional monomer methacryloylate QD and methacryloylate QN. The peak around 1750-1730 cm^{-1} was assigned to C=N stretching vibration. When *S*-omeprazole was loaded, there was no change in the position of absorption bands in the case of 4-VPD-MIP-NOM and MQD-MIP-NOM. With the addition of *S*-omeprazole, C=O peak shifted to lower frequencies about 8 cm^{-1} for MQN-MIP-NOM. In addition, new peak appeared at 2200 cm^{-1} in case of drug-MQN-MIP-NOM loaded membrane which this observed peak was assigned to the absorption peak of CO_2 (Yang and Rege, 2001). The addition of *S*-omeprazole might cause the change in the microscopic structure of MQN-MIP-NOM which this may be due to complexation formation between *S*-omeprazole and MIP.

From the binding results obtained, the possible binding sites generated on 4-VPD-MIP-NOM, MQD-MIP-NOM and MQN-MIP-NOM are shown in Figure 5.9. The higher enantioselective recognition obtained from MQN-MIP-NOM than MQD-MIP-NOM might be the consequence of stronger interaction of *S*-omeprazole enantiomer and functional monomer methacryloylate QN forming the binding site on MIP. The configuration of QN molecule would provide appropriate interaction formation with *S*-omeprazole molecule, and this might allow forming multiple intermolecular *S*-omeprazole-QN-derivative interactions, such as hydrogen bonding and π-π interaction. QD-derivative and 4-VPD molecules might have less capability to form interaction with *S*-omeprazole, and then provided lower enantioselectivity.

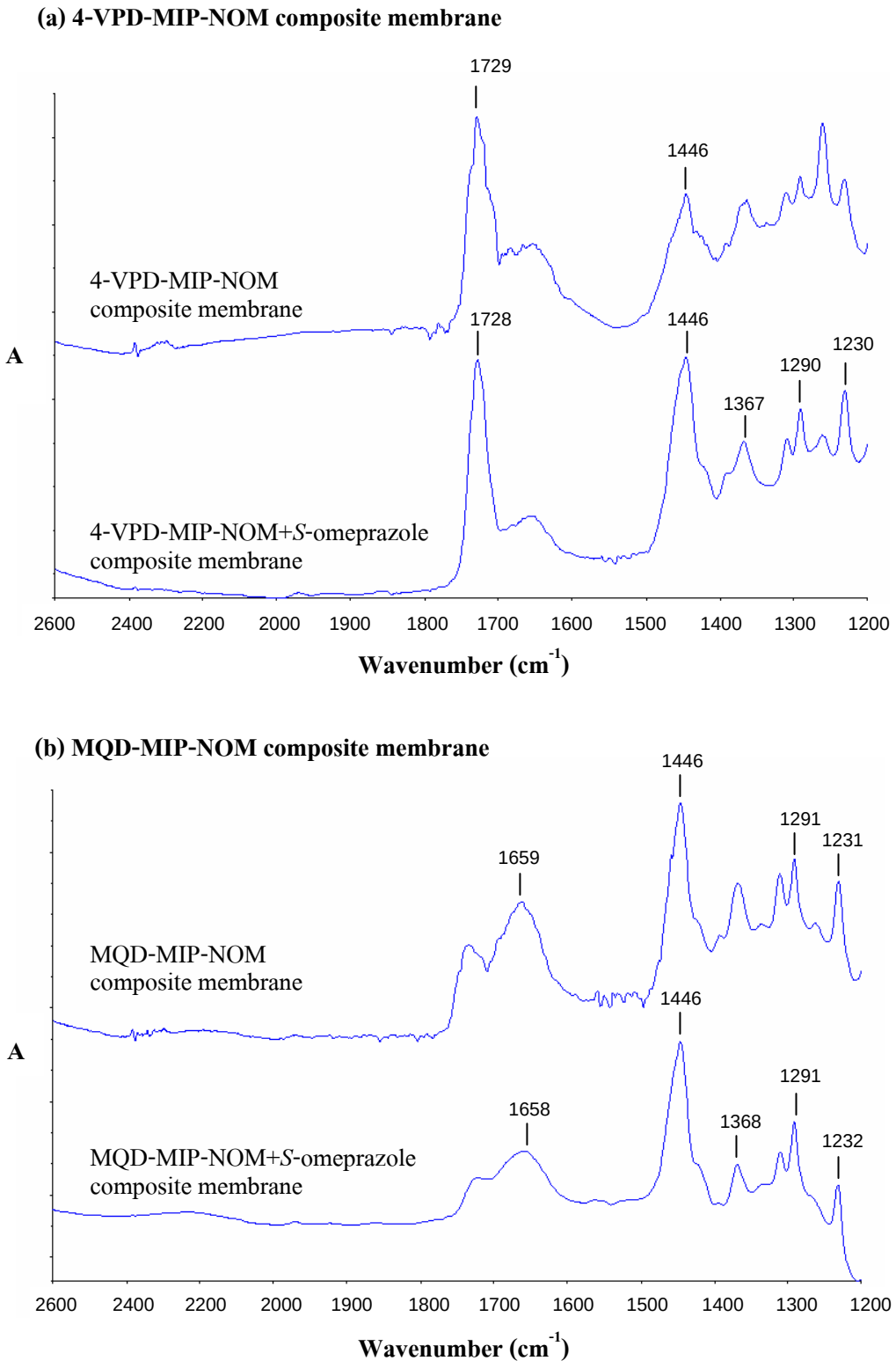

Figure 5.8. ATR-FTIR spectra of (a) 4-VPD-MIP-NOM, (b) MQD-MIP-NOM, and (c) MQN-MIP-NOM composite membranes with and without *S*-omeprazole loading.

(c) MQN-MIP-NOM composite membrane

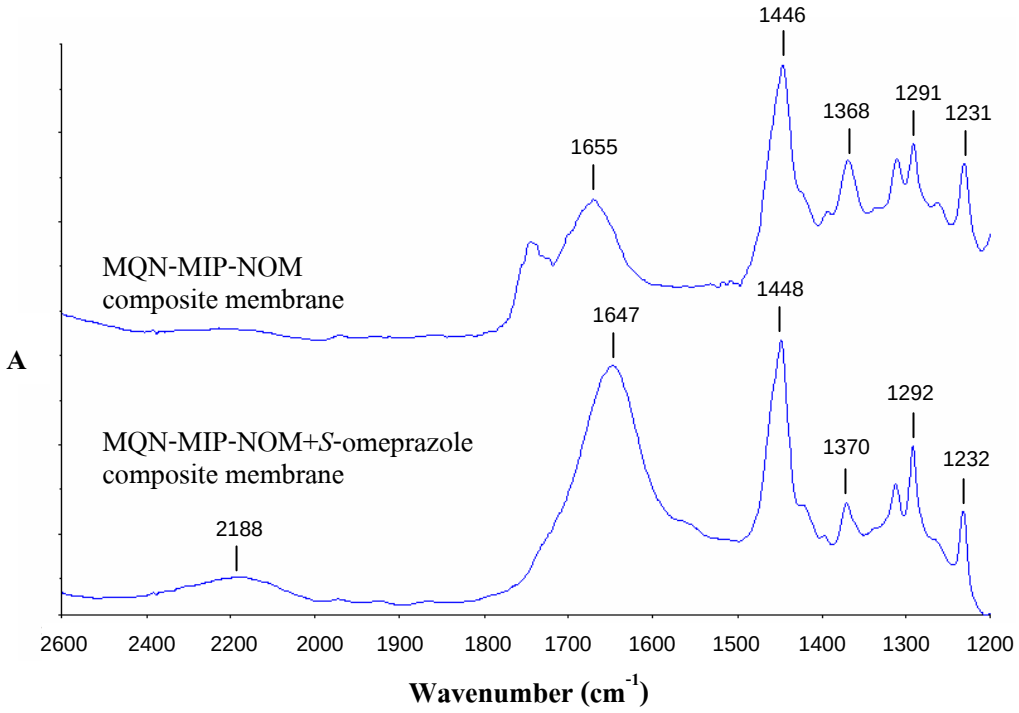

Figure 5.8. (continued)

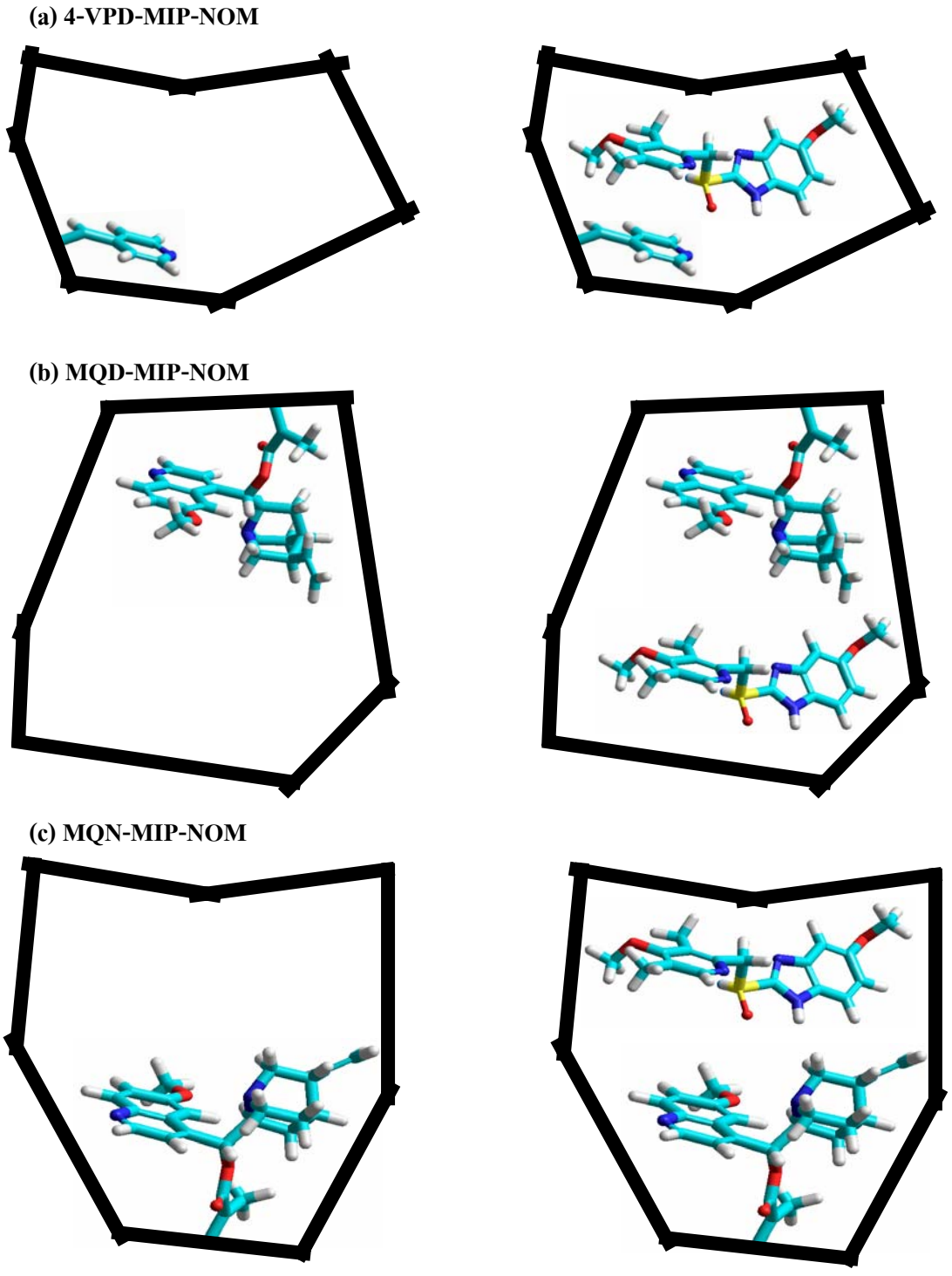

Figure 5.9. Possible binding site generation on (a) 4-VPD-MIP-NOM, (b) MQD-MIP-NOM, and (c) MQN-MIP-NOM (left column) and their assembly with template *S*-omeprazole enantiomer (right column).

5.3.7. The investigation of complexation between *S*- or *RS*-omeprazole and MIP-NOM by XRD

The XRD technique was employed to determine the complexation of the template *S*-omeprazole and *RS*-omeprazole with MIP in the composite membranes. Figure 5.10 shows XRD patterns of *RS*-omeprazole and *S*-omeprazole extracted from Nexium®, cellulose membranes: original and cast, 4-VPD-MIP-NOM, MQD-MIP-NOM and MQN-MIP-NOM composite membranes without and with *S*-omeprazole or *RS*-omeprazole loading. *RS*-omeprazole showed various diffraction peaks, indicating its crystalline nature. The extracted *S*-omeprazole showed halo diffraction pattern, indicating its amorphous structure. *S*-omeprazole powder showed crystallinity in nature (Markovic et al., 2006). The extraction process may cause the change in crystallographic structure of *S*-omeprazole. In case of the original bacterial cellulose, three broad peaks located at 2θ of 14^{o}, 16^{o} and 22^{o} were observed. The broadness of the three characteristic peaks was due to the partial crystallinity of bacterial cellulose (Wan et al., 2006). Bacterial cellulose after casting process was still observed broad peaks at 2θ of 12^{o} and 20^{o}, but rather weak intensity. This observation suggests that the casting process could decrease the crystallinity of bacterial cellulose membrane. The XRD patterns of 4-VPD-MIP-NOM, MQD-MIP-NOM and MQN-MIP-NOM composite membranes were investigated in the presence of *S*-omeprazole (3 or 4 mg) and *RS*-omeprazole at low amount (6 or 8 mg) and high amount (60 or 80 mg). The observed peak corresponding *S*-omeprazole showed the complexation of drug and MIPs. When *RS*-omeprazole was loaded at low amount, the crystalline peaks of *RS*-omeprazole were not appeared. When *RS*-omeprazole was loaded at high amount, the extra peaks were appeared by the surplus of *RS*-omeprazole diffraction peaks. These results would indicate the complexation of *RS*-omeprazole and MIPs occurred. Although, the XRD technique was useful to investigate the complexation of omeprazole and MIPs, it limited to identify the certain type of enantiomer capable to form better complexation with MIP.

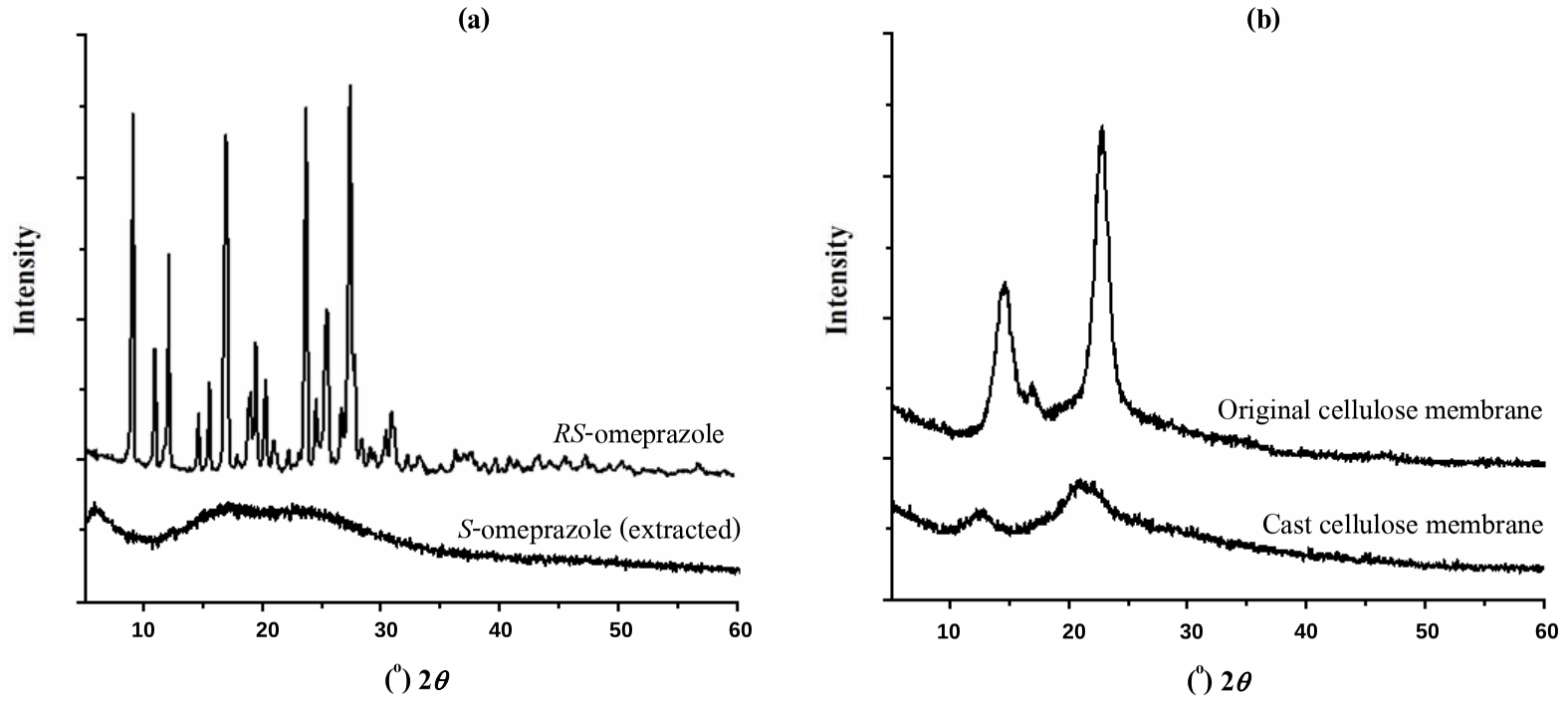

Figure 5.10. XRD patterns of (a) omeprazole (*RS*-omeprazole and extracted *S*-omeprazole); (b) cellulose membrane (original and cast cellulose membranes); (c) 4-VPD-MIP-NOM; (d) MQD-MIP-NOM; and (e) MQN-MIP-NOM composite membranes without drug loading, with *S*-omeprazole loading (3 or 4 mg) and with *RS*-omeprazole loading at low (6 or 8 mg) and at high amounts (60 or 80 mg).

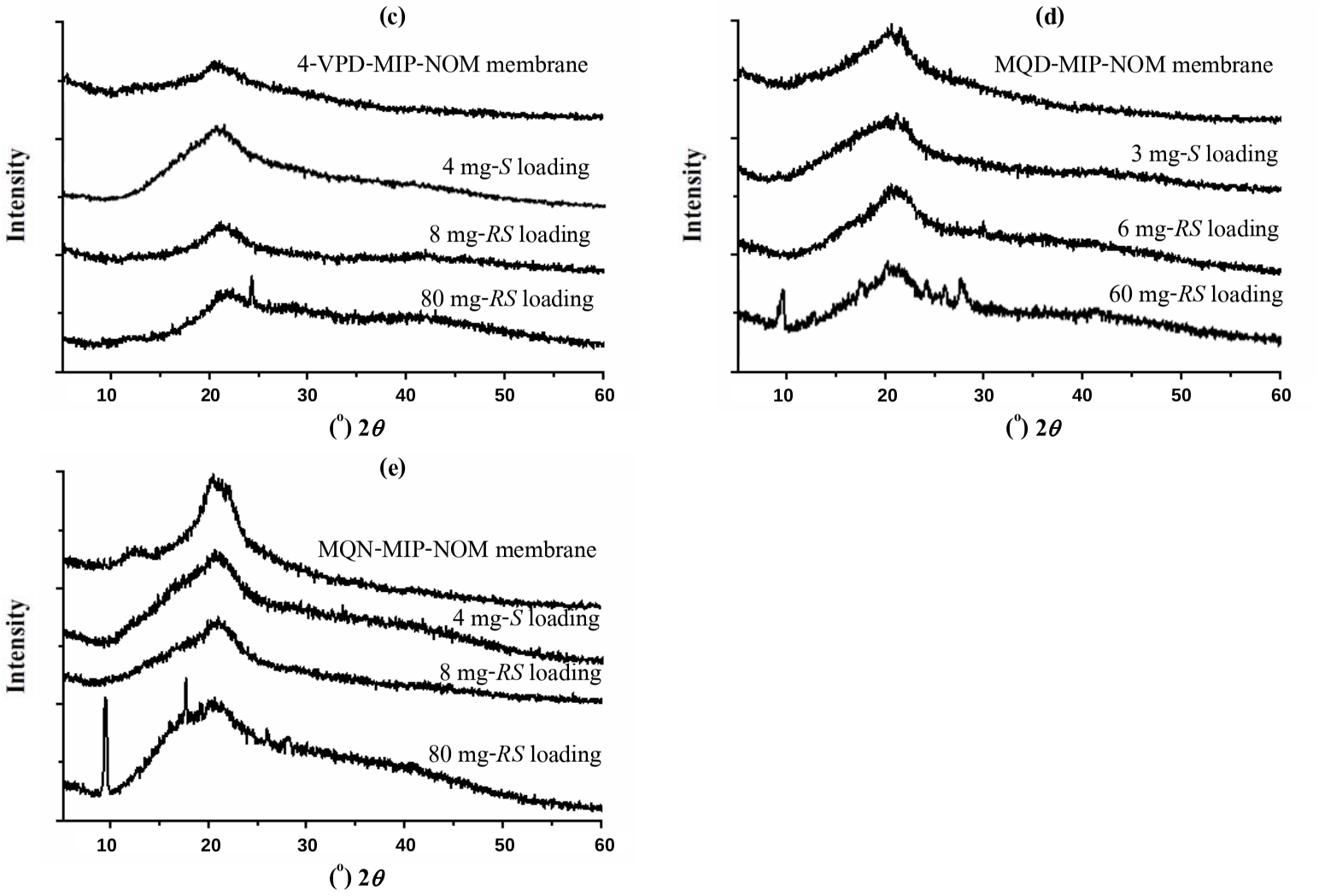

Figure 5.10. (continued)

5.3.8. DSC study

The MIP-NOM composite cellulose membranes were examined further for thermal characteristic using DSC experiments. In DSC scanning range, -50 to 250^{o}C, all the MIP-NOM composite membranes without drug exhibited a similar thermal characteristic which showed small endothermic peak at -20^{o}C and large exothermic peak at 195^{o}C (Figure 5.11), which was attributed to belong to the plain casting cellulose membrane. The small endothermic peak might result from the presence of plasticizer, poly(caprolactone triol) (PCL-T), which is viscous liquid at room temperature. And the large exothermic peak would relate to the thermal decomposition of cast cellulose membrane. The composite membranes with drug loading showed the additional endothermic peak around 140^{o}C that assigned to the melting temperature (*Tm*) of omeprazole. This observed endothermic peak shifted to higher temperature (~145^{o}C) in case of MQN-MIP-NOM composite membranes, which this may suggest the presence of chemical interactions between omeprazole enantiomer and MQN-MIP-NOM.

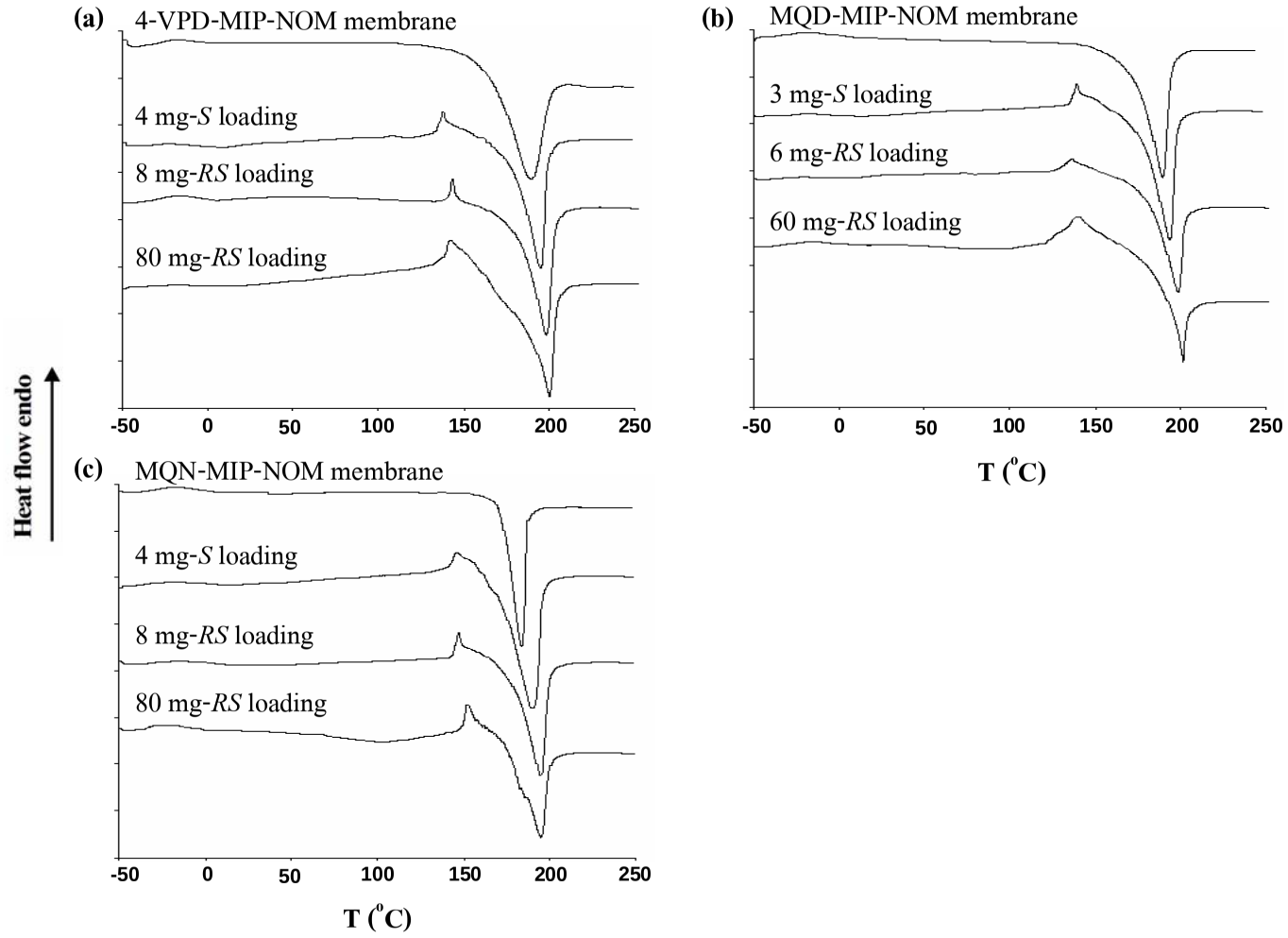

Figure 5.11. DSC thermograms of (a) 4-VPD-MIP-NOM, (b) MQD-MIP-NOM, and (c) MQN-MIP-NOM composite cellulose membranes without drug loading, with *S*-omeprazole loading (3 or 4 mg) and with *RS*-omeprazole loading at low (6 or 8 mg) and at high amounts (60 or 80 mg).

5.3.9. Enantioselective release of MIP-NOM composite membranes

The enantioselective release of omeprazole enantiomers from 4-VPD-MIP-NOM, MQD-MIP-NOM and MQN-MIP-NOM loaded composite cellulose membranes was evaluated in either aqueous or non-aqueous conditions. The release amount of drug was different in various solvents (Figure 5.12). The %release of omeprazole enantiomers from the MIP-NOM composite membranes in chloroform was higher than that in buffers. At high pH buffer, the release amount was obtained higher than at low pH. This was because of the tendency to deprotonate of NH group on benzimidazole of omeprazole at high pH. The enantioselective release of omeprazole enantiomers was found in all the MIP-NOM composite membranes in every solvent studied, while no enantioselectivity observed from the cast cellulose membrane without polymer particles loading and the control NIP-NOM composite membranes.

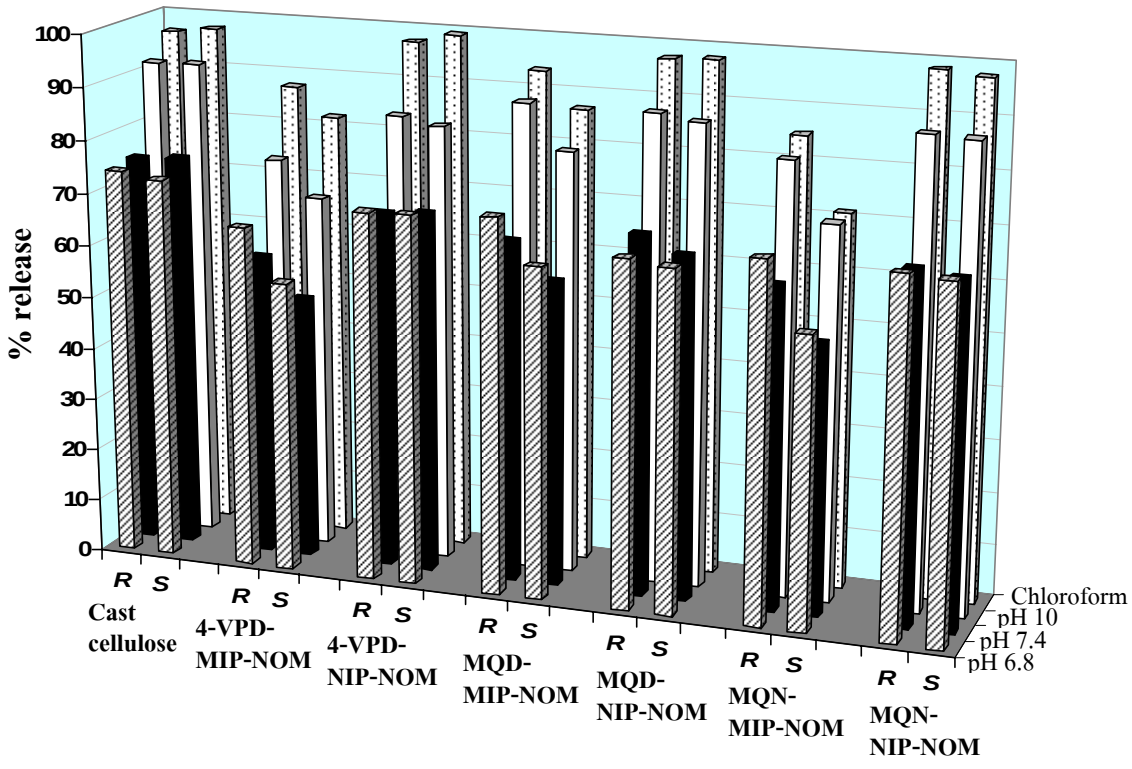

Figure 5.12. The percentage of omeprazole enantiomers release from cast cellulose membrane without polymer particles loading and composite membranes containing 4-VPD-, MQD- or MQN-MIP-NOMs and corresponding NIP-NOMs in different solvents at room temperature (25±1^{o}C).

The diffusion coefficient (*D*) and release exponent (*n*) of *R*-omeprazole, *S*-omeprazole and *RS*-omeprazole from cast cellulose without polymer particles loading, MIP-NOM and corresponding NIP-NOM composite membranes in pH 7.4 buffer are shown in Table 5.5. The MIP-NOM composite membranes gave enantioselective release of *R*-omeprazole enantiomer, while there was no enantioselectivity from any of the matching NIP-NOM composite membranes. The release of *RS*-omeprazole was slower than *R*-omeprazole enantiomer but faster than *S*-omeprazole enantiomer in every MIP-NOM composite membrane. These results can be explained by the specific recognition for the *S*-omeprazole template of MIPs, and then *R*-omeprazole was released into pH 7.4 buffer faster. MQN-MIP-NOM composite membrane showed the highest enantioselectivity compared to the other MIP-NOM composite membranes, while MQD-MIP-NOM composite membrane gave similar enantioselectivity with 4-VPD-MIP-NOM composite membrane. These results confirmed that methacryloylate QN used as functional monomer may form stronger interaction with the template than methacryloylate QD does. The release exponent (*n*) values obtained from both cast cellulose membrane without polymer particles loading and the MIP-NOM composite membranes were 0.5, indicating that the release of omeprazole enantiomers from MIP-NOM composite membranes was by Fickian diffusion mechanism.

Table 5.3. Diffusion coefficient (D) and release exponent (n) of *R*-omeprazole, *S*-omeprazole and *RS*-omeprazole from cast cellulose membrane without polymer particles loading and composite membranes containing 4-VPD-MIP-NOM, MQD-MIP-NOM, MQN-MIP-NOM and corresponding NIP-NOMs in pH 7.4 buffer at room temperature (25±1°C) (mean±S.D., n=3).

Membrane	Isomer	Diffusion coefficient (D, $cm^2.h^{-1}$)	Correlation coefficient of D	P-value	Release exponent (n)	Correlation coefficient of n
Cast cellulose	*R*	0.574±0.068	0.974	0.927	0.462±0.042	0.996
	S	0.564±0.055	0.967		0.465±0.050	0.992
	RS	0.553±0.047	0.955		0.461±0.062	0.983
4-VPD-MIP-NOM	*R*	0.419±0.025	0.982	0.021*	0.476±0.012	0.991
	S	0.366±0.037	0.976		0.479±0.022	0.990
	RS	0.384±0.043	0.989		0.472±0.021	0. 989
4-VPD-NIP-NOM	*R*	0.452±0.042	0.988	0.972	0.485±0.011	0.990
	S	0.433±0.041	0.987		0.483±0.010	0.987
	RS	0.450±0.026	0.984		0.480±0.020	0.989

* Statistically significant different of *R*- and *S*-omeprazole enantiomers (p<0.05).

Table 5.3. (continued)

Membrane	Isomer	Diffusion coefficient (D, $cm^2.h^{-1}$)	Correlation coefficient of D	P-value	Release exponent (n)	Correlation coefficient of n
QD- MIP-NOM	*R*	0.500±0.021	0.979	0.023*	0.465±0.001	0.987
	S	0.443±0.023	0.972		0.464±0.017	0.996
	RS	0.470±0.014	0.981		0.489±0.026	0.995
QD- NIP-NOM	*R*	0.520±0.078	0.955	0.959	0.478±0.013	0.991
	S	0.516±0.042	0.938		0.483±0.041	0.994
	RS	0.485±0.012	0.963		0.478±0.004	0.987
QN- MIP-NOM	*R*	0.494±0.028	0.989	0.015*	0.479±0.014	0.992
	S	0.401±0.003	0.984		0.473±0.008	0.991
	RS	0.439±0.016	0.951		0.480±0.003	0.993
QN- NIP-NOM	*R*	0.523±0.075	0.962	0.833	0.485±0.003	0.997
	S	0.512±0.067	0.945		0.489±0.010	0.988
	RS	0.495±0.010	0.951		0.488±0.005	0.989

* Statistically significant different of *R*- and *S*-omeprazole enantiomers ($p<0.05$).

5.3.10. Enantioselective permeation of racemic omeprazole across MIP-NOM composite membranes

In this section, the permeation of racemic omeprazole across MIP-NOM composite membranes was evaluated when racemic omeprazole was loaded into donor phase either with or without MIP-NOM particles. Figure 5.13 shows the flux of *RS*-omeprazole and the enantiomeric excess (%ee) of *R*-omeprazole as the function of drug concentration of *RS*-omeprazole in donor phase. It was found that the flux of *RS*-omeprazole increased with an increasing concentration of *RS*-omeprazole in donor phase, while %ee of *R*-omeprazole decreased. This suggested that the *S*-omeprazole enantiomer was retained in the MIP composite membrane, presumably at MIP binding site, while *R*-omeprazole enantiomer diffused into receiving phase, which this caused the imbalance of *R*- and *S*-omeprazole concentrations in receptor phase. This imbalance was rather high at lower concentration of racemic omeprazole than that at the higher concentration. When the drug concentration increased, *S*-omeprazole enantiomer diffused through the membrane higher. The %ee values obtained at pH 10 buffer was slightly lower than those at pH 7.4 buffer. This may be because that the interaction between the template *S*-omeprazole and MIP at pH 10 was weaker than that at pH 7.4.

When the MIP-NOM particles were added into the donor solution containing racemic omeprazole, the flux of *RS*-omeprazole decreased compared to the absence of MIP-NOM in the donor phase, whereas the %ee for *R*-omeprazole increased at lower concentration of racemic omeprazole. This can be explained as that the preferred *S*-omeprazole was bound with MIP particles in donor phase which the decrease of racemic omeprazole in membrane may cause the reduction of the *S*-omeprazole in the receiving phase. The %ee was not changed at high concentration. This may involve the limit in capacity of MIP to bind the template enantiomer.

The highest enantioselectivity in permeation study was obtained from MQN-MIP-NOM composite membrane compared to other MIP-NOM composite membranes. This confirmed that the methacryloylate QN might form stronger interaction with template *S*-omeprazole enantiomer than methacryloylate QD.

(a) pH 7.4

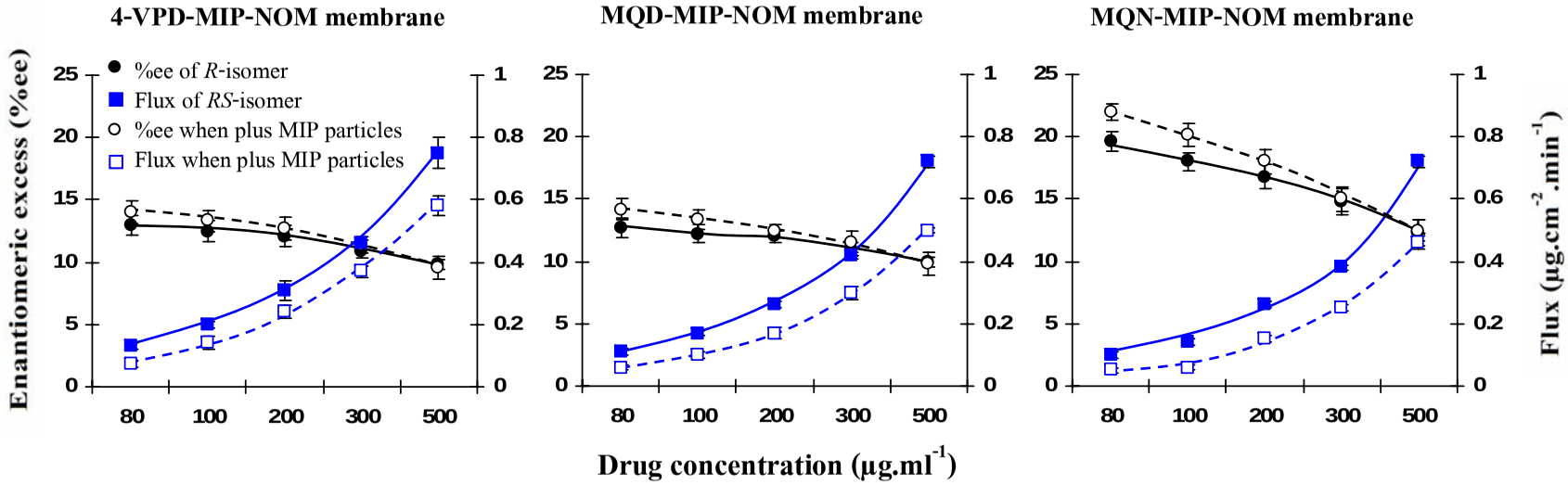

Figure 5.13. Flux of *RS*-omeprazole and enantiomeric excess (%ee) of *R*-omeprazole from permeation study of racemic omeprazole across 4-VPD-MIP-NOM, MQD-MIP-NOM, and MQN-MIP-NOM composite membranes when racemic omeprazole was loaded either with or without MIP-NOM particles in (a) pH 7.4 and (b) pH 10 buffers at room temperature (25±1°C) (mean±S.D., n=3).

(b) pH 10

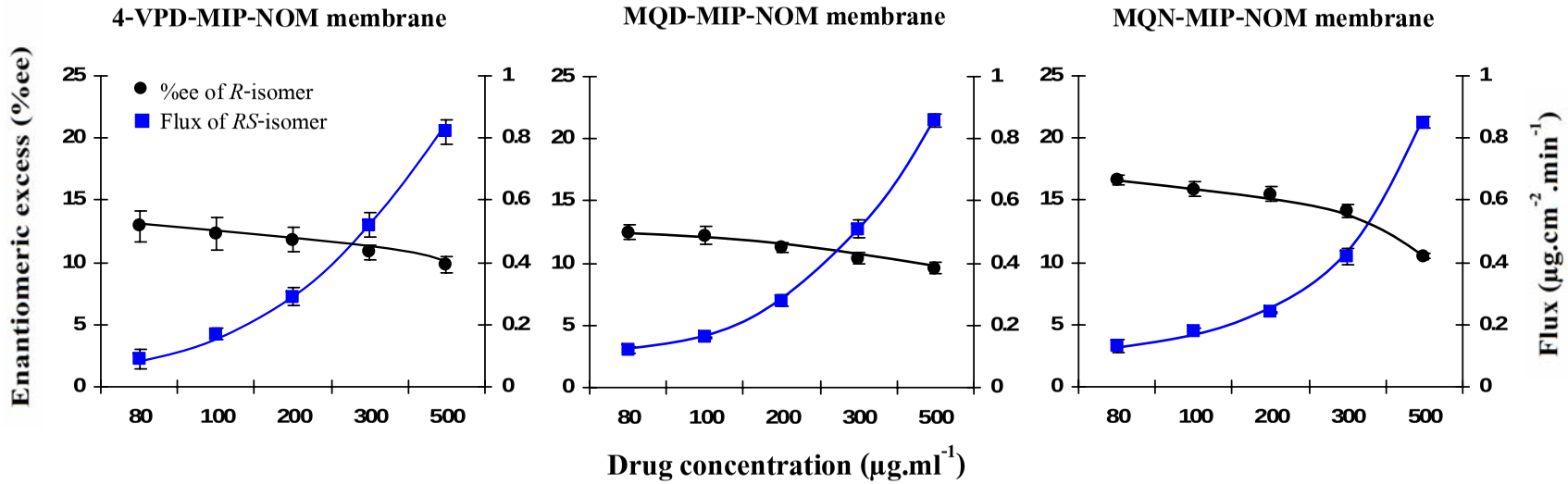

Figure 5.13. (continued)

5.3.11. CLSM study

The CLSM study of MIP-NOM composite membranes was carried out since QN and QD are fluorescent compounds, which allowed the diffusion of omeprazole enantiomers in the composite membranes to be investigated. Figure 5.14 shows fluctuated fluorescence of (a) MQN-MIP-NOM and (b) MQD-MIP-NOM composite membranes at *Z*-stack, the distance in *Z* direction (depth), of 5, 20 and 50 μm when exposure to *S*-omeprazole, *S*-omeprazole and *RS*-omeprazole sequentially. When *S*-omeprazole was added to MQN-MIP-NOM composite membrane, the fluctuated fluorescence increased (Figure 5.14a). When the sequential addition of *S*-omeprazole, the fluctuated fluorescence gradually increased until reach the maximum at ~0.7. When the addition of *RS*-omeprazole to the MQN-MIP-NOM membrane, the fluctuated fluorescence decreased about one third before reaching the plateau at 0.7. These results indicated that *S*-omeprazole enantiomer was bound with MIP cavity and this caused fluorescence quenching. The presence of *RS*-omeprazole would cause the *S*-omeprazole enantiomer discarded the imprinted sites that occupied again by *RS*-omeprazole. The overlay CLSM images of composite membranes before and after exposure to the test compounds are shown in Figure 5.15. As shown in Figure 5.15, the appearance of fluorescence from MQN-MIP-NOM composite membrane was relatively changed by the elapse of time at *Z*-stack of 5 and 50 μm, whereas no fluorescence changed was observed at *Z*-stack of 20 μm. In the case of MQD-MIP-NOM composite membrane, there was little change of fluorescence in every *Z*-stack by the elapse of time. The fluctuated fluorescence was not observed in the middle of membranes (*Z*-stack of 20 μm). This may be due to the release and occupation of template *S*-omeprazole was taking place at the same time or this area may not have specific cavities for binding of *S*-omeprazole. The slight fluctuated fluorescence observed in the case of MQD-MIP-NOM composite membrane (Figure 5.14b) can be accounted by taking that the lower specific recognition of MQD-MIP-NOM for the template *S*-omeprazole. The results obtained in CLSM would be the support evidence in drug permeation study that the presence of *RS*-omeprazole especially at high concentration induced the release of *S*-omeprazole enantiomer to receptor phase and hence the decrease in the enantiomeric excess of *R*-omeprazole.

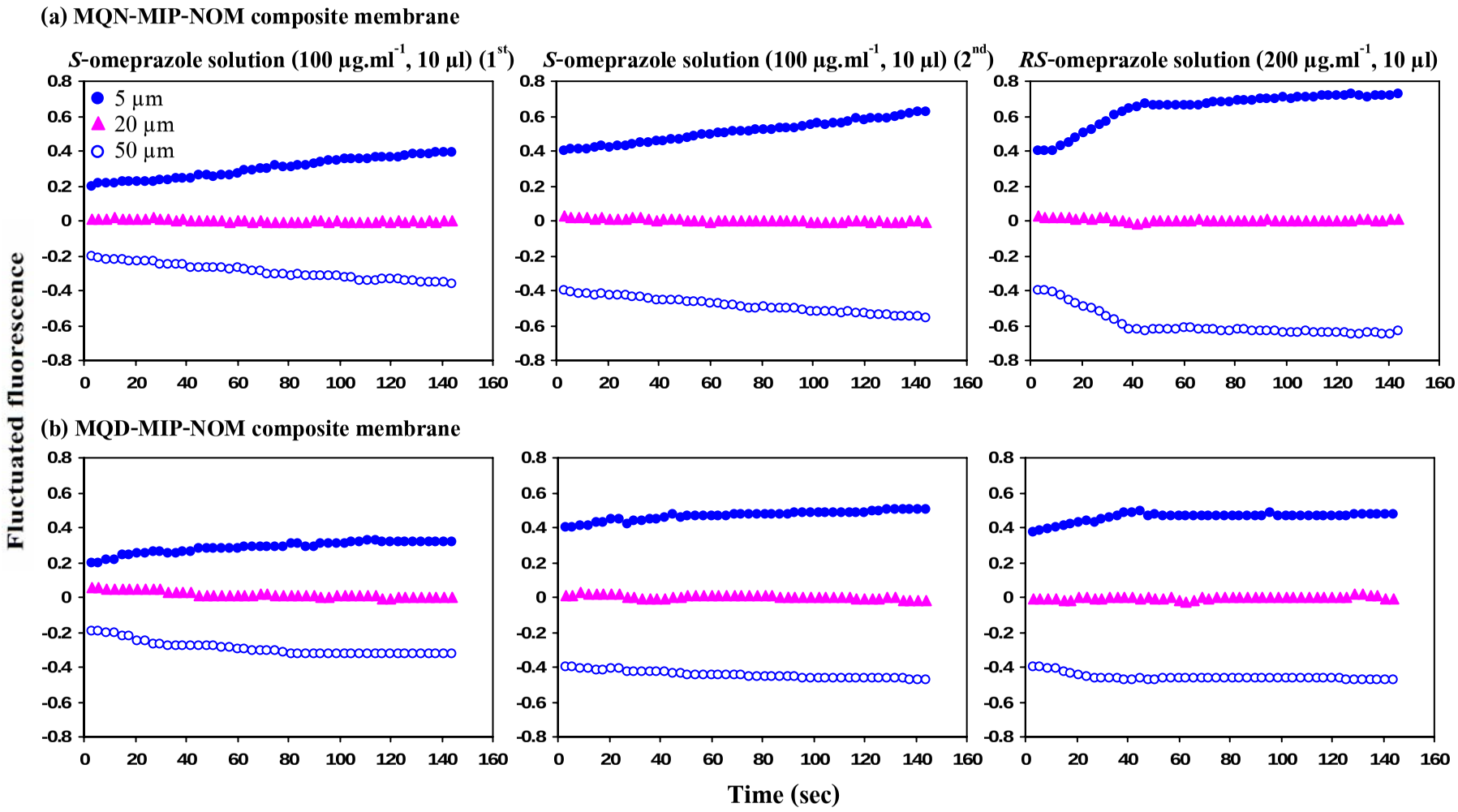

Figure 5. 14. Fluctuated fluorescence of (a) MQN-MIP-NOM and (b) MQD-MIP-NOM composite membranes at *Z*-stack of 5, 20 and 50 µm by the elapse of time (sec) when exposure to *S*-omeprazole, *S*-omeprazole and *RS*-omeprazole solutions (pH 7.4) sequentially.

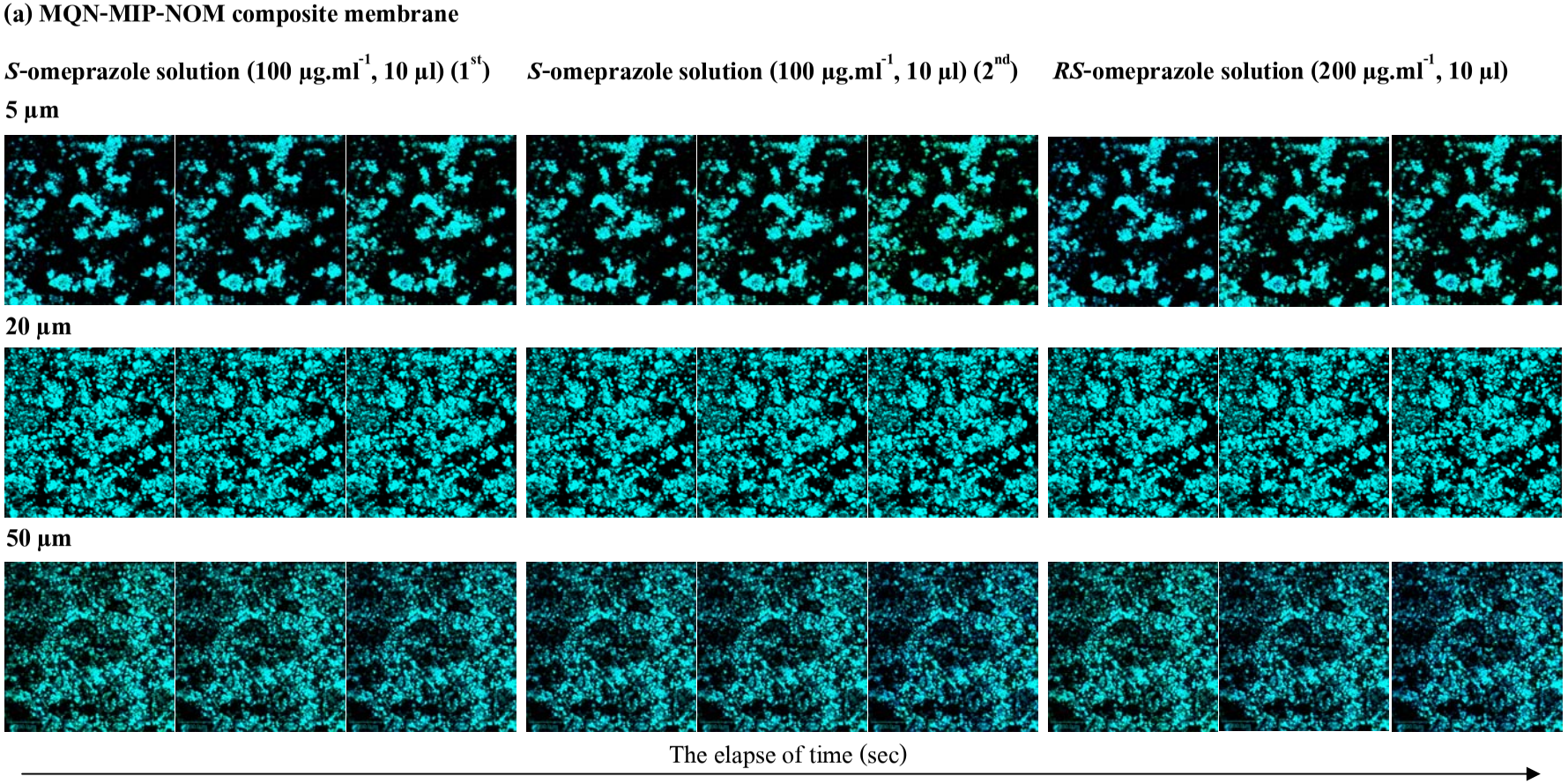

Figure 5. 15. Overlay CLSM images of (a) MQN-MIP-NOM and (b) MQD-MIP-NOM composite membranes at *Z*-stack of 5, 20 and 50 µm by the elapse of time (sec) before (green) and after (red) exposure to *S*-omeprazole, *S*-omeprazole and *RS*-omeprazole solutions (pH 7.4) sequentially.

(b) MQD-MIP-NOM composite membrane

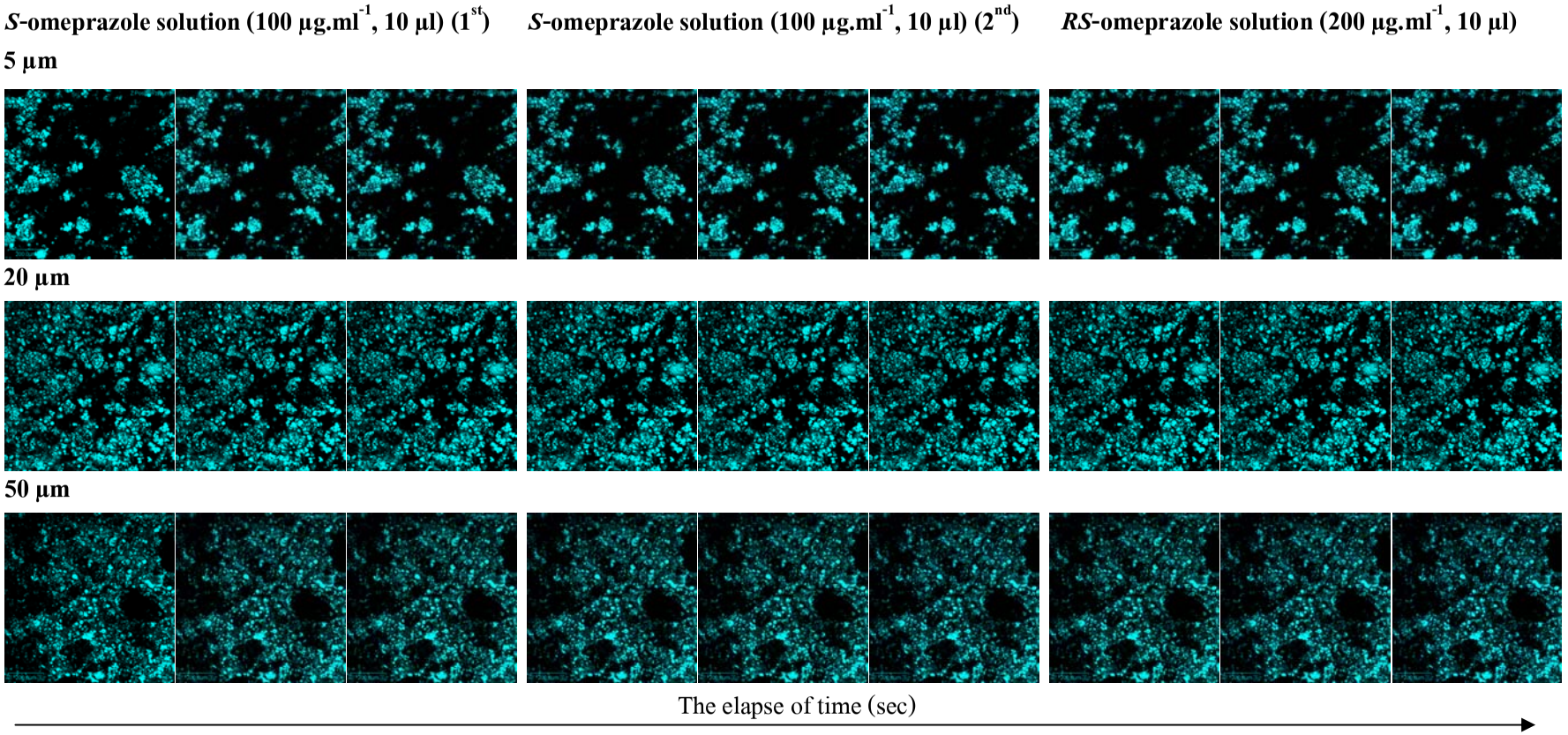

Figure 5.15. (continued)

CHAPTER 6

THE EVALUATION OF MIP NANOPARTICLE-ON-MICROSPHERE DELIVERY SYSTEM FOR THE ENANTIOSELECTIVE CONTROLLED RELEASE OF RACEMIC OMEPRAZOLE

6.1. Introduction and objectives

In a drug delivery system (DDS), the *S*-omeprazole enantiomer should be selectively released from DDS, whereas the *R*-omeprazole enantiomer should be retained inside DDS as long as possible. In this study, the DDS for enantioselective release of racemic omeprazole was designed as a hollow cylindrical reservoir-type delivery system. This design would allow the enantioselective release of omeprazole enantiomers occurred priory in reservoir. *R*-omeprazole enantiomer would be selectively released from polymer matrix into reservoir, whereas *S*-omeprazole enantiomer would be remained in the polymer matrix in higher amount than *R*-omeprazole enantiomer. By the effect that *S*-omeprazole enantiomer was retained in the reservoir wall higher than *R*-omeprazole enantiomer and the effect of drug in the reservoir, *S*-omeprazole enantiomer could be selectively released from the DDS.

Figure 6.1 shows schematic representation of DDS designed as a hollow cylindrical reservoir-type delivery system. The racemic omeprazole was loaded with MIP particles and cellulose into poly(2-hydroxyethyl methacrylate) (poly(HEMA)) matrix. The core of DDS was filled with pH 7.4 buffer as vehicle. The poly(HEMA) cap that fit with the cylindrical delivery system was used to seal liquid into the reservoir. Poly(HEMA) is widely used in pharmaceutical technologies and exhibit good biocompatibility, also, with its compact structure hydrogel, DDS based on poly(HEMA) may possibly be adjusted to control the release of drug from the system.

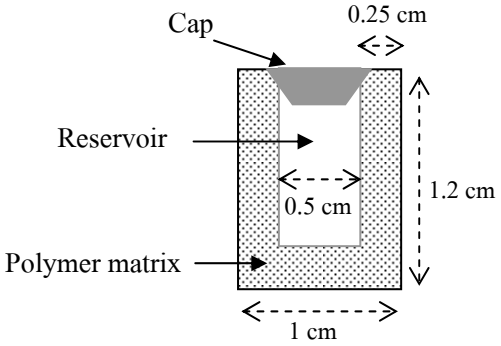

Figure 6.1. Schematic representation of a hollow cylindrical reservoir-type delivery system used in this study.

The objectives of this study were to develop the DDS for enantioselective-controlled delivery of racemic omeprazole with the use of MIP-NOM as a recognition phase and to evaluate the ability in enantioselective release of prepared DDS. Three different types of MIP-NOM were used including: 4-VPD-MIP-NOM, MQD-MIP-NOM and MQN-MIP-NOM and the enantioselective release of omeprazole enantiomers from the prepared DDS was examined *in vitro* using dissolution apparatus. The dissolution test was carried out at different pH media, i.e., pH 1.2 medium (0.1 N HCl), pH 6.8 and pH 8 buffers. The enantioselective dissolution of prepared DDS was evaluated, and compared with the commercial formulations for either racemic omeprazole or single *S*-omeprazole enantiomer formulations.

6.2. Experimental

6.2.1. Materials

2-Hydroxyethyl methacrylate (HEMA) was purchased from Sigma-Aldrich (Milwaukee, WI, USA) and purified by distilled under reduce pressure before use. The commercial racemic omeprazole and single *S*-omeprazole formulations were used with the brand names Losec® and Nexium® MUPS tablets 20 mg (AstraZeneca, Södertälje, Sweden). All chemicals used for preparation of dissolution media were of reagent grade quality or higher and

were used without further purification. Various dissolution media were prepared as follows: pH 1.2 medium (0.1 N HCl, μ=0.1): add 0.1 mol of HCl in 1 L volume distilled water; pH 8 buffer (0.1 M, μ=0.26): add 21 mmol of NaH_2PO_4 and 79 mmol of Na_2HPO_4 in 1 L volume distilled water.

6.2.2. Preparation of MIP-NOM-contained DDS

The polymer matrix incorporated with racemic omeprazole was prepared by free-radical photo-polymerization at room temperature (25±1^{o}C). The mold for DDS preparation was prepared from a polypropylene tube (1.0 cm of outer diameter, 0.5 cm of inner diameter and 1.5 cm of height). In preliminary study, the compositions for the preparation of polymer matrix had been optimized in order to obtain high quality of the system, which had good integrity and good appearance. Cellulose was used as powder obtained from cast cellulose membrane without polymer particle loading subsequently ground with mortar mill. PCL-T was used as plasticizer and pore former in the polymer matrix. A DDS, equivalent to 20 mg of racemic omeprazole, was prepared by mixing MIP-NOM selective to *S*-omeprazole enantiomer (100 mg), cellulose (50 mg), PCL-T (150 mg) and racemic omeprazole in ethanol (0.2 ml) containing HEMA (0.5 g), EDMA (6 mg) and AIBN (4 mg). The mixture was blended by mechanical agitation and gently placed into the mold by using micropipette tip. The mold was immediately exposed to UV light at 365 nm for 30 min. The resulting polymer matrix was removed from the mold and washed with distilled water and dried in air for 24 h at room temperature (25±1^{o}C). Buffer pH 7.4 (500 μl) was filled into the reservoir and capped with the HEMA-based polymer, sealing liquid into the reservoir. After 24 h, the DDS prepared was examined *in vitro* dissolution.

6.2.3. Morphologic analysis

Morphology of cylindrical DDS in both surface and cross-section was examined using scanning electron microscopy (SEM) (Jeol serie JSM 5800LV, CA, USA) at an accelerating voltage of 20 kV with the sample being sputter-coated with gold before imaging.

6.2.4. *In vitro* dissolution study

The release of omeprazole enantiomers from the DDS was examined in different pH media: pH 1.2 medium, pH 6.8 and pH 8 buffers. The release test was performed in compliance with USP 30 testing, apparatus I (basket) (VK7000, VanKel Industries, Inc., Cary, NC). The rotating speed of basket was set at 50 rpm and temperature of dissolution bath was maintained at 37±0.5^{o}C. Dissolution testing of all DDS was performed in set of six. The DDS were placed into the baskets and transferred to dissolution vessels, containing 500 ml of pH 1.2 medium. Dissolution testing carried out in pH 1.2 medium for 2 h, and then pH 6.8 buffer for 2 h and finally pH 8 buffer for 2 h. 2 ml samples were withdrawn with fresh medium replacement at 120 min for the first 2 h (in pH 1.2 medium) and at 15, 30, 60 and 120 min for the test in both pH 6.8 and pH 8 buffers. The amounts of omeprazole enantiomers in pH 1.2 medium samples were measured by mass spectroscopy (MAT 95 XL Mass Spectrometer, Thermo Finnigan, Bremen, Germany), and the samples in pH 6.8 and pH 8 buffers were analyzed by stereospecific HPLC method. Dissolution profiles were presented as percentage of drug release *versus* time curves. After dissolution process, the remained amount of omeprazole enantiomers in reservoir and polymer matrix was measured. The drug remained in polymer matrix was calculated by subtracting the total amount of drug released in dissolution media and the amount of drug remained in reservoir from the total amount of drug incorporated in polymer matrix. Moreover, the dissolution of the commercial omeprazole formulations of both racemic and single *S*-omeprazole enantiomer was tested for comparison purpose in drug release behavior.

6.3. Results and discussion

6.3.1. MIP-NOM-contained DDS preparation and morphologic analysis

Figure 6.2 shows typical scanning electron micrographs of polymer matrix of DDS: (a, b) outer surface and (c, d) cross-section. The DDS showed an intact outer surface with

some small cracks. The polymer particles were fabricated in the compact structural poly(HEMA) matrix.

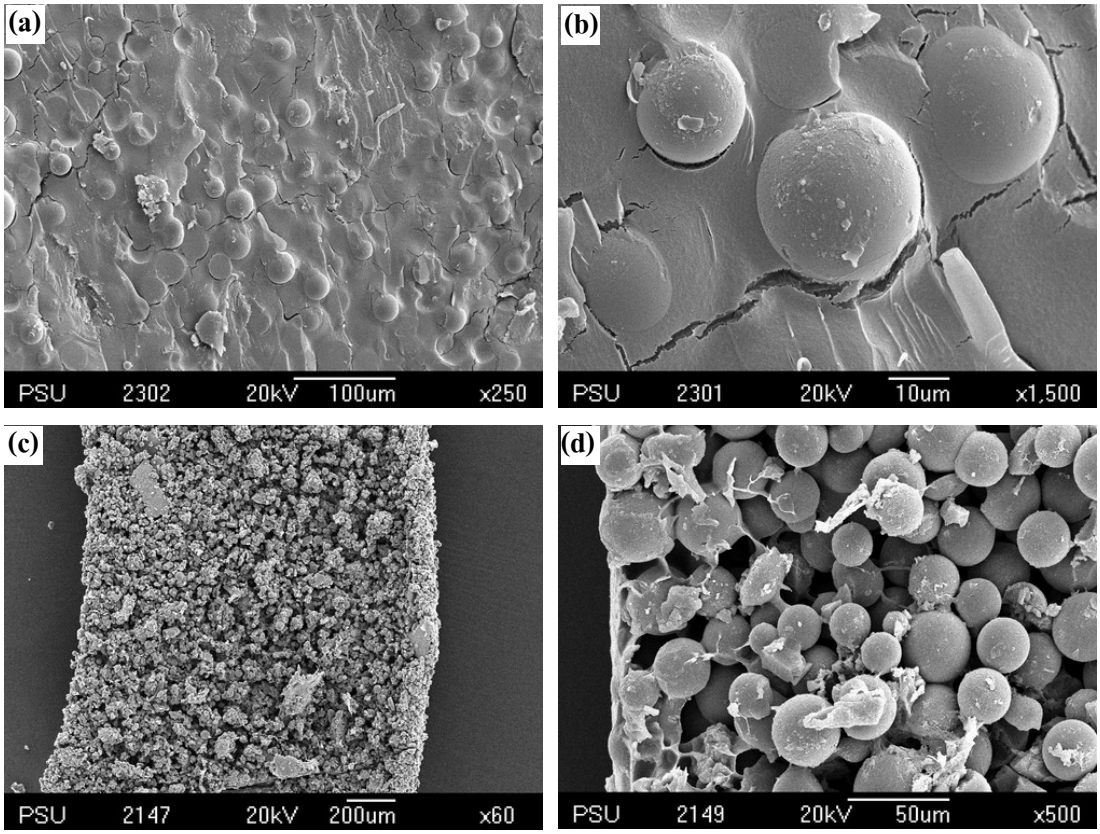

Figure 6.2. SEM images of (a, b) outer surface and (c, d) cross-section of polymer matrix of DDS.

6.3.2. Dissolution studies

6.3.2.1. Dissolution profile

Figure 6.3 shows dissolution profiles of omeprazole enantiomers from DDS contained MIP-NOMs and corresponding NIP-NOMs. It can be seen that in pH 1.2 medium omeprazole enantiomers were not released from all types of MIP-NOM- and NIP-NOM-contained DDS. Omeprazole enantiomers were gradually released from DDS in pH 6.8 buffer to reach about 50% within 4 h dissolution. The release of omeprazole enantiomers from DDS in pH

8 buffer was also gradually increased and reached the maximum at about 80% of drug released within 6 h period. HEMA based hydrogel is sensitive to the pH of aqueous environment; expanding at high pH and shrinking at low pH (John et al., 2002; Sutani et al., 2002), the DDS based on poly(HEMA) matrix was able to protect the release of drug in the acidic pH medium. The total omeprazole enantiomers released in dissolution media, the remained omeprazole enantiomers in reservoir and the drug in the polymer matrix after the 6 h dissolution test are shown in Table 6.1. The omeprazole enantiomers released in reservoir were almost the maximum value of drug solubility and *R*-omeprazole enantiomer was found in higher amount than *S*-omeprazole enantiomer obtained from MIP systems. On the other hand, *S*-omeprazole enantiomer was released into the dissolution medium in higher amount than *R*-omeprazole enantiomer. Figure 6.4 demonstrates the proposed mechanism underlying the release of omeprazole enantiomers from the MIP delivery system. In an entirely aqueous environment the delivery system comprising the MIPs in a controlled-release system gave partial selective delivery for the *S*-enantiomer over the *R*-enantiomer. Filling buffer pH 7.4 in the reservoir of system rendered the poly(HEMA) matrix of the initial surface of polymeric membrane to be swelled, and this pH favored the complex formation between MIP and enantiomer, thereby, the excess racemic omeprazole along with non-bound *R*-omeprazole transfered into the reservoir of the delivery systems. As dissolution proceeded, a pressure driving force was applied to force water through the MIP in the polymer matrix, immediately the delivery of *S*-omeprazole enantiomer occurred, as facilitated by racemic omeprazole, though the *R*-isomer also diffused from the system but at a significantly lower rate. The enantioselective dissolution of racemic omeprazole was not observed from the corresponding NIP-NOM-contained DDSs.

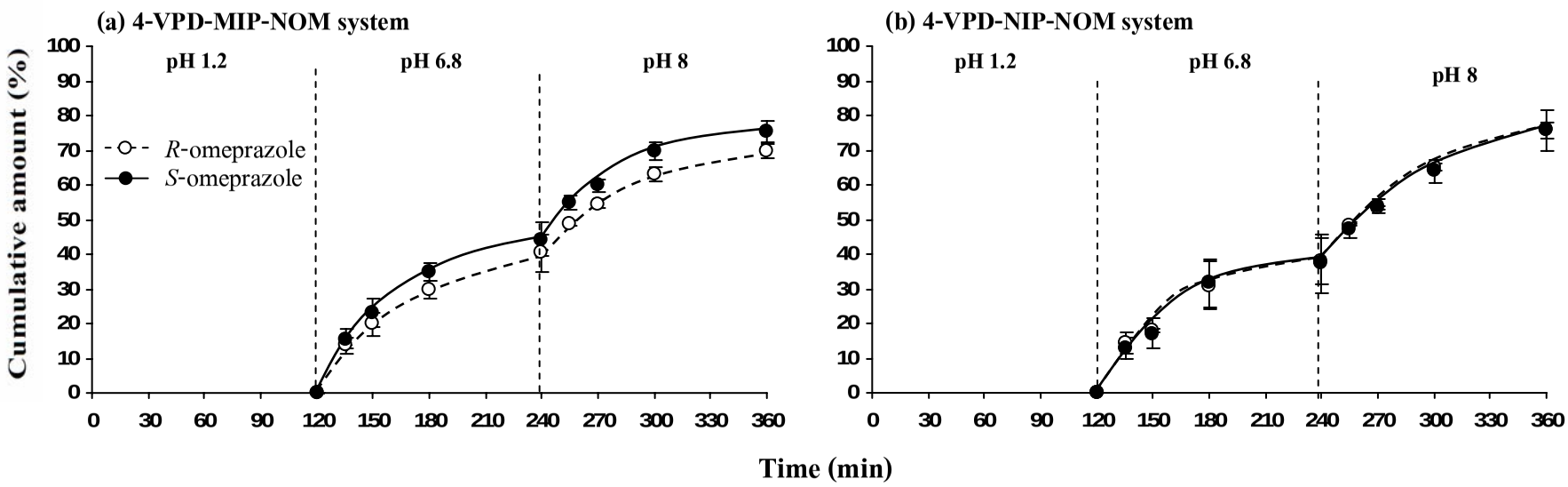

Figure 6.3. Dissolution profiles of omeprazole enantiomers from DDS containing (a) 4-VPD-MIP-/ (b) NIP-NOMs, (c) MQD-MIP-/ (d) NIP-NOMs, (e) MQN-MIP-/ (f) NIP-NOMs, (g) commercial racemic and (h) *S*-omeprazole formulations in pH 1.2 medium, pH 6.8 and pH 8 buffers at 37±0.5°C (mean±S.D., n=6).

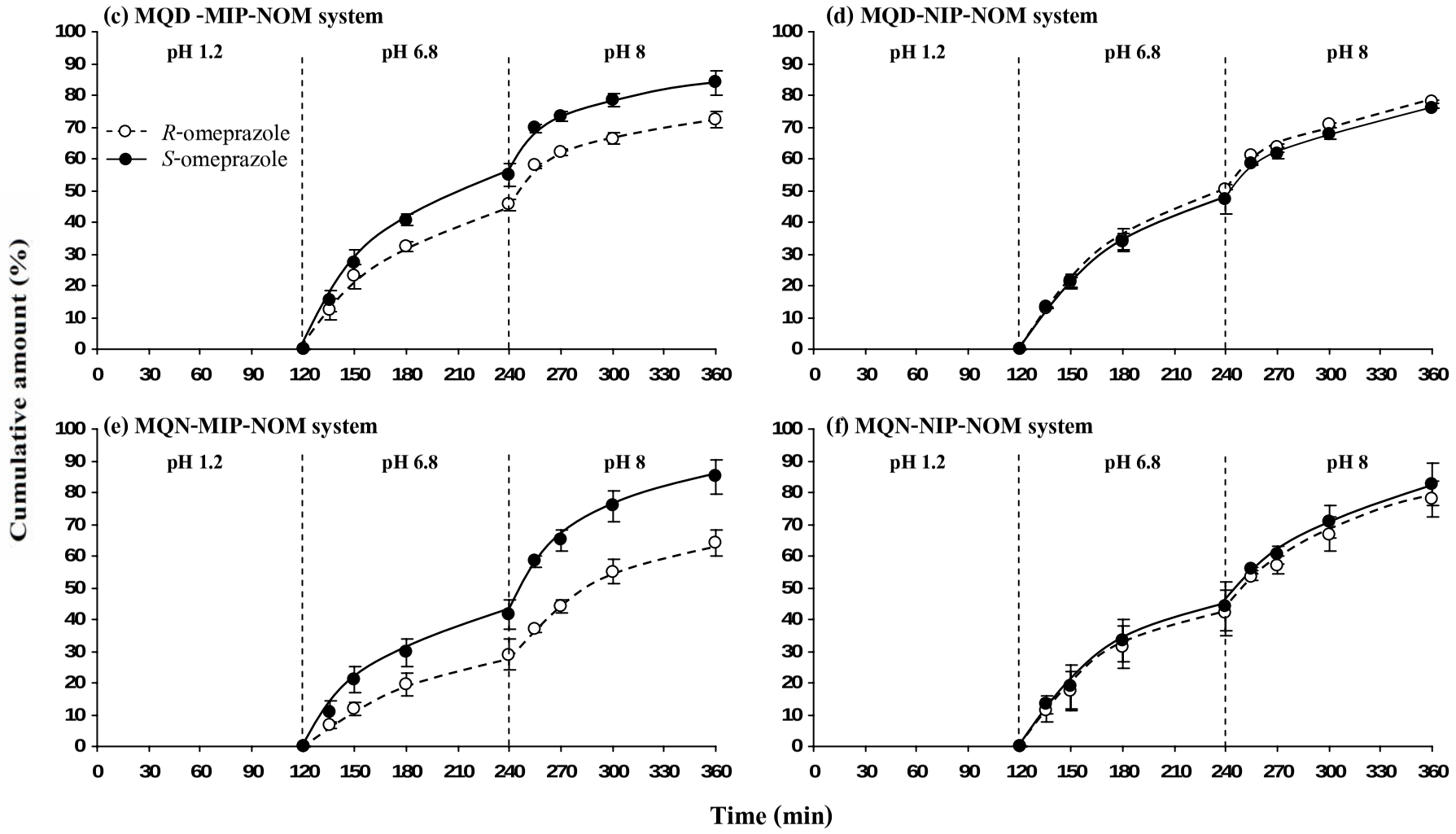

Figure 6.3. (continued)

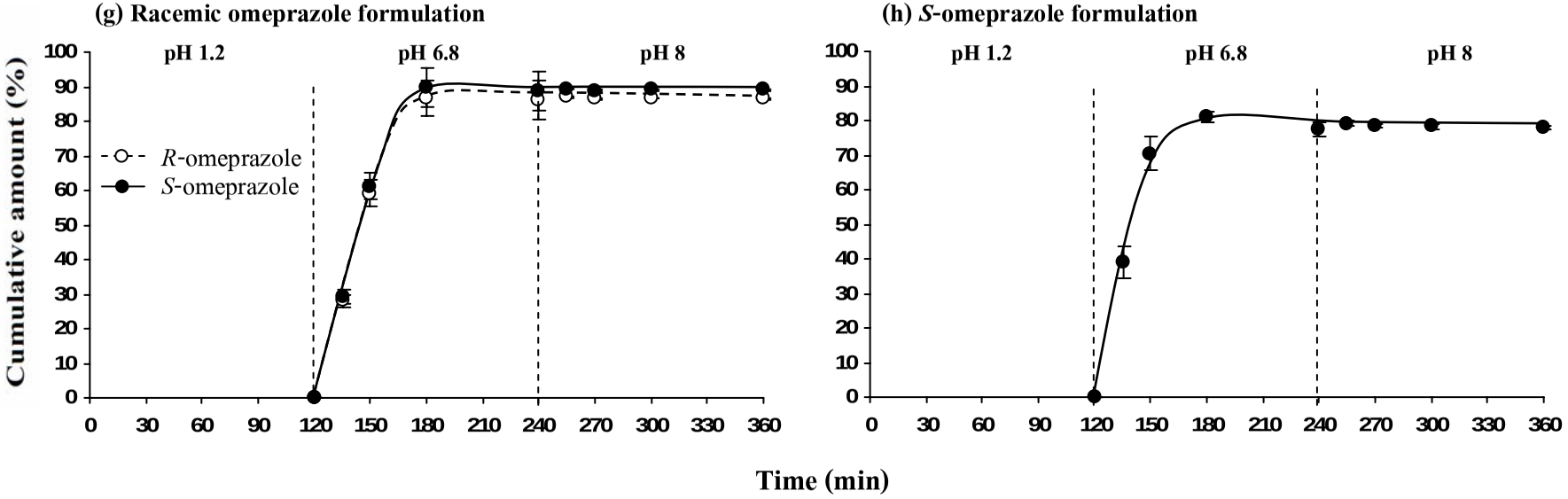

Figure 6.3. (continued)

Table 6.1. Total omeprazole enantiomers in polymer matrix, total omeprazole enantiomers in dissolution media, and remained omeprazole enantiomers in reservoir and in polymer matrix after 6 h dissolution test (mean±S.D., n=6).

System	Total drug in system (mg)		Total drug in dissolution media (mg)		Drug remained in reservoir (mg)		Drug remained in polymer matrix (mg)	
	R	*S*	*R*	*S*	*R*	*S*	*R*	*S*
4-VPD-MIP-NOM	10.30±0.18	10.28±0.31	6.97±0.21	7.53±0.34	0.88±0.02	0.73±0.02	2.19±0.17	1.63±0.19
4-VPD-NIP-NOM	10.86±0.37	10.76±0.25	7.57±0.23	7.58±0.59	0.68±0.01	0.64±0.07	1.84±0.16	1.91±0.27
MQD-MIP-NOM	10.21±0.37	10.10±0.37	7.23±0.25	8.39±0.37	0.76±0.03	0.51±0.01	2.04±0.25	1.08±0.12
MQD-NIP-NOM	10.48±0.83	10.51±0.26	7.78±0.15	7.58±0.16	0.52±0.02	0.52±0.09	1.76±0.30	1.97±0.11
MQN-MIP -NOM	10.25±0.39	10.15±0.51	6.41±0.42	8.49±0.54	0.87±0.04	0.46±0.02	2.79±0.26	1.11±0.20
MQN-NIP-NOM	10.63±0.14	10.58±0.10	7.78±0.58	7.93±0.65	0.63±0.01	0.64±0.05	1.54±0.14	1.31±0. 09

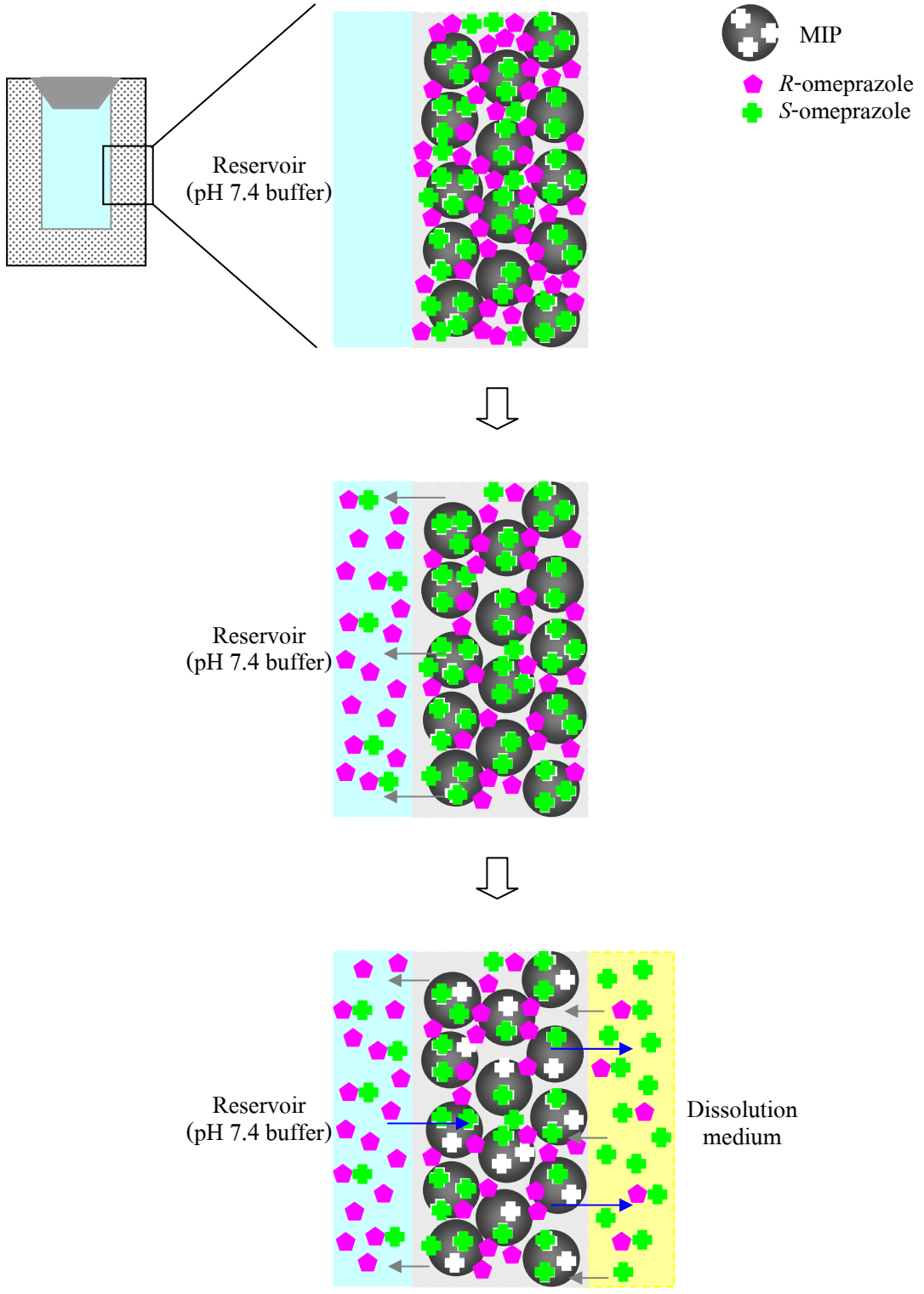

Figure 6.4. Schematic mechanism underlying the release of omeprazole enantiomers from the MIP delivery system.

The release rates of omeprazole enantiomers as function of time of prepared DDS and commercial formulations, according to the data obtained in release study as above, are presented in Figure 6.5. The release rates of omeprazole enantiomers from every DDS were likely as two pulses. This behavior may be the consequence that omeprazole enantiomers were contained in the DDS likely as in two compartments: in the polymer matrix and in the reservoir. The first pulse may be occurred mainly from the effect of drug in polymer matrix and the following pulse may be occurred mainly from the effect of drug in reservoir. In the case of DDS containing MQN-MIP-NOM, the two pulses of release rate was seemingly symmetry, while the other systems were asymmetry. The release rate of omeprazole enantiomers from MQN-MIP-NOM-contained DDS was slightly slower than the other systems but the higher enantioselectivity was obtained. These results indicated the greater enantioselective-controlled release for *S*-omeprazole enantiomer of the MQN-MIP-NOM-contained DDS than the MQD-MIP-NOM-contained DDS. The enantioselective release of omeprazole enantiomers to dissolution medium of MQN-MIP-NOM-contained system would be influenced greatly the highly enantioselective recognition ability of MQN-MIP-NOM binding site, resulting in the obtained high enantioselectivity in both two pulses as well as proper control release behavior. In other DDSs, the release rate of omeprazole enantiomers in dissolution medium pH 8 was lower than in pH 6.8 with slightly decreased of *S*/*R* enantioselectivity. This may be because at third fluid (pH 8), the release of drug from the remained drug in DDS occurred. The *R*-omeprazole enantiomer would compete to release when the time progressed, resulting in the decrease of enantioselectivity obtained in the second pulse.

The fast release of drug would be preference if the absorption of drug also occurred in the fast with high amount absorption to reach therapeutic index. However, in the most cases, the absorption of drug depends on the number of binding sites at absorption region, which capable to attain saturation and limit the drug absorption. Many attempts have made to develop sustained release preparations with extended clinical effects and reduced dosing frequency. For the release study of commercial racemic and *S*-omeprazole enteric formulations (Figure 6.3g and h), the drug was protected to be released in acidic pH medium, and the drug was released very fast in pH 6.8 buffer and reach the drug plateau within 30 min. The commercial *S*-omeprazole formulation showed the drug release slightly faster than commercial racemic omeprazole

formulation, and both formulations showed one pulse of drug release (Figure 6.4g and h). According to the dissolution study, the prepared DDSs especially MQN-MIP-NOM-contained DDS appeared to prolong the release of omeprazole enantiomers which allowed the drug to be gradually released up to about 80% within 6 h. In addition, the appearance as two pulses in drug release of MQN-MIP-NOM-contained DDS may provide efficient drug absorption and therapeutic effects.

6.3.2.2. Kinetic evaluation of drug release

Drug release mechanism of the DDS was evaluated by using the Korsmeyer-Peppas semi-empirical model as described in Section 5.3.9. The release exponents (n) of omeprazole enantiomers obtained from various DDSs and commercial formulations are shown in Table 6.2. Drug release data of prepared DDS showed a good fit into Korsmeyer-Peppas model (R^2>0.97) in both pH 6.8 and pH 8 buffers. The n values of all DDS were within the limit of the non-Fickian release mechanism in both pH 6.8 and pH 8 buffers. The n values especially in the case of MQN-MIP-NOM-contained system were quite high, which nearly 1 (n≈0.8) compared to other systems, indicating that the release mechanism was nearly ideal zero-order kinetic of MQN-MIP-NOM-contained DDS than other systems. The n values of commercial racemic and *S*-omeprazole formulations were also within the limit of the non-Fickian release mechanism except racemic omeprazole formulation in pH 8 buffer (n≈0.5; Fickian release mechanism). In *S*-omeprazole formulation, the n could be calculated only in pH 6.8 buffer because the drug was released almost completely in this pH buffer. The n value of commercial *S*-omeprazole formulation was quite low compared to the prepared DDS and racemic omeprazole formulation, indicating the release mechanism was rather far from zero-order kinetic.

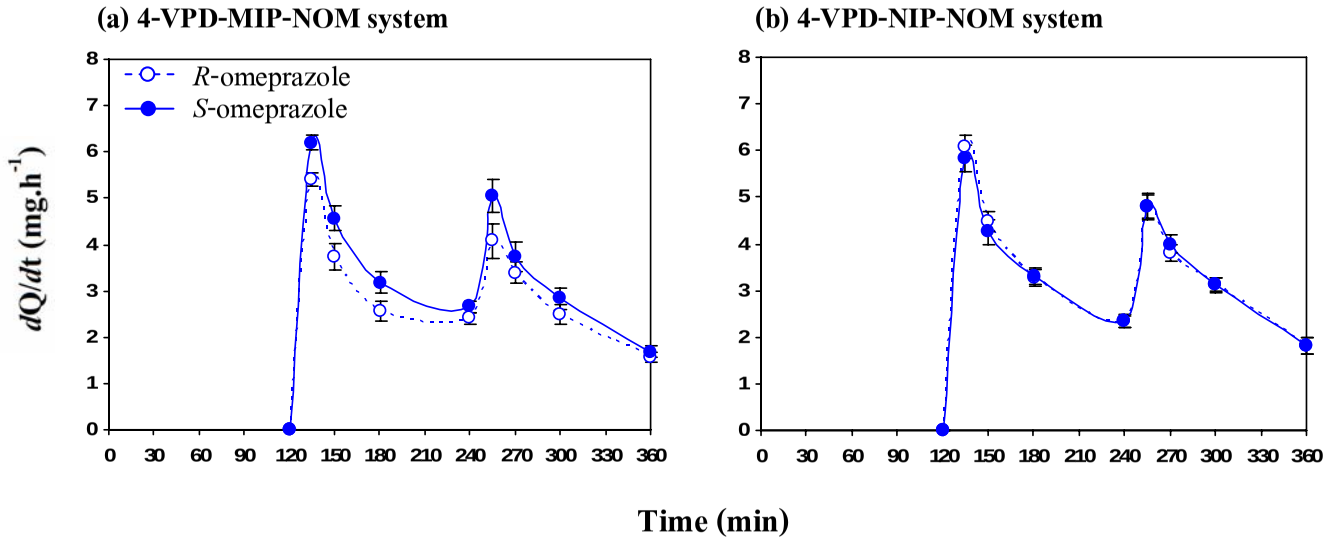

Figure 6.5. Release rates of omeprazole enantiomers from DDS containing (a) 4-VPD-MIP-/ (b) NIP-NOMs, (c) MQD-MIP-/ (d) NIP-NOMs, (e) MQN-MIP-/ (f) NIP-NOMs, (g) commercial racemic and (h) *S*-omeprazole formulations according to the release study.

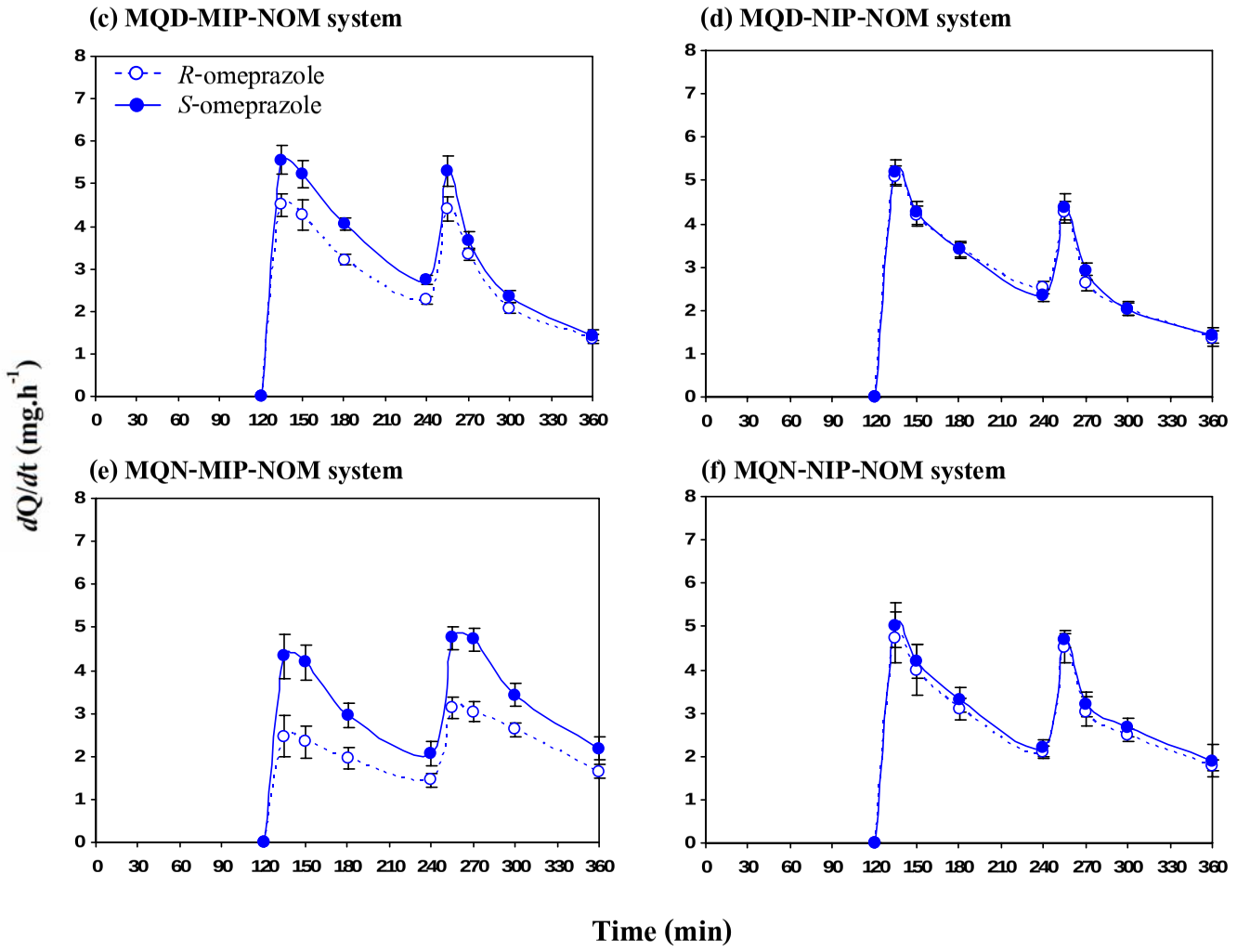

Figure 6.5. (continued)

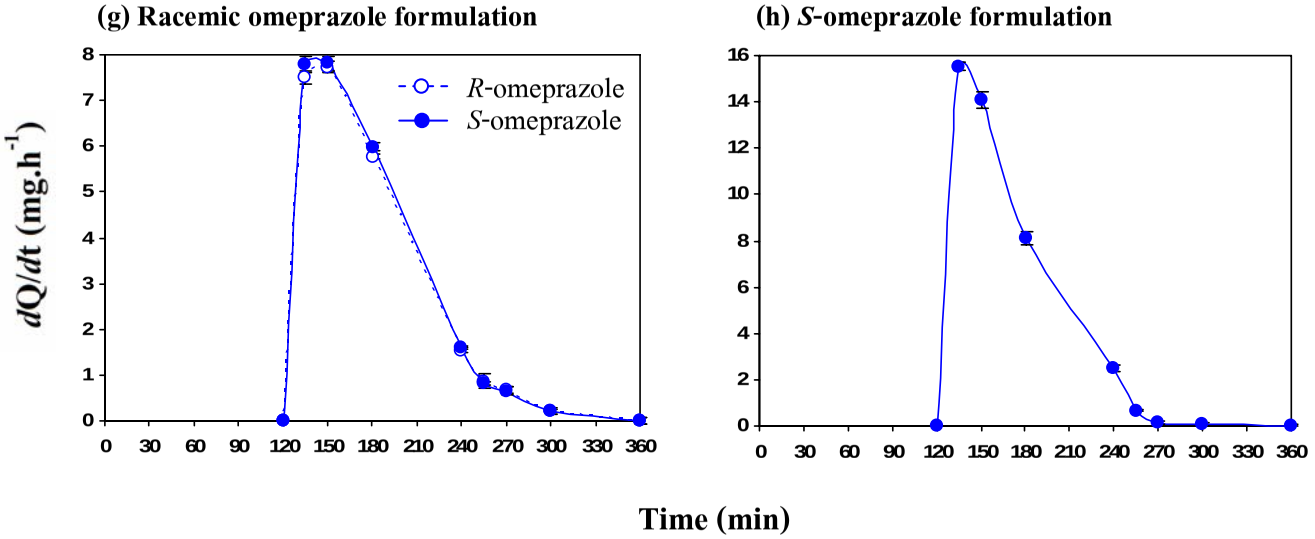

Figure 6.5. (continued)

Table 6.2. The release exponent (*n*) of *R*- and *S*-omeprazole enantiomers from DDS containing different MIP- and corresponding NIP-NOMs and from commercial formulations in pH 6.8 and pH 8 buffers at 37±0.5°C (mean±S.D., n=6).

System	Isomer	Release exponent (*n*)			
		pH 6.8	R^2	pH 8	R^2
4-VPD-MIP-NOM	*R*	0.712±0.013	0.991	0.699±0.032	0.980
	S	0.706±0.025	0.986	0.662±0.030	0.976
4-VPD-NIP-NOM	*R*	0.698±0.026	0.989	0.674±0.034	0.998
	S	0.716±0.022	0.975	0.663±0.031	0.985
MQD-MIP-NOM	*R*	0.719±0.043	0.995	0.672±0.044	0.984
	S	0.718±0.031	0.979	0.677±0.046	0.983
MQD-NIP-NOM	*R*	0.736±0.018	0.996	0.684±0.032	0.993
	S	0.733±0.028	0.995	0.682±0.032	0.995
MQN-MIP-NOM	*R*	0.865±0.076	0.994	0.826±0.041	0.989
	S	0.835±0.028	0.992	0.813±0.038	0.988
MQN-NIP-NOM	*R*	0.768±0.023	0.988	0.757±0.045	0.987
	S	0.761±0.021	0.987	0.729±0.031	0.980
Formulation RS	*R*	0.791±0.013	0.989	0.474±0.017	0.867
	S	0.792±0.028	0.988	0.477±0.019	0.866
Formulation S	*R*	-	-	-	-
	S	0.607±0.057	0.930	N/A	N/A

N/A: not applicable.

CHAPTER 7

CONCLUSION

In this thesis, the design and optimization of molecularly imprinted polymer (MIP) composite membrane and MIP-contained drug delivery system for application in drug delivery and membrane separation of chiral drugs were involved. Firstly, the composite membrane derived from MIP and cellulose was prepared, and its application for the enantioselective-controlled release of NSAIDs was studied. The conditions for manufacturing MIP and MIP composite cellulose membranes with regards of different monomer mixtures were established. The attachment of polymer layer on cellulose membranes was appeared after grated with poly(4-VPD-*co*-EDMA) or poly(ACM-*co*-MBA). The cellulose membrane modified with MIP layer comprising of poly(ACM-*co*-MBA) demonstrated higher enantioselective release of racemic ibuprofen than cellulose membrane modified with MIP layer comprising of poly(4-VPD-*co*-EDMA). However, the cellulose membrane modified with MIPs comprising of either poly(ACM-*co*-MBA) or poly(4-VPD-*co*-EDMA) did not give enantioselective release of racemic naproxen. The facilitated release of template *S*-ibuprofen enantiomer from the *S*-ibuprofen-(ACM-*co*-MBA)-MIP composite membrane was observed and this could be influenced from the selective adsorption of the template enantiomer by MIP grafted onto cellulose membrane together with the mobility of the molecule at the binding site. Although the difference of release of ibuprofen enantiomers from cellulose membrane modified with *S*-ibuprofen-(ACM-*co*-MBA)-MIP was statistically significant ($p<0.05$), the enantioselectivity obtained was modest. There was no enantioselectivity of the diffusion of ibuprofen enantiomers across such MIP grafted cellulose membrane placed on the mouse skin. The low enantioselective release obtained from MIP grafted cellulose membrane may be due to the deposition of MIP layer on the membrane surface.

Secondly, the cellulose composite membrane comprising MIP granules was produced. MIP granules selective to propranolol enantiomer either *R*- or *S*-propranolol was synthesized by bulk polymerization using methacrylic acid as a functional monomer and ethylene glycol dimethacrylate as a cross-linker and the MIP granules were loaded into cellulose membrane by phase inversion method. The ratio of cellulose and MIP granules content was

optimized to obtain integrity membrane with good appearance. For enantioselective transport evaluation, the MIP granule composite cellulose membrane revealed the facilitated non-template isomer transport across membrane, i.e., the *R*-propranolol imprinted polymer composite membrane facilitated the transport of eutomer (*S*-propranolol), whilst delayed the transport of distomer (*R*-propranolol). For enantioselective release evaluation, the MIP composite membrane tended to release the template enantiomer, i.e., the *S*-propranolol imprinted polymer composite membrane tended to release *S*-propranolol enantiomer in greater amount than *R*-propranolol enantiomer. However, the enanantioselective release obtained from *S*-propranolol MIP granule composite membrane was quite low with low permeability of propranolol enantiomers due to heterogeneous morphology and a broad population of binding sites of MIP granule, and low dispersity of MIP in composite membrane.

Thirdly, the MIP nanoparticle-on-microsphere (NOM) was successfully prepared by suspension polymerization involving agitation the polymerizing mixture at high speed. The MIP-NOM was fabricated into a self-assembled porous bacterial cellulose membrane using a phase inversion method. The resultant composite membrane demonstrated enantioselectivity of release for racemic propranolol. Such membrane displayed greater enantioselective release than membrane containing the same polymer but presented as granules. The increased surface area of the MIP-NOM allowed rebinding of the template molecule to occur more effectively. Moreover, the diffusivity of MIP-NOM composite membrane was improved compared to MIP granule composite membrane due to the greater dispersity of MIP-NOM in the membrane. The potential of using the generated *S*-propranolol MIP-NOM bacterial cellulose composite membrane to the enantioselective-controlled delivery of the *S*-isomer of racemic propranolol and its prodrug analogs was demonstrated *in vitro* evaluation using rat skin.

Finally, the design and synthesis of a NOM-MIP that contains achiral functional group (4-VPD) and chiral cinchona alkaloid functional group (QN, QD) within the binding sites was described. The application of the resulting NOM-MIPs in the enantioselecive controlled delivery of omeprazole was reported. The MIP-NOMs with selective binding sites for *S*-omeprazole enantiomer were synthesized by suspension polymerization from a polymeric mixture comprising of either the methacryloyl derivatized quinine or quinidine as functional monomer, and ethylene glycol dimethacrylate as a cross-linker and *S*-omeprazole as template molecule. The

%binding and selectivity of the MIPs made by either cinchona monomers were investigated, which differential binding of omeprazole enantiomers on MQN-MIP-NOM was evident in buffer solutions and was the greatest in pH 7.4 buffer. The FT-IR and XRD results revealed the microscopic structures of MQN- or MQD-MIP-NOM within the polymer matrix in the presence of *S*-omeprazole, and racemic omeprazole. The cellulose composite membranes containing the MQN-MIP-NOM were able to partially affect a selective transport flux of *S*-omeprazole enantiomer, from racemic omeprazole at pH 7.4. This evident was confirmed by confocal laser scanning microscopic study. These developed MIPs have been used to design delivery systems for the partial selective release of omeprazole enantiomers from racemic omeprazole. The delivery device was comprised of a hollow cylindrical poly(2-hydroxyethyl methacrylate) (poly(HEMA)) membrane fabricates, racemic omeprazole and MIP and pH 7.4 buffer as the vehicle. Release pattern of the prepared delivery systems was influenced by the poly(HEMA) matrix that provided enantiomer in sustain release and pH-dependent release. Release profiles showed 2:1 enantiomeric ratio of the active *S*-enantiomer of omeprazole to *R*-enantiomer released from MQN-MIP-NOM delivery systems, with a controlled release profile in media of different pH values. The delivery system containing molecularly imprinted *S*-omeprazole nanoparticle-on-microsphere QN-polymer displayed enantioselective controlled release for omeprazole model drug, which may have the potential for maximizing efficacy while minimizing dose frequency and toxicity.

To this end, the key aspects to achieve the enantioselection of release for the membranes and drug delivery devices in this study are: (1) the selection of functional monomer, (2) the morphology of MIP, and (3) the design of enantioselective-controlled release system. Thus, the future work should be the use of chiral functional monomer for MIP synthesis selective to propranolol enantiomer. Taking advantage that the high surface area of MIP provides good site accessibility and good enantioselectivity, the MIP format may be prepared as nanofilament membrane in order to improve the surface area of MIP. The cellulose membrane may be modified to obtain the symmetric pore structure before grafted with MIP. Additionally, the drug delivery device for racemic omeprazole should be further developed to reduce the size in order to obtain the system which is suitable for use in human.

REFERENCES

Abelo, A., Andersson, T.B., Antonsson, M., Naudot, A.K., Skanberg, I., Weidolf, L., 2000. Stereoselective metabolism of omeprazole by human Cytochrome P450 enzymes. Drug Metab. Dispos. 28, 966-972.

Adams, S.S., Bresloff, P., Mason, C.G., 1976. Pharmacological differences between the optical isomers of ibuprofen: evidence for metabolic inversion of (-)-isomer. J. Pharm. Pharmacol. 28, 256-257.

Ahmed, S., Imai, T., Yoshigae, Y., Otagiri, M., 1997. Stereospecific activity and nature of metabolizing esterases for propranolol prodrug in hairless mouse skin, liver and plasma. Life Sci. 61, 1879-1887.

Allender, C.J., Richardson, C., Woodhouse, B., Heard, C.M., Brain, K.R., 2000. Pharmaceutical application for molecularly imprinted polymers. Int. J. Pharm. 195, 39-43.

Allison, B., Applegate, B.M., Youngblood, J.P., 2007. Hemocompatibility of hydrophilic antimicrobial copolymers of alkylated 4-vinylpyridine. Biomacromolecules 8, 2995-2999.

Alvarez, C., Torrado, J.J., Cadorniga, R., 1999. Stereoselective drug release from ketoprofen and ricobendazole matrix tablets. Chirality 11, 611-615.

Amnuaikit, C., Ikeuchi, I. Ogawara, K., Higaki, K., Kimura, T., 2005. Skin permeation of propranolol from polymeric film containing terpene enhancers for transdermal use. Int. J. Pharm. 289, 167-175.

Ansell, R.J., 2005. Molecularly imprinted polymers for the enantioseparation of chiral drugs. Adv. Drug Deliv. Rev. 57, 1809-1835.

Arshady, R., Mosbach, K., 1981. Synthesis of substrate-selective polymer by host-guest polymerization. Macromol. Chem. 182, 687-692.

Asnin, L., Götmar, G., Guiochon, G., 2005. Chromatographic behavior of the enantiomers of 2,2,2-trifluoro-1-(9-anthryl)ethanol on a quinidine-carbamate chiral stationary phase. J. Chromatogr. A 1091, 183-186.

Atkins, R.C., Carey, F.A., 2002. Stereochemistry. In: Organic chemistry: a brief course, 3rd ed. (Peterson, K.A., Oberbroeckling, S.R., eds.), McGraw-Hill, New York, pp. 182-205.

Avgerinos, A., Noormohammadi, A., Hutt, A.J., 1991. Disposition of ibuprofen enantiomers following the oral administration of a novel controlled release formulation to healthy volunteers. Int. J. Pharm. 68, 97-103.

Barrett, A.M., Cullum, V.A., 1968. The biological properties of the optical isomers of propranolol and their effects on cardiac arrythemias. Br. J. Pharmacol. 34, 43-55.

Bataille, P., Van, B.T., Pharm, Q.B., 1982. Emulsion polymerization of styrene: I. Review of experimental data and digital simulation. J. Polym. Sci. Polym. Chem. 20, 795-810.

Bodhibukkana, C., Srichana, T., Kaewnopparat, S., Tangthong, N., Bouking, P., Martin, G.P., Suedee, R., 2006. Composite membrane of bacterially-derived cellulose and molecularly imprinted polymer for use as a transdermal enantioselective controlled-release system of racemic propranolol. J. Contr. Release 113, 43-56.

Brown, A., 1886. On an acetic acid ferment which forms cellulose. J. Chem. Soc. 49, 432-439.

Brueggemann, O., Haupt, K., Ye, L., Yilmaz, E., Mosbach, K., 2000. New configurations and applications of molecularly imprinted polymers. J. Chromatogr. A 889, 15-24.

Brunton, L.L., 1990. Drugs affecting gastrointestinal function - agents for control of gastric acidity and treatment of peptic ulcers. Goodman and Gilman's The pharmacological basis of therapeutics, 8th ed. (Gilman, A.G., Rall, T.W., Nies, A.S., Taylor, P., eds.), Pargamon Press, Inc., New York, pp. 897-913.

Bryjak, M., Kozlowski, J., Wieczorek, P., Kaferski, P., 1993. Enantioselective transport of amino acid through supported chiral liquid membranes. J. Membr. Sci. 85, 221-228.

Burke, D., Henderson, D.J., 2002. Chirality: a blueprint for the future. Br. J. Anaesth. 88, 563-576.

Cahn R.S., Ingold, S.C., Prelog, V., 1966. Specification of molecular chirality. Angew. Chem. Int. Ed. Engl. 5, 385-415.

Caner, H., Groner, E., Levy, L., 2004. Trends in the development of chiral drugs. Drug Discov. Today 9, 105-110.

Cattani, M., Bassalo§, J.M.F., 1997. On the stability of optical activity: a two-level approach. J. Quant. Spectrosc. Radiat. Transfer 61, 299-302.

Charman, S.A., Charman, W.N., 2003. Oral modified-release delivery systems. In: Modified-release drug delivery technology (Rathbone, M.J., Hadgraft, J., Roberts, M.S., eds.), Marcel Dekker, Inc., New York, pp. 1-10.

Cheng, H., Rogers, J.D., Demetriades, J.L., Holland, S.D., Depuy, E., et al., 1994. Pharmacokinetics and bioinversion of ibuprofen enantiomers in humans. Pharm. Res. 11, 824-830.

Chronakis, I.S., Jakob, A., Hagström, B., Ye, L., 2006. Encapsulation and selective recognition of molecularly imprinted theophylline and 17^{β}-estradiol nanoparticles within electrospun polymer nanofibers. Langmuir 22, 8960-8965.

Ciardelli, G., Borrelli, C., Silvestri, D., Cristallini, C., Barbani, N., Giusti, P., 2006. Supported imprinted nanospheres for the selective recognition of cholesterol. Biosens. Bioelectron. 21, 2329-2338.

Cormack, P.A.G., Elorza, A.Z., 2004. Molecularly imprinted polymer: synthesis and characterization - review. J. Chromatogr. B 804, 173-182.

Costa, P., Lobo, J.M.S., 2001. Modeling and comparison of dissolution profiles - review. Eur. J. Pharm. Sci. 13, 123-133.

Crossley, R., 1995. Chirality and aspects of drug development. In: Chirality and the biological activity of drugs, CRC Press, New York, pp. 161-187.

Cunliffe, D., Kirby, A., Alexander, C., 2005. Molecularly imprinted drug delivery systems. Adv. Drug Deliv. Rev. 57, 1836-1853.

Danel, C., Foulon, C., Goossens, J.F., Bonte, J.P., Vaccher, C., 2006. Kinetics of racemization of enantiopure *N*-imidazole derivatives, aromatase inhibitors: studies in organic, aqueous, and biomimetic media. Tetrahedron: Asymmetry 17, 2317-2321.

Daugherty, A.L., Mrsny, R.J., 1999. Transcellular uptake mechanisms of the intestinal epithelial barrier. Pharm. Sci. Technol. Today 4, 144-151.

Devine, D.M., Derery, S.M., Lyons, L.T., Geever, L.M., Kennedy, J.E., Higginbotham, C.L., 2006. Multifunctional polyvinylpyrrolidinone-polyacrylic acid copolymer hydrogels for biomedical applications. Int. J. Pharm. 326, 50-59.

Dixit, N., Bali, V., Baboota, S., Ahuja, A., Ali, J., 2007. Iontophoresis - an approach for controlled drug delivery - review. Curr. Drug Deliv. 4, 1-10.

Donato, L., Figoli, A., Drioli, E., 2005. Novel composite poly(4-vinylpyridine)/polypropylene membranes with recognition properties for (*S*)-naproxen. J. Pharm. Biomed. Anal. 37, 1003-1008.

Drayer, D.E., 1988. Pharmacodynamic and pharmacokinetic differences between drug enantiomers in humans: an overview. Clin. Pharmacol. Ther. 40, 125-133.

Duddu, S.P., Vakilynejad, M., Jamali, F., Grant, D.J.W., 1993. Stereoselective dissolution of propranolol hydrochloride from hydroxypropyl methylcellulose matrices. Pharm. Res. 10, 1648-1653.

Dzgoev, A., Haupt, K., 1999. Enantioselective molecularly imprinted polymer membranes. Chirality 11, 465-469.

Easson, L.H., Stedman, E., 1933. Studies on the relationship between chemical constitution and physiological action. Biochem. J. 27, 1257-1266.

Eikeren, P.V., 1997. Commerical manufacture of chiral pharmaceuticals. In: Chiral separation – application and technology, (Ahuja, S., ed.), American Chemical Society, Washington, DC., pp. 9-35.

Erlandsson, P., Isaksson, R., Lorentzon, P., Lindberg, P., 1990. Resolution of the enantiomers of omeprazole and some of its analogues by liquid chromatography on a trisphenylcarbamoylcellulose-based stationary phase. The effect of the enantiomers of omeprazole on gastric glands. J. Chromatogr. 532, 305-319.

Fellenius, E., Berglindh, T., Sachs, G., Olbe, L., Elander, B., Sjöstrand, S.-E., Wallmark, B., 1981. Substituted benzimidazoles inhibit gastric acid secretion by blocking (H^+/K^+) ATPase. Nature (London) 290, 159-161.

Fink, H.P., Weigel, P., Purz, H.J., Ganster, J., 2001. Structure formation of regenerated cellulose materials from NMMO-solutions. Prog. Polym. Sci. 26, 1473-1524.

Flynn, G.L., Weiner, N.D., 1993. Topical and transdermal delivery - provinces of realism. In: Dermal and transdermal drug delivery - new insights and perspectives (Gurny, R, Teubner, A., eds.), Wissenschaftliche Verlagsgesellschaft GmbH, Stuttgart, pp. 33-65.

Foss, A.C., Peppas, N.A., 2004. Investigation of the cytotoxicity and insulin transport of acrylic-based copolymer protein delivery systems in contact with caco-2 cultures. Eur. J. Pharm. Biopharm. 57, 447-455.

Friend, D.R., 1992. *In vitro* skin permeation technique. J. Contr. Release 18, 235-248.

Gomollon, F., Calvet, X., 2005. Optimising acid inhibition treatment. Drugs 65 (Suppl. 1), 25-33.

Gummer, C.L., 1989. The *in vitro* evaluation of transdermal delivery. In: Transdermal drug delivery - developmental issues and research initiatives (Hadgraft, J., Guy, R.H., eds.), Marcel Dekker, Inc., New York, pp. 177-196.

Gyo Lee, E., Soon Won, H., Hyun Chung, B., 2001. Enantioselective hydrolysis of racemic naproxen methyl ester by two-step acetone-treated *Candida rugosa* lipase. Process Biochem. 37, 293-298.

Hadgraft, J., 2004. Skin deep - review. Eur. J. Pharm. Biopharm. 58, 291-299.

Hadik, P., Kotsis, L., Eniszne-Bodogh, M., Szabo, L.P., Nagy, E., 2005. Lactic acid enantiseparation by means of porous ceramic disc and hollow fiber organic membrane. Sep. Purif. Technol. 41, 299-304.

Haigh, J.M., Smith, E.W., 1994. The selection and use of natural and synthetic membranes for *in vitro* diffusion experiments - review. Eur. J. Pharm. Sci. 2, 311-330.

Han, C., Wang, B., 2005. Factors that impact the developability of drug candidates: an overview. In: Drug delivery - principles and applications, John Wiley & Sons, Inc., New Jersey, pp. 1-14.

Hansen, F.K., Ugelstad, J., 1978. Particle nucleation in emulsion polymerization; I. Theory of homogeneous nucleation. J. Polym. Sci. Polym. Chem. 16, 1953; 1979. II. Nucleation in emulsifier-free systems investigated by seed polymerization; III. Nucleation in systems with anionic emulsifier investigated by seeded and unseeded polymerization; IV. Nucleation in monomer droplets. J. Polym. Sci. Polym. Chem. 17, pp. 3033, 3047, 3069.

Hattori, K., Hiwatari, M., Iiyama, C., Yoshimi, Y., Kohori, F., Sakai, K., Piletsky, S.A., 2004. Gate effect of theophylline-imprinted polymers grafted to the cellulose by living radical polymerization. J. Membr. Sci. 233, 169-173.

Heinze, T., Koschella, A., 2005. Solvents applied in the field of cellulose chemistry - a mini review. Polímeros: Ciência e Tecnologia 15, 84-90.

Higaki, K., Amnuaikit, C., Kimura, T., 2003. Strategies for overcoming the stratum corneum - chemical and physical approaches. Am. J. Drug Deliv. 1, 187-214.

Higuchi, A., Yomogita, H., Yoon, B.O., Kojima, T., Hara, M., Maniwa, S., Saitoh, H., 2002. Optical resolution of amino acid by ultrafiltration using recognition sites of DNA. J. Membr. Sci. 205, 203-212.

Hilal, N., Kochkodan, V., 2003. Surface modified microfiltration membranes with molecularly recognizing properties. J. Membr. Sci. 213, 97-113.

Hilal, N., Kochkodan, V., Busca, G., Kochkodan, O., Atkin, B.P., 2003. Thin layer composite molecularly imprinted membranes for selective separation of cAMP. Sep. Purif. Technol. 31, 281-289.

Hiratani, H., Alvarez-Lorenzo, C., 2002. Timolol uptake and release by imprinted soft contact lenses made of *N,N*-diethylacrylamide and methacrylic acid. J. Contr. Release 83, 223-230.

Hosoya, K., Yoshizako, K., Tanaka, N., Kimata, K., Araki, T., Haginaka, J., 1994. Uniform-size macroporous polymer-based stationary phase for HPLC prepared through molecular imprinting technique. Chem. Lett. 23, 1437-1438.

Howe, R., Shanks, R.G., 1966. Optical isomers of propranolol. Nature (London) 210, 1336-1338.

Hyneck, M., Dent, J., Hook, J.B., 1990. Chirality: Pharmacological action and drug development. In: Chirality in drug design and synthesis (Brown, C., ed.), Academic Press Limited, London, pp. 1-28.

Johnson, B., Niedermaier, D.J., Crone, W.C., Moorthy, J., Deebe, D.J., 2002. Mechanical properties of a pH sensitive hydrogel. Society for Experimental Mechanics, 2002 SEM Annual Conference Proceedings, Milwaukee, WI, 2002 (from http://mandm.engr.wisc.edu/faculty_pages/crone/PDF/SEM2002_Buck_paper_02_PREPRINT.pdf, access on April 2009).

Jonas, R., Farah, L.F., 1998. Production and application of microbial cellulose. Polym. Degrad. Stab. 59, 101-106.

Kanazawa, H., Okada, A., Higaki, M., Yokota, H., Mashige, F., Nakahara, K., 2003. Stereospecific analysis of omeprazole in human plasma as a probe for CYP2C19 phenotype. J. Pharm. Biomed. Anal. 30, 1817-1824.

Karadag, E., Saraydin, D., Cetinkaya, S., Güven, O., 1996. *In vitro* swelling studies and preliminary biocompatibility evaluation of acrylamide-based hydrogels. Biomaterials 17, 67-70.

Kempe, M., Fischer, L., Mosbach, K., 1993. Chiral separation using molecularly imprinted heteroaromatic polymers, J. Mol. Recognit. 6, 25-29.

Kempe, M., Mosbach, K., 1994. Direct resolution of naproxen on non-covalently molecularly imprinted chiral stationary phase. J. Chromatogr. 664, 276-279.

Kempe, M., Mosbach, K., 1995. Molecular imprinting used for chiral separations. J. Chromatogr. A 694, 3-13.

Keurentjes, L.J., Nabuurs, W.M., Vegter, E.A., 1996. Liquid membrane technology for the separation of racemic mixtures. J. Membr. Sci. 113, 351-360.

Kim, J.H., Kim, J.H., Jegal, J., Lee, K-H., 2003. Optical resolution of α-amino acids through enantioselective polymeric membranes based on polysaccharides. J. Membr. Sci. 213, 273-283.

Klemm, D., Schumann, D., Udhardt, U., Marsch, S., 2001. Bacterial synthesized cellulose-artificial blood vessels for microsurgery. Prog. Polym. Sci. 26, 1561-1603.

Klotz, U., 2006. Clinical impact of *CYP2C19* polymorphism on the action of proton pump inhibitors: a review of a special problem. Int. J. Clin. Pharmacol. Ther. 44, 297-302.

Kobayashi, T., Wang, H.Y., Fujii, N., 1998. Molecular imprint membranes of polyacrylonitrile copolymers with different acrylic acid segments, Anal. Chim. Acta 365, 81-88.

Kochkodan, V., Weigel, W., Ulbricht, M., 2002. Molecularly imprinted composite membranes for selective binding of desmetryn from aqueous solutions. Desalination 149, 323-328.

Komiyama, M., Takeuchi, T., Mukawa, T., Asanuma, H., 2003. Fundamentals of molecular imprinting. In: Molecular imprinting - from fundamentals to applications. Wiley-VCH Verlag GmbH & Co. KGaA, Weinheim, pp. 9-19.

Lavelle, E.C., Sharif, S., Thomas, N.W., Holland, J., Davis, S.S., 1995. The importance of gastrointestinal uptake of particles in the design of oral delivery systems. Adv. Drug Deliv. Rev. 18, 5-22.

Lee, E.J.D., Williams, K., Day, R., Graham, G., Champion, D., 1985. Stereoselective disposition of ibuprofen enantiomers in man. Br. J. Clin. Pharmacol. 19, 669-674.

Lehmann, M., Brunner, H., Tovar, G.E.M., 2002. Selective separations and hydrodynamic studies: a new approach using molecularly imprinted nanosphere composite membranes. Desalination 149, 315-321.

Maggi, L., Massolini, G., De Lorenzi, E., Conte, U., Caccialanza, G., 1996. Evaluation of stereoselective dissolution of verapamil hydrochloride from matrix tablets press-coated with chiral excipients. Int. J. Pharm. 136, 43-52.

Maier, N.M., Franco, P., Lindner, W., 2001. Separation of enantiomers: needs, challenges, perspectives. J. Chromatogr. A 906, 3-33.

Mandl, A., Nicoletti, L., Lämmerhofer, M., Lindner, W., 1999. Quninine *versus* carbamoylated quinine-based chiral anion exchangers - a comparison regarding enantioselectivity for N-protected amino acids and other chiral acids. J. Chromatogr. A 858, 1-11.

Markovic, N., Agotonovic-Kustrin, S., Glass, B., Prestidge, C.A., 2006, Physical and thermal characterization of chiral omeprazole sodium salts. J. Pharm. Biomed. Anal. 42, 25-31.

Martens-Lobenhoffer, J., Reiche, I., Tröger, U., Mönkemüller, Malfertheiner, P., Bode-Böger, S.M., 2007. Enantioselective quantification of omeprazole and its main metabolites in human serum by chiral HPLC-atmospheric pressure photoionization tandem mass spectrometry. J. Chromatogr. B 857, 301-307.

Maruyama, A., Adachi, N., Takatsuki, T., Torii, M., Sanui, K., Ogata, N., 1990. Enantioselective permeation of α-amino acid isomers through poly(amino acid)-derived membranes. Macromolecules 23, 2748-2752.

Mathew, M., Gupta, V.D., Bailey, R.E., 1995. Stability of omeprazole solutions at various pH values as determined by high-performance liquid chromatography. Drug Dev. Ind. Pharm. 21, 965-971.

Mathew-Krotz, J., Shea, K.J., 1996. Imprinted polymer membranes for the selective transport of targeted neutral molecules. J. Am. Chem. Soc. 118, 8154-8155.

Maximini, A., Chmiel, H., Holdik, H., Maier, N.W., 2006. Development of a supported liquid membrane process for separating enantiomers of N-protected amino acid derivatives. J. Membr. Sci. 276, 221-231.

Mayes, A.G., Mosbach, K., 1996. Molecularly imprinted polymer beads: suspension polymerization using a liquid perfluorocarbon as the dispersing phase. Anal. Chem. 68, 3769-3774.

Mayes, A.G., Whitcombe, M.J., 2005. Synthetic strategies for the generation of molecularly imprinted organic polymers. Adv. Drug Deliv. Rev. 57, 1742-1778.

McConalthy, J., Owens, M.J., 2003. Stereochemistry in drug action. Prim. Care Companion J. Clin. Psychiatry 5, 70-73.

Meier, M.M., Danis, L.A., Soldi, V., 2004. Characterization and drug-permeation profiles of microporous and dense cellulose acetate membranes: influence of plasticizer and pore forming agent. Int. J. Pharm. 278, 99-110.

Mosbach, K., Ramson, O., 1996. The emerging technique of molecular imprinting and its future impact on biotechnology. Bio/Technology 14, 163-170.

Namdeo, A., Jain, N.K., 2002. Liquid crystalline pharmacogel based enhanced transdermal delivery of propranolol hydrochloride. J. Contr. Release 82, 223-236.

Newcomb, M., Helgeson, R.C., Cram, D.J., 1974. Enantiomer differentiation in transport through bulk liquid membranes. J. Am. Chem. Soc. 96, 7367-7369.

Nguyen, L.A., He, H., Pharm-Huy, C., 2006. Chiral drugs - an overview. Int. J. Biomed. Sci. 2, 85-100.

Norell, M.C., Andersson, H.S., Nicholls, I.A., 1998. Theophylline molecularly imprinted polymer dissociation kinetics: a novel sustained release drug dosage mechanism. J. Mol. Recognit. 11, 98-102.

Olbe, L., Carlsson, E., Lindberg, P., 2003. A proton-pump inhibitor expedition: the case histories of omeprazole and esomeprazole. Nat. Rev. Drug Discov. 2, 132-139.

Park, E.S., Chang, S.Y., Hahn, M., Chi, S.C., 2000. Enhancing effect of polyoxyethylene alkyl ethers on the skin permeation of ibuprofen. Int. J. Pharm. 209, 109-119.

Pérez, N., Whitcombe, M.J., Vulfson, E.N., 2001. Surface imprinting of cholesterol on submicrometer coreshell emulsion particles. Macromolecules 34, 830-836.

Pérez-Moral, N., Mayes, A.G., 2004. Comparative study of imprinted polymer particles prepared by different polymerization methods. Anal. Chim. Acta 504, 15-21.

Pettersson, C., 1984. Chromatographic separation of enantiomers of acids with quinine as chiral counter ion. J. Chromatogr. A 316, 553-567.

Pettersson, C., Schill, G., 1986. Separation of enantiomers in ion-pair chromatographic systems. J. Liq. Chromatogr. 9, 269-290.

Pham-Huy, C., Radenen, B., Sahui-Gnassi, A., Claude, J.R., 1995. High-performance liquid chromatographic determination of (*S*)- and (*R*)-propranolol in human plasma and urine with a chiral β-cyclodextrin bounded phase. J. Chromatogr. B 665, 125-132.

Pickering, P.J., Chaudhuri, J.B., 1997. Enantioselective extraction of (D)-phenylalanine from racemic (D/L)-phenylalanine using chiral emulsion liquid membranes. J. Membr. Sci. 127, 115-130.

Piette, V., Kindner, W., Crommen, J., 2002. Enantiomeric separation of N-protected amino acids by non-aqueous capillary electrophoresis with dimeric forms of quinine and quinidine derivatives serving as chiral selectors. J. Chromatogr. A 948, 295-302.

Piette, V., Lindner, W., Crommen, J., 2000. Enantioseparation of anionic analytes by non-aqueous capillary electrophoresis using quinine and quinidine derivatives as chiral counter-ions. J. Chromatogr. A 894, 63-71.

Piletsky, S.A., Dubey, I.Y., Fedoryak, D.M., Kukhar, V.P., 1990. Substrate-selective polymeric membranes. Selective transfer of nucleic acid components. Biopolym. Kletka 6, 55-58.

Piletsky, S.A., Matuschewski, H., Schedler, U., Wilpert, A., Piletskaya, E.V., Thiele, T.A., Ulbricht, M., 2000. Surface functionalization of porous polypropylene membranes with molecularly imprinted polymers by photograft copolymerization in water. Macromolecules 33, 3092-3098.

Piletsky, S.A., Panasyuk, T.L., Piletskaya, E.V., Nicholls, I.A., Ulbricht, M., 1999. Receptor and transport properties of imprinted polymer membranes. J. Membr. Sci. 157, 263-278.

Piletsky, S.A., Piletskaya, E.V., Panasyuk, T.L., El'skaya, A.V., Levi, R., Karube, I., Wulff, G., 1998. Imprinted membranes for sensor technology: opposite behavior of covalently and noncovalently imprinted membranes. Macromolecules 31, 2137-2140.

Qin, L., He, X.W., Li, W.Y., Zhang, Y.K., 2008. Molecularly imprinted polymer prepared with bonded β-cyclodextrin and acrylamide on functionalized silica gel for selective recognition of tryptophan in aqueous media. J. Chromatogr. A 1187, 94-102.

Quigley, J.M., Jordan, C.G.M., Timoney, R.F., 1994. The synthesis, hydrolysis kinetics and lipophilicity of O-acyl esters of propranolol. Int. J. Pharm. 101, 145–163.

Ramamoorthy, M., Ulbricht, M., 2003. Molecular imprinting of cellulose acetatesulfonated polysulfone blend membranes for rhodamine B by phase inversion technique. J. Membr. Sci. 217, 207-214.

Ranade, V.V., 1991. Drug delivery systems (6); transdermal drug delivery. J. Clin. Pharmacol. 31, 401-418.

Reddy, P.S., Kobayashi, T., Fujii, N., 1999. Molecular imprinting in hydrogen bonding networks of polyamide nylon for recognitions of amino acids. Chem. Lett. 293-294.

Reddy, P.S., Kobayashi, T., Fujii, N., 2002. Recognition characteristics of dibenzofuran by molecularly imprinted polymers made from common polymers. Eur. Polym. J. 38, 79-785.

Ross, P., Mayer, R., Benziman, M., 1991. Cellulose biosynthesis and function in bacteria. Microbiol. Rev. 55, 35-58.

Schmook, F.P., Meingassner, J.G., Billich, A., 2001. Comparison of human skin or epidermis models with human and animal skin in *in-vitro* percutaneous absorption. Int. J. Pharm. 215, 51-56.

Sellergren, B., Allender, C.J., 2005. Molecularly imprinted polymers: a bridge to advanced drug delivery. Adv. Drug Deliv. Rev. 57, 1733-1741.

Sergeyeva, T.A., Matuschewski, H., Piletsky, S.A., Bendig, J., Schedler, U., Ulbricht, M., 2001. Molecularly imprinted polymer membranes for substance-selective solid-phase extraction from water by surface photo-grafing polymerization. J. Chromatogr. A 907, 89-99.

Sheldon, R.A., 1993. Chirality and biological activity. In: Chirotechnology - industrial synthesis of optically active compounds, Marcel Dekker, Inc., New York, pp. 39-72.

Shinbo, T., Yamaguchi, T., Yanagishita, H., Sakai, K., Kitamoto, D., Sugiura, M., 1993. Supported liquid membranes for enantioselective transport of amino acid mediated by chiral crown ether - effect of membrane solvent on transport rate and membrane stability J. Membr. Sci. 84, 241-248.

Smith, L.E., Rimmer, S., MacNeil, S., 2006. Examination of the effects of poly(*N*-vinylpyrrolidinone) hydrogels direct and indirect contact with cells. Biomaterials 27, 2806-2812.

Solinís, M.A., de la Cruz, Y., Hernández, R.M., Gascón, A.R., Calvo, B., Bedraz, J.L., 2002. Release of ketoprofen enantiomres from HPMC K100M matrices - diffusion studies. Int. J. Pharm. 239, 61-68.

Srichana, T., Suedee, R., 2001. Evaluation of stereoselective dissolution of racemic salbutamol matrices prepared with commonly used excipients and ^{1}H-NMR study. Drug Dev. Ind. Pharm. 27, 454-464.

Stinson, S.C., 1998. Counting on chiral drugs. Chem. Eng. News 76, 83-103.

Stott, P.W., Williams, A.C., Barry, B.W., 2001. Mechanistic study into the enhanced transdermal permeation of a model β-blocker, propranolol, by fatty acids: a melting point depression effect. Int. J. Pharm. 219, 161-176.

Suedee, R., Bodhibukkana, C., Tangthong, N., Amnuaikit, C., Kaewnopparat, S., Srichana, T., 2008. Development of a reservoir-type transdermal enantioselective-controlled delivery system for racemic propranolol using a molecularly imprinted polymer composite membrane. J. Contr. Release 129, 170-178.

Suedee, R., Srichana, T., Chotivatesin, R., Martin, G.P., 2002a. Stereoselective release behaviors of imprinted bead matrices. Drug Dev. Ind. Pharm. 28, 547-556.

Suedee, R., Srichana, T., Martin, G.P., 2000. Evaluation of matrices containing molecularly imprinted polymers in the enantioselective-controlled delivery of β-blockers. J. Contr. Release 66, 135-147.

Suedee, R., Srichana, T., Rattananont, T., 2002b. Enantioselective release of controlled delivery granules based on molecularly imprinted polymers. Drug Del. 9, 19-30.

Sutani, K., Saetsu, I., Uchida, K., Matsubara, Y., 2002. Stimulus responsive drug release from polymer gel. Controlled release of ionic drug from polyampholyte gel. Rad. Phys. Chem. 64, 331-336.

Swarbrick, J., Boylan, J.C., 1995. Percutaneous absorption. In: Encyclopedia of pharmaceutical technology, Marcel Dekker, Inc., New York, pp. 413-447.

Testa, B., Carrupt, P.A., Gal, J., 1993. The so-called “interconversion” of stereoisomeric drugs: an attempt at clarification. Chirality 5, 105-111.

Thoelen, C., De bruyn, M., Theunissen, E., Kondo, Y., Vankelecom, I.F.J., Grobet, P., Yoshikawa, M., Jacobs, P.A., 2001. Membranes based on poly(γ-methyl-L-glutamate): synthesis, characterization and use in chiral separations. J. Membr. Sci. 186, 153-163.

Torres-Lugo, M., Garcia, M., Record, R., Peppas, N.A., 2002. Physicochemical behavior and cytotoxic effects of p(methacrylic acid-g-ethylene glycol) nanospheres for oral delivery of proteins. J. Contr. Release 80, 197-205.

Tucker, G.T., Lennard, M.S., 1990. Enantiomer specific pharmacokinetics. Pharmacol. Ther. 45, 309-329.

Ulbricht, M., 2004. Membrane separations using molecularly imprinted polymers. J. Chromatogr. B, 804, 113-125.

Ulbricht, M., 2006. Molecularly imprinted membranes. In: Molecular imprinting of polymers - biotechnology intelligence unit (Piletsky, S., Turner, A., eds.), Landes Bioscience, Texas, pp. 80-94.

Ulbricht, M., Belter, M., Langenhangen, U., Schneider, F., Weigel, W., 2002. Novel moleculary imprinted polymer (MIP) composite membranes *via* controlled surface and pore functionalizations. Desalination 149, 293-295.

Wan, Y.Z., Huang, Y. Yuan, C.D., Raman, S., Zhu, Y., Jiang, H.J., He., F., Gao, C., 2006. Biomimetic synthesis of hydroxyapatite/bacterial cellulose nanocomposites for biomedical applications. Mater. Sci. Eng. C 27, 855-864.

Wang, J., Cormack, P.A.G., Sherrington, D.C., Khoshdel, E., 2003. Monodisperse, molecularly imprinted polymer microspheres prepared by precipitation polymerization for affinity separation applications. Angew. Chem. Int. Ed. 42, 5336-5338.

Whitcombe, M.J., Rodriguez, M.E., Villar, P., Vulfson, E.N., 1995. A new method for the introduction of recognition site functionality into polymers prepared by molecular imprinting - synthesis and characterization of polymeric receptors for cholesterol. J. Am. Chem. Soc. 117, 7105-7111.

Wilson, D.J., Chenery, D.H., Bowring, H.K., Wilson, K., Turner, R., Maughan, J., West, P.J., Ansell, C.W., 2005. Physical and biological properties of a novel siloxane adhesive for soft tissue application. J. Biomater. Sci. Polym. Ed. 16, 449-472.

Wulff, G., 1995. Molecular imprinting in cross-linked materials with the aid of molecular templates - a way towards artificial antibodies. Angew. Chem. Int. Ed. Engl. 34, 1812-1832.

Wulff, G., 1993. The role of binding-site interactions in the molecular. Imprinting of polymers. Trends Biotechnol. 11, 85-87.

Wulff, G., Sarhan, A., 1972. The use of polymers with enzyme analogous structures for the resolution of racemates. Angew. Chem. Int. Ed. Engl. 11, 341-343.

Yang, R.T., Rege, S.U., 2001. A novel FTIR method for studying mixed gas adsorption at low concentrations: H_2O and CO_2 on NaX zeolite and γ-alumina. Chem. Eng. Sci. 56, 3781-3796.

Yang, S.K., Lu, X.L., 1992. Resolution and stability of oxazepam enantiomers. Chirality 4, 443-446.

Ye, L., Mosbach, K., 2001. Molecularly imprinted microspheres as anti-body binding mimics. React. Funct. Polym. 48, 149-157.

Yoshikawa, M., Izumi, J., Kitao, T., Koya, S., Sakamoto, S., 1995. Molecular imprinted polymeric membranes for optical resolution. J. Membr. Sci. 108, 171-175.

Yoshikawa, M., Murakoshi, K., Kogita, T., Hanaoka, K., Guiver, M.D., Robertson, G.P., 2006. Chiral separation membranes from modified polysulfone having myrtenal-derived terpenoid side groups. Eur. Polym. J. 42, 2532-2539.

Yoshikawa, M., Ooi, T., Izumi, J., 1999. Alternative molecularly imprinted membranes from a derivative of a natural polymer, cellulose acetate. J. Appl. Polym. Sci. 72, 493-499.

Yoshimi, Y., Ohdaira, R., Iiyama, C., Kiyotaka, S., 2001. “Gate effect” of thin layer of molecularly-imprinted poly(methacrylic acid-*co*-ethyleneglycol dimethacrylate). Sens. Actuators B 73, 49-53.

http://en.wikipedia.org/wiki/cellulose, access on November 2008.

http://en.wikipedia.org/wiki/Epidermis_(skin), access on November 2008.

http://www.fda.gov/cder/guidance/stereo.htm, access on October 2008.

http://www.res.titech.ac.jp/~junkan/english/cellulose, access on November 2008.

http://www.scf-online.com/german/43_d/absorption43_d.htm, access on November 2008.

APPENDIX A

FT-IR AND ^{1}H NMR SPECTRA OF METHACRYLOYLATE QUININE AND METHACRYLOYLATE QUINIDINE

A.1. FT-IR spectra of methacryloylate quinine and methacryloylate quinidine

Instrument: FT-IR spectrometer, Perkin-Elmer system 2000

A.2. ^{1}H NMR spectra of methacryloylate quinine and methacryloylate quinidine

Instrument: Bruker DRX 200 MHz spectrometer

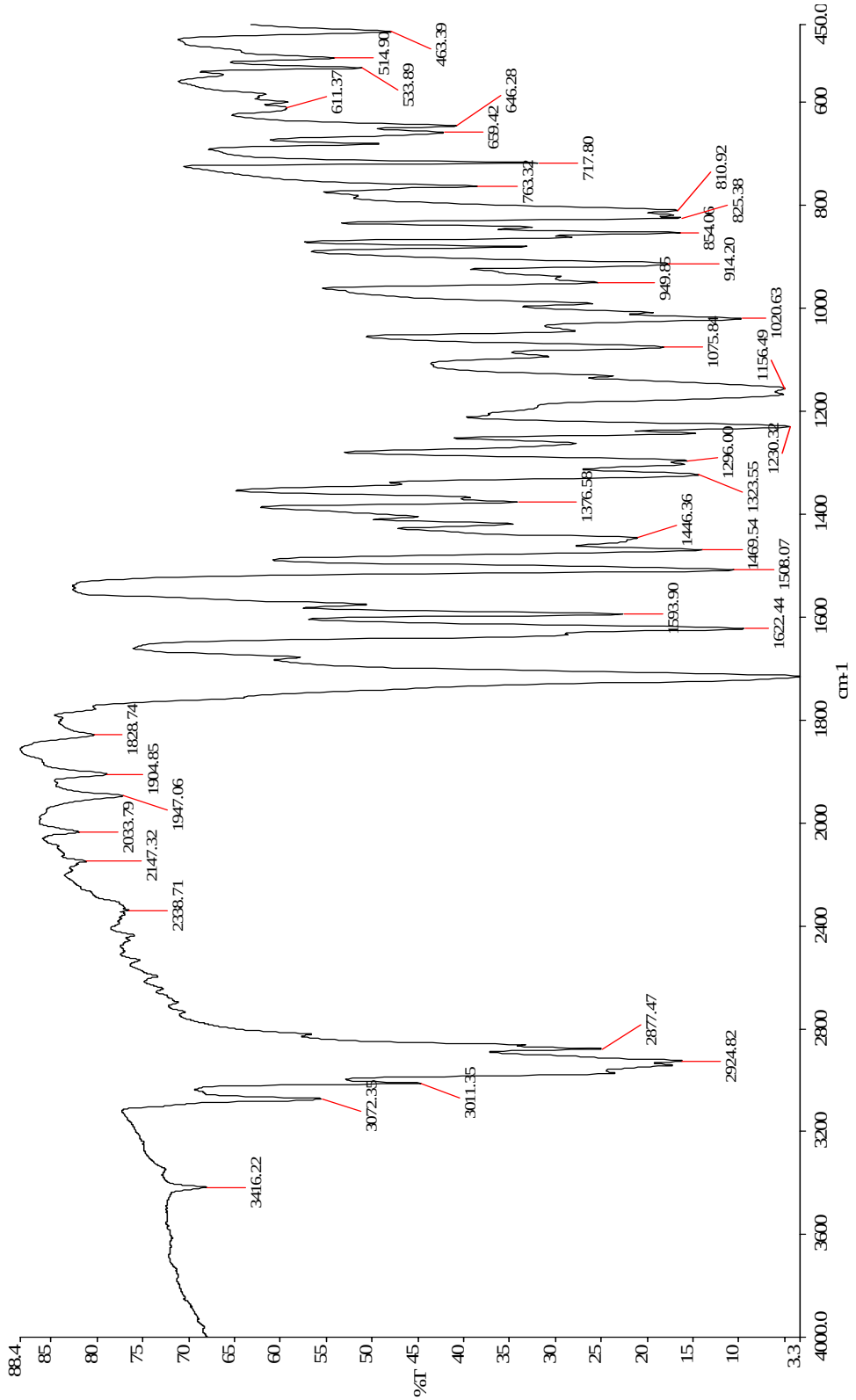

Figure A.1. FT-IR spectrum of methacryloylate quinine.

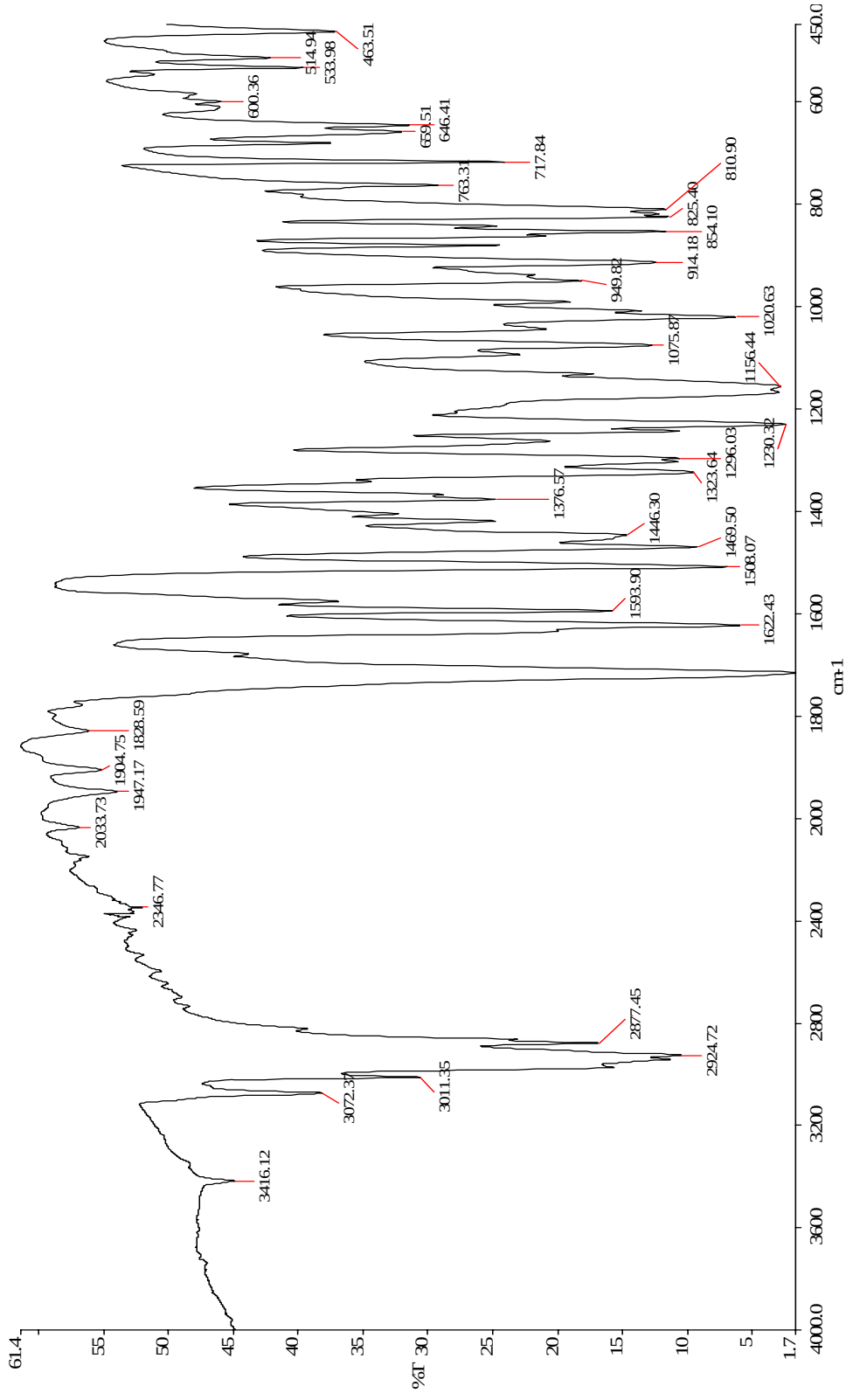

Figure A.2. FT-IR spectrum of methacryloylate quinidine.

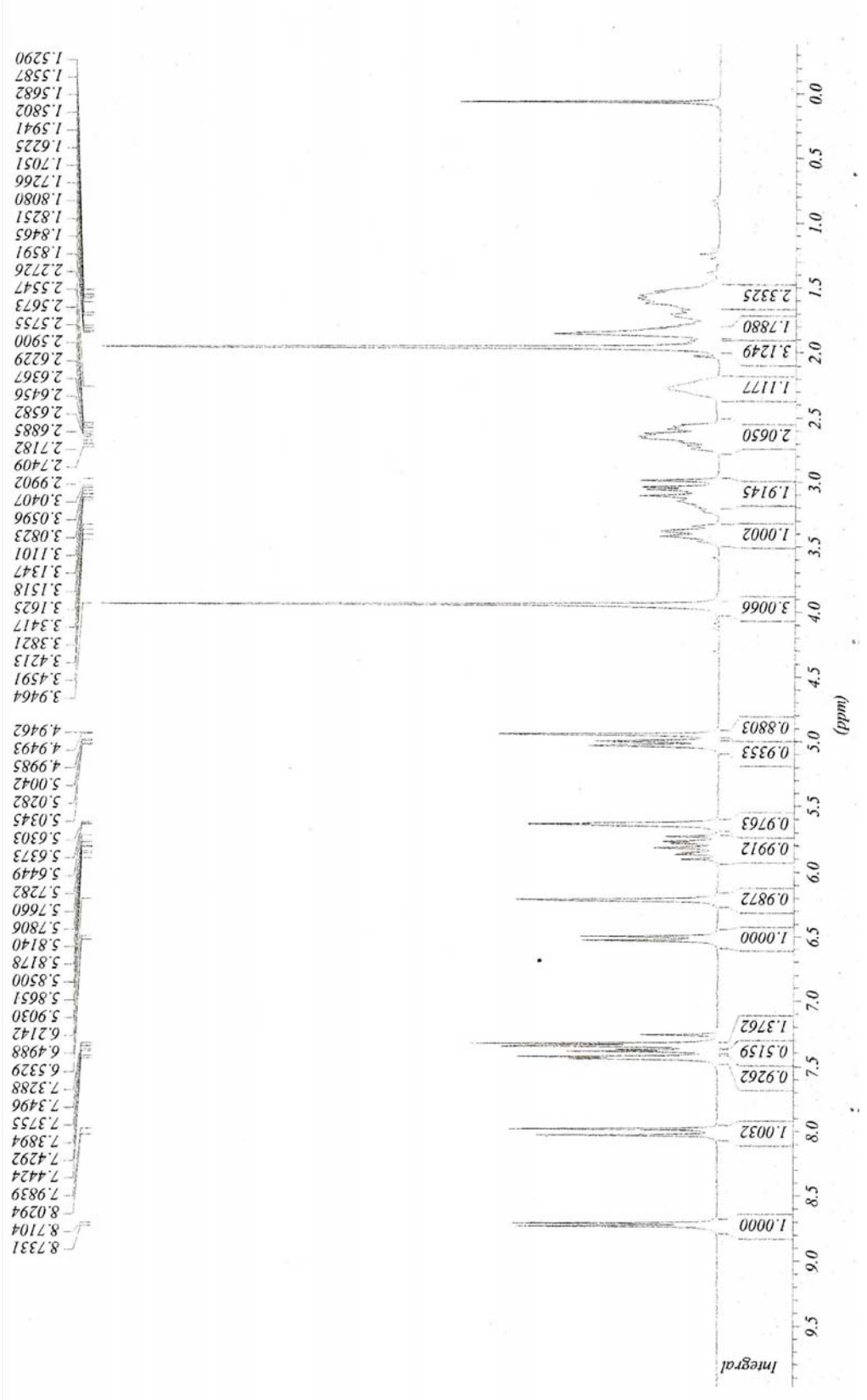

Figure A.3. ^{1}H NMR spectrum of methacryloylate quinine.

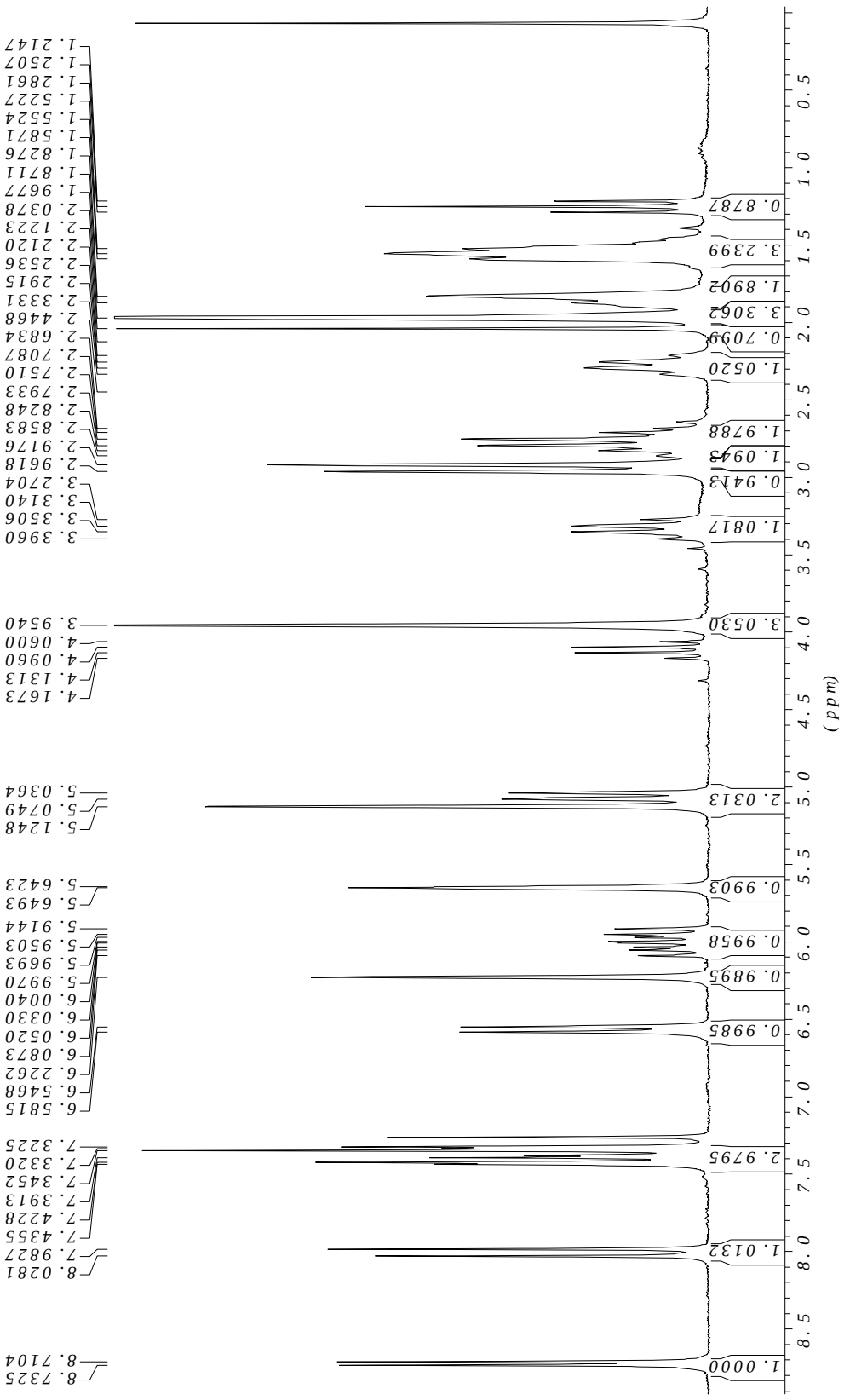

Figure A.4. ^{1}H NMR spectrum of methacryloylate quinidine.